Performance Evaluation of Ultra-Dense Networks with Applications in Internet-of-Things

Mahmoud Kamel

A Thesis

In the Department

of

Electrical and Computer Engineering

Presented in Partial Fulfillment of the Requirements

For the Degree of

Doctor of Philosophy (Electrical and Computer Engineering) at

Concordia University

Montréal, Québec, Canada

March, 2019

CONCORDIA UNIVERSITY

SCHOOL OF GRADUATE STUDIES

This is to certify that the thesis prepared

By: Mahmoud Kamel

Entitled: Performance Evaluation of Ultra-Dense Networks with Applications in Internet-of-Things

and submitted in partial fulfillment of the requirements for the degree of

Doctor of Philosophy (Electrical and Computer Engineering)

complies with the regulations of the University and meets the accepted standards with respect to originality and quality.

Signed by the final examining committee:

Chair

Dr. Govind Gopakumar

External Examiner

Dr. Hossam S. Hassanein

External to Program

Dr. Chadi Assi

Examiner

Dr. Dongyu Qiu

Examiner

Dr. Yousef R. Shayan

Thesis Co-Supervisor

Dr. Walaa Hamouda

Thesis Co-Supervisor

Dr. Amr Youssef

Approved by:

Dr. Mustafa Mehmet Ali, Graduate Program Director

May 7, 2019

Dr. Amir Asif, Dean
Gina Cody School of Engineering & Computer Science

ABSTRACT

Performance Evaluation of Ultra-Dense Networks with Applications in Internet-of-Things

Mahmoud Kamel, Ph.D.

Concordia University, 2019

The new wireless era in the next decade and beyond would be very different from our experience nowadays. The fast pace of introducing new technologies, services, and applications requires the researchers and practitioners in the field be ready by making paradigm shifts. The stringent requirements on 5G networks, in terms of throughput, latency, and connectivity, challenge traditional incremental improvement in the network performance. This urges the development of unconventional solutions such as network densification, massive multiple-input multiple-output (massive MIMO), cloud-based radio access network (C-RAN), millimeter Waves (mmWaves), non-orthogonal multiple access (NOMA), full-duplex communication, wireless network virtualization, and proactive content-caching to name a few.

Ultra-Dense Network (UDN) is one of the preeminent technologies in the racetrack towards fulfilling the requirements of next generation mobile networks. Dense networks are featured by the deployment of abundant of small cells in hotspots where immense traffic is generated. In this context, the density of small cells surpasses the active users density providing a new wireless environment that has never been experienced in mobile communication networks. The high density of small cells brings the serving cells much closer to the end users providing a two-fold gain where better link quality is achieved and more spatial reuse is accomplished.

In this thesis, we identified the distinguishing features of dense networks which include: close proximity of many cells to a given user, potential inactivity of most base stations (BSs)due to lack of users, drastic inter-cell interference in hot-spots, capacity limitation by virtue of the backhaul bottleneck, and fundamentally different propagation environments. With these features in mind, we recognized several problems associated with the performance evaluation of UDN which require a treatment different from traditional cellular networks. Using rigorous advanced mathematical techniques along with extensive

Monte Carlo simulations, we modelled and analytically studied the problems in question. Consequently, we developed several mathematical frameworks providing closed-form and easy-computable mathematical instruments which network designers and operators can use to tune the networks in order to achieve the optimal performance. Moreover, the investigations performed in this thesis furnish a solid ground for addressing more problems to better understand and exploit the UDN technology for higher performance grades.

In Chapter 3, we propose the multiple association in dense network environment where the BSs are equipped with idle mode capabilities. This provides the user with a "data-shower," where the user's traffic is split into multiple paths, which helps overcoming the capacity limitations imposed by the backhaul links. We evaluate the performance of the proposed association scheme considering general fading channel distributions. To this end, we develop a tractable framework for the computation of the average downlink rate.

In Chapter 4, we study the downlink performance of UDNs considering Stretched Exponential Path-Loss (SEPL) to capture the short distances of the communication links. Considering the idle mode probability of small cells, we draw conclusions which better reflect the performance of network densification considering SEPL model. Our findings reveal that the idle mode capabilities of the BSs provide a very useful interference mitigation technique. Another interesting insight is that the system interference in idle-mode capable UDNs is upper-bounded by the interference generated from the active BSs, and in turn, this is upper-bounded by the number of active users where more active users is translated to more interference in the system. This means that the interference becomes independent of the density of the small cells as this density increases.

In Chapter 5, we provide the derivation of the average secrecy rate in UDNs considering their distinct traits, namely, idle mode BSs and LOS transmission. To this end, we exploit the standard moment generating function (MGF)-based approach to derive relatively simple and easily computable expressions for the average secrecy rate considering the idle mode probability and Rician fading channel. The result of this investigation avoids the system level simulations where the performance evaluation complexity can be greatly reduced with the aid of the derived analytical expressions.

In Chapter 6, we model the uplink coverage of mMTC deployment scenario considering a UDN environment. The presented analysis reveals the significant and unexpected impact of the high density of small cells in UDNs on the maximum transmit power of the MTC

nodes. This finding relaxes the requirements on the maximum transmit power which in turn allows for less complexity, brings more cost savings, and yields much longer battery life. This investigation provides accurate, simple, and insightful expressions which shows the impact of every single system parameter on the network performance allowing for guided tunability of the network. Moreover, The results signify the asymptotic limits of the impact of all system parameters on the network performance. This allows for the efficient operation of the network by designing the system parameters which maximizes the network performance.

In Chapter 7, we address the impact of the coexistence of MTC and HTC communications on the network performance in UDNs. In this investigation, we study the downlink network performance in terms of the coverage probability and the cell load where we propose two association schemes for the MTC devices, namely, *Connect-to-Closest (C2C)* and *Connect-to-Active (C2A)*. The network performance is then analyzed and compared in both association schemes.

In Chapter 8, we model the uplink coverage of HTC users and MTC devices paired together in NOMA-based radio access. Closed-form and easy-computable analytical results are derived for the considered performance metrics, namely the uplink coverage and the uplink network throughput. The analytical results, which are validated by extensive Monte Carlo simulations, reveal that increasing the density of small cells and the available bandwidth significantly improves the network performance. On the other side, the power control parameters has to be tuned carefully to approach the optimal performance of both the uplink coverage and the uplink network throughput.

Acknowledgments

I would like to express my special appreciation to my advisors Professor Dr. Walaa Hamouda and Professor Dr. Amr M. Youssef. I could not reach this day without your extreme encourage and constant support. I would like to thank you Dr. Hamouda for being such a great advisor, and for all the support you provided me both technically and personally. Your support and insightful advices were crucial to my academic achievement and my development as a research scientist. Prof. Walaa, thank you for all the technical and ethical values I have learned from you. Also, I would like to thank you Dr. Youssef. You have been a tremendous mentor for me. I would like to thank you for encouraging my research and for allowing me to grow as a research scientist. Your advices on both research as well as on my career have been invaluable. Prof. Youssef, thank you for all the research skills and writing skills I have gained throughout the time I worked with you.

I would also like to thank my committee members, Professor Dr. Y.R. Shayan, Professor Dr. C. Assi, and Professor Dr. D. Qiu for serving as my committee members even at hardship. I also want to thank you for your brilliant comments and suggestions, thanks to you.

I am sincerely thankful to Concordia Graduate Student Support Program (GSSP) for funding my PhD's studies. Also, I would like to seize the opportunity to thank Concordia University Student Parents Centre (CUSP) for the support they provided to my family, especially, my beloved kids.

Last but not least, I would like to express my deepest gratitude to my wife, Marwa Ismail, for the unlimited support and love she has given to me. Your belief in my dreams is the sole energy driving me to success. Without your great sacrifices, I would not reach this level in my research career. You really deserve a special acknowledgment for all you have given to me, which I could not enumerate by any means. Thanks so much Marwa! My beloved kids, Fares, Seif, and Jawad, how delightful and rewarding is the raising of kids like you. I thank you so much for your patience sacrificing so many hours of good family time and playing.

To my beloved wife, Marwa,

To my inspiring kids, Fares, Seif and Jawad, and

To my Mother.

Contents

List of Figures

List of Tables

List of Acronyms

ACA	Advanced Carrier Aggregation
AE	Antenna Element
AR	Augmented Reality
ASE	Area Spectral Efficiency
BBU	Base Band Unit
BPP	Binomial Point Process
BS	Base Station
C2A	Connect-to-Active
C2C	Connect-to-Closest
CA	Carrier Aggregation
CAPEX	Capital Expenditure
CC	Component Carrier
CCDF	Complementary Cumulative Distribution Function
CDF	Cumulative Distribution Function
CDMA	Code-Division Multiple Access
CE	Coverage Enhancements
CIoT	Cellular Internet of Things
CoMP	Coordinated MultiPoint
CSG	Closed Subscriber Group

CSI	Channel State Information
D2D	Device-to-Device
DAS	Distributed Antenna System
DC	Dual Connectivity
DI	Dominant Interferer
DSL	Digital Subscriber Line
eCA	enhanced Carrier Aggregation
eDCM	enhanced Dynamic Cell Muting
eICIC	enhanced Inter-Cell Interference Cancellation
FiWi	Fiber-Wireless
FRP	Frequency Reuse Planning
FTTC	Fiber-To-The-Cell
H2H	Human to Human
HetNet	Heterogeneous Networks
HCPP	Hard Core Point Process
HTC	Human-Type Communications
HSPA	High Speed Packet Access
IoT	Internet of Things
KPI	Key Performance Indicator
LOS	Line-Of-Sight
LT	Laplace Transform
LTE	Long-Term Evolution
LTE-A	Long Term Evolution- Advanced

M2M Machine to Machine

MAC Medium Access Control

MCA massive Carrier Aggregation

MC-UDN Multi-Carrier UDN

MDE Most Detrimental Eavesdropper

MFG Mean-Field Game

MGF Moment Generating Function

MIMO Multiple-Input Multiple-Output

mmWaves millimeter Waves

mMTC massive Machine-Type Communication

MRP Maximum Rank Planning

MS Mobile Stations

MTC Machine-Type Communication

NAAR Network Aggregate Average Rate

NLOS Non Line-Of-Sight

NOMA Non-Orthogonal Multiple Access

OFDMA Orthogonal Frequency-Division Multiple Access

OMA Orthogonal Multiple Access

ONF Open Networking Foundation

OPEX Operational Expenditure

PCP Poisson Cluster Process

PDF Probability Distribution Function

PF Proportional Fair

PGFL Probability Generating Functional

PHY Physical Layer

PLS Physical Layer Security

PP Point Process

PPP Poisson Point Process

QoE Quality of Experience

QoPE Quality-of-Physical Experience

QoS Quality of Service

RACH Random Access CHannel

RAN Radio Access Network

RAT Radio Access Technology

RB Resource Block

RE Range Expansion

RR Round Robin

RRH Remote Radio Head

RRM Radio Resource Management

RSS Received Signal Strength

SDN Software-Defined Network

SDWN Software-Defined Wireless Network

SE Spectral Efficiency

SEPL Stretched Exponential Path Loss

SIC Successive Interference Cancellation

SINR Signal to Interference-plus-Noise Ratio

SNR	Signal-to-Noise Ratio
TCI	Truncated Channel Inversion
TDD	Time-Division Duplex
ucICIN	user-centric Inter-Cell Interference Nulling
UE	User Equipment
UDN	Ultra-Dense Network
VR	Virtual Reality

List of Symbols

Φ_s	PPP of small cells
λ_s	Density of small cells
Φ_u	PPP of users
λ_u	Density of users
Φ_h	PPP of HTC users
λ_h	Density of HTC users
Φ_m	PPP of MTC devices
λ_m	Density of MTC devices
ρ_m	Activity ratio of MTC devices
Φ_e	PPP of eavesdroppers
λ_e	Density of eavesdroppers
κ	Densification ratio
p_a	Probability of active mode
p_o	Probability of idle mode
λ_a	Density of active cells
P_s	BS transmit power
P_{ho}	Power control cutoff threshold of HTC users
P_h^{max}	Maximum transmit power of HTC users
P_{mo}	Power control cutoff threshold of MTC devices
P_m^{max}	Maximum transmit power of MTC devices
B	Component carrier bandwidth
$\mathcal{S}$	Signal power
$\mathcal{I}$	Interference power
σ^2	Noise power
τ	Coverage threshold
$\mathcal{P}$	Probability of coverage
M	*Multicell* size

g_o	Tagged BSs fading channel
g_b	Interfering BSs fading channel
U_o	Typical user
B_o or B_k	Tagged BS
r_k	Distance from U_o to the tagged BS B_k
γ	Signal-to-Noise ratio (SNR)
$\mathbb{E}\{\cdot\}$	Expectation operator
$\mathcal{M}_X(\cdot)$	MGF of random variable X
$f_X(\cdot)$	PDF of random variable X
$F_X(\cdot)$	CDF of random variable X
$\mathcal{L}(\cdot)$	Laplace Transform
${}_2F_1(\cdot,\cdot,\cdot,\cdot)$	Hypergeometric function X
$\Gamma(\cdot)$	Gamma function
$\gamma(\cdot,\cdot)$	Lower incomplete Gamma function
$\mathrm{Li}_{(k)}(\cdot)$	The k^{th} order poly-logarithmic function
$\ln(\cdot)$	Natural logarithmic function

1. Introduction

1.1 Ultra-Dense Networks (UDNs)

The ever-evolving requirements on mobile communication networks are principally fueled by three main drivers: deeper coverage, higher capacity, and massive connectivity. The wireless standards in the next decade (beyond 2020) are facing extremely diverse demands where both enormous traffic and gigantic number of connections are required [3]. Applications like Virtual Reality (VR) [4], Augmented Reality (AR) [5], Internet-of-Things (IoT) [6], social networks, and cloud offices generate mammoth traffic and request massive number of connections that has been never witnessed or imagined. In this way, UDN is a key player and we would claim it as the main candidate technology to satisfy the various requirements. Moving from network-centric mode of operation to user-centric mode largely supports this claim. In user-centric paradigm, a single user would generate traffic that needs the entire spectrum of one BS [7]. Moreover, a single household may contain 50+ IoT devices asking for connections [8], let alone the devices in the building and in the street. Deploying a huge number of small cells in UDN is then in a perfect alignment with this networking paradigm shift. With a number of BSs that exceeds the number of active users, each user can connect to one or more BSs harvesting all the spectrum to his own need. At the same time, this large number of cells provide a uniform and deep coverage to reach the IoT devices in harsh deployment scenarios (like basements, underground facilities, and concrete structures). Besides, the surplus availability of small cells affords massive scalable connectivity for the potential IoT applications.

The concept of Ultra-Dense Network (UDN) represents a new paradigm shift in future networks. The basic idea is to get the access nodes as close as possible to the end users. The realization of this is simply done by the dense deployment of small cells in the hotspots where immense traffic is generated. These small cells are access nodes with

small transmission power, and hence, a small coverage. These cells are deployed by the customers in their premises, or by the operators in the streets (e.g., on lampposts, trees, and walls) and hotspots (e.g., airports, metro/train stations, and markets). Thus, UDN deployment scenarios introduce a different coverage environment where any given user would be in close proximity to many cells.

The densification of wireless networks is motivated by the traffic trends measured in the current decade. For instance, Cisco, in the Cisco Virtual Networking Index, predicts a 10 fold increase in the mobile data worldwide for the period $2014 - 2019$ [9]. With the scarce spectrum resources, one vital and long-term solution is to increase the reuse per unit area of the existing spectrum. This spectrum reuse is a two fold gain; the spectrum is increasingly reused, which significantly improves the network capacity, and the link to the end user becomes shorter which improves the link quality. Obviously, the network densification cannot continue endlessly. There would be a fundamental limit for network densification which requires extensive research for realistic system models to capture the reality of dense networks.

1.2 Internet of Things (IoT)

IoT refers to a network of devices with Internet connectivity to communicate directly without human-intervention in order to provide smart services to users [6]. The connectivity of such devices eases the collaborative decision making through processing of real-time data and the improved access to information. The achievements in smart sensors, wireless communication technologies [10], context-aware computing, cloud technologies, and Internet protocols can be considered as the building blocks of IoT architecture [11]. Also, the research and standardization efforts in machine-to-machine (M2M) communication plays a significant role in the development of the state-of-the-art of IoT [12]. Applications in health [13], smart security, and smart cities found their way to the market and realizes the potential benefits of this technology [14]. In addition, many other applications of IoT can be enumerated such as agriculture, industry, natural resources (water, forests, etc.) monitoring, transport system design, and military applications [15].

Many challenges are facing the fruition of IoT technology, namely, addressing and identification of the connected devices, the standardization of the technology for optimal

interoperability, the privacy of the information, the security of the sensors or actuators, the provisioning of wireless backhaul and storage resources for billions of connected devices, and the energy efficient deployment of edge-devices and communication nodes [15].

Network densification is considered as an enabler for the successful diffusion of IoT services and application in the society. The availability of nearby communication links alleviates the strict requirements on the wireless network infrastructure. The deployment of indoor small cells (picocells and femtocells) stems as an excellent solution for providing connectivity to home smart devices and offloads a great portion of the traffic from the macro-cellular network.

1.3 Motivations

Many aspects of Ultra-Dense Networks (UDNs) require comprehensive investigations in order to accurately evaluate the performance of such networks. The wireless environment of UDNs has never been experienced before, consequently, this urges identifying what features make UDN different. In addiction, these features have to be considered in the modelling of UDN in order to develop tractable results. Thus, the network performance can be characterized in terms of relevant key performance indicators (KPIs). The fundamental distinguishing features of UDN are: i) the close proximity of many cells to a given user, ii) the high probability for a cell being inactive due to the lack of connected users, iii) the fundamentally different propagation environment, and iv) the drastic inter-cell interference in hot-spots.

Considering the above mentioned distinguishing features, we recognized several problems associated with the performance evaluation of UDN. Accordingly, we defined our problem as to model dense networks considering the distinct traits of such networks in order to investigate some of the previously mentioned challenges and to study their impact on the performance of UDNs. In addition, we exploited the UDN features to propose innovative solutions concerning the user association, physical layer security, and uplink coverage of MTC devices in UDN environment. Moreover, we addressed the impact of the coexistence of HTC users and MTC devices on the downlink coverage and downlink load in UDN environments. Furthermore, we investigated the impact of deploying UDNs on the coexistence of HTC and MTC considering NOMA in the uplink.

1.4 Thesis Contributions

Considering the preceding discussion, the main challenges in evaluating the performance of UDN and exploiting their distinct traits in supporting the applications of Internet of Things (IoT) are i) capturing of the fundamental differences associated with the deployment of UDNs in the modeling of such networks, ii) providing tractable mathematical frameworks to compute the main performance metrics of UDNs, and iii) developing of association schemes to satisfy the diverse requirements of both Human-Type Communication (HTC) users and Machine-Type Communication (MTC) devices in a coexisting scenario. Tackling these challenges provides the ultimate goal of this thesis. The contributions of this thesis are summarized in the following items:

Multiple Association in UDNs. In Chapter 3, we consider the modeling of multiple association in dense network environment where the BSs are equipped with idle mode capabilities. We evaluate the performance of the proposed association scheme considering general fading channel distributions. To this end, the MGF-based approach is exploited to develop a tractable framework for the computation of the average downlink rate. To highlight the contributions of this investigation, a simple and accurate framework is developed to compute the average downlink rate of the links connecting the typical user to the tagged BSs in a multiple association context. The framework considers general *multicell* size M, and general fading channel distributions in both the signal and interference links. Moreover, we develop a recursive form to provide a simpler way for the computation of the average downlink considering Rayleigh fading channels. The recursion is easy to manipulate and avoids the tedious work required for the computation of folded integrals involved in averaging out the downlink rate over the distance distributions and channel fading distributions.

Downlink Coverage and Capacity Analysis considering SEPL in UDNs. In Chapter 4, we study the downlink performance of UDNs considering a more accurate path loss model, i.e., SEPL model. Different from existing research, we further consider the idle mode probability of small cells in UDNs, thus, we assume that a given user connects to the nearest BS and if there exist a BS with no connected users, it is turned off to mitigate its interference. Based on this assumption, we draw different conclusions which better reflect the performance of network densification considering SEPL model. Our

findings reveal that the idle mode capabilities of the BSs provide a very useful interference mitigation technique besides the energy efficiency of operating such dense networks. Another interesting insight is that the system interference in idle-mode capable UDNs is upper-bounded by the interference generated from the active BSs, and in turn this is upper-bounded by the number of active users where more active users is translated to more interference in the system. This means that the interference becomes independent of the density of the small cells as this density increases. In the light of the above discussion, we conclude that the coverage probability converges to a constant value at very high small cell densities where this value is a function of the user's density.

Physical layer security in UDNs. In Chapter 5, the main contribution is the derivation of the average secrecy rate in UDNs considering their distinct traits, namely, idle mode BSs and LOS transmission. The high density of small cells makes it quite probable for a BS to have no connected users. Consequently, turning off those inactive BSs provides a simple yet effective interference mitigation scheme. Moreover, the close proximity of the users/Eves to the BSs increases the probability of having a LOS transmission in both the main link and the leakage link. To this end, we exploit the standard moment generating function (MGF)-based approach to derive relatively simple and easily computable expressions for the average secrecy rate considering the idle mode probability and Rician fading channel. The result of this investigation avoids the system level simulations where the performance evaluation complexity can be greatly reduced with the aid of the derived analytical expressions. Finally, we highlight that two eavesdropping scenarios have been considered in the literature; active eavesdropping and passive eavesdropping. In active eavesdropping, the instantaneous channel state information (CSI) of the eavesdropper is known to the transmitter through feedback. Practical scenarios for this case includes broadcast channels where all users except the intended user can be dealt as eavesdroppers. In this scenario, perfect secrecy is always guaranteed. In passive eavesdropping, the CSI of the main channel is available while the CSI of the eavesdropper's channel is not known. As such, the transmitter selects a constant secrecy rate and perfect secrecy is not always guaranteed. The considered analysis in this investigation provides a guaranteed average secrecy rate in the case of active eavesdropping while in the case of passive eavesdropping it provides statistical characterization of the performance of secrecy communication in UDNs. Specifically, one can gain insights of how the

secrecy performance in UDN scales with the density of various network nodes, namely, the legitimate users, the eavesdroppers, and the BSs.

Uplink Coverage of mMTC in UDNs. In Chapter 6, we investigate the uplink coverage of massive Machine-Type Communication (mMTC) considering an Ultra-Dense Network (UDN) environment. The small-scale fading is modeled using a general ($\alpha - \mu$) channel model and the large-scale fading is modeled by SEPL to capture the short distances in Ultra-Dense Networks (UDNs). In particular, the system model captures the impact of the system parameters which characterizes the environment of massive machine-type communications (mMTC). The provided analysis reveals the significant and unexpected impact of the high density of small cells in UDNs on the maximum transmit power of the MTC nodes. This finding relaxes the requirements on the maximum transmit power which in turn allows for less complexity, brings more cost savings, and yields much longer battery life. Thanks to the high density of the serving small cells. This investigation provides accurate, simple, and insightful expressions. The expressions are readily readable and shows the impact of every single system parameter on the network performance allowing for guided tunability of the network. Furthermore, the results signify the asymptotic limits of the impact of all system parameters on the network performance. This allows for the efficient operation of the network by designing the system parameters which maximizes the network performance. Remarkably, there is a critical saturation point where increasing these system parameters has no further impact on the performance. Accordingly, this saturation limit can be chosen as a limit for the corresponding system parameter. Finally, an interesting finding is that the uplink coverage performance in the considered scenario has two distinct regions of operation, noise-limited region and interference-limited one where the power control parameters solely controls the border between the two regions.

Coexistence of MTC and HTC in UDN. In Chapter 7, we address the impact of the coexistence of MTC and HTC communications on the network performance in UDNs. In this investigation, we study the downlink network performance in terms of the coverage probability and the cell load where we proposed two association schemes for the MTC devices, namely, *Connect-to-Closest (C2C)* and *Connect-to-Active (C2A)*. The network performance is then analyzed and compared in both association schemes. The investigation of the proposed system model shows a tradeoff between the two performance

metrics with respect to the considered association schemes. Accordingly, this suggests the design of association schemes to find a balance between them. On the positive side, the consideration of UDNs to support MTC devices traffic provides a scalable and a viable solution to the connectivity problem in future massive deployments of MTC devices.

Combined HTC and MTC considering NOMA in UDNs. In Chapter 8, we investigate a NOMA-based radio access where a pair of HTC user and MTC device is encouraged to use the same resource block in the uplink simultaneously. This allows to host the diverse requirements of both types of users while operating the network at its optimal point. The results confirm this claim where both types of users, i.e., HTC and MTC, enjoy a high uplink coverage and an enormous uplink network throughput. The analytical results which is validated by extensive Monte Carlo simulations provide a mathematical framework to assess the performance of such scenario and to tune the system parameters to operate the network at an optimal and efficient point. Increasing the density of small cells and the available bandwidth significantly improves the network performance. On the other hand, the power control parameters has to be tuned carefully to approach the optimal performance of both the uplink coverage and the uplink network throughput.

1.5 Thesis Organization

The rest of the thesis is organized as follows. In Chapter 2 we provide a comprehensive introduction to UDN. Also, we present the state-of-the-art in different research directions in the context of Ultra-Dense Networks. The multiple association scheme is then proposed and investigated in Chapter 3. In Chapter 4, we study the coverage and capacity of UDNs considering SEPL model and idle mode capabilities. The physical layer security in UDN is studied in Chapter 5 and the uplink coverage of MTC devices is analyzed in Chapter 6. In Chapter 7, the impact of the coexistence of MTC and HTC users on the downlink coverage and cell load of UDN is studied. The uplink coverage of combined HTC and MTC considering NOMA is investigated in Chapter 8. Finally, in Chapter 9 the conclusions of this thesis are drawn and the future trends are discussed.

2. Background and Literature Review

The evolution of mobile devices and applications in the current decade have drawn a new picture for wireless networks, where the concept of Ultra-Dense Network (UDN) represents a new paradigm shift in future networks [16–19]. The basic idea is straightforward; bring the access nodes as close as possible to the end users. The realization of this is simply done by the dense deployment of small cells in the hotspots where immense traffic is generated. These small cells are access nodes with small transmission power, and hence, a small footprint. The cells are deployed by the customers in their premises, or by the operators in the streets (e.g., on lampposts, trees, and walls) and hotspots (e.g., airports, metro/train stations, and markets), as illustrated in Figure 2.1. Thus, the UDN deployment scenarios introduce a different coverage environment where any given user would be in close proximity to many cells.

2.1 Definitions of UDN

Ultra-Dense Networks can be defined as those networks where there are more cells than active users [20–24]. In other words, $\lambda_b \gg \lambda_u$, where λ_b is the density of access points, and λ_u is the density of users. Another definition of UDN was solely given in terms of the cell density, irrespective of the users density. Ding *et al.* [25] provided a quantitative measure of the density at which a network can be considered ultra-dense ($\geq 10^3$ cells/km^2). In fact, the first definition converges to the second given that the active users density considered in dense urban scenarios is upper bounded by about 600 active users/km^2 [26].

Generally, the small cells in UDN can be classified into fully-functioning base stations (BSs) (picocells and femtocells) and macro-extension access points (relays and Remote

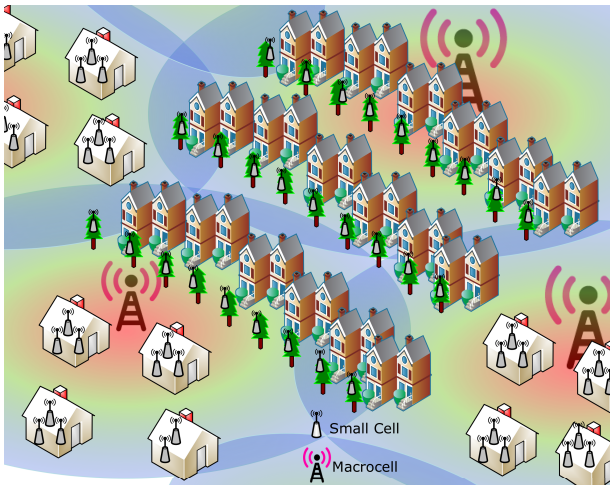

Figure 2.1: The network is densified by deploying small cells indoors in buildings and stores, and outdoors on trees, lampposts, and building walls. Small cell networks coexist with macrocells, either in the same spectrum or on a dedicated carrier.

Radio Heads (RRHs)). The fully-functioning BS is capable of performing all the functions of a macrocell with a lower power in a smaller coverage area. Specifically, the fully-function BS performs all the functions of the entire protocol stack [27]. On the other hand, a macro-extension access node is an extension for the macrocell to effectively extend the signal coverage, and it performs all or some of the PHY layer functions only. Moreover, the small cells feature different capabilities, transmission powers, coverage, and deployment scenarios [28, 29]. Table 2.1 summarizes the features of different small cell types. In what follows we explain the different types of small cells [30]:

- **Picocells** are small BSs which are installed by operators to cover a small coverage area in a range of one hundred meters. Usually picocells are deployed in hotspots (indoor or outdoor) to serve tens of active users by offloading their traffic from the macrocell. The transmission power of picocells is typically up to 33 dBm, and they are mainly deployed for capacity purposes. The backhauling of picocells is similar to that of the macrocells (fiber or microwave links) in order to provide ideal high-bandwidth low-latency links.

- **Femtocells** are user-deployed indoor BSs which are installed to cover indoor spots (homes, offices, and meeting rooms) in order to serve a small set of users. The transmission power of femtocells typically is less than 20 dBm and the coverage range is in the order of tens of meters. Thus, a femtocell provides a large indoor signal strength for the home users where most of the data traffic is generated. The

Table 2.1: Different Types of Small Cells

Type of small cell	Deployment Scenario	Coverage	Power	Access Scenario	Backhaul
Picocells (fully-functioning)	indoor/outdoor (planned)	up to 100 meters	indoor ($\leq$ 100 mW) outdoor (0.25 – 2 W)	Open Access	Ideal
Femtocells (fully-functioning)	indoor (unplanned)	10 – 30 meters	$\leq$ 100 mW	Open/Closed/Hybrid Access	Non-Ideal
Relays (macro-extension)	indoor/outdoor (planned)	up to 100 meters	indoor ($\leq$ 100 mW) outdoor (0.25 – 2 W)	Open Access	Wireless (in-band/out-of-band)
RRHs (macro-extension)	outdoor (planned)	up to 100 meters	outdoor (0.25 – 2 W)	Open Access	Ideal

femtocells can be connected to the network via any of the consumers' broadband connections such as Digital Subscriber Line (DSL), cable, or fiber.

- **Relays** are operator deployed access points which are usually deployed for coverage purposes to cover the dead zones and to improve the edge performance of the macrocells. They transmit the users data back and forth from and to the macrocell, featuring what is considered as wireless backhaul. Both relays and picocells have the same coverage and transmit power, but they mainly differ in three properties. First, a picocell is a fully-functioning BS while the relay is an extension for the macrocell. Second, picocells are deployed for capacity, but relays are deployed for coverage. Finally, the backhaul of the picocell is an ideal backhaul while the relay backhaul is a wireless in-band or out-of-band backhaul.

- **RRHs** are RF units which are deployed in order to extend the coverage of a central BS to a remote geographic location. RRHs are connected to the central BS via high speed fiber or microwave links [31]. They are deployed for coverage extension of the macrocell and can be used as a centralized densification alternative as compared to the distributed densification performed by the picocells or femtocells.

It is important to highlight that indoor small cells (femtocells) operate in three different access modes: open, closed, and hybrid. In open access mode, all subscribers of a given operator can access the node, while in closed access mode the access is restricted to a closed subscriber group (CSG). In hybrid mode, all subscribers can connect to the femtocell with the priority always given to the subscribers of the CSG. The deployment of small cells with regular macrocells is termed in the literature and standards as HetNet. HetNets in general represents a paradigm shift from homogeneous networks [32]. As depicted in Figure 2.2, UDN serves as another evolution from HetNets.

2.2 Fundamental Features of UDN

In order to understand the current state of the research activities in UDN, the differences between dense networks and traditional networks need to be highlighted. These fundamental differences of UDN from traditional networks can be summarized as follows:

1. Many small cells are in the vicinity of a given user. The network access nodes in UDN environments are low-power small cells with a small footprint, or in other words, with a small coverage area. Accordingly, the inter-site distance would be in the range of meters or tens of meters. This defines a different wireless coverage environment where many small cells would be in a very close distance to the users.

2. Idle mode capabilities are of a great interest. Due to the high density of small cells, many small cells would be inactive. This motivates the idle mode concept, where inactive small cells are turned off to partially or fully mitigate their interference [33].

3. Drastic interference between neighboring cells is a limiting factor. Close proximity of the small cells to each other in UDN environments generates high interference. Hence, strict interference management schemes are unavoidable to mitigate the interference of neighboring cells [34–38].

4. Innovative frequency reuse techniques are required. In traditional cellular networks, the spectrum is reused at the level of a cluster of cells where a reuse pattern is repeated in each cluster. This reuse scheme touches its limit in code-division multiple access (CDMA) and orthogonal frequency-division multiple access (OFDMA) systems where the spectrum is reused in each cell, i.e., the frequency reuse factor is one. In UDN environments, there would be a need for a paradigm shift in the frequency reuse concept.

5. Backhauling in UDN environments is challenging. It might be difficult for operators to guarantee an ideal high-speed low-delay backhaul for each small cell. Also, the backhaul of a small cell might be the bottleneck of its capacity, where the backhaul capacity would limit the air-interface capacity [21, 39–43].

6. High probability of Line-of-Sight (LOS) transmissions. In UDN, the distance between BSs and users is small enough to have a high probability of LOS trans-

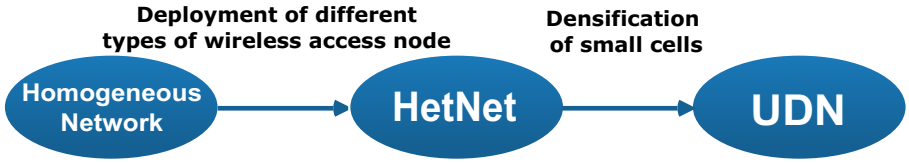

Figure 2.2: The traditional homogeneous network is evolved to HetNet, and in turn the UDN is a densified HetNet.

missions [25, 44, 45]. Accordingly, the need for a different propagation modelling becomes a necessity. Moreover, the propagation modelling in UDN should also consider a Rician channel model for multi-path fading due to the dominant LOS component in the received signal.

2.3 Horizontal and Vertical Densification

The densification of wireless networks takes place mainly by the deployment of increasing number of small cells. Accordingly, the network densification comes in two different flavors, either horizontal densification or vertical densification. In horizontal densification, the access nodes are densified in the horizontal plane, e.g., in the streets or hotspots. On the other hand, the vertical densification evolves in the elevation plane where the customers deploy BSs in their apartments, offices, meeting rooms, and buildings interior. Figure 2.3 depicts vertical and horizontal network densification. The aforementioned classification highlights three major aspects of the densification schemes, specifically, the modelling of the densification scheme (vertical/horizontal) to consider appropriate propagation models, the backhauling alternatives for the different densification schemes, and the performance evaluation of the corresponding densification scheme. Consequently, the investigation of UDNs requires different modelling for the two densification schemes, namely vertical and horizontal. In this manner, the three-dimensional (3D) modelling of the vertically densified networks is inescapable to reflect the reality of such networks. Only a few papers addressed the 3D modelling of cellular networks [46, 47] over the past decade. Recently, the modelling of wireless networks in 3D has been addressed in the work of Gupta *et al.* considering a UDN context [44]. Furthermore, the modelling and analysis of coverage in 3D cellular networks is conducted by Pan and Zhu [48]. Consequently, this gives rise to the consideration of 3D-MIMO [49] which might be used as a

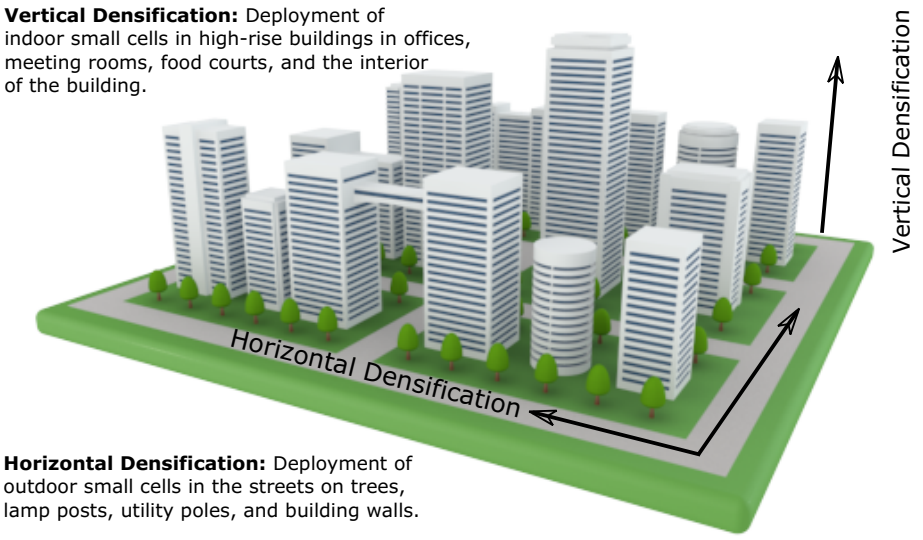

Figure 2.3: Vertical densification versus horizontal densification in small cell networks.

backhauling alternative in vertically densified networks. Also, this in turn motivates the modelling and analysis of 3D fading channels [50]. Moreover, the performance of network densification in the vertical plane is different from that of the horizontal plane. In vertical densification, the area spectral efficiency for the same area improves in high-rise buildings with more floors. This suggests incorporating the clutter of the buildings into the performance evaluation of such densification schemes.

2.4 Centralized and Distributed Densification

In centralized densification, a central entity takes the coordination role between different elements in order to boost the network performance. This central entity can be a BS equipped with a massive-MIMO system [51], a BS extended with a Distributed Antenna System (DAS) [52], or a cloud of base band processing units in a Cloud- Radio Access Network (Cloud-RAN) [53]. On the other hand, the distributed densification of wireless nodes in small cell networks or the distributed densification of wireless links in Device-to-Device (D2D) requires scalable algorithms for the collaboration amongst different nodes. Densification of wireless networks can be realized either by the deployment of increasing number of access nodes or by the densification of the number of links per unit area. In the first approach, the densification of access nodes can be achieved in a distributed manner by the deployment of small cells (picocells and femtocells) or via a centralized scheme

using DAS or Cloud-RAN. Also, in the second theme, the increasing of the number of links per unit area is realized either in a distributed way in D2D communication, or by a centralized massive-MIMO deployment.

2.5 Motivation Behind Network Densification

The motivation behind densification of wireless networks is the traffic trends measured in the current decade. For instance, Cisco, in the Cisco Virtual Networking Index, predicts a 10 fold increase in the mobile data worldwide for the period 2014-2019 [9]. With the scarce spectrum resources, one vital and long-term solution is to increase the reuse per unit area of the existing spectrum. This is a two fold gain, the spectrum is increasingly reused which significantly improves the network capacity, and the link to the end user becomes shorter which improves the link quality.

2.6 UDN in a Practical Sense

One of the most distinguishing traits of UDNs is the high density of the BSs. A quantitative measure of how high this density can be given in terms of the relative density of the BSs with regard to the active users' density (e.g. see Definition 1 in [54] and the references therein) which is also consistent with the UDN definition in other references such as in [21, 55–57]. We emphasized in [58] on how to define a UDN, or in other words, at what level of densification we consider a network as UDN. An early comprehensive simulation study is conducted in [21] to shed lights on the potential gains of network densification, where densities as high as $20,000$ cells/km^2 are considered while the maximum considered users' density was limited to 600 users/km^2.

In Apr. 2014, Qualcomm reported in [59] the world's densest LTE small cell deployment with equivalent cell density of 1107 cells/km^2 with an average site-to-site distance of 22m, minimum site-to-site distance of 7m and a total coverage area of 0.028 km^2. Based on the trial deployments in this report, one could imagine more dense UDN implementations to come in the near future. In fact, the trends reported for the new technologies, applications, and services show that the anticipated data rates to fulfill the requirements will be in the order of multi-Gbps. This requires networks with densities that may appear impractical for the time being, however, these densities will be very practical in the near

future. Moreover, we quote Nokia's definition of a UDN [60] *"UDN can be defined as a network with sites on every lamp post or having indoor sites less than* $10m$ *apart"*. According to this definition and considering the fact that the active user's density in dense urban scenarios is typically bounded by about 600 users/km^2 [61], the assumption of BSs density is higher than the active users' density in UDN would be fairly practical in future deployments of UDNs.

2.7 Literature Review

Liu *et al.* [62] comprehensively surveyed the user association schemes in 5G networks. They considered the state-of-the-art association mechanisms in three paradigms of the 5G networks: HetNets, massive MIMO networks, and mmWaves networks. Lie *et al.* delved into the aspects of user association in 5G networks where they discussed different modelling techniques, performance metrics, and network topology models. Liu and Wang [63] investigated a general random cell association scheme to study the fundamental correlation between cell association and void cell probability (AKA idle mode probability). The findings in [63] reveal accurate bounds for the idle mode probability in a PPP modelled cellular network where they claim that the existing result [20] is not accurate in a general setting, or in other words its accuracy is conditioned on the considered association scheme (e.g., nearest cell association).

Various downlink interference mitigation techniques are investigated by Soret *et al.* [37] where two algorithms are proposed, a time domain and a frequency domain small cell interference coordination. They considered four interference scenarios, and they highlighted the role of the dominant interferer (DI). On the other hand, Polignano *et al.* [36] addressed the inter-cell interference dilemma in dense outdoor small cell networks. The impairment to the user experience due to inter-cell interference is investigated to evaluate the conditions that make the interference coordination preferred to the universal frequency reuse. In a different direction, an enhanced dynamic cell muting scheme (eDCM) is proposed by Wang *et al.* in [38] where the authors exploit the Coordinated MultiPoint (CoMP) framework of LTE Rel-11 to develop a dynamic muting mechanism to mute some resources at certain small cells for the benefit of other small cells. In their work, the inter-cell coordination function to generate the muting patterns considers a benefit metric for individual

users and a proportional fairness scheduling amongst all users.

In a MIMO setting, Tavares *et al.* [64] utilized MIMO spatial multiplexing to mitigate the inter-cell interference in small cell networks. Rather than the traditional frequency reuse planning (FRP), they proposed maximum rank planning (MRP). In their proposal, the reduction of spatial multiplexing streams increases the probability of higher degree-of-freedom for the interference rejection receivers to reject the dominant interference. In a different setting, Li *et al.* investigated a user-centric inter-cell interference nulling (ucICIN) scheme [34, 35]. In their work, the authors derived an approximate expression for the success probability of a typical user. In this model, a user requests the suppression of the interference of some neighbouring BSs based on their relative distance to the serving BS. Moreover, the simulation results confirmed the accuracy of the approximation to some extent. Furthermore, the authors studied the effect of limited channel state information (CSI) on the performance of the interference nulling technique.

Using game theory concepts, Al-Zahrani *et al.* [65] exploited game-theoretic approaches to investigate the cross-tier and co-tier interference management. To overcome the curse of dimensionality in case of dense networks, the authors modelled their problem using mean-field game theory. In mean-field game theory [66], a player takes an action based on the average of the effect of other players' actions rather than the individual effects. In another setting, Liu *et al.* [67] exploited game theoretic approaches combined with graph-coloring algorithms to model a joint CoMP clustering and inter-cell resource allocation for interference mitigation. A scalable algorithm is proposed to account for the large number of cells in a dense network. The distributed two-step algorithm is evaluated and potential performance improvements are concluded. A power allocation algorithm is proposed by Yuehong *et al.* [68] to coordinate the interference especially for the benefit of edge users. Non-cooperative game theory is applied to find the Nash Equilibrium for the power allocations in the downlink of a dense network. A non-cooperative game is formulated by Sun *et al.* [69] to investigate the role of cluster-based spectrum allocation and CoMP transmission to mitigate the sever interference in UDNs. In this investigation, the authors consider the load condition of the cells to associate the users to the best cell in order to optimize the network performance.

In the uplink direction, Cho *et al.* [70] considered a power control scheme designed for interference management in a time-division duplex (TDD) setting where the individ-

ual users tune their transmission power to keep a preset interference threshold to other BSs. Consequently, each BS schedules the users having the best normalized channel gains according to the corresponding transmission power. Wang *et al.* surveyed the backhauling solutions for 5G small cells from the perspective of radio resource management [71]. They discussed the relation between the emergent backhauling solutions and some radio resource management (RRM)issues including, but not limited to, cell association, interference management, scheduling, and inter-cell coordination. In [42], Ge *et al.* studied the throughput and energy efficiency of 5G wireless backhaul networks. Specifically, they adopted two traffic models, namely centralized backhauling model and distributed backhauling model. In the centralized model, a given macrocell aggregates the traffic of the small cells in its coverage area assuming an ideal backhaul link between the macrocell and each small cell. This assumption is rather ideal in UDN environments since the large number of small cells in the coverage area of a macrocell makes it almost impossible to provide the small cell tier with ideal backhaul links. In the distributed model, a small cell which is connected to the core network via fiber-to-the-cell (FTTC) link collects the traffic of the small cells in its vicinity through mmWaves communication links.

The wireless backhauling, although non-ideal, emerged as a viable solution for the backhauling in dense small cell networks. Amin *et al.* [43] studied the performance of self-backhauled small cells. In their model, a Long Term Evolution (LTE)macrocell backhauls High Speed Packet Access (HSPA)small cells. A massive MIMO backhauling solutions were investigated in [40, 41]. Also Chen *et al.* [39] proposed a hierarchical network model to investigate the backhauling in small cell networks, where they considered both wired and wireless backhaul. They derived analytical expressions for the backhaul delay and the average delay seen by a typical user considering two scenarios, namely, static (i.e., no mobility case), and extreme mobility case. Björnson et al., by the aid of a stochastic geometry model, studied the energy efficient deployment of dense small cell networks [72, 73]. In their work, they considered the uplink of a multi-cell multi-user MIMO network. The closed-form expressions obtained via solving the energy efficiency maximization problems shed lights on the role of all the considered parameters and optimization variables. In a different setting, Li *et al.* [74] modelled the downlink of a dense multi-transmission antennae small cell network to quantify the performance in terms of ASE and energy efficiency. A tractable expression for the outage probability is derived via stochastic geometry ap-

proach and then exploited in the computation of the ASE and the energy efficiency. In this, Liu *et al.* assessed the effect of deploying more BSs and more transmit antennas per BS on the aforementioned performance metrics. Moreover, the optimal BS density and the optimal number of antennas per BS to optimize the energy efficiency is computed.

A comparison between three network densification scenarios is conducted by Yunas *et al.* [75]. These scenarios are the densification of the outdoor macrocell tier, the densification of the indoor femtocell tier, and the densification of DASs. The results of the study confirmed that the resources efficiency in terms of spectrum and energy is much higher in the second and third densification strategies, compared to the first scenario. Consequently, the rule of thumb in network densification is to densify the small cells, not the macrocells. Moreover, they found out that the densification of indoor femtocells not only improves the indoor network capacity, but also improves the outdoor network capacity in case of open access mode (i.e., the indoor femtocells are open to serve outdoor users in their vicinity). Finally, the results obtained verified the efficacy of the dense deployment of dynamic DAS in terms of resource efficiency. Another stochastic geometry analytical study considered the performance of UDN in terms of energy efficiency along with cell average spectral efficiency and area throughput [76]. Ren *et al.* [76] concluded that the three performance indicators cannot be optimized simultaneously, and a tradeoff is unavoidable to meet the required network performance. Using game-theoretic approach, Samarakoon *et al.* [77, 78] investigated a joint power control and user scheduling in dense scenario to optimize the energy efficiency. They formulated a dynamic stochastic game and analyzed the mean-field equilibrium. In another venue, Yang [79] studied three important performance metrics in a dense network setting: spectrum, energy, and cost efficiencies. The author formulated a Nash-product form of the corresponding utility function, and analyzed the tradeoff equilibrium amongst the considered metrics

The fast discovery of small cells in dense networks is another emerging research direction. Due to the large number of small cells in the vicinity of a user, there is a need for optimized cell discovery mechanisms. Many features in UDN, such as idle mode capabilities [33], CoMP [80], load balancing [81], and enhanced Inter-cell Interference Cancellation (eICIC) [30], require fast and efficient discovery of small cells. In that direction, Prasad *et al.* [82] evaluated disparate cell discovery mechanisms especially designed for energy-efficient detection of small cells. A graph coloring based scheme for small cell discovery

is proposed and evaluated by Shuai *et al.* [83]. In this scheme, the small cells in the same vicinity are clustered into disjoint groups and each cluster takes a turn to transmit the synchronization sequence. Only minimal changes to the conventional synchronization scheme are required, and thus guaranteeing backward compatibility. The scheme improves the detection probability of small cells.

The dense deployment of indoor and outdoor small cells requires the provisioning of a new spectrum to alleviate the interference. The spectrum sharing thus stems as a viable solution. In spectrum sharing, the UDN cells are allocated a spectrum as secondary users in a cognitive network regime. Another alternative, is the inter-network spectrum sharing where the spectrum is shared amongst multiple operators [84]. Another key aspect is the multiple access and resource management in dense small cells. In spite of the small probability of having multiple users in the coverage area of a small cell in a dense network, still there would be a chance that many users are served by a small cell in a given hotspot. The authors in [85] studied the spectrum sharing for UDN in the radar bands. They modelled a primary/secondary spectrum sharing scenario, where the primary system is the radar system and the secondary system is the dense small cell network. They developed deployment regulations, namely, area power regulation and deployment location regulation, and studied its effectiveness in different environments. Different from the former cognitive radio regime, Teng *et al.* [86] considered the inter-network spectrum sharing, in particular the co-primary spectrum sharing. In co-primary spectrum sharing, two or more operators pool their licenses to achieve flexible spectrum sharing amongst their network nodes which is co-located but with only relative displacement. Stefanatos and Alexiou [22] studied the effect of multiple access and the density of BSs on the performance of a dense network scenario. They also derived a lower bound for the optimal number of bandwidth partitions and a closed-form upper bound for the BS density to guarantee an asymptotically small rate outage probability.

In terms of resources management, Jafari *et al.* [87] studied the performance of different scheduling techniques. In particular, they compared the performance of proportional fair (PF) scheduler and round robin (RR) scheduler. The key aspect of their model is to consider the LOS transmission which is more probable in dense networks. Furthermore, Chen *et al.* [88] investigated a distributed spectrum resource allocation and proposed a learning algorithm. The algorithm is proven to converge to Nash equilibrium

and the performance results asserts that co-tier and cross-tier interference is mitigated. The throughput performance of the proposed system model is investigated and potential performance improvements verified by simulations. The propagation modelling is a vital part of the investigation of wireless communication problems. Since the network densification brings the access point closer to the users, the LOS transmission components become most probable. Hence, the study of dense networks requires a different propagation model where the LOS transmission is considered. Also, in dense indoor networks, the cells are deployed in buildings with many floors, thus a three-dimensional propagation environment should be considered. This suggests two major modifications to the traditional propagation modelling in macrocellular networks; the consideration of dual-slope or multi-slope path loss model while the path loss exponent becomes a function of the distance to the user, and employing Rician fading channel instead of the simple Rayleigh fading model [87].

In [54], the asymptotic average downlink in a UDN scenario is computed in a closed-form, however, a Rayleigh fading is considered in a single association scenario. We noted that the results in [54] cannot be extended to consider either general fading channels or the multiple association scenario. In [55], the spectral efficiency (SE) is evaluated in closed-form for single association and a Rayleigh fading channel in UDNs. Closed-form bounds for average downlink rate are provided in [89] in a single connectivity model considering Rayleigh fading channel. Although, the analytical results are in closed-form, extending the results for multiple association and general fading channels is not straightforward. In [90], simple integrals and closed-form approximations are presented for the average downlink rate in mmWaves cellular network assuming noise-limited scenario, however, less tractable results are reported for interference-limited case. Moreover, in [90] the small-scale fading and single connectivity are considered. Also, the average downlink rate in [91] considers Rayleigh fading and single connectivity. In [2], the SEPL model is considered to evaluate the performance of a dense cellular network. However, it is assumed that all BSs are turned on and each cell has exactly one active user. This implies a very high number of active users at very high BSs densities, which would not capture the reality of cellular networks where the number of active users in real traffic scenarios is typically bounded by 600 users/km^2 [61]. We differently assume that a given user connects to the nearest BS and if there exist a BS with no connected users, it is turned off to mitigate

its interference. Based on these assumptions, we draw different conclusions which better reflect the performance of network densification. In [54] a closed-form is provided for the asymptotic average downlink rate in a UDN scenario, however, a standard decaying path loss model $r^{-\alpha}$ is used, where r is the link distance and α is the path loss exponent. A multi-slope path loss model is investigated in [92] where an activity probability of one is assumed.

The concept of "data-showers" [32] refers to the future possibility for a user to connect to multiple BSs. This stems from the capacity problem that is facing operators now. The fast pace of introducing new data-hungry services and applications changes the picture of wireless networks where there are too many users requiring immense amounts of traffic. To this end, Dual Connectivity (DC) is an emerging association scheme which is under investigation in the LTE standard [93]. In DC association, the user connects to a primary macro cell and a set of secondary small cells. This ensures robustness of the mobility management of the users since they connect to two cell tiers. The main advantage of this connectivity scheme is the splitting of users traffic amongst a set of small cells to satisfy the high demand of the users.

In [94], we introduced a multiple association scenario where a typical user connects to the nearest M cells in its neighborhood to form what we call a *multicell*. In [54], the asymptotic average downlink in a UDN scenario is computed in a closed-form, however, a Rayleigh fading is considered in a single association scenario. We noted that the results in [54] cannot be extended to consider either general fading channels or the multiple association scenario. In [55], the spectral efficiency (SE) is evaluated in closed-form for single association and a Rayleigh fading channel in UDNs. Closed-form bounds for average downlink rate are provided in [89] in a single connectivity model considering Rayleigh fading channel. Although, the analytical results are in closed-form, extending the results for multiple association and general fading channels is not straightforward. In [90], simple integrals and closed-form approximations are presented for the average downlink rate in mmWaves cellular network assuming noise-limited scenario, however, less tractable results are reported for interference-limited case. Moreover, in [90] the small-scale fading and single connectivity are considered. Also, the average downlink rate in [91] considers Rayleigh fading and single connectivity.

In [2], the SEPL model is considered to evaluate the performance of a dense cellular

network. However, it is assumed that all BSs are turned on and each cell has exactly one active user. This implies a very high number of active users at very high BSs densities, which would not capture the reality of cellular networks where the number of active users in real traffic scenarios is typically bounded by 600 users/km^2 [61]. In [54] a closed-form is provided for the asymptotic average downlink rate in a UDN scenario, however, a standard decaying path loss model $r^{-\alpha}$ is used, where r is the link distance and α is the path loss exponent. A multi-slope path loss model is investigated in [92] where an activity probability of one is assumed.

In [95], the secrecy throughput along with secrecy probability are investigated considering a heterogeneous network (HetNet). The secrecy outage probability is studied in a multiple radio access technology (multi-RAT) scenario in [96]. In [97], the secrecy rate in a multi-tier HetNet is investigated considering generalized fading model; however, the significant role of the relative density of the users with respect to the small cells' density is not considered. A dense network environment was assumed in [98] to validate the approximation of the secrecy outage probability. However, the key features of dense networks, such as the users' relative density, the high probability of idle BSs and the high probability of Line-of-Sight (LOS) transmission [58], were not considered. Furthermore, the analytical approximations provided in [8] are shown to be loose as the BSs density gets high, contradicting one of the main aspects of dense networks.

Recently, some researchers investigated the uplink coverage in MTC scenarios (e.g., [99–102]). However, UDN characteristics (e.g., high density of small cells, short distance links, accurate path loss modeling, and general fading channels) have not been considered. Moreover, the power control of the uplink transmission from MTC devices is overlooked. In [99], the coverage performance of randomly distributed data collectors, which collect data of wireless sensors in a single-hop scenario, was investigated, and answers to the required number of data collectors, the required transmit power of the sensors, and the impact of the propagation environment were provided. However, a simple path loss model was considered and power control was not included in the system model. In [100], uplink coverage performance was addressed in a multi-hop aggregation scenario where power control was considered but not the features of UDN. Also, a simple power decay path loss was used for the sake of tractability. The power decay path loss model was adopted also in [103] which cannot fit precisely the short-range communication scenario of a UDN

serving a massive MTC deployment. A Device-to-Device MTC scenario was modeled in [101] where the transmitted packets of the sensors are relayed using D2D to the serving cell. The authors in [101] adopted a power control mechanism, however, the densification of the BSs was not considered. In addition, effective capacity was investigated in ultra-reliable MTC scenario where an optimal power allocation scheme was devised for high SNR regime [102]. The authors considered a simple point-to-point scenario where neither the impact of the interference in a dense network nor the influence of power control was included in the analysis. In [2], SEPL model was adopted in the downlink of a dense network. Nevertheless, a single user per cell is considered and the uplink coverage is not investigated.

2.8 Theory and Techniques

2.8.1 Stochastic Geometry

Topological randomness is a characteristic feature of small cells (e.g., femto cells) as a consequence of their independent and unplanned deployment. Thus, stochastic geometry emerged as a handy tool that suits the modelling of such networks [104]. The stochastic modelling of the spatial distribution of small cells has achieved significant results in the literature (e.g., see [104–106]). In the literature of traditional networks and heterogeneous networks (HetNets), there are many results have been reported using stochastic geometry [107–109]. Moreover, the application of stochastic geometry is expected to meet substantial success in dense environments (e.g., see [58] and the references therein).

Locations of small cells can be modeled in two- or three-dimensional Euclidean space, which is termed as a point process (PP). A PP is a a set of random points existing in some space which abstract the locations of wireless nodes such as small cells and user equipment [105]. The Poisson point process (PPP) is one of the most tractable point processes. In PPP, the number of BSs in a given area A in two-dimensional space or in a given volume V in three-dimensional space has a Poisson distribution with mean $\lambda_s A$ or $\lambda_s V$, respectively. The parameter λ_s represents the density of the BSs per unit area or unit volume. The proprieties of a PPP that model a wireless network can be computed for a reference point which is termed as "typical user". The concept of a typical user in stochastic geometry refers to a user residing at the origin and represents any randomly

picked user. This allows Palm analysis by the aid of Slivnyak's theorem [106]. Most of the properties of a wireless network can be expressed as a function of the distance between the network nodes and the typical user. Hence, the distance from the typical user to the nth nearest BS is of a special importance in stochastic modelling of wireless networks.

The close proximity of access nodes in a dense network requires researchers to propose and investigate a class of distributed clustering techniques to exploit the cooperation of cells in the cluster. The of such structures requires more advanced techniques from stochastic geometry. Besides Poisson point process (PPP), there exist many other point processes that match different applications. Binomial point process (BPP), Hard core point process (HCPP), and Poisson cluster process (PCP) are a few examples of the stochastic geometry toolbox [105]

2.8.2 Performance Metrics

In this section, we explain the set of commonly used performance metrics in the modelling of UDN problems. These metrics are basically related to either the signal to interference-plus-noise ratio (SINR)(e.g., coverage (success) probability and outage probability) or the rate (e.g., rate coverage, average spectral efficiency, and ASE).

1. **Coverage/Success Probability and Outage Probability/SINR Distribution:** The coverage probability is defined as the probability that the SINR of a randomly selected user is above a certain threshold. In other words, the link quality is good enough to proceed to a successful connection. The coverage probability is also termed as the success probability. On the other hand, the outage probability or the SINR distribution is the probability that the SINR of an arbitrary user falls below a minimum threshold. A given user is considered in outage if the SINR of the link to the serving BS is not enough for a successful connection. The coverage probability, the success probability, the outage probability, and the SINR distribution quantify the quality of the link between the user and the serving BS.

2. **Rate Coverage and Rate Outage:** In small cell networks, a better coverage performance metric is the rate coverage, which is defined as the probability that the achievable rate of an arbitrary user is above a certain minimum. Conversely, the rate outage is the probability that the achievable rate of an arbitrary user falls below

a certain threshold. It is known that the rate distribution and SINR distribution are strongly correlated in macrocell homogeneous networks [32]. Conversely, this is not the case in HetNets and then as well in UDN. In small cell networks, not only the SINR determines the achievable rate, but also the backhaul capabilities and the load of individual cells.

3. **Average Spectral Efficiency:** The average number of transmitted bits per secondper unit bandwidth represents the efficiency of the spectrum. The efficiency of the spectrum is a crucial performance metric in 5G networks due to the scarcity of spectrum along with the high data rate requirements [110]. Also, the cell spectral efficiency is another form of this metric to measure the performance of a single cell.

4. **Area Spectral Efficiency:** Densification of cellular networks increases the reuse of spectrum per unit area. Thus, the ASE is an important metric to quantify the performance of UDN. ASE is defined as the average achievable data rate per unit bandwidth per unit area [111].

5. **Network Throughput:** The network throughput is another metric to quantify the performance of UDN and is defined as the average number of successfully transmitted bits per sec. per Hz. per unit area [74]. This metric considers the success probability in the evaluation of the ASE of a given network with a certain BS density and is defined as

$$R_n = \lambda_s p_a (1 - p_{out}) R_o, \tag{2.1}$$

0 where λ_s is the BSs density, p_a is the probability of active BSs, p_{out} is the outage probability, and $R_o \triangleq \log_2(1 + \hat{\gamma})$ is the link capacity with a signal-to-interference ratio (SINR) threshold $\hat{\gamma}$.

6. **Energy Efficiency:** The ratio of the network throughput or the ASE to the power consumption per unit area is defined as the energy efficiency [73, 74]. The energy efficiency metric is a performance indicator that measures the benefit-cost ratio by comparing the achievable rate to the energy costs to achieve this rate [73].

7. **Fairness:** A crucial performance indicator to the evaluation of a given cell association, scheduling, or resource management scheme is the fairness between different

users. The fairness index measures how likely a given resource allocation scheme is fair. Jain's fairness index [112] is a widely-adopted index that computes the fairness of a set of user rates or resource allocations [62] and is given by

$$\mathcal{J}(r_1, \cdots, r_N) \triangleq \frac{(\sum_{n=1}^{N} r_n)^2}{N \sum_{n=1}^{N} r_n^2}, \tag{2.2}$$

where N is the number of users, and r_n is the rate of the n-th user.

It is however important to note that the context of dense networks to a large extent is different from traditional networks. Thus, the need for other metrics to quantify the performance of UDN is a significant requirement. Andrews *et al.* [110] introduced a new metric, the BS densification gain ρ, which is defined as the ratio between the ratio of the rates corresponding to two different BS densities and the ratio of the corresponding BS densities, i.e.,

$$\rho = \frac{R_2/R_1}{\lambda_2/\lambda_1} = \frac{R_2\lambda_1}{R_1\lambda_2}, \tag{2.3}$$

where R_1 is the rate corresponding to a BS density of λ_1, while R_2 is the rate if the density is increased to λ_2. In other words, this measure quantifies the payoff ratio in terms of rate relative to the cost ratio in terms of BS density.

3. Multiple Association in UDNs

3.1 Introduction

Ultra-Dense Network (UDN) is one of the preeminent technologies in the racetrack towards fulfilling the requirements of next generation mobile networks [58]. Dense networks are featured by the deployment of abundant of small cells in hotspots where immense traffic is generated. Small cells will thus be of a density that may exceed the density of the active users [113]. On one hand, increasing small cells density improves the signal quality and the reuse of the spectrum per unit area. On the other hand, providing an economical backhaul connectivity for this large number of cells per unit area emerges as a severe problem [39]. In this context, wireless backhauling is considered to address the backhaul challenges of 5G networks [114].

The capacity of the backhauling solutions in dense networks imposes a limit on the capacity of the small cells. In other words, the radio interface capacity of the small cells might be bottlenecked by the capacity of the backhauling solution whether wired or wireless [21]. Thus, the association of a user to a single base station (BS) restricts the maximum achievable rate by this user to the capacity of the backhaul link. Moreover, the delay in the backhauling link can significantly decline the latency performance of the connected users.

Throughout this chapter, the term multiple association is used to refer to the scenario where a user connects to multiple BSs. Typically, the number of BSs exceeds the number of active mobile stations in ultra-dense networks, and in this case one can expect an operating point where each user equipment (UE) is associated to one cell [21]. However, considering the fast pace of introducing new services and technologies that are data-hungry, further expectations rather consider the association of a user to many BSs in its neighborhood. This would provide the user with cloud-like "data-showers" connections of *Gbps* rates [32].

Furthermore, this dramatic increase in link capacities to end users significantly improves the user experience and make science-fiction communication services like hologram videos become real [115].

In multiple association, a UE connects to many BSs in its vicinity [116] to form a *multicell* [94]. This comes with the price of sophisticated UE which must be equipped with many RF chains. However, in dense networks, the close proximity of the user to the serving BSs relaxes the requirements on these RF circuits [117]. In LTE-Advanced Release 10 and beyond, the 3GPP introduced carrier aggregation (CA) technology with the intention to hit or even exceed the target of 1 Gbps/UE peak data rate [118]. CA is the support of transmission over wide frequency bandwidths by using multiple available component carriers. Two different types of CA are introduced, contiguous CA and non-contiguous CA . In the contiguous CA, the available component carriers (CCs) are adjacent to each other, which is apparently difficult in the current state of spectrum allocation in mobile spectrum bands. On the other hand, the non-contiguous CA provides a practical alternative in which the available CCs do not need to be adjacent. In this case, the deployment of multiple RF receiving units is unavoidable [118]. Therefore, the multiple association requirement of many RF chains would not be a limiting factor.

In order to further boost user peak data rates, the 3GPP considered a radical increase in the spectrum resources available to the network nodes and UE. To this end, massive CA (MCA) or enhanced CA (eCA) is introduced allowing up to 32 component carriers for a UE in LTE-A Release 13 compared to only 5 CCs in Releases 10-12. Consequently, the supported peak downlink data rate is increased to about 25 Gbps [119]. Continuing in this way forward, more advanced techniques and technologies are introduced in Release 14 and beyond to support advanced CA (ACA) and multi-carrier UDN (MC-UDN) where many clusters of small cells get much closer to each other forming a continuously dense areas [119].

The introduction of these radically different techniques motivates a distinct view of user association in dense networks. This view considers a user-centric association paradigm where the user is the central point in any considered association scheme. Evidently, this results in unprecedented mobile network environment where there are no more *edge users* experiencing weak channels and low service grades. On the contrary, the user will be always in the center of any cell in the considered association scheme as depicted in

Figures 3.1 and 3.2. In a continuously dense network, this user-centric association takes place in order to improve the user experience, which would be the dominant factor in the network operation of future networks [120]. To conclude, those advancements encourage and motivate the concept of multiple association of a UE to a cluster of small cells.

3.2 State-of-the-Art

The concept of "data-showers" [32] refers to the future possibility for a user to connect to multiple BSs. This stems from the capacity problem that is facing operators now. The fast pace of introducing new data-hungry services and applications changes the picture of wireless networks where there are too many users requiring immense amounts of traffic. To this end, Dual Connectivity (DC) is an emerging association scheme which is under investigation in the LTE standard [93]. In DC association, the user connects to a primary macro cell and a set of secondary small cells. This ensures robustness of the mobility management of the users since they connect to two cell tiers. The main advantage of this connectivity scheme is the splitting of users traffic amongst a set of small cells to satisfy the high demand of the users.

In [94], we introduced a multiple association scenario where a typical user connects to the nearest M cells in its neighborhood to form what we call a *multicell*. In [54], the asymptotic average downlink in a UDN scenario is computed in a closed-form, however, a Rayleigh fading is considered in a single association scenario. We noted that the results in [54] cannot be extended to consider either general fading channels or the multiple association scenario. In [55], the spectral efficiency (SE) is evaluated in closed-form for single association and a Rayleigh fading channel in UDNs. Closed-form bounds for average downlink rate are provided in [89] in a single connectivity model considering Rayleigh fading channel. Although, the analytical results are in closed-form, extending the results for multiple association and general fading channels is not straightforward. In [90], simple integrals and closed-form approximations are presented for the average downlink rate in mmWaves cellular network assuming noise-limited scenario, however, less tractable results are reported for interference-limited case. Moreover, in [90] the small-scale fading and single connectivity are considered. Also, the average downlink rate in [91] considers Rayleigh fading and single connectivity.

3.3 Contributions

Different from previous works (e.g., see [1,22,24,54,55,89–91,121]), in this investigation, we consider the modeling of multiple association in dense network environment where the BSs are equipped with idle mode capabilities. We evaluate the performance of the proposed association scheme considering general fading channel distributions. To this end, the MGF-based approach is exploited to develop a tractable framework for the computation of the average downlink rate. To highlight the contributions of this investigation, a simple and accurate framework is developed to compute the average downlink rate of the links connecting the typical user to the tagged BSs in a multiple association context. The framework considers general *multicell* size M, and general fading channel distributions in both the signal and interference links. Moreover, we develop a recursive form to provide a simpler way for the computation of the average downlink considering Rayleigh fading channels. The recursion is easy to manipulate and avoids the tedious work required for the computation of folded integrals involved in averaging out the downlink rate over the distance distributions and channel fading distributions.

3.4 System Model

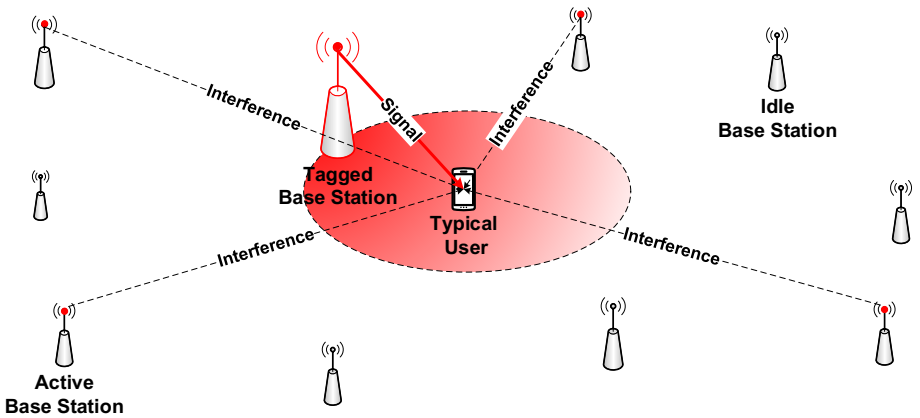

Figure 3.1: The typical user at the origin is associated to the tagged (serving) BS that provides the maximum long-term averaged received power. In UDN environments, the tagged BS would be at a close proximity to the typical user with a high probability of Line-of-Sight (LOS) transmission in the useful signal link. Only active cells contribute to the aggregate interference seen by the typical user in the interference signal.

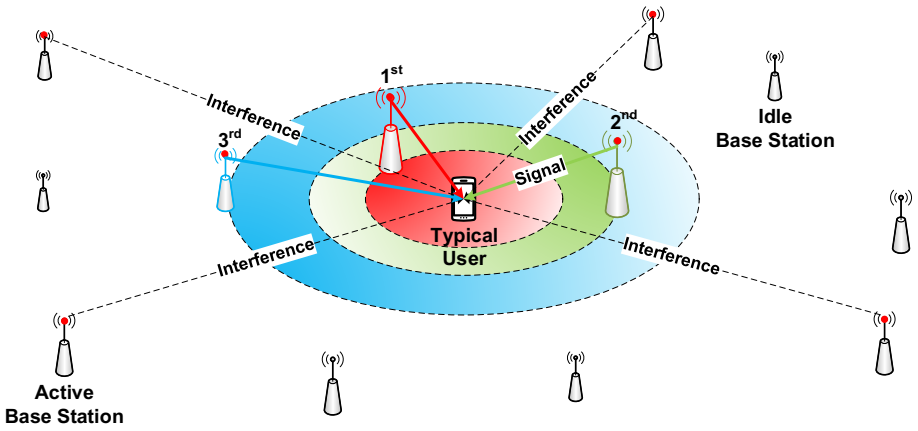

Figure 3.2: In multiple association, the typical user connects to the set of the M-th nearest BSs according to the maximum long-term averaged received power from the BSs in its neighborhood.

We consider the downlink of a UDN comprised of a single tier of small cells. UDNs are characterized by the high density of small cells relative to the density of active users [58]. We employ techniques from stochastic geometry [105, 106, 109, 122] to lay out a general mathematical framework for the evaluation of the network performance. Throughout our study, we consider the characterization of the network performance in the context of multiple association of a user to many BSs.

3.4.1 Network Model

We consider a single tier of small cells modeled as an independent homogenous PPP Φ_s with density λ_s on two-dimensional plane. A realization of BSs locations is drawn from Φ_s as $\{b_1, b_2, \ldots\}$ where b_i is the location of the i-th BS. The users form another independent homogenous PPP positions $\Phi_u = \{u_1, u_2, \ldots\}$ with a density λ_u where u_j is the location of the j-th user. In general, we assume that $\lambda_s \gg \lambda_u$ which implies that many BSs are in idle mode by virtue of the lack of connected users [21]. BSs in the idle mode are turned off to fully mitigate their interference. Without loss of generality, we elaborate in the analysis of this investigation considering a typical mobile user U_o located at the origin [105]. A typical user in stochastic geometry refers to a user residing at the origin where the properties of the point process (PP) can be computed. To explain, the typical user is assumed to be a representative to all users. Also, each BS transmits with a power P_s and operates in open access mode [28]. Consequently, the typical user is allowed to connect to any BS in the network without any access restrictions as imposed by the Closed Subscriber Group (CSG) mode.

3.4.2 Spectrum Allocation Model

We consider that M orthogonal component carriers each of bandwidth B Hz are available in the system. Each BS of the M BSs comprising the *multicell* is allocated a single component carrier, i.e. no carrier aggregation is implemented in the small cells. Moreover, we assume that the capacity of the small cell is mainly limited by its backhaul link capacity, hence, suitable component carrier bandwidth should be chosen. These orthogonal component carriers carry M simultaneous data streams from the cells of the *multicell* to the user in the downlink. Thus, the aggregate downlink rate of any user is no longer directly limited by the backhaul capacity of any of the cells in the *multicell*. In fact, the aggregate rate is mainly limited by the size of the *multicell* M, and this in turn is limited by the complexity constraints of the user equipment.

We also assume that the bandwidth allocation of the small cells in a *multicell* is managed by the macrocell covering the area where these small cells are deployed. This is known in the literature and LTE Release 12 as "dual connectivity" [93] where the user can connect to a macrocell (primary cell) for coverage and mobility and connects to one or more small cells (secondary cells) for capacity enhancement. In this way, the macrocell provides the signaling and control required to manage the association of the user to the cells of the *multicell* and the bandwidth allocation as well. In addition, we assume that a BS serves only one user on a single component carrier and if another user attempts to connect to an active cell the admission control rejects the connection and this user can connect to other nearby small cells.

3.4.3 Propagation Model

To maintain the generic structure of the proposed framework, we consider a general propagation environment which is comprised of two components, namely, a large scale fading component and a small scale fading component. On one hand, the large scale fading is modeled by a general decaying power law with a path loss exponent ($\alpha > 2$) [123]. In this model, the received signal power at a distance d from a BS is $P_s d^{-\alpha}$. On the other hand, all small cells are assumed to have multipath fading channels that are independent and identically distributed (i.i.d). The fading channel distribution for the serving BSs g_o is in general different from that of the interfering BSs g_b [1].

3.4.4 Association Model

Two modes of cell association are considered in this study; single association where a given user associates to only one BS, and multiple association where a user can connect to more than one cell in its vicinity. We refer to the BSs connected to the typical user U_o as tagged BSs. Let B_o denote the tagged BS in case of single association and B_k the k-th tagged BS in multiple association where $k \in \{1, 2, \ldots, M\}$. The association criterion in both modes depends on the maximum long-term averaged received power of the received signal at U_o. Accordingly, U_o connects to the BSs that provide the maximum average received power, or in other words the nearest BSs. The distance between U_o and the tagged BS B_k is in general random due to the randomness of the positions of the BSs. This applies to the distance between U_o and the interfering BSs as well. This randomness in the distance requires the use of the distance distribution functions while computing the average performance metrics such as the average ergodic downlink rate.

3.4.5 Problem Statement and Performance Metrics

Having considered the described network, channel, and association models, the signal to interference-plus-noise ratio (SINR)of the downlink from the tagged BS B_k to the typical user U_o is computed as:

$$\texttt{SINR}_k^M = \frac{S(r_k)}{\sigma^2 + I(r_M)}, \tag{3.1}$$

where M is the *multicell* size i.e., the number of BSs connected to the typical user and $k = 1, 2, \cdots, M$. Also, $S(r_k) = P_s g_o r_k^{-\alpha}$ is the signal power of the link between U_o and B_k, σ^2 is the noise power, and $I(r_M) = \sum_{b \in \Phi_a^c / \mathcal{V}_o} P_s g_b r_b^{-\alpha}$ is the aggregate interference power from the set Φ_a^c of all active cells on a given component carrier c, except the set of tagged BSs $\mathcal{V}_o$. An active cell is a cell with one user connected, and the tagged BSs are those BSs belonging to the same *multicell*.

In multiple association, r_k is the distance from the U_o to the k-th tagged BS B_k, while r_M is the distance to the M-th tagged BS in a *multicell* of size M. r_M represents the radius of the exclusion region of the typical user [123]. The exclusion zone refers to a circular area around the typical user where no interfering BSs exist. In other words, all interfering BSs with respect to U_o lie outside a disk of radius r_M. The distances r_k and r_M are random

variables with a probability distribution function $\mathcal{F}_{r_k}(k)$ and $\mathcal{F}_{r_M}(M)$, respectively. The aforementioned distance distribution function can be in general expressed as:

$$\mathcal{F}_{r_n}(n) = \frac{2(\pi\lambda_s)^n}{\Gamma(n)} \; {r_n}^{2n-1} \; e^{-\lambda_s \pi {r_n}^2}, \tag{3.2}$$

where $\Gamma(n) = \int_0^\infty t^n e^{-t} \mathrm{d}t$ is the gamma function, and for integer positive n, $\Gamma(n) = (n-1)!$. In single association, (3.1) is simplified to

$$\mathtt{SINR} = \frac{S(r)}{\sigma^2 + I(r)}, \tag{3.3}$$

where $M = k = 1$ and both are omitted for brevity, and r is the distance between U_o and B_o.

In this investigation, we adopt two performance metrics to evaluate the performance of the considered system model: the average (ergodic) downlink rate of the individual connection(s) from the tagged BSs to U_o, denoted as $\mathcal{R}_k^M$, and the network aggregate average rate (NAAR), denoted as $\mathcal{R}_{naar}$. The rate of the downlink connection between U_o and its tagged BS B_k in a *multicell* of size M is computed as:

$$R_k^M = \ln(1 + \mathtt{SINR}_k^M) \quad \text{nats/sec/Hz}. \tag{3.4}$$

The average rate is then computed by averaging the rate in (3.4) over the fading channels and the distances to serving BSs and interfering BSs. Denote by $\mathcal{G}(\cdot)$ the fixed association average rate which is the rate averaged over the fading channels of the useful and interfering links g_o, g_b, respectively, conditioned on a fixed association distance and it can be expressed as:

$$\mathcal{G}(r_k, r_M) = \mathbb{E}_{g_o, g_b} \left\{ \ln \left(1 + \frac{P_s g_o r_k^{-\alpha}}{\sigma^2 + I(r_M)} \right) \right\}, \tag{3.5}$$

and the overall average downlink rate is then given by

$$\mathcal{R}_k^M = \mathbb{E}_{r_k, r_{k+1}, \ldots, r_M} \left\{ \mathcal{G}(r_k, r_M) \right\}, \tag{3.6}$$

where the expectation is computed with respect to the marginal distribution of the distances $r_k, r_{k+1}, \ldots, r_M$. In single association, the average rate is simplified to

$$\mathcal{R} = \mathbb{E}_r \left\{ \mathcal{G}(r) \right\} \tag{3.7}$$

where

$$\mathcal{G}(r) = \mathbb{E}_{g_o, g_b} \left\{ \ln \left(1 + \frac{P_s g_o r^{-\alpha}}{\sigma^2 + I(r)} \right) \right\}. \tag{3.8}$$

The network aggregate average rate $\mathcal{R}_{naar}$ is the aggregate average downlink rate of all users in a given area normalized by the area and is then can be defined as:

$$\mathcal{R}_{naar} = \lambda_u \sum_{k=1}^{M} B\mathcal{R}_k^M. \tag{3.9}$$

3.5 Analytical Results

3.5.1 Single Association in UDNs

In this section, we study the association of the typical user to the tagged BS in a single association context. Considering general fading channels in both signal and interference links, we exploit the standard MGF approach to compute the average downlink rate. While the analytical result is simple and easily computable using standard mathematical packages (e.g., Matlab), it is also significantly accurate and matches the simulation results as we shall discuss in the simulation results section.

We consider an association policy based on the long-term averaged maximum-received power, where the typical user at the origin associates to the nearest BS as depicted in Figure 3.1. The average rate of the downlink $\mathcal{R}$ is expressed as [122]:

$$\begin{aligned}\mathcal{R} &= \mathbb{E}_r\left\{\mathcal{G}(r)\right\} \\ &= \int_0^\infty 2\lambda_s \pi r^2 e^{-\lambda_s \pi r^2} \mathcal{G}(r) \mathrm{d}r\end{aligned} \tag{3.10}$$

In the following theorem we give an expression for the average rate of the downlink in terms of small cells density, active users density, and signal and interference fading channels. We consider the use of the MGF-based approach [1] for the sake of reduced computational complexity.

Theorem 1. *The average downlink rate of a typical user associated to its nearest base station over general fading channels in both signal and interference links is given by:*

$$\mathcal{R} = \int_0^\infty \frac{1 - \mathcal{M}_o(\gamma y)}{y} \mathcal{Q}(y)\ \mathrm{d}y \tag{3.11}$$

where $\gamma = P_s/\sigma^2$ is the signal-to-noise ratio (SNR), $\mathcal{M}_o(s) = \mathbb{E}(e^{sg_o})$ is the MGF of the

signal fading channel

$$\mathcal{Q}(y) = \frac{1}{\mathcal{W}_I(\gamma y)} - \frac{\alpha y}{\mathcal{W}_I(\gamma y)}\mathcal{A}(y) \tag{3.12}$$

$$\mathcal{A}(y) = \int_0^\infty r^{\alpha-1} e^{-r^\alpha y} e^{-\pi\lambda_s r^2 \mathcal{W}_I(\gamma y)}\, \mathrm{d}r \tag{3.13}$$

$$\mathcal{W}_I(z) = p_o + (1-p_o)\mathcal{Z}_I(z) \tag{3.14}$$

$$\mathcal{Z}_I(z) = \mathcal{M}_I(z) + \mathcal{T}_I(z) \tag{3.15}$$

$$\mathcal{T}_I(z) = \Gamma(1-\tfrac{2}{\alpha}) \sum_{j=0}^{\infty} z^{j+1} \mathcal{M}_I^{(j)}(z) \left[\Gamma(2-\tfrac{2}{\alpha}+j)\right]^{-1} \tag{3.16}$$

$$\mathcal{M}_I^{(j)}(z) = \mathbb{E}\left\{g_b^{j+1} e^{-z g_b}\right\} \tag{3.17}$$

and $\mathcal{M}_I(s) = \mathbb{E}(e^{s g_b})$ *is the MGF of the interference fading channel.*

Proof. Considering the expectation in the fixed association average rate in (3.7), this expectation can be rewritten as:

$$\mathcal{G}(r) = \mathbb{E}\left\{\ln\left(1 + \frac{X}{1+Y}\right)\right\} \tag{3.18}$$

where $X = (P_s g_o r^{-\alpha})/\sigma^2$ and $Y = (I(r))/\sigma^2$, and by using [124, Lemma 1] with $N = M = 1$ we obtain

$$\begin{aligned}\mathcal{G}(r) &= \mathbb{E}\left\{\ln\left(1 + \frac{X}{1+Y}\right)\right\} \\ &= \int_0^\infty \left(\mathcal{M}_Y(z) - \mathcal{M}_{X,Y}(z)\right) \frac{e^{-z}}{z}\, \mathrm{d}z \\ &\overset{(a)}{=} \int_0^\infty \mathcal{M}_Y(z)\left(1 - \mathcal{M}_X(z)\right) \frac{e^{-z}}{z}\, \mathrm{d}z\end{aligned} \tag{3.19}$$

where X and Y are arbitrary non-negative random variables, $\mathcal{M}_X(z)$ and $\mathcal{M}_Y(z)$ are the respective MGF of these random variables, $\mathcal{M}_{X,Y}(z)$ is the MGF of $X+Y$, i.e., $\mathcal{M}_{X,Y}(z) = \mathbb{E}\left\{e^{z(X+Y)}\right\}$, and (a) holds if X and Y are independent.

Now, the expectation in (3.7) can be expressed as:

$$\mathcal{G}(r) = \int_0^\infty \mathcal{M}_I(\gamma z; r)\left(1 - \mathcal{M}_o(\gamma r^{-\alpha} z)\right) \frac{e^{-z}}{z}\, \mathrm{d}z \tag{3.20}$$

where $\gamma = P_s/\sigma^2$ is the SNR, and $\mathcal{M}_o(\cdot)$ is the moment generating function of the useful signal fading channel. $\mathcal{M}_I(.; r)$ is the MGF of the aggregate interference in the downlink, which is generated by all interferes that lie outside a disk of radius r and centered at the

typical user. A closed form expression for $\mathcal{M}_I(.;r)$ is derived in [1, Eq. 36], however in this derivation the aggregate interference is considered as the sum of interference from all BSs except the tagged BS, which is the nearest one to the user.

This is not the case in UDN, where many BSs will be turned off due to inactivity [58]. Here, we consider the interference generated from the active BSs which are using the same component carrier only. According to the investigated system model, a given BS is active if one user is associated to it. The probability of BS activation is $p_a = 1 - p_o$, where p_o is the idle mode probability and is given by [20, 23]:

$$p_o = \left(\frac{3.5\kappa}{1 + 3.5\kappa} \right)^{3.5}. \tag{3.21}$$

where $\kappa \triangleq \lambda_s/\lambda_u$ is the densification ratio of the small cell network.

In fact, the interferers point process is generally not homogenous. This is due to the location dependency of the BS activation probability [54]. However, considering the special features of UDN, this location dependency disappears since the variance in the cell sizes vanishes with the increasing density of the small cells. Using the approximation in [54, Lemma (1)], we can approximate the interferers process to be homogenous PPP. Accordingly, we use the idle mode probability p_o to perform an independent thinning of the small cells point process Φ_s to form the thinned PPP Φ_a. Thus, Φ_a represents the PPP of the active cells, where $\Phi_a \equiv \Phi_a^c$ since all cells are using the same channel c in the case of single association. Since we assume that a small cell in idle mode is turned off to fully mitigate its interference, therefore we account only for the interference generated from the active small cells in the computation of the interference. The interfering small cells which are active and transmit at the same time with the tagged base station of the typical user form a thinned version of the original PPP [106]. This thinned PP has the same distribution of the original one with a density $p_a\lambda_s$. By using [1, Eq. (36)] and considering the thinned PPP Φ_a, $\mathcal{M}_I(.;r)$ is expressed as:

$$\begin{aligned} \mathcal{M}_I(z;r) = &\exp\left\{\pi p_a \lambda_s r^2\right\} \exp\left\{-\pi p_a \lambda_s r^2 \mathcal{M}_I(zr^{-\alpha})\right\} \\ &\times \exp\left\{-\pi p_a \lambda_s r^2 \mathcal{T}_I(zr^{-\alpha})\right\} \end{aligned} \tag{3.22}$$

Now, we substitute (3.22) in (5.10) and then in (3.10). To simplify, we perform a change of variables $y = zr^{-\alpha}$, and apply integration by parts to (3.10) to obtain (3.11), which completes the proof. ■

The result in Theorem (1) generalizes the results in [1, Theorem (1)] considering the realistic impact of high small cells density in UDNs. In particular, the average downlink rate expression in (3.11) is expressed in terms of the function $\mathcal{W}_I(z)$ instead of $\mathcal{Z}_I(z)$. However, one can show that $\mathcal{W}_I(z)$ converges to $\mathcal{Z}_I(z)$ when the idle mode probability p_o is zero, which is the case in traditional cellular networks where the density of the cells are low or moderate with regard to the density of the active users.

In most cases, cellular networks are limited by interference rather than noise and this is the typical scenario especially in UDNs. Thus, the noise becomes very small compared to the aggregate interference, this yields to $\gamma = P_s/\sigma^2 \to \infty$. Considering this remark, Theorem 1 can be simplified to the following corollary:

Corollary 1. *Considering a UDN environment which is limited by interference rather than noise, the average rate of the downlink in* (3.11) *simplifies to*

$$\hat{\mathcal{R}} = \mathcal{R}|_{\gamma\to\infty} = \int_0^\infty \frac{1-\mathcal{M}_o(z)}{z\mathcal{W}_I(z)}\,\mathrm{d}z \tag{3.23}$$

Proof. Manipulating $\mathcal{Q}(y)$ by using the change of variables $z = \gamma y$, and taking the limit as $\gamma \to \infty$, $\mathcal{Q}(\gamma^{-1}z)$ evaluates to $1/\mathcal{W}_I(z)$. Thus completing the proof. ■

It is interesting to note that the results in Theorem 1 and Corollary 1 extend the results in [1] to account for the BS density. In the numerical evaluations section, we discuss the effect of the network densification on the average rate of the downlink.

In this section, we studied the single association in a UDN context as a special case of a more general scenario. In the general scenario, we assume that the typical user can associate to M BSs in its vicinity. We investigate this scenario in the following section to give the general solution parametrized with the *multicell* size M. In this way, the special case of single association can be deduced from the general solution by setting $M = 1$.

3.5.2 Multiple Association in UDNs

3.5.2.1 Average Downlink Rate in the General Case

In this section, we consider the association of the typical user to the nearest M BSs in the vicinity. The association of the typical user to the tagged BSs follows the same criteria as in the single association. However, instead of connecting to the BS providing the maximum average received power, the typical user connects to M BSs providing the

strongest average received power. The average downlink rate $\mathcal{R}_k^M$ in (3.6) of the link from the k-th tagged BS, $k \in \{1, 2, \ldots, M\}$, to the typical user involves averaging the downlink rate over all fading channels and random distances.

The function $\mathcal{G}(r_k, r_M)$ in (3.5) represents the downlink rate averaged over the fading channel distributions g_o, g_b of the serving BS and the interfering BSs, respectively. $S(r_k)$ is the signal power of the connection between the typical user residing at the origin and the kth serving BS in the *multicell*, BS_k. The serving BS is at a random distance r_k from the typical user, and the channel fading distribution of this link is g_k. We consider a general fading distribution in this investigation where all the fading channels of serving BS $1, \cdots, M$ are identical and independent from each other and also independent from the fading distribution of the interfering BSs. For the sake of simplicity, we denote by g_o the fading distribution of the link from U_o to any serving BS in the set of serving BSs $\mathcal{V}_s \subset \Phi_s$. However, the fading distribution of the interfering BSs g_b although independent from g_o but in general they are not identical, i.e., g_b can follow any general distribution.

The interference signal power $I(r_M)$ on a given component carrier considers all the interference links using this component carrier outside the *multicell*. We assume that all the serving BS in a *multicell* are using orthogonal component carriers in order to mitigate the interference. In other words, the interference experienced by the typical user is generated by all the interferers using a certain component carrier that lie outside a disk of radius r_M, and centered at the typical user. This region around the typical user is called the exclusion region [123]. In the scenario of multiple association, we consider the allocation of orthogonal channels to the links from the cells of the *multicell* to a given user. Intuitively, each *multicell* has only one cell that contributes to the interference on a given channel. In other words, a *multicell* appears from the interference point of view as a single interfering cell on one of the available channels. The only difference in this case is that the active BS that contributes to the interference on a given channel is not always the nearest BS to the typical user as in the case of traditional single association, it can be the first, the second, up to the M-th nearest BS. Moreover, it is equally likely to have this active BS at different relative distance from the typical user. Considering the displacement theorem [125, 126], assume that each active user location is displaced randomly and independently to the location of one of the activated BSs in a *multicell*, the interfering BSs process thus forms another homogeneous PPP with a density λ_u. Recall

that the active BSs density $p_a\lambda_s$ converges to the density of the users λ_u at very high BSs density λ_s. Considering the above discussion, we perform independent thinning for the small cells process Φ_s by the probability of active BS $p_a = 1 - p_o$, where p_o is the idle mode probability. The thinned PPP $\Phi_a^c \subset \Phi_s$ is the set of all active BS allocated the same component carrier c in the region outside the exclusion region from r_M to infinity. The density of this thinned process is $\lambda_a = p_a\lambda_s$.

The computation of the average downlink rate involves averaging over the positions of the serving and the interfering small cells. For this reason, we consider the joint distribution function of the distances from the typical user to the cells in the *multicell* denoted as $\mathcal{F}(r_1, \ldots, r_M)$ and is given by [127].

$$\mathcal{F}(r_1, \ldots, r_M) = (2\pi\lambda_s)^M \; r_1 \ldots r_M \; e^{-\lambda_s \pi r_M^2} \tag{3.24}$$

where $0 \leq r_1 \leq r_2 \leq \ldots \leq r_k \leq \ldots \leq r_M \leq \infty$. This can be interpreted as follows. The distance from the typical user to the 1st nearest BS, r_1, is a continuous random variable ranging from 0 to r_2. Subsequently, r_2 is the random distance from the typical user to the 2nd nearest BS and ranges from 0 to r_3. In general, the distance to the kth nearest BS is bounded in the interval $[0, r_{k+1}]$. Moreover, we denote by $\mathcal{F}(r_k, \ldots, r_M)$ the marginal joint distribution function of the distances $r_k, \ldots, r_M$. This can be expressed as:

$$\begin{aligned}
&\mathcal{F}(r_k, \ldots, r_M) = \\
&\int_0^{r_k} \int_0^{r_{k-1}} \cdots \int_0^{r_1} \mathcal{F}(r_1, \ldots, r_M) \mathrm{d}r_1 \ldots \mathrm{d}r_{k-1} \\
&= \frac{(2\pi\lambda_s)^M}{2^{k-1}\Gamma(k)} \; r_k^{2k-1} \ldots r_M \; e^{-\lambda_s \pi r_M^2}
\end{aligned} \tag{3.25}$$

The averaging in (3.6) is carried out over all the distances from the typical user to the serving BSs in the *multicell*. For this purpose, we use the marginal joint probability distribution function $\mathcal{F}(r_k, \ldots, r_M)$. Finally, the probability distribution of the distance to the nth nearest BS can be obtained by integrating successively the joint distribution in (3.24) w.r.t r_1 from 0 to r_2, w.r.t r_2 from 0 to r_3 up to r_{n-1} from 0 to r_n. This yields to [127]:

$$\mathcal{F}_r(n) = \frac{2(\pi\lambda_s)^n}{\Gamma(n)} \; r^{2n-1} \; e^{-\lambda_s \pi r^2} \tag{3.26}$$

In the following theorem, we provide a framework to compute the average downlink rate in (3.6).

Theorem 2. *Assuming general fading channels in both the signal and interference links, the average downlink rate of a typical user associated to its kth nearest BS in a* multicell *of size M where $k = 1, 2, \cdots, M$ is given by*

$$\mathcal{R}_k^M = \frac{(2\pi\lambda_s)^M}{2^{k-1}\Gamma(k)} \int_0^\infty \int_0^\infty r_M \mathcal{I}(r_M) e^{-\lambda_s \pi r_M^2 \mathcal{W}_I(M\gamma y)} \frac{e^{-y r_M^\alpha}}{y} \mathrm{d}r_M \mathrm{d}y \tag{3.27}$$

where:

$$\mathcal{I}(r_k) = 1 - \mathcal{M}_o(\beta r_k^{-\alpha}) \tag{3.28}$$

$$\mathcal{I}(r_{k+1}) = \int_0^{r_{k+1}} r_k^{2k-1} \mathcal{I}(r_k) \mathrm{d}r_k \tag{3.29}$$

$$\mathcal{I}(r_j) = \int_0^{r_j} r_{j-1} \mathcal{I}(r_{j-1}) \mathrm{d}r_{j-1}, \ j \in \{k+2, \ldots, M\} \tag{3.30}$$

Proof. Using [124, Lemma 1], the fixed association average rate $\mathcal{G}(r_k, r_M)$ can be expressed as:

$$\begin{aligned} \mathcal{G}(r_k, r_M) &= \mathbb{E}_{g_o, g_b} \left\{ \ln \left(1 + \frac{S(r_k)}{\sigma_N^2 + I(r_M)} \right) \right\} \\ &= \int_0^\infty \mathcal{M}_I(\gamma z; r_M) \left(1 - \mathcal{M}_o(\gamma r_k^{-\alpha} z) \right) \frac{e^{-z}}{z} \, \mathrm{d}z \end{aligned} \tag{3.31}$$

Considering [123, Eq.(18)] and [1, Eq.(36)], the aggregate interference moment generating function $\mathcal{M}_I(.; r_M)$ can be expressed as:

$$\begin{aligned} \mathcal{M}_I(s; r_M) &= \exp\left\{ \pi p_a \lambda_s r_M^2 \right\} \exp\left\{ -\pi p_a \lambda_s r_M^2 \mathcal{M}_I(s r_M^{-\alpha}) \right\} \exp\left\{ -\pi p_a \lambda_s r_M^2 \mathcal{T}_I(s r_M^{-\alpha}) \right\} \\ &= \exp\left\{ \pi p_a \lambda_s r_M^2 \left(1 - \mathcal{Z}_I(s r_M^{-\alpha}) \right) \right\} \end{aligned} \tag{3.32}$$

Now, we can compute the average downlink rate $\mathcal{R}_k^M$. Substituting (3.32) in (3.31) and then substituting (3.31) along with (3.25) in (3.6)

$$\begin{aligned} \mathcal{R}_k^M &= \int_0^\infty \int_0^{r_M} \cdots \int_0^{r_{k+1}} \mathcal{F}(r_k, \ldots, r_M) \ \mathcal{G}(r_k, r_M) \mathrm{d}r_k \ldots \mathrm{d}r_M \\ &= \frac{(2\pi\lambda_s)^M}{2^{k-1}\Gamma(k)} \int_0^\infty \int_0^{r_M} \cdots \int_0^{r_{k+1}} r_k^{2k-1} \ldots r_M \left(\int_0^\infty e^{\pi p_a \lambda_s r_M^2 \mathcal{W}_I(\gamma z r_M^{-\alpha})} \left(1 - \mathcal{M}_o(\gamma z r_k^{-\alpha}) \right) \frac{e^{-z}}{z} \, \mathrm{d}z \right) \\ &\qquad \mathrm{d}r_k \ldots \mathrm{d}r_M \\ &\overset{(a)}{=} \frac{(2\pi\lambda_s)^M}{2^{k-1}\Gamma(k)} \int_0^\infty \int_0^\infty \int_0^{r_M} \cdots \int_0^{r_{k+1}} r_k^{2k-1} \ldots r_M e^{-\lambda_s \pi r_M^2 \mathcal{W}_I(\gamma y)} \frac{e^{-y r_M^\alpha}}{y} \left(1 - \mathcal{M}_o(\beta r_k^{-\alpha}) \right) \mathrm{d}r_k \ldots \mathrm{d}r_M \mathrm{d}y \end{aligned} \tag{3.33}$$

where $\beta = \gamma y r_M^\alpha$ and $\mathcal{W}_I(z) = p_o + (1 - p_o)\mathcal{Z}_I(z)$. Note that, step (a) follows from changing the order of integration, and by the change of variables $y = z r_M^{-\alpha}$.

To compute the integral in (3.33), we evaluate this folded integral successively w.r.t the distances $(r_k, r_{k+1}, \ldots, r_M)$. Denote by $\mathcal{I}(r_j)$ this successive integration up to the distance r_{j-1}, $j \in \{k+2, \ldots, M\}$. This integral can be expressed as:

$$\mathcal{I}(r_j) = \int_0^{r_j} r_{j-1} \mathcal{I}(r_{j-1}) \mathrm{d}r_{j-1} \tag{3.34}$$

where the seeds of the above recursive integral are $\mathcal{I}(r_k)$ and $\mathcal{I}(r_{k+1})$ and are expressed as

$$\mathcal{I}(r_k) = 1 - \mathcal{M}_o(\beta r_k^{-\alpha}) \tag{3.35}$$

$$\mathcal{I}(r_{k+1}) = \int_0^{r_{k+1}} r_k^{2k-1} \left(1 - \mathcal{M}_o(\beta r_k^{-\alpha})\right) \mathrm{d}r_k \tag{3.36}$$

The average downlink rate in (3.6) is then simplified to:

$$\mathcal{R}_k^M = \tfrac{(2\pi\lambda_s)^M}{2^{k-1}\Gamma(k)} \int_0^\infty \int_0^\infty r_M \mathcal{I}(r_M) e^{-\lambda_s \pi r_M^2 \mathcal{W}_I(\gamma y)} \frac{e^{-y r_M^\alpha}}{y} \mathrm{d}r_M \mathrm{d}y. \tag{3.37}$$

This completes the proof. ■

The mathematical framework in Theorem 2 considers general channel fading distributions. Consequently, the average downlink rate $\mathcal{R}_k^M$ can be computed for general signal and interference fading channels. Therefore, one can employ a fading channel for the useful link that is suitable for dense network environments, where the serving BSs would be at very close distances to the active users. In the propagation environments where Rayleigh fading channel would be considered in dense network (e.g., indoor coverage), a simpler form of the solution can be derived. In the following theorem we consider a Rayleigh channel fading distribution in the useful link which yields to a more tractable solution.

Theorem 3. *Assuming a Rayleigh fading channel in the signal link, the average rate of the downlink of a typical user associated to its kth nearest BS in a* multicell *of size M where $k = 1, 2, \cdots, M$ is given by*

$$\mathcal{R}_k^M = \int_0^\infty \frac{G_k^M(\gamma y)\mathcal{P}(y)}{y} \, \mathrm{d}y \tag{3.38}$$

where:

$$\mathcal{P}(y) = \frac{1}{[\mathcal{W}_I(\gamma y)]^M} - \frac{\alpha y}{\mathcal{W}_I(\gamma y)} \mathcal{H}(y) \tag{3.39}$$

$$\mathcal{H}(y) = \int_0^\infty r_M^{\alpha-1} e^{-r_M^\alpha y} e^{-\pi\lambda_s r_M^2 \mathcal{W}_I(\gamma y)} \sum_{n=0}^{M-1} \frac{[\pi\lambda_s r_M^2 \mathcal{W}_I(\gamma y)]^n}{n!} \, \mathrm{d}r_M \tag{3.40}$$

Proof. Let the useful link experiences a Rayleigh fading, the MGF of the fading channel is then $\mathcal{M}_o = (1+z)^{-1}$ [128, Table 2.2]. We begin using the mathematical framework of Theorem (2) by computing the integral $\mathcal{I}(r_{k+1})$

$$\begin{aligned}\mathcal{I}(r_{k+1}) &= \int_0^{r_{k+1}} r_k^{2k-1}\left(1-\mathcal{M}_o(\beta r_k^{-\alpha})\right)\mathrm{d}r_k. \\ &\overset{(a)}{=} \frac{1}{2k} r_{k+1}^{2k}\, {}_2F_1\left(1, \frac{2k}{\alpha}; \frac{2k}{\alpha}+1; -\frac{r_{k+1}^{\alpha}}{\beta}\right)\end{aligned} \tag{3.41}$$

where ${}_2F_1(\cdot,\cdot,\cdot,\cdot)$ is the Gauss hypergeometric function [129, Ch. (15)]. Step (a) follows from simple manipulation and evaluating the integral.

We proceed by evaluating the next integral in the folded integrals

$$\begin{aligned}\mathcal{I}(r_{k+2}) &= \int_0^{r_{k+2}} r_{k+1}\mathcal{I}(r_{k+1})\mathrm{d}r_{k+1} \\ &= \tfrac{1}{2k}\int_0^{r_{k+2}} r_{k+1}^{2(k+1)-1}\Upsilon(r_{k+1},2k)\mathrm{d}r_{k+1} \\ &= (\tfrac{1}{2})^2\left(\tfrac{1}{(k+1)k}\right) r_{k+2}^{2(k+1)}\left((k+1)\Upsilon(r_{k+2},2k) - k\Upsilon(r_{k+2},2(k+1))\right) \\ &= (\tfrac{1}{2})^2\left(\tfrac{1}{(k+1)k}\right) r_{k+2}^{2(k+1)}\Upsilon^{(1)}(r_{k+2},k)\end{aligned} \tag{3.42}$$

where

$$\Upsilon(r,n) = {}_2F_1\left(1, \tfrac{n}{\alpha}; \tfrac{n}{\alpha}+1; -\tfrac{r^{\alpha}}{\beta}\right) \tag{3.43}$$

$$\Upsilon^{(1)}(r,k) = (k+1)\Upsilon(r,2k) - k\Upsilon(r,2(k+1)) \tag{3.44}$$

We notice that the parametrized Gauss hypergeometric function $\Upsilon(\cdot,n)$ appears with different values for the parameter n in the integral w.r.t the next distance. To show this, we evaluate the next integral

$$\begin{aligned}\mathcal{I}(r_{k+3}) &= \int_0^{r_{k+3}} r_{k+2}\mathcal{I}(r_{k+2})\mathrm{d}r_{k+2} \\ &= (\tfrac{1}{2})^2\left(\tfrac{1}{(k+1)k}\right)\int_0^{r_{k+3}} r_{k+2}^{2(k+2)-1}\Upsilon^{(1)}(r_{k+2},k)\mathrm{d}r_{k+2} \\ &= (\tfrac{1}{2})^3\left(\tfrac{1}{(k+2)(k+1)k}\right) r_{k+3}^{2(k+2)}\left(\tfrac{1}{2}(k+2)\Upsilon^{(1)}(r_{k+3},k) - \tfrac{1}{2}k\Upsilon^{(1)}(r_{k+3},k+1)\right) \\ &= (\tfrac{1}{2})^3\left(\tfrac{1}{(k+2)(k+1)k}\right) r_{k+3}^{2(k+2)}\Upsilon^{(2)}(r_{k+3},k)\end{aligned} \tag{3.45}$$

where

$$\Upsilon^{(2)}(r,k) = \tfrac{1}{2}(k+2)\Upsilon^{(1)}(r,k) - \tfrac{1}{2}k\Upsilon^{(1)}(r,k+1) \tag{3.46}$$

Subsequently, we can compute the integrals up to $\mathcal{I}(r_M)$

$$\begin{aligned}\mathcal{I}(r_M) &= \int_0^{r_M} r_{M-1}\mathcal{I}(r_{M-1})\mathrm{d}r_{M-1} \\ &= (\tfrac{1}{2})^{M-k}\tfrac{\Gamma(k)}{\Gamma(M)}\, r_M^{2(M-1)} G_k^M(\gamma y)\end{aligned} \tag{3.47}$$

The function $G_k^M(\cdot)$ plays a central role in the characterization of the average downlink rate. This function depends mainly on the fading distribution of the channel between the typical user and the serving BS, the size of the *multicell* M, and the index of the serving BS k. We shall discuss the role of this function and evaluate its special cases in the following section.

Substituting (3.47) in (3.37) we obtain

$$\mathcal{R}_k^M = \tfrac{2}{\Gamma(M)}(\pi\lambda_s)^M \int_0^\infty \int_0^\infty r_M^{2M-1} e^{-\lambda_s \pi r_M^2 \mathcal{W}_I(M\gamma y)} \tfrac{e^{-y r_M^\alpha}}{y} G_k^M(\gamma y)\mathrm{d}r_M\mathrm{d}y \tag{3.48}$$

Finally, by evaluating the inner integral w.r.t r_M using integration by parts, the integral in (3.48) simplifies to (3.38). ■

Corollary 2. *Considering a UDN environment which is limited by interference rather than noise, the average rate of the downlink in* (3.38) *simplifies to*

$$\hat{\mathcal{R}}_k^M = \mathcal{R}_k^M|_{\gamma\to\infty} = \int_0^\infty \frac{G_k^M(z)}{z[\mathcal{W}_I(z)]^M}\,\mathrm{d}z \tag{3.49}$$

Proof. Manipulating $\mathcal{P}(y)$ by using the change of variables $z = \gamma y$, and taking the limit as $\gamma \to \infty$, $\mathcal{P}(\gamma^{-1}z)$ is reduced to $1/[\mathcal{W}_I(z)]^M$, which completes the proof. ■

It is interesting to highlight that the result of the single association in (3.23) is a special case of the above result in (3.49) by setting $M = 1, k = 1$, and considering that $G_1^1(z) = 1 - \mathcal{M}_o(z)$

3.5.2.2 Evaluation of the Function $G_k^M(\cdot)$

The function $G_k^M(\cdot)$ is essential to compute the average downlink rate in Theorem (3) and Corollary (2). In this section, we provide a recursive integral to evaluate the function $G_k^M(\cdot)$. This recursive integral significantly simplifies the computation of a closed-form of $G_k^M(\cdot)$ for arbitrary M, k. In addition, we provide a general integral form to further simplify the computations of the recursive integral.

Corollary 3. *The function $G_k^M(z)$ can be evaluated to a closed-form by using the recursive integral*

$$G_k^M(z) = \tfrac{2k}{r_{k+1}^{2k}} \int_0^{r_{k+1}} r_k^{2k-1} G_{k+1}^M(r_k) \mathrm{d}r_k \tag{3.50}$$

The seed of this recursive integral is $G_M^M(r_M)$ and it is expressed as:

$$G_M^M(r_M) = 1 - \mathcal{M}_o(r_M^{-\alpha}\beta(r_M)) \tag{3.51}$$

where in the case of a Rayleigh fading channel $\mathcal{M}_o(z) = (1+z)^{-1}$ and $\beta(r_k) = zr_k^{\alpha}$. Moreover, evaluating this recursive integral involves integrals of the form

$$\mathcal{J} = \int r^m \Upsilon(r, n) \mathrm{d}z, \tag{3.52}$$

which evaluates to

$$\mathcal{J} = \tfrac{r^{m+1}}{(m+1)-n} \left(\Upsilon(r, n) - \tfrac{n}{m+1} \Upsilon(r, m+1) \right) \tag{3.53}$$

Proof. We begin by computing $\mathcal{R}_M^M$ from (3.33)

$$\mathcal{R}_M^M = \tfrac{2(\pi\lambda_s)^M}{\Gamma(M)} \int_0^{\infty} \int_0^{\infty} r_M^{2M-1} e^{-\lambda_s \pi r_M^2 \mathcal{W}_I(M\gamma y)} \frac{e^{-y r_M^{\alpha}}}{y} \left(1 - \mathcal{M}_o(\beta r_M^{-\alpha})\right) \mathrm{d}r_M \mathrm{d}y \tag{3.54}$$

comparing the result in (3.54) to (3.48), we can express G_M^M as

$$G_M^M = 1 - \mathcal{M}_o(\beta r_k^{-\alpha}) \tag{3.55}$$

Proceeding in a similar manner and computing $\mathcal{R}_{M-1}^M$ from (3.33)

$$\begin{aligned} \mathcal{R}_{M-1}^M = \tfrac{2(\pi\lambda_s)^M}{\Gamma(M)} \int_0^{\infty} \int_0^{\infty} r_M^{2M-1} \frac{e^{-y r_M^{\alpha}}}{y} e^{-\lambda_s \pi r_M^2 \mathcal{W}_I(\gamma y)} \times \\ \tfrac{2(M-1)}{r_M^{2(M-1)}} \left(\int_0^{r_M} r_{M-1}^{2(M-1)-1} \left(1 - \mathcal{M}_o(\beta r_{M-1}^{-\alpha})\right) \mathrm{d}r_{M-1} \right) \mathrm{d}r_M \mathrm{d}y \end{aligned} \tag{3.56}$$

Now, the comparison of the above result to (3.48) yields

$$G_{M-1}^M = \tfrac{2(M-1)}{r_M^{2(M-1)}} \int_0^{r_M} r_{M-1}^{2(M-1)-1} G_M^M(r_{M-1}) \mathrm{d}r_{M-1} \tag{3.57}$$

Continuing by computing $\mathcal{R}_{M-2}^M$ from (3.33), we obtain

$$\begin{aligned} \mathcal{R}_{M-2}^M = \tfrac{2(\pi\lambda_s)^M}{\Gamma(M)} \int_0^{\infty} \int_0^{\infty} r_M^{2M-1} \frac{e^{-y r_M^{\alpha}}}{y} e^{-\lambda_s \pi r_M^2 \mathcal{W}_I(\gamma y)} \times \\ \int_0^{r_{M-1}} \tfrac{2(M-1)}{r_M^{2(M-1)}} \left(\tfrac{2(M-2)}{r_{M-1}^{2(M-2)}} \left(\int_0^{r_{M-1}} r_{M-2}^{2(M-2)-1} G_M^M(r_{M-2}) \mathrm{d}r_{M-2} \right) \mathrm{d}r_{M-1} \right) \mathrm{d}r_M \mathrm{d}y \end{aligned} \tag{3.58}$$

By comparing (3.58) to (3.48) we obtain

$$G_{M-2}^{M} = \frac{2(M-1)}{r_M^{2(M-1)}} \int_0^{r_M} r_{M-1}^{2(M-1)-1} G_{M-1}^{M}(r_{M-2}) \mathrm{d}r_{M-1} \tag{3.59}$$

Evidently, from the results (3.55), (3.57), (3.59) one can find the general result in (3.50). In case of Rayleigh fading channels, $\mathcal{M}_o(\beta r_k^{-\alpha}) = \frac{1}{1+\beta r_k^{-\alpha}}$ and the evaluation of G_k^M for $k \in \{1, 2, \ldots, M-2\}$ involves integrals of the hypergeometric function ${}_2F_1(\cdot,\cdot,\cdot,\cdot)$ of the form in (3.52) which evaluates to the general form in (3.53). This completes the proof. ■

In the following section we show some case studies of the function $G_k^M(z)$.

3.5.2.3 Case Study of the Function $G_k^M(\cdot)$ (Rayleigh Fading)

In this section, we exploit the result in Corollary 3 to show how to use the recursive form in (3.50). We give four examples for the cases where $k \in \{M, M-1, M-2, M-3\}$. The result in Corollary 3 is for Rayleigh fading channel where a closed-form simple result is provided in each case.

Case $k = M$

The function $G_M^M(z)$ can be computed by using (3.51). In this case it is given by

$$\begin{aligned} G_M^M(r_M) = 1 - \mathcal{M}_o(r_M^{-\alpha}\beta(r_M)) &= \frac{\beta(r_M)}{\beta(r_M) + r_M^{\alpha}} \\ &= \frac{z r_M^{\alpha}}{z r_M^{\alpha} + r_M^{\alpha}} \end{aligned} \tag{3.60}$$

This yields to the general form of $G_M^M(z)$

$$G_M^M(z) = \frac{z}{z+1} \tag{3.61}$$

Case $k = M - 1$

In this case, we substitute $k = M - 1$ in (3.50)

$$\begin{aligned} G_{M-1}^{M}(z) &= \tfrac{2(M-1)}{r_M^{2(M-1)}} \int_0^{r_M} r_{M-1}^{2(M-1)-1} G_M^M(r_M) \mathrm{d}r_M \\ &= \tfrac{2(M-1)}{r_M^{2(M-1)}} \int_0^{r_M} \frac{\beta r_{M-1}^{2(M-1)-1}}{r_M + \beta} \\ &= \tfrac{2(M-1)}{r_M^{2(M-1)}} \tfrac{r_M^{2(M-1)}}{2(M-1)} \, {}_2F_1\left(1, \tfrac{n}{\alpha}; \tfrac{n}{\alpha} + 1; -\tfrac{r_M^{\alpha}}{\beta}\right) \\ &\overset{(a)}{=} {}_2F_1\left(1, \tfrac{2(M-1)}{\alpha}; \tfrac{2(M-1)}{\alpha} + 1; -\tfrac{1}{z}\right) \\ &= \Upsilon_g(z, 2(M-1)) \end{aligned} \tag{3.62}$$

In step (a), we substitute $\beta = \beta(r_M) = z r_M^{\alpha}$.

Case $k = M - 2$

Similarly, we substitute $k = M - 2$ in (3.50)

$$\begin{aligned} &G_{M-2}^{M}(z) = \tfrac{2(M-2)}{r_{M-1}^{2(M-2)}} \int_0^{r_{M-1}} r_{M-2}^{2(M-2)-1} G_{M-1}^M(r_{M-1}) \mathrm{d}r_{M-1} \\ &= \tfrac{2(M-2)}{r_{M-1}^{2(M-2)}} \int_0^{r_{M-1}} r_{M-2}^{2(M-2)-1} \, {}_2F_1\left(1, \tfrac{2(M-1)}{\alpha}; \tfrac{2(M-1)}{\alpha} + 1; -\tfrac{r_{M-1}^{\alpha}}{\beta}\right) \mathrm{d}r_{M-1} \\ &\overset{(a)}{=} (M-1)\Upsilon_g(z, 2(M-2)) - (M-2)\Upsilon_g(z, 2(M-1)) \\ &= \Upsilon_g^{(1)}(z, M-2) \end{aligned} \tag{3.63}$$

We used the recursive form in (3.53) to evaluate the integral in step (a) where $m = 2(M-2) - 1$ and $n = 2(M-1)$. Also, we substitute $\beta = \beta(r_{M-1}) = z r_{M-1}^{\alpha}$

Case $k = M - 3$

In this case, we substitute $k = M - 3$ in (3.50) and use (3.53) with $m = 2(M-3) - 1$. Since G_{M-2}^M is composed of two $\Upsilon(\cdot, \cdot)$ with respective parameters $n = 2(M-1)$ and $n = 2(M-2)$, we use the respective n with each instance. This yields to

$$\begin{aligned} &G_{M-3}^{M}(z) = \tfrac{1}{2}(M-1)\Upsilon_g^{(1)}(z, M-3) - \tfrac{1}{2}(M-3)\Upsilon_g^{(1)}(z, M-2) \\ &= \Upsilon_g^{(2)}(z, M-3) \end{aligned} \tag{3.64}$$

The provided case studies allow the numerical computation of *multicell* sizes up to $M = 4$. Extending these results to higher sizes, i.e., $(M > 4)$, can be done following the same approach. The function G_k^M is tabulated in Table 3.1 for $M \leq 4$ and $k \in \{1, 2, \ldots, M\}$.

Table 3.1: Some examples for the function G_k^M (Rayleigh Fading)

$G_M^M(z)$	$\frac{z}{z+1}$
$G_1^2(z)$	${}_2F_1(1, \frac{2}{\alpha}, \frac{2}{\alpha}+1, -\frac{1}{z})$
$G_2^3(z)$	${}_2F_1(1, \frac{4}{\alpha}, \frac{4}{\alpha}+1, -\frac{1}{z})$
$G_1^3(z)$	$2\,{}_2F_1(1, \frac{2}{\alpha}, \frac{2}{\alpha}+1, -\frac{1}{z}) - {}_2F_1(1, \frac{4}{\alpha}, \frac{4}{\alpha}+1, -\frac{1}{z})$
$G_3^4(z)$	${}_2F_1(1, \frac{6}{\alpha}, \frac{6}{\alpha}+1, -\frac{1}{z})$
$G_2^4(z)$	$3\,{}_2F_1(1, \frac{4}{\alpha}, \frac{4}{\alpha}+1, -\frac{1}{z}) - 2\,{}_2F_1(1, \frac{6}{\alpha}, \frac{6}{\alpha}+1, -\frac{1}{z})$
$G_1^4(z)$	$3\,{}_2F_1(1, \frac{2}{\alpha}, \frac{2}{\alpha}+1, -\frac{1}{z}) - 3\,{}_2F_1(1, \frac{4}{\alpha}, \frac{4}{\alpha}+1, -\frac{1}{z}) +$ ${}_2F_1(1, \frac{6}{\alpha}, \frac{6}{\alpha}+1, -\frac{1}{z})$

Also, it is important to realize that the function $\Upsilon(r, .)$ and $\Upsilon_g(z, .)$ have similar structure except that the latter is a simplified version of the former. This simplification takes place by substituting $\beta = zr^\alpha$ in $\Upsilon(r, .)$. Another key point is that the function G_k^M is a weighted sum of the basis function $\Upsilon_g(z, n)$ for different values of the parameter n.

3.5.2.4 Network Aggregate Average Rate (NAAR)

The network aggregate average rate, denoted by $\mathcal{R}_{naar}$, is defined as the aggregate average downlink rate of all users in a given area normalized by this area and is expressed in (3.9). To further simplify, considering the interference-limited scenario in UDN:

$$\begin{aligned}
\mathcal{R}_{naar} &= \lambda_u \sum_{k=1}^{M} B\hat{\mathcal{R}}_k^M \\
&= \lambda_u B \sum_{k=1}^{M} \int_0^\infty \frac{G_k^M(z)}{z[\mathcal{W}_I(z)]^M}\, \mathrm{d}z \\
&= \lambda_u B \int_0^\infty \sum_{k=1}^{M} \frac{G_k^M(z)}{z[\mathcal{W}_I(z)]^M}\, \mathrm{d}z \\
&= \lambda_u B \int_0^\infty \frac{\sum_{k=1}^{M} G_k^M(z)}{z[\mathcal{W}_I(z)]^M}\, \mathrm{d}z \\
&= \lambda_u B \int_0^\infty \frac{G_M(z)}{z[\mathcal{W}_I(z)]^M}\, \mathrm{d}z. \qquad (3.65)
\end{aligned}$$

Considering Rayleigh fading and using Corollary 3, $G_M(z)$ can be further simplified to:

$$\begin{aligned} G_M(z) &= \sum_{k=1}^{M} G_k^M(z) \\ &= \frac{z}{z+1} + (M-1)\,{}_2F_1(1, \tfrac{2}{\alpha}, \tfrac{2}{\alpha}+1, -\tfrac{1}{z}) \end{aligned} \tag{3.66}$$

3.6 Simulation Results

In this section, we assess the accuracy of the presented analytical framework through simulations. We also show the impact of different system parameters on the average downlink rate. To this end, we consider a simulation environment where the small cells' positions and the users' positions are drawn from PPP with the respective densities. Also, we generate independent channel fading gains which follow Rayleigh and Rician fading distributions to show the effect of the channel on the average downlink rate. Moreover, we study the impact of the *multicell* size M on the network performance in terms of the average downlink rate.

3.6.1 Impact of the multicell size

Figure 3.3 depicts the average downlink rate of the connections to the BSs in a *multicell* of size 4. The rate is an increasing function of the small cells density. However, in the propagation environments of higher pathloss exponents, the average downlink rate improves significantly. This can be explained in the light of the fact that higher pathloss exponents translate into less interference impact due to the high attenuation of the interference signals.

On the other side, the average rate of the link to the farthest BSs is less than that of the nearest BS which reflects the fact that the link to the farther BSs is always weaker than the link to the nearest BS. At the same time, the rate of the connections to the farther BSs is considerably high especially at higher cell densities. Undoubtedly, connecting using the whole available bandwidth to the nearest BS provides the user with the maximum rate. However, this capacity would be censored by the limits on the backhaul capacity of this individual cell. In this way, the splitting of the user traffic to different BSs in its neighborhood provides the user with a data-shower where each data path is limited by the corresponding backhaul capacity of this cell only. To further show the

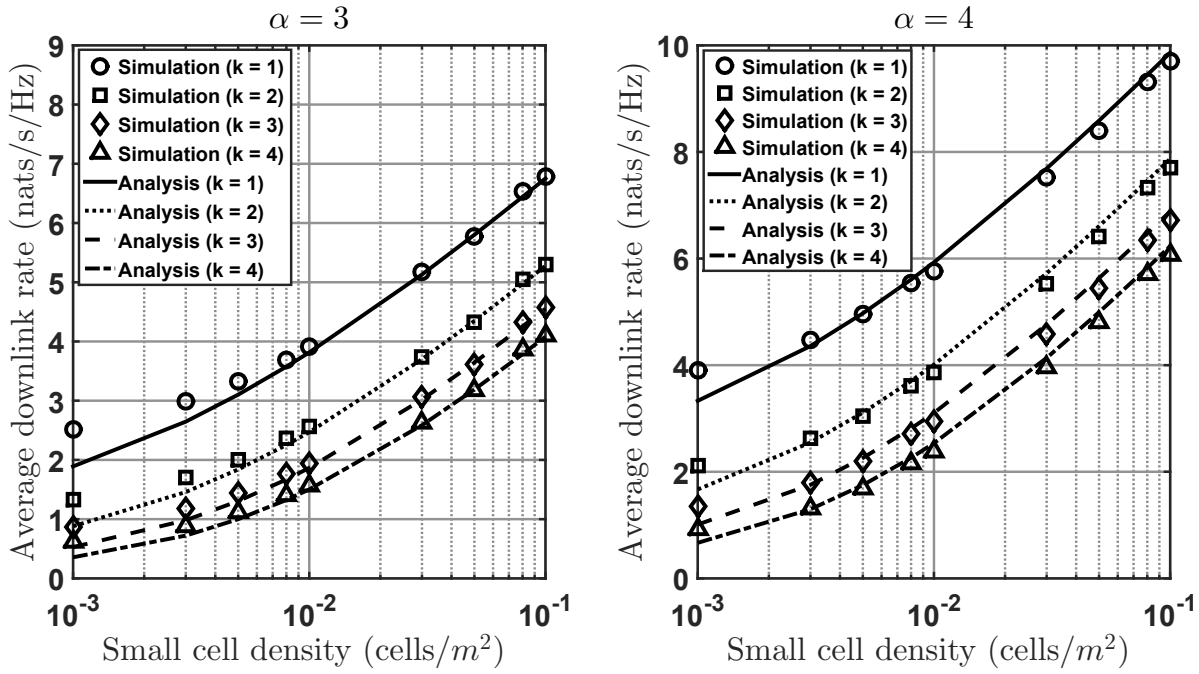

Figure 3.3: Average downlink rate with the small cells density over Rayleigh fading in multiple association for different pathloss exponents. *Multicell* size 4 is considered with user density $\lambda_u = 500$ users/Km^2. The analytical results are computed using Corollary (2).

impact of the *multicell* size on the performance, Figure 3.4 depicts the network aggregate average rate for different *multicell* sizes. The results show significant improvement in the network performance with larger *multicell* sizes. However, this comes with a price, i.e., the increasing complexity of the user equipment.

3.6.2 Impact of the small cells density

Figure 3.5 depicts the impact of the small cells density on the average downlink rate. The results show the significant boost in the average downlink rate with the increasing small cells density for different pathloss exponents. This improvement shed lights on the important impact of the idle mode capabilities on mitigating the interference in dense networks. In other words, turning off the idle BSs is vital for the fruition of the gains of network densification. In Figure 3.5, we compare with the results presented in [1] to show the impact of this important parameter on the performance of the network. In addition, Figure 3.4 depicts the significant improvement in the network aggregate average rate with the higher small cell densities. Higher BSs density brings the user much closer to the serving BSs. Consequently, the link quality improves significantly leading to the

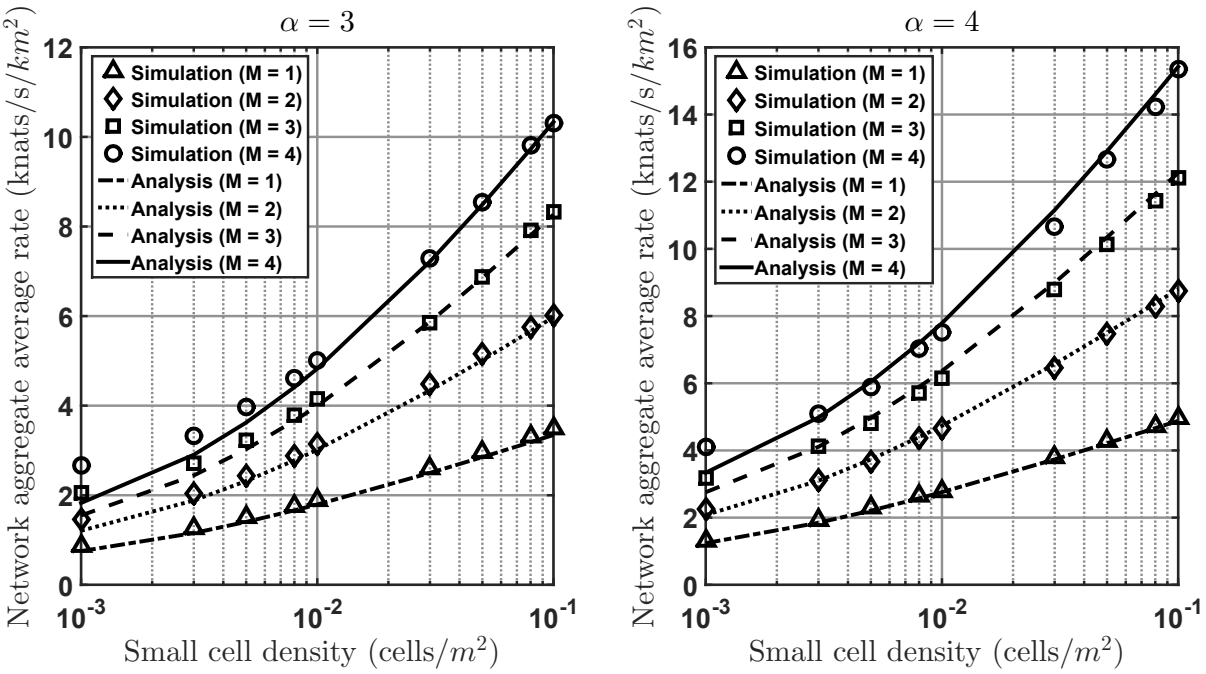

Figure 3.4: Network aggregate average rate with the small cells density over Rayleigh fading in multiple association for different pathloss exponents. A user density $\lambda_u = 500$ users/Km^2 and various *multicell* sizes are considered. The analytical results are computed using Corollary (2) and Eq. (3.65) and (3.66).

considerable increase in the average downlink rate and the network aggregate average rate.

3.6.3 Impact of the users density

Figure 3.6 shows how the average downlink rate decreases with the users density. This is a result of the activation of more BSs as the density of users increases. More active cells yield to more interference in the system, and hence the SINR is severely affected. However, in a realistic situation the density of active users is moderate and in the range of $300 - 600$ users/km^2 [21]. In this scenario, the impact of the activation of many cells in multiple association can be considered marginal. However, if we considered the network aggregate average rate as depicted in Figure 3.6, the network performance improves significantly with higher users density. More users in the network activate more BSs which enhances the frequency reuse of the available bandwidth. Although, with more active BSs the network experiences more interference, aggregating more component carriers for each user and reusing the available bandwidth more compensates for the negative impact of the interference.

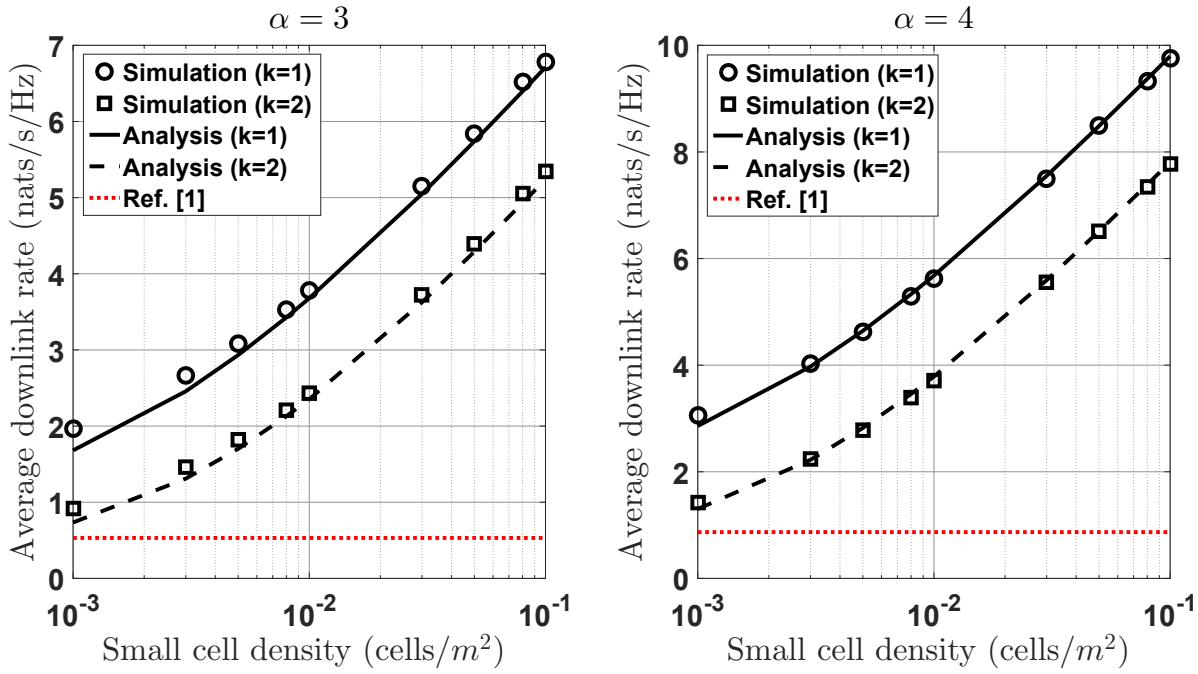

Figure 3.5: Average downlink rate in single association with the small cells density for Rayleigh fading channel in multiple association for different pathloss exponents. User density $\lambda_u = 500$ users/Km^2 is considered. The results are compared with the results in [1], and the analytical results are computed using Corollary (2).

3.6.4 Impact of the fading channels

In order to study the impact of fading channels on the average downlink rate, we considered the comparison between Rayleigh fading and Rician fading distributions. To this end, we considered the MGF of a Rayleigh fading channel $\mathcal{M}_o = (1+z)^{-1}$ [128, Table (2.2)]. Correspondingly, we consider the approximation of Rice fading channels using Nakagami-m fading which is a more general fading distribution whose parameters can be adjusted to fit different fading scenarios [130]. The MGF of Nakagami-m fading is $\mathcal{M}_o = (1+z/m)^{-m}$ [128, Table (2.2)] where for Rayleigh fading distribution $m = 1$. Remarkably, the Nakagami-m distribution usually gives accurate representation of land-mobile and indoor-mobile multipath propagation which is most appropriate in UDNs [128]. Interestingly, there is a one-to-one mapping between the m parameter and the Rician K factor $\left(m = \frac{(K+1)^2}{2K+1}\right)$, which allows Nakagami-m distribution to closely approximate the Rice distribution [128]. On the positive side, considering the Nakagami-m approximation to the Rician fading slightly contribute to the complexity of the numerical computations of the average downlink rate. In this simulation scenario, we considered $K = 32$ [87, Eq.

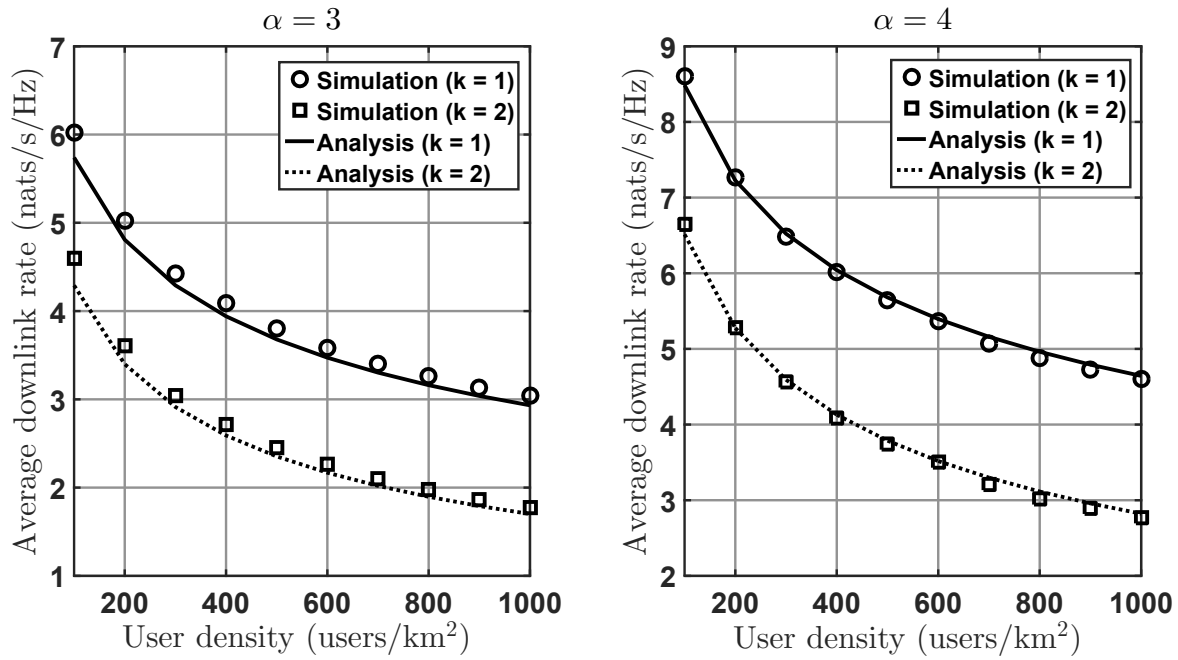

Figure 3.6: Downlink rate with the users density over Rayleigh fading in multiple association for different pathloss exponents. *Multicell* size 2 is considered with small cells density $\lambda_s = 10^4$ cells/Km^2. The analytical results are computed using Corollary (2).

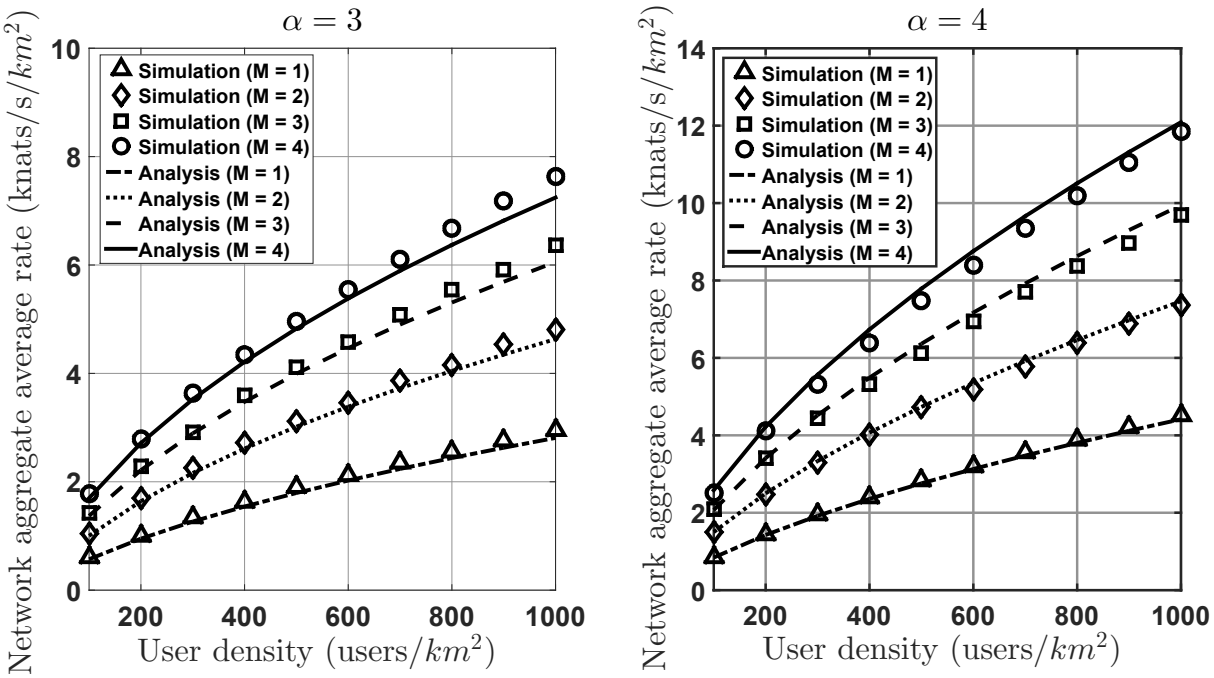

Figure 3.7: Network aggregate average rate with the users density over Rayleigh fading in multiple association for different pathloss exponents. Different *multicell* sizes and a small cells density $\lambda_s = 10000$ cells/Km^2 are considered. The analytical results are computed using Corollary (2). and Eq. (3.65) and (3.66) .

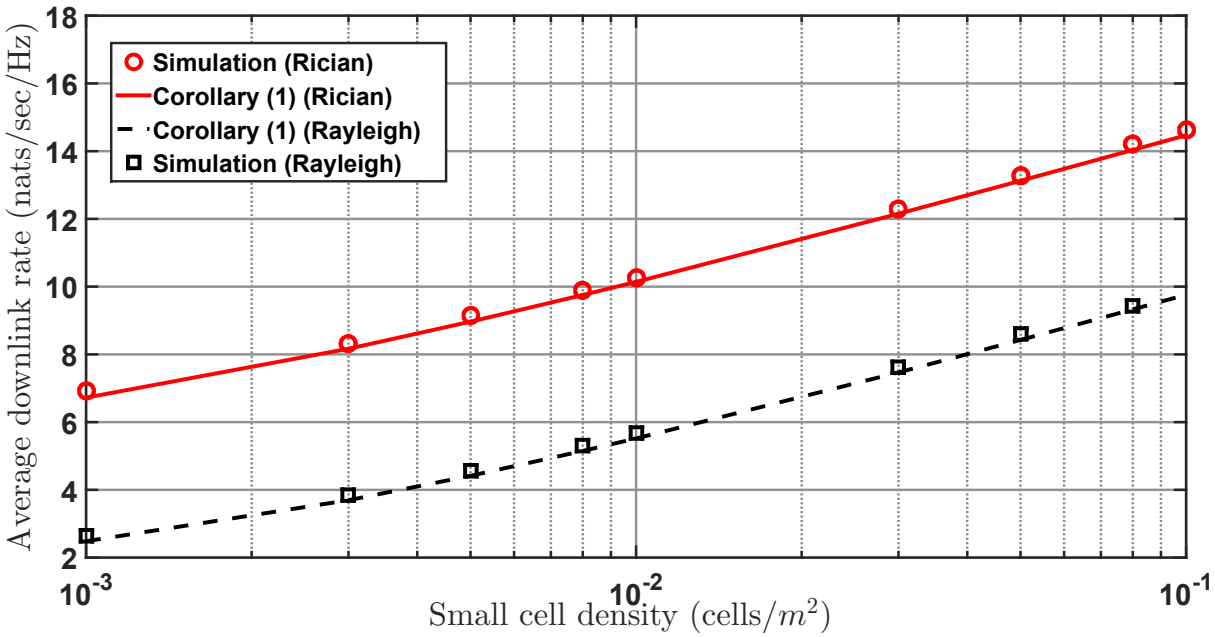

Figure 3.8: Average downlink rate in single association with the small cells density for different fading channels. Pathloss exponent $\alpha = 4$ is considered with user density $\lambda_u = 500$ users/Km^2.

(3)] where the average distance to the tagged BS (server) in dense networks is usually in the considered range of $d < 18$ m.

In Figure 3.8, the average downlink rate is plotted considering Rician and Rayleigh fading channels in the signal link. Due to the proximity of the users to the tagged BS, the probability of LOS transmission considerably increases. As depicted in Figure 3.8, the average downlink rate in the case of Rician fading channel is significantly higher than the case of Rayleigh fading channel.

3.7 Conclusions

We developed a mathematical framework for the computation of the average downlink rate of the connections from the typical user to many BSs in its neighborhood. The framework provides a high degree of accuracy as confirmed by our extensive simulations for the considered system model. The performance of the multiple association sheds light on the gains and losses of such association scheme. Although the average rate decreases when connecting to farther cells, this is compensated by expanding beyond the bottleneck of the limited backhaul capacity. The aggregate downlink rate of the connections to many cells exceeds the limits imposed by the backhaul capacity of the individual cells. Moreover,

considering general channel fading distributions in both the signal and the interference links provides a way to handle different propagation environment in dense networks. In addition, the presented framework provides a starting point to fully characterize the performance of multiple association in dense networks in subsequent investigations.

4. Coverage and Capacity Analysis considering SEPL in UDNs

4.1 Introduction

Network densification is widely believed, by both industry and academia, as the potential technology that would satisfy the stringent requirements of the 5G networks [58, 59, 110]. According to [131], the capacity of wireless communication has expanded 1 million times in 50 years (1950 – 2000), Astonishingly, the gain achieved by spatial reuse through network densification was 2700x, where other factors such as: wider spectrum, better medium access/modulation techniques and better coding techniques, have contributed by 15x, 5x and 5x, respectively [21]. Based on this successful history, Ultra-Dense Networks (UDNs) are expected to dominate other solutions in approaching the 5G networks in the near future. In UDNs, a surplus of small cells is deployed in the hotspots where enormous amounts of traffic is generated. Increasing the density of small cells brings the serving cells much closer to the end users which provides a two-fold gain where better link quality is achieved and more spatial reuse is accomplished. This scenario would define a new wireless environment that has never been experienced in mobile communication where the density of base stations (BSs) outpaces the density of active users [54, 58].

Evidently, the network densification cannot grow indefinitely and there will be fundamental limits [132] and more importantly economical and business limits on the density of UDNs [24]. Nevertheless, the high density of BSs in UDNs is the most distinguishing feature of such networks. Quantifying how dense is a UDN can be determined in terms of the relative density of the BSs with regard to the active users' density (e.g. see Definition 1 in [54] and the references therein). In 2014, Qualcomm has provided a prototype implementation for an early UDN. In particular, the world's densest LTE small cell de-

ployment was reported by Qualcomm in [59] with cell density of 1107 cells/km^2, average site-to-site distance of 22m, minimum site-to-site distance of 7m and a total coverage area of 0.028 km^2. Moreover, the trends reported for the surge in mobile traffic demands urge more dense network deployments to come in the near future.

Considering the realistic modeling of the special features of UDN, in this work we employed a Stretched Exponential Path-Loss (SEPL) model where the signal power decays with the distance r as $e^{-\alpha r^{\beta}}$. SEPL model accurately captures the signal propagation properties in UDN environments featuring short distances between the (serving/interfering) BSs and the associated users. A recent study considers this path loss model which is better fit to the propagation environment in UDNs (e.g., see [2, Table I] where a comprehensive survey of several path loss models is provided).

BSs equipped with idle mode capability turn off to mitigate the interference [21] in case there are no connected users. The control of this capability can be classified into user equipment driven, small cell driven, and core network driven approaches [133]. Energy efficient operation of the network and interference mitigation are of the main benefits of such capability. In this chapter, we study the impact of idle mode capability on the network performance considering a SEPL model. We provide an accurate analytical model to compute the coverage probability and the network capacity in terms of network throughput and area spectral efficiency (ASE).

The deployment of small cells is usually done by consumers in case of indoor femtocells and by operators in case of outdoor picocells. In both cases, the small cells are placed randomly due to the less restrictive network planning guidelines. In quest of an accurate modelling for such location randomness, stochastic geometry stems as a perfect tool (e.g., see [104–106]). The modelling and analytical tools provided by stochastic geometry are widely used in investigating problems in cellular, heterogeneous, and dense networks [104]. Small cells' locations in two-dimensional or three-dimensional space are modeled as a point process (PP) where the Homogeneous Poisson Point Process (HPPP) is one of the most tractable PP. In HPPP, the number of points in some area A has a Poisson distribution with an average of λA, where λ is the cells' density. Moreover, the points abstracting the small cells are uniformly distributed in this area [106].

4.2 State-of-the-Art and Contributions

In this chapter, we study the downlink performance of UDNs considering a more accurate path loss model, i.e., SEPL model. In [2], the SEPL model is considered to evaluate the performance of a dense cellular network. However, it is assumed that all BSs are turned on and each cell has exactly one active user. This implies a very high number of active users at very high BSs densities, which would not capture the reality of cellular networks where the number of active users in real traffic scenarios is typically bounded by 600 users/km^2 [61]. In [54] a closed-form is provided for the asymptotic average downlink rate in a UDN scenario, however, a standard decaying path loss model $r^{-\alpha}$ is used, where r is the link distance and α is the path loss exponent. A multi-slope path loss model is investigated in [92] where an activity probability of one is assumed.

We differently consider the idle mode probability of small cells in UDNs, thus, we assume that a given user connects to the nearest BS and if there exist a BS with no connected users, it is turned off to mitigate its interference. Based on this assumption, we draw different conclusions which better reflect the performance of network densification considering SEPL model. Our findings reveal that the idle mode capabilities of the BSs provide a very useful interference mitigation technique besides the energy efficiency of operating such dense networks. Another very interesting insight is that the system interference in idle-mode capable UDNs is upper-bounded by the interference generated from the active BSs, and in turn this is upper-bounded by the number of active users where more active users is translated to more interference in the system. This means that the interference becomes independent of the density of the small cells as this density increases. In the light of the above discussion, we conclude that the coverage probability converges to a constant value at very high small cell densities where this value is a function of the user's density.

4.3 System Model

In this investigation, we consider a dense network comprised of a single tier of small cells where we assume that the BSs are equipped with advanced idle mode capabilities to perfectly mitigate their interference in case of inactivity due to lack of connected

users. The BSs spatial locations are modeled as a Homogeneous Poisson Point Process (HPPP) Φ_s with density λ_s. The users also form another HPPP Φ_u with density λ_u. We assume that in UDN the density of BSs is higher than the density of the active users, i.e., $\lambda_s \gg \lambda_u$ leaving many of the BSs in idle mode where no users are connected [21]. All BSs and users are assumed to be equipped with a single antenna, the BSs transmit with a unit power, and all component carriers are utilized in each cell, i.e., frequency reuse factor of one. We evaluate the performance metrics for a typical mobile user located at the origin, and without loss of generality, this represents the average of the performance for all users and is allowed by Slivnyak's theorem [105]. The typical user connects to the BS providing the maximum average received power, i.e., the closest BS. We refer to the serving BS of the typical user as the tagged BS b_o. Notably, the distance R from any BS (serving or interfering) to the typical user is a random variable due to the randomness of BSs locations. The probability distribution function (PDF) of this distance is expressed as [20]:

$$f_R(r) = 2\pi\lambda_s r e^{-\pi\lambda_s r^2} \tag{4.1}$$

Moreover, we consider a propagation environment that consists of large scale fading attenuation as well as small scale fading effects. The large scale fading component is modeled by a stretched exponential decaying power law with parameters (α and β) [2], thus the received signal power at a distance r from a BS transmitting with a unit power is $e^{-\alpha r^\beta}$. All small cells are assumed to have multipath fading channels that are independent and identically distributed (i.i.d) to model the small scale fading and are assumed to follow Rayleigh distribution. Hence, the power fading channel gain of the serving BS, h_o, and interfering BSs, h_b follow exponential distribution with mean one ($\sim Exp(1)$).

We consider the interference-limited scenario which is the typical scenario in UDN. Accordingly, the downlink signal to interference ratio (SIR) can be expressed as:

$$\texttt{SIR} = \frac{\mathcal{S}}{\mathcal{I}_a} = \frac{h_o e^{-\alpha r^\beta}}{\sum_{b\in\Phi_a/b_o} h_b e^{-\alpha r_b^\beta}} \tag{4.2}$$

where $\Phi_a \subset \Phi_s$ is the interfering BSs point process which is the set of all active cells.

In this study, we consider three performance metrics:

1. Downlink Coverage Probability $\mathcal{P}_c(\tau)$: The coverage probability is defined as:

$$\mathcal{P}_c(\tau) = \mathbb{P}\left\{\texttt{SIR} \geq \tau\right\} \tag{4.3}$$

where τ is the coverage threshold.

2. Network Throughput $\mathcal{R}_a$: The network throughput is defined as [74]:

$$\mathcal{R}_a = \lambda_a \mathcal{P}_c(\tau) \ln(1+\tau) \quad \text{nats/sec/Hz}, \tag{4.4}$$

where $\lambda_a = p_a \lambda_s$ is the density of the active BSs represented by the point process Φ_a.

3. Area Spectral Efficiency $\mathcal{A}_{se}$: The area spectral efficiency is defined as [2]:

$$\mathcal{A}_{se} = \mathbb{E}\left[\lambda_a \ln(1+\texttt{SIR})\right] \quad \text{nats/sec/Hz} \tag{4.5}$$

where the expectation is with respect to the channel fading gains and the random distances of the links to the serving and interfering BSs (e.g., see the definition of SIR in (7.1)).

4.4 Analytical Results

4.4.1 Downlink Coverage

In this section, we analyze the downlink coverage probability of an interference-limited UDN as defined in (7.4). In the following theorem we present the main result considering a SEPL model with general parameters α and β.

Theorem 1. *The downlink coverage probability of a UDN satisfying the system model presented in Section 4.3 is given by:*

$$\mathcal{P}_c(\tau) = 2\pi\lambda_s \int_0^\infty r e^{-\pi\lambda_s r^2} \mathcal{L}_{\mathcal{I}_a}(\tau e^{\alpha r^\beta}) \mathrm{d}r \tag{4.6}$$

where:

$$\mathcal{L}_{\mathcal{I}_a}(\tau e^{\alpha r^\beta}) = \exp\left\{ (-1)^{\frac{2}{\beta}} \frac{2\pi p_a \lambda_s \tau}{\beta \alpha^{\frac{2}{\beta}}} \int_0^1 \frac{\left(\ln(x) - \alpha r^\beta\right)^{\frac{2-\beta}{\beta}}}{1+\tau x} \mathrm{d}x \right\} \tag{4.7}$$

Theorem 1 provides a general result, yet not simple to draw conclusions or intuitive insights. For the sake of simplicity, in the following Corollary, we study a less general case with the special values $\beta = \frac{2}{n+1}$ where $n \in \{0, 1, 2, 3, \cdots\}$ which corresponds to the values $\beta = 2, 1, \frac{2}{3}, \frac{1}{2}, \cdots$.

Corollary 1. *Considering the special case* $\beta = \frac{2}{n+1}$ *where* $n \in \{0, 1, 2, 3, \cdots\}$, *the downlink coverage probability stated in Theorem 1 simplifies to*

$$\mathcal{P}_c(\tau) = 2\pi\lambda_s \int_0^\infty r \exp\left\{ \sum_{k=0}^{n+1} p_a \lambda_s a_k(\tau) r^{\frac{2k}{n+1}} \right\} \mathrm{d}r \tag{4.8}$$

where

$$a_k(\tau) = \begin{cases} \frac{\pi(n+1)!}{k!\alpha^{n-k+1}} \mathrm{Li}_{(n-k+1)}(-\tau), & 0 \leq k \leq n. \\ -\frac{\pi}{p_a}, & k = n+1. \end{cases} \tag{4.9}$$

and $\mathrm{Li}_{(k)}(\cdot)$ *is the* k^{th} *order poly-logarithmic function [134], which can be expressed as:*

$$\mathrm{Li}_{(n-k+1)}(\tau) = -\frac{\tau}{\Gamma(n-k+1)} \int_0^\infty \frac{x^{n-k}}{e^x - \tau} \mathrm{d}x \tag{4.10}$$

Remark 1: The downlink coverage probability reduces to its simplest form at $\beta = 2$ which corresponds to $n = 0$, and it is expressed as:

$$\mathcal{P}_c(\tau) = \exp\left\{ -\frac{\pi p_a \lambda_s}{\alpha} \ln(1+\tau) \right\}. \tag{4.11}$$

This follows from Corollary 1 by simple manipulations.

Remark 2: The idle mode capabilities of the BSs provide a very useful interference mitigation technique besides the energy efficiency of operating such dense networks. More interestingly, the results in Theorem 1 and Corollary 1 provide insights for the impact of the idle mode probability on the coverage probability. The term $p_a\lambda_s$ shows up in the expressions of the coverage probability in (7.8), (7.9), (7.12) where it represents the density of the active BSs, or in other words, the interfering BSs. As the density of the small cells λ_s increases, the term $p_a\lambda_s$ converges to the user's density λ_u, i.e., $\lim_{\lambda_s \to \infty} p_a\lambda_s = \lambda_u$. This provides a very interesting insight; the system interference in idle-mode capable UDNs is upper-bounded by the interference generated from the active BSs, and in turn this is upper-bounded by the number of active users where more active users is translated to more interference in the system. This means that the interference becomes independent of the density of the small cells as this density increases. In the light of the above discussion, we conclude that the coverage probability converges to a constant value at very high small cell densities where this value is a function of the user's density.

4.4.2 Network Throughput

The network throughput can be expressed as a function of the coverage probability as given by the definition in (4.4). In the following corollary, we provide an expression for the network throughput in a general case and two special cases.

Corollary 2. *The network throughput of a UDN satisfying the system model presented in Section 4.3 is given by:*

$$\mathcal{R}_a = 2\pi p_a \lambda_s^2 \ln(1+\tau) \int_0^\infty r e^{-\pi\lambda_s r^2} \mathcal{L}_{\mathcal{I}_a}(\tau e^{\alpha r^\beta}) \mathrm{d}r, \tag{4.12}$$

where $\mathcal{L}_{\mathcal{I}_a}(\cdot)$ *is given in* (7.8). *Moreover, in the special case* $\beta = \frac{2}{n+1}$ *where* $n \in \{0, 1, 2, 3, \cdots\}$, *the network throughput further simplifies to*

$$\mathcal{R}_a = 2\pi p_a \lambda_s^2 \ln(1+\tau) \int_0^\infty r \exp\left\{ \sum_{k=0}^{n+1} p_a \lambda_s a_k(\tau) r^{\frac{2k}{n+1}} \right\} \mathrm{d}r \tag{4.13}$$

where $a_k(\cdot)$ *is given in* (7.10). *Furthermore, for the special value* $\beta = 2$, *the network throughput can be reduced to*

$$\mathcal{R}_a = p_a \lambda_s \ln(1+\tau) \exp\left\{ -\frac{\pi p_a \lambda_s}{\alpha} \ln(1+\tau) \right\} \tag{4.14}$$

4.4.3 Area Spectral Efficiency

In the following theorem, we provide the main result of area spectral efficiency.

Theorem 2. *The area spectral efficiency of a UDN satisfying the system model presented in Section 4.3 is given by:*

$$\mathcal{A}_{se} = 2\pi p_a \lambda_s^2 \int_0^\infty \int_0^\infty r e^{-\pi\lambda_s r^2} \mathcal{L}_{\mathcal{I}_a}(w e^{\alpha r^\beta}) \frac{1}{w+1} \mathrm{d}r \mathrm{d}w, \tag{4.15}$$

where $\mathcal{L}_{\mathcal{I}_a}(\cdot)$ *is given in* (7.8).

The area spectral efficiency expression in Theorem 2 requires three folded integrals for the evaluation of numerical result. In quest of more tractable results where insights can be read out, we provide the following corollary.

Corollary 3. *Considering the special case* $\beta = \frac{2}{n+1}$ *where* $n \in \{0, 1, 2, 3, \cdots\}$, *The area spectral efficiency stated in Theorem 2 simplifies to*

$$\mathcal{A}_{se} = 2\pi p_a \lambda_s^2 \int_0^\infty \int_0^\infty \exp\left\{ \sum_{k=0}^{n+1} p_a \lambda_s a_k(w) r^{\frac{2k}{n+1}} \right\} \frac{r \mathrm{d}r \mathrm{d}w}{w+1} \tag{4.16}$$

where $a_k(\cdot)$ *is given in* (7.10). *Moreover, for the special value* $\beta = 2$, *the area spectral efficiency can be further reduced to*

$$\mathcal{A}_{se} = \frac{\alpha}{\pi} \tag{4.17}$$

4.5 Simulation Results

In this section, we assess the accuracy of the analytical results by simulating the UDN model provided in the system model. The network is realized by the generation of HPPP with corresponding densities for the small cells and the users. We consider a simulation area of 1 km^2 where we generated 1000 spatial realizations of the PPP. The channel variation is simulated by a realization of 100 time slots drawn from an exponential random variable with a mean one. We consider a SEPL model $e^{-\alpha r^\beta}$ to compute the path losses for the serving BS links as well as the interference links.

Figure 4.1 depicts the downlink coverage probability versus the coverage threshold τ. The results show that the coverage in UDNs is significantly high even in high coverage thresholds, thanks to turning off the idle BSs. The impact of mitigating the interference of the inactive BSs is further highlighted by contrasting it with the coverage probability results in [2] where the coverage probability drops significantly in higher coverage thresholds. The impact of users density is also depicted where higher users' density is translated to more active BSs which in turn adds more interference to the system. Thus, the coverage probability is less in higher users' density.

This conclusion is further settled by assessing the impact of higher small cells' densities on the coverage probability. Figure 4.2 depicts the coverage probability versus the small cells' density λ_s where the coverage probability is very high and almost invariant with small cells' density. To explain, turning off the idle BSs defines an upper bound for the interference where this bound is solely controlled by the user's density.

The network throughput versus small cell's density is depicted in Figure 4.3 for different users' density. The results show that the network throughput increases with higher

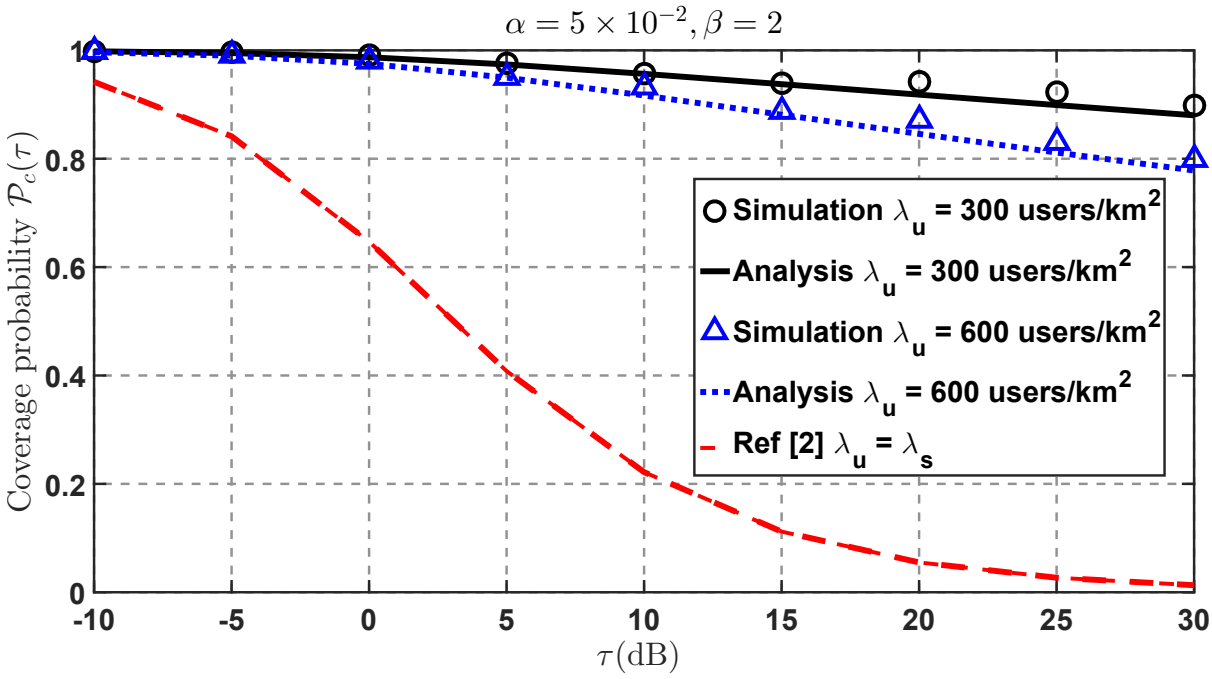

Figure 4.1: Downlink coverage probability versus the coverage threshold τ for different user's density with small cells' density $\lambda_s = 10^4$ cells/km^2. The results are compared to the results in [2] which assumes that all BSs are active and are serving exactly one user each.

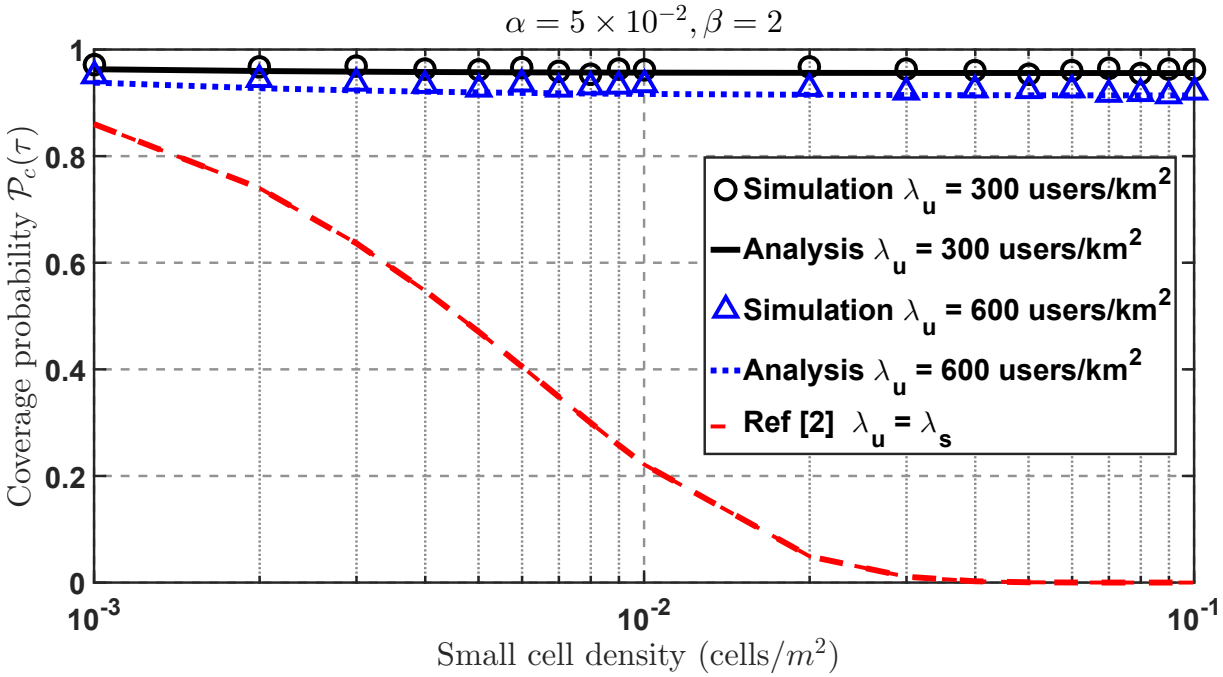

Figure 4.2: Downlink coverage probability versus the small cells' density λ_s for different user's density and coverage threshold $\tau = 10$ dBs. The results are compared to the results in [2].

small cells' density, also it improves significantly with higher user's density. Moreover, the network throughput saturates at a value which depends on the number of active users.

To explain, more active users activate more BSs which in turn improves the network throughput. In Figure 4.4, we compare our results to the results in [2] which show a different behavior, the network throughput is maximized at a certain BSs density and then drops exponentially to zero with higher small cells' density. This is due to the increasing unbounded interference based on the assumptions of [2] where all BSs are turned on and each BS serves exactly one user. In our work, the consideration of idle mode capabilities drives to different conclusions. Interestingly, our results converge to the results in [2] at very high users' density as indicated.

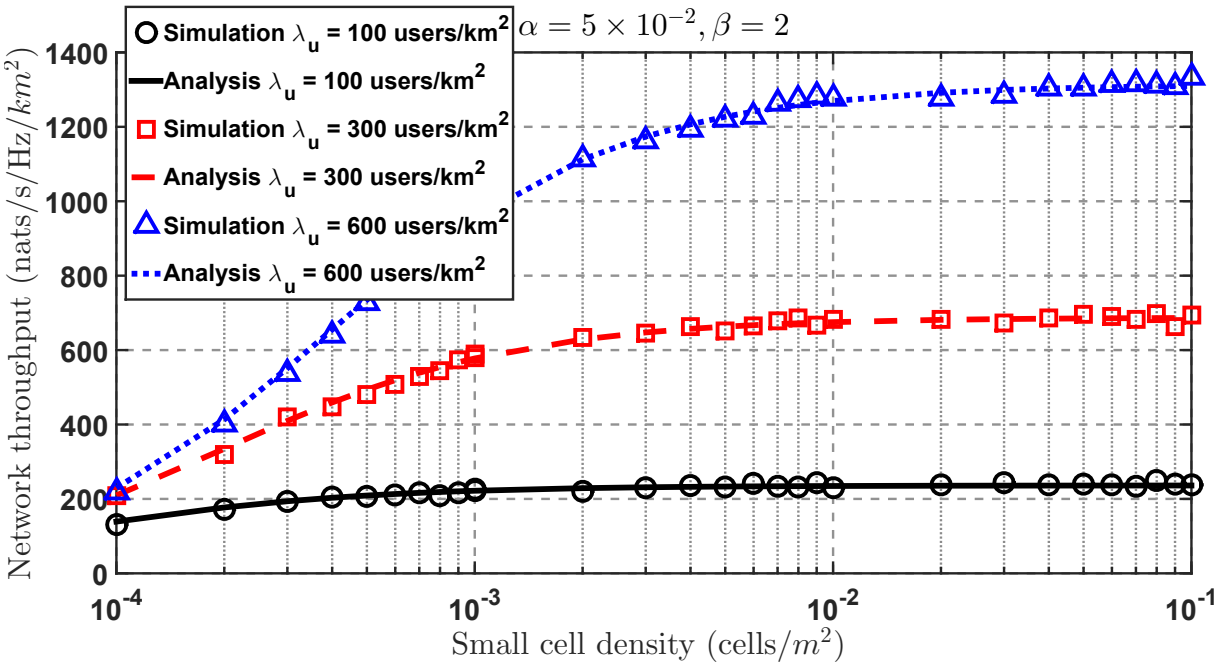

Figure 4.3: Network throughput versus the small cells' density λ_s for different user's density and coverage threshold $\tau = 10$ dBs..

Figure 4.5 depicts the area spectral efficiency versus the small cells' density for different users' density considering the special case $\beta = 1$. The results show that the area spectral efficiency increases with higher small cells' approaching a saturation value. Also, the ASE is independent of the users' density which is also confirmed in the special case $\beta = 2$ in (4.17).

In conclusion, both the ASE and the network throughput saturate at a given small cell density for the considered path loss model leaving no room for enhancing the network performance by increasing the small cell density beyond this density. Moreover, turning off the idle BSs keeps the network performance from dropping to zero at very high cell densities.

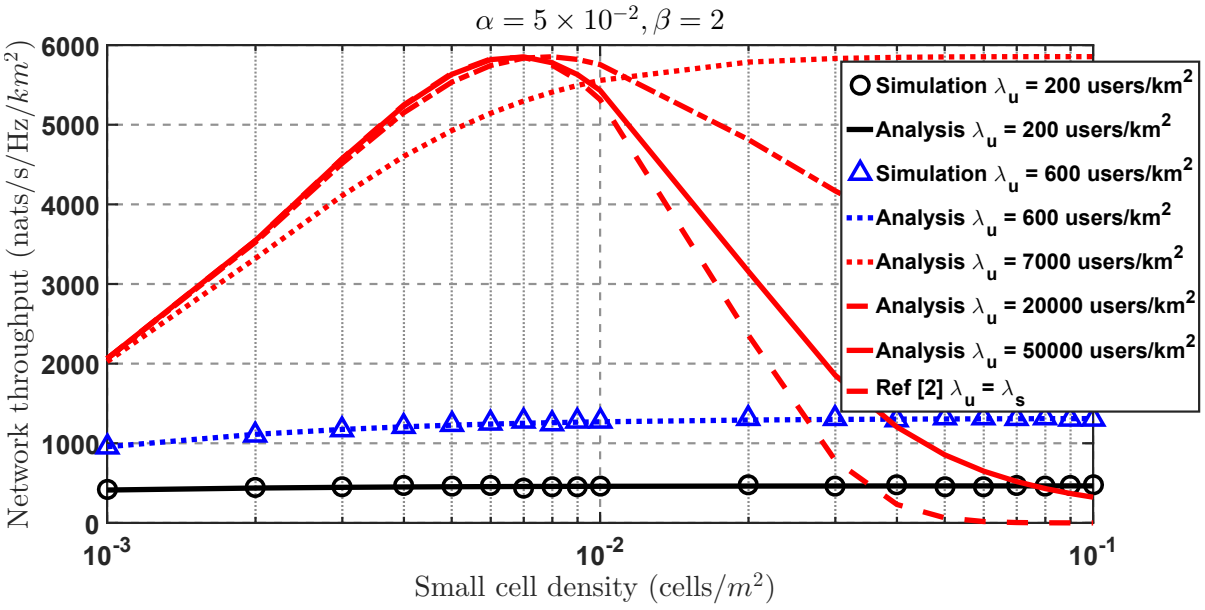

Figure 4.4: Network throughput versus the small cells' density λ_s for different user's density and coverage threshold $\tau = 10$ dBs. The results are compared to the results in [2].

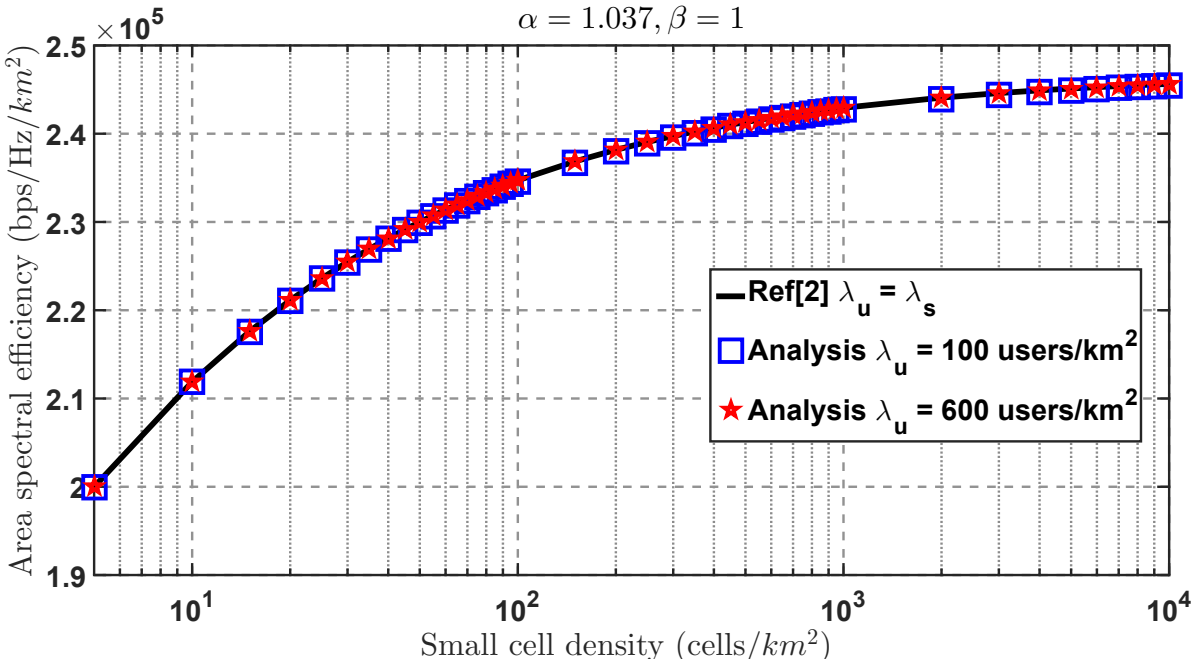

Figure 4.5: Area spectral efficiency versus the small cells' density λ_s for different user's density. The results are compared to the results in [2].

4.6 Conclusions

We investigated the downlink performance of UDNs where inactive BSs are turned off to mitigate their interference. We employ SEPL model to capture the propagation environment in UDN where the serving and interfering BSs are within short distances from the

user. The idle mode capability imposes an upper-bound on the system interference where at very high small cells' densities the number of active BSs converges to the number of the active users, e.g., each user activates the closest BS to its location. The impact of bounding the interference on the network performance influences the coverage as well as the capacity of the network. To summarize, under the utilized assumptions, the coverage probability as well as the capacity are invariant with the small cells' density at high densities. However, it is strongly tied to the user's density. Moreover, the coverage probability and the network throughput never drop to zero at very high BSs density due to the interference upper-bound set by the density of the active users.

5. Physical layer security in UDNs

5.1 Introduction

In 5G networks where Internet of Things (IoT) is a key player, low-cost security is inevitable [58]. For this reason, Physical Layer Security (PLS) stems as an important and effective solution. PLS signifies the attempt to achieve information-theoretic security in digital communication systems by exploiting the randomness in the transmission media. Particularly, PLS can be realized in wireless networks by designing effective channel coding techniques [135]. This means that PLS would provide the wireless communication networks with a cheap security solution in terms of the computational complexity where there is no need for sophisticated encryption schemes.

In PLS context, the maximum achievable transmission rate to the legitimate user, at which the eavesdropper is completely confused and cannot decode the messages, is termed as the *secrecy capacity* [135]. The close proximity of the users to the serving base stations (BSs) in Ultra-Dense Network (UDN)environments suggests the positivity of the secrecy capacity [56, 136]. In this investigation, we aim to investigate the inherent high secrecy capacity of UDNs which plays a key role in providing a highly secured connectivity alternative. For a comprehensive survey of PLS in wireless networks, we refer the reader to [135] and the references therein.

5.2 State-of-the-Art

In [95], the secrecy throughput along with secrecy probability are investigated considering a heterogeneous network (HetNet). The secrecy outage probability is studied in a multiple radio access technology (multi-RAT) scenario in [96]. In [97], the secrecy rate in a multi-tier HetNet is investigated considering generalized fading model; however, the

significant role of the relative density of the users with respect to the small cells' density is not considered. A dense network environment was assumed in [98] to validate the approximation of the secrecy outage probability. However, the key features of dense networks, such as the users' relative density, the high probability of idle BSs and the high probability of Line-of-Sight (LOS) transmission [58], were not considered. Furthermore, the analytical approximations provided in [8] are shown to be loose as the BSs density gets high, contradicting one of the main aspects of dense networks.

5.3 Contributions

The main contribution of this investigation is the derivation of the average secrecy rate in UDNs considering their distinct traits, namely, idle mode BSs and LOS transmission. The high density of small cells makes it quite probable for a BS to have no connected users. Consequently, turning off those inactive BSs provides a simple yet effective interference mitigation scheme. Moreover, the close proximity of the users/Eves to the BSs increases the probability of having a LOS transmission in both the main link and the leakage link. To this end, we exploit the standard moment generating function (MGF)-based approach [1] to derive relatively simple and easily computable expressions for the average secrecy rate considering the idle mode probability and Rician fading channel. The result of this investigation avoids the system level simulations where the performance evaluation complexity can be greatly reduced with the aid of the derived analytical expressions. Finally, we highlight that two eavesdropping scenarios have been considered in the literature; active eavesdropping and passive eavesdropping. In active eavesdropping, the instantaneous channel state information (CSI) of the eavesdropper is known to the transmitter through feedback. Practical scenarios for this case includes broadcast channels where all users except the intended user can be dealt as eavesdroppers. In this scenario, perfect secrecy is always guaranteed. In passive eavesdropping, the CSI of the main channel is available while the CSI of the eavesdropper's channel is not known. As such, the transmitter selects a constant secrecy rate and perfect secrecy is not always guaranteed [137]. The considered analysis in this investigation provides a guaranteed average secrecy rate in the case of active eavesdropping while in the case of passive eavesdropping it provides statistical characterization of the performance of secrecy communication in UDNs. Specifically,

one can gain insights of how the secrecy performance in UDN scales with the density of various network nodes, namely, the legitimate users, the eavesdroppers, and the BSs.

5.4 System Model

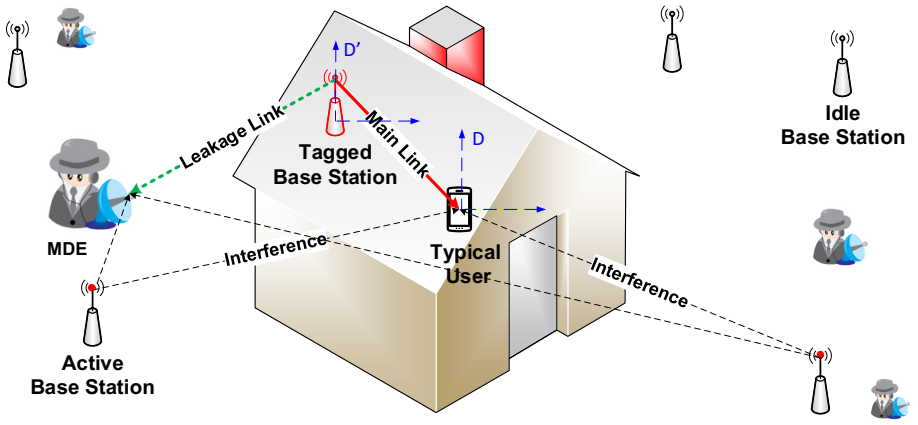

Figure 5.1: The main link connects the typical user to the tagged BS and the leakage link connects the tagged BS to the most detrimental eavesdropper (MDE).

In this investigation, we consider the downlink of a UDN comprised of small cell BSs which transmit at a power P_s. The BSs locations are spatially distributed according to a homogeneous PPP Φ_s with a density λ_s. The locations of the mobile stations (MSs), which are assumed to be held by legitimate users, are drawn from another homogeneous PPP Φ_u with a density λ_u which is independent from the BSs PPP. We assume that passive eavesdroppers (Eves) coexist with the legitimate users and are attempting to intercept the secret messages intended to these legitimate users. We further assume that the Eves locations are distributed according to a homogeneous PPP Φ_e with a density λ_e which is also independent from both Φ_s and Φ_u. According to the definitions of UDN [58], we assume that the density of the BSs is much greater than the density of the active MSs, i.e., $\lambda_s \gg \lambda_u$. Also, we consider scenarios where the density of the Eves is less than the density of users (i.e., $\lambda_e < \lambda_u$) which is mostly the case in various environments. We utilize a standard propagation model with a path loss ($\alpha > 2$) where the received signal power at a distance d from a BS is $Pd^{-\alpha}$. The small scale channel fading considered in this study accounts for the fundamental properties of UDNs, where LOS propagation is most probable. Thus, we assume that the main link h_m between the legitimate users and the BSs is modeled as a Rician channel with a parameter K_m. Furthermore, we model

the leakage link h_e representing the channel between the Eves and the transmitting BS with another Rician fading channel with a parameter K_e.

5.5 Analytical Results

In this section, we evaluate the average secrecy rate $\bar{\mathcal{R}}_s = \mathbb{E}(\mathcal{R}_s)$ in UDNs. Denote by $\mathcal{R}_s$ the secrecy rate which is given by [136]

$$\mathcal{R}_s = [\mathcal{R}_m - \mathcal{R}_e]^+ \tag{5.1}$$

where $[x]^+ = \max\{x, 0\}$, $\mathcal{R}_m$ is the rate of the main link and $\mathcal{R}_e$ is the rate of leakage link. In UDN environments, the probability of nonzero secrecy rate is very high (i.e., $\mathbb{P}\{\mathcal{R}_s > 0\} > 0.95$) [56, 136]. Thus, the secrecy rate can be approximated to:

$$\mathcal{R}_s \approx \mathcal{R}_m - \mathcal{R}_e \tag{5.2}$$

and hence, the average secrecy rate is then given by:

$$\bar{\mathcal{R}}_s \approx \bar{\mathcal{R}}_m - \bar{\mathcal{R}}_e \tag{5.3}$$

where $\bar{\mathcal{R}}_m$ is the average rate of the main link and $\bar{\mathcal{R}}_e$ is the average rate of the leakage link.

Having considered this approximation, one can evaluate the average rate of each link individually. The main link connects the typical user at the origin of the system of coordinates D with the tagged BS, which is the nearest BS according to the considered association criterion. Taking another system of coordinates D', the leakage link is the link connecting the tagged BS at the origin of the new coordinates to the nearest Eve or in other words the most detrimental eavesdropper (MDE) as depicted in Figure 5.1. We assume non-colluding Eves in this investigation [135], where each Eve decodes the intercepted messages of the legitimate users independently, i.e., there no cooperation between the Eves. Thus, the worst case information leakage considers only the MDE. In what follows, we proceed in the analysis starting with the leakage link, and following similar line of thought, we provide the analysis of the main link.

5.5.1 Leakage Link

In the system of coordinates D', we consider the tagged BS as a typical point where the nearest Eve is considered as the MDE. The average rate of the leakage link from this

typical BS to the MDE can be expressed as:

$$\bar{\mathcal{R}}_e = 2\pi\lambda_e \int_0^\infty \zeta e^{-\pi\lambda_e\zeta^2} \mathbb{E}\left\{\ln\left(1+\frac{P_s h_{eo}\zeta^{-\alpha}}{\sigma^2+I_e(\zeta)}\right)\right\} \mathrm{d}\zeta \tag{5.4}$$

where $\mathbb{E}\{\cdot\}$ denotes the expectation operator, h_{eo} is the channel gain of the leakage link, ζ is the distance between the typical BS b_o and the nearest Eve, and $I_e(\zeta) = \sum_{b\in\Phi_a/b_o(\zeta)} P_s h_{eb}\zeta_b^{-\alpha}$ is the aggregate interference in the leakage link from all active BSs except the tagged BS, b_o. We consider BSs equipped with idle mode capability where an idle BS is turned off to mitigate its interference. In this scenario, the PPP $\Phi_a \subset \Phi_s$ is a thinned version of the small cells point process Φ_s with a probability of activation $p_a = 1 - p_o$ where p_o is the idle mode probability. It is worth mentioning that $I_e(\zeta)$ approximates the interference seen by the MDE to the interference at the typical BS. In the following theorem, we provide a tractable expression for the average rate of the leakage link. UDN environments are rather interference limited. Thus, we consider evaluating the rate of the leakage link where the noise is negligible relative to the interference (*i.e.*, $\sigma^2 \to 0$). This assumption always holds in dense cellular networks ($\lambda_s > 10^{-3}$) for any pathloss exponent, and for traditional sparse cellular networks ($\lambda_s < 10^{-4}$) for low pathloss exponents ($\alpha < 4$) [1].

Theorem 1. *The average rate of the leakage link from the tagged base station of the typical user to the most detrimental eavesdropper (MDE) in the downlink considering interference limited scenarios can be approximated as:*

$$\bar{\mathcal{R}}_e \approx \int_0^\infty \frac{1-\mathcal{M}_{eo}(z)}{z\mathcal{J}_{I_e}(z)}\,\mathrm{d}z \tag{5.5}$$

where:

$$\mathcal{J}_{I_e}(z) = 1-(1-p_o)\frac{\lambda_s}{\lambda_e} + (1-p_o)\frac{\lambda_s}{\lambda_e}\mathcal{Z}_{I_e}(z) \tag{5.6}$$

$$\mathcal{Z}_{I_e}(z) = \mathcal{M}_{I_e}(z) + \mathcal{T}_{I_e}(z) \tag{5.7}$$

$$\mathcal{T}_{I_e}(z) = \Gamma(1-\tfrac{2}{\alpha})\sum_{j=0}^{\infty} z^{j+1}\mathcal{M}_{I_e}^{(j)}(z)\left[\Gamma(2-\tfrac{2}{\alpha}+j)\right]^{-1} \tag{5.8}$$

$$\mathcal{M}_{I_e}^{(j)}(z) = \mathbb{E}\left\{h_{eb}^{j+1}e^{-zh_{eb}}\right\} \tag{5.9}$$

and, $\mathcal{M}_{eo}(z)$ is the MGF of the useful signal fading channel h_{eo} in the leakage link.

Proof. Using the standard MGF approach [1] and considering [124, Lemma 1] with $N =$

$M = 1$, the expectation in (5.4) can be expressed as:

$$\mathbb{E}\left\{\ln\left(1+\frac{P_s h_{eo}\zeta^{-\alpha}}{\sigma^2+I_e(\zeta)}\right)\right\} = \int_0^{\infty} \mathcal{M}_{I_e}(\gamma z;\zeta)\left(1-\mathcal{M}_{eo}(\gamma\zeta^{-\alpha}z)\right)\frac{e^{-z}}{z}\,\mathrm{d}z \tag{5.10}$$

where $\gamma = P_s/\sigma^2$ is the signal-to-noise ratio (SNR), $\mathcal{M}_{I_e}(.;\zeta)$ is the MGF of the approximated aggregate interference in the leakage link. This interference is approximated as the interference generated by all interferes that lie outside a disk of radius ζ and centered at the tagged BS of the typical user. A closed form expression for $\mathcal{M}_{I_e}(.;\zeta)$ is derived in [1, Eq. (36)]. In here, we consider a UDN which is featured by the high density of the small cells and hence a high probability of idle BSs p_o. Therefore, we consider the active BSs only in the evaluation of the aggregate interference [58]. A given BS is active if at least one user is associated to it. The probability of BS activation $p_a = 1 - p_o$, where $p_o = \left(\frac{3.5\kappa}{1+3.5\kappa}\right)^{3.5}$ is the idle mode probability where $\kappa \triangleq \lambda_s/\lambda_u$ is the densification ratio of the small cell network. By using [1, Eq. (36)] and considering the thinned PPP $\Phi_a \subset \Phi_s$, $\mathcal{M}_{I_e}(.;\zeta)$ is expressed as:

$$\begin{aligned}\mathcal{M}_{I_e}(z;\zeta) = \exp\left\{\pi p_a\lambda_s\zeta^2\right\}\exp\left\{-\pi p_a\lambda_s\zeta^2\mathcal{M}_I(z\zeta^{-\alpha})\right\} \\ \times\exp\left\{-\pi p_a\lambda_s\zeta^2\mathcal{T}_I(z\zeta^{-\alpha})\right\}.\end{aligned} \tag{5.11}$$

Now, we substitute (5.11) in (5.10) and then in (5.4). To simplify, we perform a change of variables $y = z\zeta^{-\alpha}$, and apply integration by parts to (5.4) and taking the limit as $\sigma^2 \to 0$ to obtain (5.5) which completes the proof. ■

5.5.2 Main Link

We consider a user association policy based on the long-term maximum averaged-received power, where the typical user at the origin of the system of coordinates D associates to the nearest BS as depicted in Figure 5.1. The average rate of the main link $\bar{\mathcal{R}}_m$ can be expressed as:

$$\bar{\mathcal{R}}_m = 2\pi\lambda_s\int_0^{\infty} re^{-\pi\lambda_s r^2}\mathbb{E}\left\{\ln\left(1+\frac{P_s h_{mo} r^{-\alpha}}{\sigma^2+I_m(r)}\right)\right\}\mathrm{d}r \tag{5.12}$$

where h_{mo} is the channel gain of the main link, r is the distance between the typical user and the nearest BS b_o, and $I_m(r) = \sum_{b\in\Phi_a/b_o(r)} P_s h_{mb} r_b^{-\alpha}$ is the aggregate interference of the active BSs in the main link considering interference limited network.

In the following theorem, we provide an expression for the average downlink rate in the main link.

Theorem 2. *The average downlink rate in the main link from the tagged base station to the typical user considering interference limited scenarios can be given as:*

$$\bar{\mathcal{R}}_m = \int_0^\infty \frac{1 - \mathcal{M}_{mo}(z)}{z\mathcal{W}_{I_m}(z)} \, \mathrm{d}z \tag{5.13}$$

where:

$$\mathcal{W}_{I_m}(z) = p_o + (1 - p_o)\mathcal{Z}_{I_m}(z) \tag{5.14}$$

$$\mathcal{Z}_{I_m}(z) = \mathcal{M}_{I_m}(z) + \mathcal{T}_{I_m}(z) \tag{5.15}$$

$$\mathcal{T}_{I_m}(z) = \Gamma(1 - \tfrac{2}{\alpha}) \sum_{j=0}^{\infty} \frac{z^{j+1}\mathcal{M}_{I_m}^{(j)}(z)}{\left[\Gamma(2 - \frac{2}{\alpha} + j)\right]} \tag{5.16}$$

$$\mathcal{M}_{I_m}^{(j)}(z) = \mathbb{E}\left\{h_{mb}^{j+1} e^{-z h_{mb}}\right\} \tag{5.17}$$

and, $\mathcal{M}_{mo}(z)$ is the MGF of the useful signal fading channel h_{mo} in the main link.

Proof. Following similar arguments as in the proof of Theorem (1) we arrive at the result in (5.13). ■

Finally, one can find the approximate average secrecy in (5.3) by combining the results in (5.5) and (5.13). The rate expressions of the main and the leakage links are integrals which involve special functions. However, the numerical computation of these integrals is quite straightforward and it can be done efficiently using commercial software packages (e.g., Matlab).

Moreover, it is worth mentioning that the average secrecy rate in terms of the average main link rate and the average leakage link rate is a function of the eavesdroppers density λ_e, the legitimate users density λ_u and the BSs density λ_s. Thus, the nodes' densities are the key system parameters.

5.6 Simulation Results

In this section, we assess the accuracy of the provided expressions for the average secrecy rate in the investigated system model via simulations. Considering the PPP of the BSs, the legitimate users, and the eavesdroppers; we generate 1000 spatial realization of the

positions with the corresponding densities in a square area of a side 500 m. The channel variations are simulated by generating 100 time slots with channel gains drawn from Rician channel with different values for the K parameter to represent the main link and the leakage link. We assume interference-limited networks, i.e., $\sigma^2 \to 0$.

Figure 5.2 depicts the average secrecy rate versus the small cells density for different relative densities of the Eves. We consider a Rician channel in the main link and Rayleigh fading in the leakage link. The results show that the average secrecy rate significantly improves with higher cell density which confirms the inherent physical layer security of dense networks. Moreover, the results show that the approximation in the analytical result improves in higher cell densities. To explain, the positivity of the secrecy rate becomes almost sure at very high small cell density which improves the positivity approximation.

The slight variation in the average secrecy rate with the relative density of the Eves is due to the assumption that the Eves experience Rayleigh fading channel. In this scenario, the leakage rate varies slightly in the considered Eve's relative density range as depicted in Figure 5.6.

In Figures 5.3 and 5.4, we consider Rician fading in both the main and the leakage links with different values for the corresponding K parameter. Although the average secrecy rate degrades slightly in both cases, the results unveil that the secrecy feature of UDNs is a strong function in the small cell density where the average secrecy rate is high in higher small cell densities even with a LOS channel for the Eve. The average secrecy rate is depicted in Figure 5.5 versus the users density for different small cell densities considering Rician fading in both the main and the leakage links. The results show that the average secrecy rate degrades with higher users density. As the users density increases, more BSs are activated adding up to the aggregate interference in the main link which negatively impacts the main link average rate. Moreover, in the considered scenario, the Eves density is proportional to the users density and increasing the users density means higher Eves density, and hence higher information leakage. As a final investigation, Figure 5.6 depicts the average rate of the leakage link versus the Eves relative density for different small cell density. The results show the significant increase of the leakage link rate with higher Eves relative densities where Rayleigh fading is considered in the leakage link.

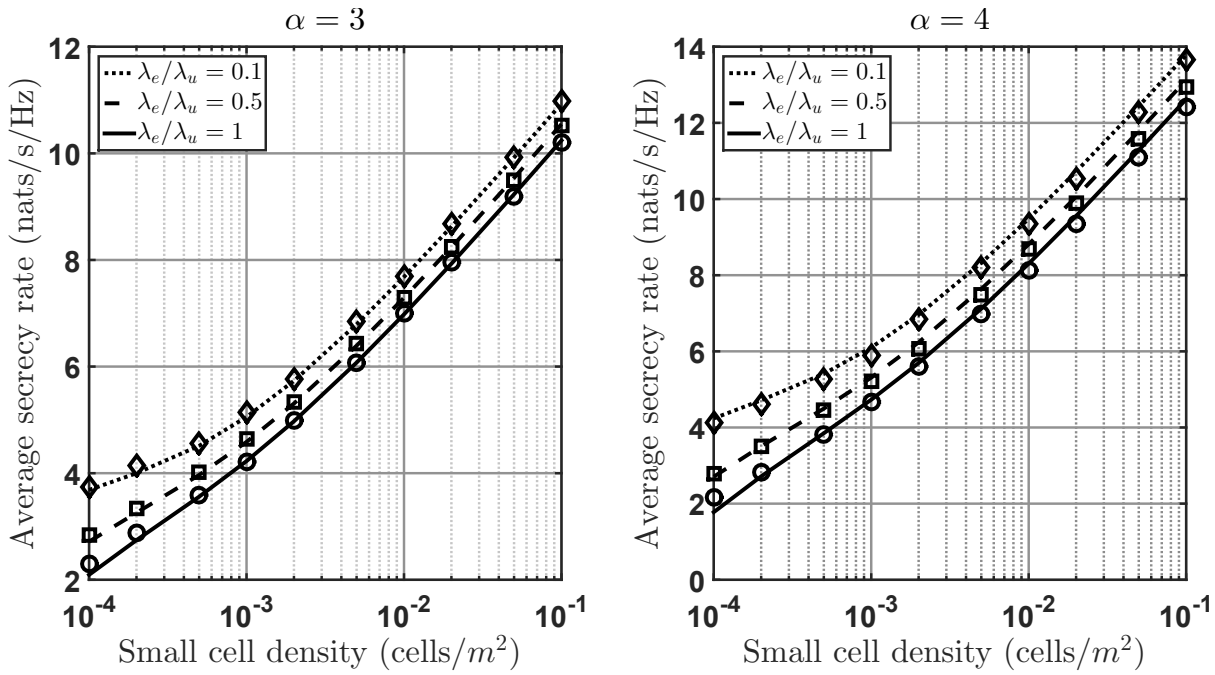

Figure 5.2: The average downlink secrecy rate versus small cell density considering Rician channel in the main and Rayleigh channel in the leakage link ($K_m = 32, K_e = 0, \lambda_u = 600$ users/km^2). Lines show the analytical results computed using Theorems 1 and 2, and Markers show simulation results.

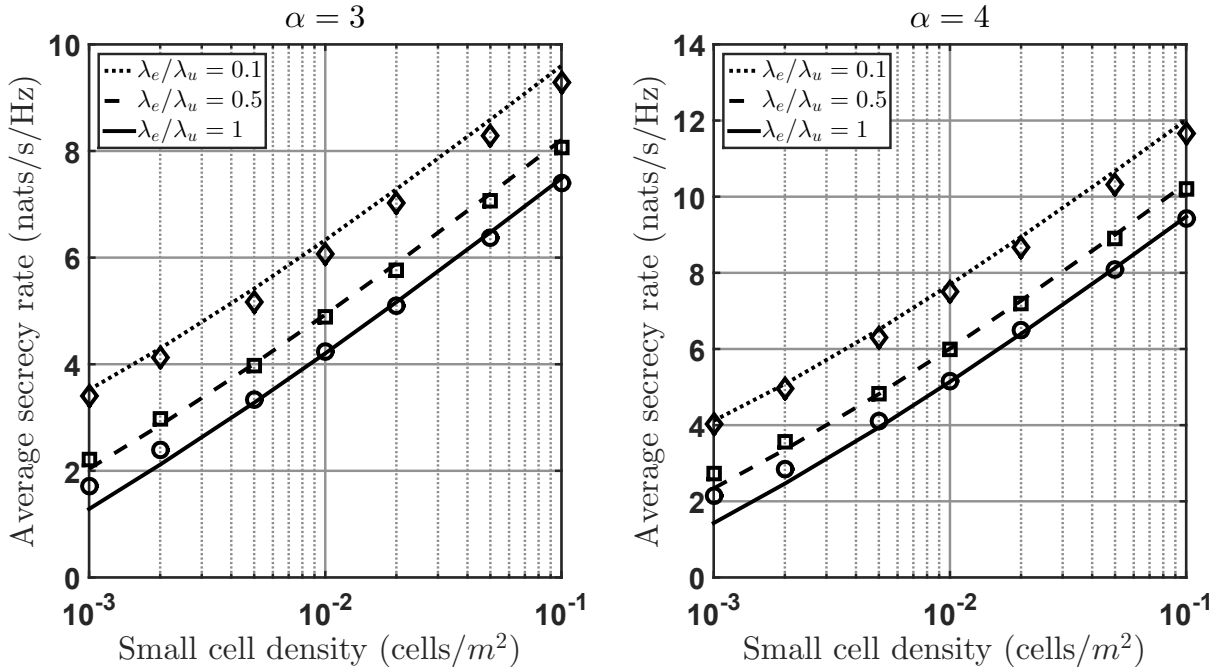

Figure 5.3: The average downlink secrecy rate versus small cell density considering Rician channel in both the main and the leakage links ($K_m = 32, K_e = 16, \lambda_u = 600$ users/km^2). Lines show the analytical results computed using Theorems 1 and 2, and Markers show simulation results.

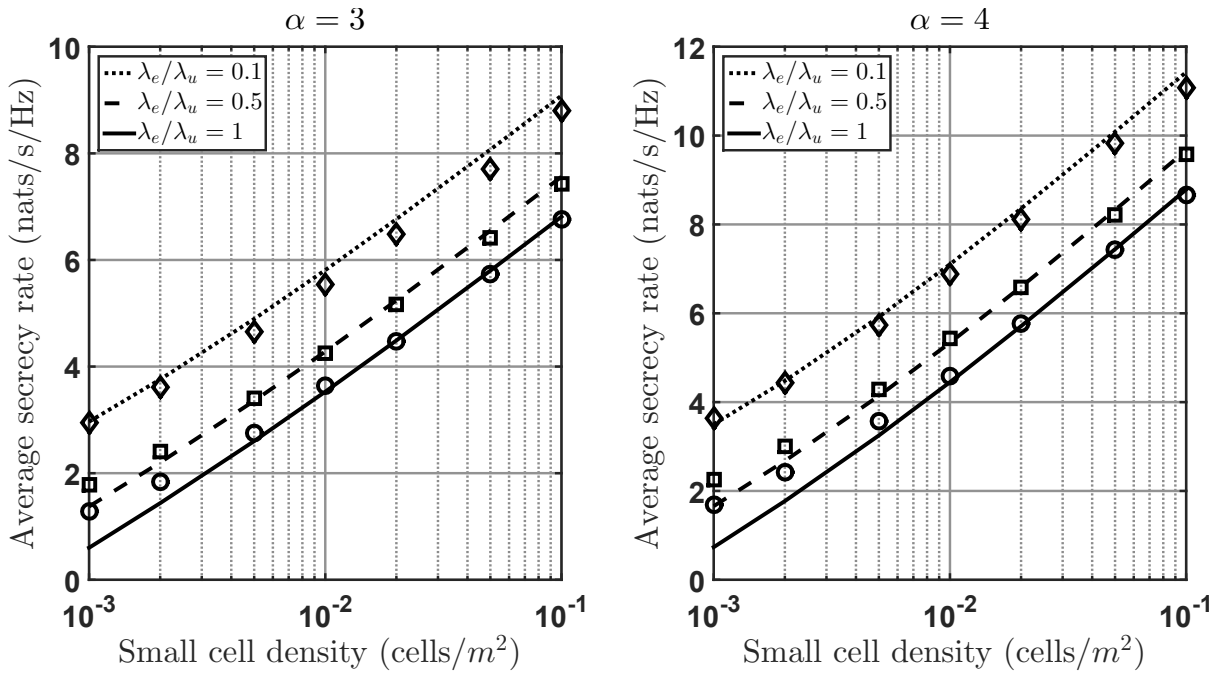

Figure 5.4: The average downlink secrecy rate versus small cell density considering Rician channel in both the main and the leakage links ($K_m = 32, K_e = 32, \lambda_u = 600$ users/km^2). Lines show the analytical results computed using Theorems 1 and 2, and Markers show simulation results.

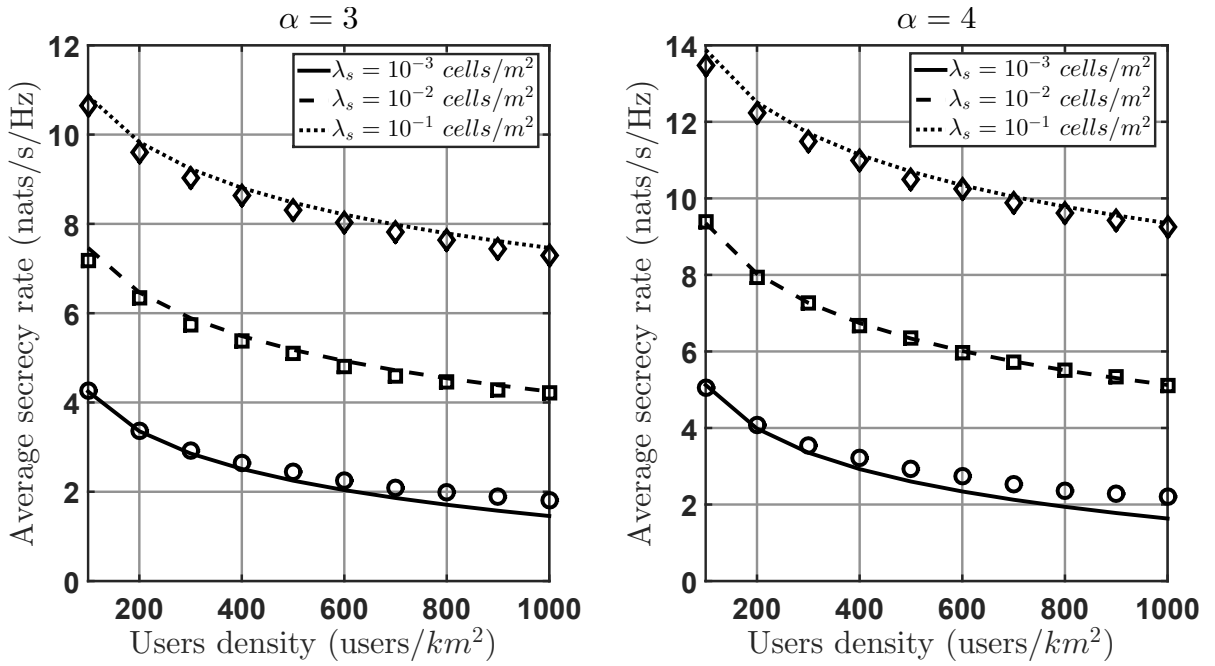

Figure 5.5: The average downlink secrecy rate versus users density considering Rician channel in both the main and the leakage links ($K_m = 32, K_e = 16, \lambda_e = 0.5\lambda_u$). Lines show the analytical results computed using Theorems 1 and 2, and Markers show simulation results.

5.7 Conclusions

The high secrecy capacity of UDN networks is an inherent feature by virtue of the high density of the cells. Users in dense networks connect via strong connections to very close

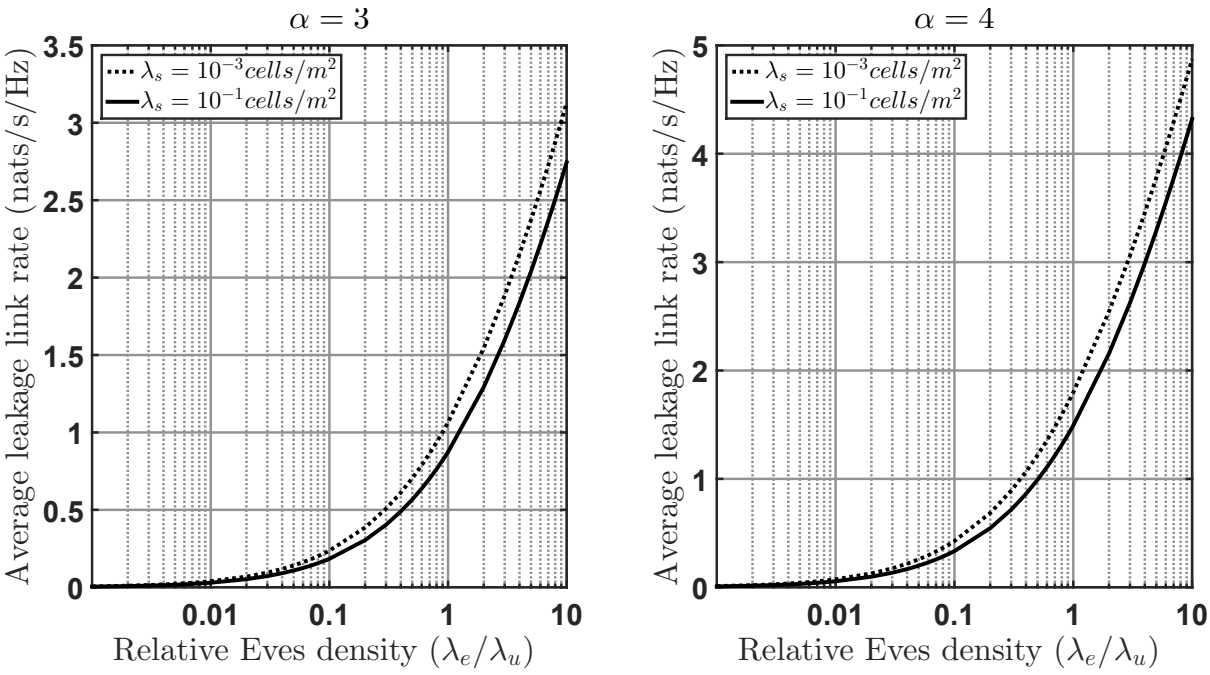

Figure 5.6: The average rate of the leakage link versus relative density of Eves ($\lambda_u = 600$ users/km^2, $K_e = 0$).

cells. The close proximity of the small cells to the users induces a secure environment where the cells can whisper encoded messages to the legitimate users confusing the Eves and providing the users with high average secrecy rate. The average secrecy rate in UDNs is an increasing function in the small cells density even with the consideration of LOS transmission in the leakage link. On the contrary, the average secrecy rate decreases in environments with high users density where the activation of more BSs results in increasing the interference in the main link which in turn negatively impacts the average secrecy rate.

6. Uplink Coverage of mMTC in UDNs

6.1 Introduction

Smart living is the core of a set of trending concepts and technologies. Smart city, smart building, and smart home are all synonyms in the sense of having the same essential element: devices that sense the surrounding environment to extract data, compute a given logic on this data, and communicate the data with other devices through a shared cloud. In this way, Machine-Type Communication (MTC) is the umbrella encompassing these devices with the aforementioned capabilities. Ensuring the versatility of these devices, to cover a wide range of applications that is not even imaginable, is not an easy task. To this end, the MTC nodes are usually powered by long-lasting batteries and in sometimes equipped with actuators to provide control [138]. Fostering the low cost of MTC nodes dictates their features. Limited communication capabilities, limited computation resources, and limited power consumption are amongst the most distinguishing features of such devices [139]. These features in turn give rise to a set of challenges to the large scale application of MTC. Challenges include connectivity, coverage, and security. Reported predictions assert that gigantic number of MTC nodes will connect to the cloud in order to report their measurements. Consequently, significant improvements to the connectivity procedures in both PHY and MAC layers would be required [140].

The nature of mMTC deployment scenarios suggests a set of considerations with regard to the analysis of the network performance. The limited complexity of the mMTC nodes presumes a strict maximum transmission power. This is due to the limitations on the RF chain of the mMTC nodes. Also, the limited power consumption imposed by the battery requires the consideration of a power control scheme. Moreover, power control

in the uplink is effective in mitigating the excessive interference in massive deployment scenarios. In addition, the scalable connectivity is an essential requirement in any future mMTC deployment. Thus, a dense network to collect the uplink traffic can provide seamless scalability [99]. Accordingly, the distinguishing features of dense networks must be considered in the network performance analysis.

Many challenges are facing the maturity of MTC applications including connectivity, coverage, and security. Massive numbers of MTC devices are expected to report their measurements to the network requiring the network to significantly improve the connectivity procedures in both PHY and MAC layers [140,141]. The diversity of the deployment scenarios also calls for extending the coverage of the network to reach nodes in dead zones like basements, forests, and underground facilities. Last but not least, the privacy and integrity of the exchanged information require a new vision to the security procedures especially with low complexity/cost MTC nodes.

The traffic characteristics in mMTC are a direct consequence to its inherent features [142]. In particular, the uplink traffic load is much higher than the downlink traffic which is different from the scenario of the Human-Type Communication (HTC). In some applications (e.g., smart metering), the traffic is periodic and sporadic where at any given time only a fraction of the deployed devices will be actively transmitting data. In some other scenarios (e.g., monitoring), the traffic is very low in normal conditions and bursty at the detection of events. Finally, the mobility of MTC nodes spans a wide range of speeds. In most scenarios the devices are stationary. In wearables, the mobility is moderate (e.g., like the mobility of HTC). At the other extreme (e.g., high-speed vehicular applications), MTC devices undergo very high mobility conditions.

6.2 State-of-the-Art

One of the main challenges of a cellular network serving MTC devices is the coverage. In most applications, MTC nodes transmit in the uplink. Although many coverage enhancements (CE) for the Long-Term Evolution (LTE) standard are proposed by the third generation partnership project (3GPP) [143], the uplink coverage analysis of such scenarios has not received much attention. Moreover, while network densification is a trend in both academia and industry, the significant role UDNs can play in fostering the diverse

application scenarios of MTC is often overlooked [144]. At the same time, the analytical framework of the deployment of UDNs in MTC scenarios requires a different propagation environment modelling where short-range communication links are dominant. In addition, the adoption of a power control technique in the uplink transmission of the battery-powered MTC devices is unavoidable [145].

Recently, some researchers investigated the uplink coverage in MTC scenarios (e.g., [99–102]). However, UDN characteristics (e.g., high density of small cells, short distance links, accurate path loss modeling, and general fading channels) have not been considered. Moreover, the power control of the uplink transmission from MTC devices is overlooked. In [99], the coverage performance of randomly distributed data collectors, which collect data of wireless sensors in a single-hop scenario, was investigated, and answers to the required number of data collectors, the required transmit power of the sensors, and the impact of the propagation environment were provided. However, a simple path loss model was considered and power control was not included in the system model. In [100], uplink coverage performance was addressed in a multi-hop aggregation scenario where power control was considered but not the features of UDN. Also, a simple power decay path loss was used for the sake of tractability. The power decay path loss model was adopted also in [103] which cannot fit precisely the short-range communication scenario of a UDN serving a massive MTC deployment. A Device-to-Device MTC scenario was modeled in [101] where the transmitted packets of the sensors are relayed using D2D to the serving cell. The authors in [101] adopted a power control mechanism, however, the densification of the BSs was not considered. In addition, effective capacity was investigated in ultra-reliable MTC scenario where an optimal power allocation scheme was devised for high SNR regime [102]. The authors considered a simple point-to-point scenario where neither the impact of the interference in a dense network nor the influence of power control was included in the analysis. In [2], SEPL model was adopted in the downlink of a dense network. Nevertheless, a single user per cell is considered and the uplink coverage is not investigated.

6.3 Contributions

Motivated by the challenges facing the successful deployment of mMTC, we model the uplink coverage of mMTC deployment scenario considering a UDN environment. Stochastic geometry techniques are adopted for the modelling of the scenario under investigation considering the natural randomness of the deployment of both small cells and MTC devices.

Different from previous works [2, 99–103, 146], in what follows we summarize the contributions of this investigation:

- The small-scale fading is modeled using a general $\alpha - \mu$ channel model. We then, in quest for tractable and insightful expressions, studied the special case of Rayleigh fading. More tractable results for the general $\alpha - \mu$ channel model scenario can be considered in extended versions of this investigation.

- The Stretched Exponential Path Loss (SEPL) is considered to capture the short distances in Ultra-Dense Networks (UDNs). SEPL model can be seen as a limiting case of the multi-slope model (recommended by the 3GPP LTE standard [147]) with an infinite number of slopes.

- The system model captures the impact of the system parameters which characterizes the environment of massive machine-type communications (mMTC) including the density of the MTC node λ_m, the activity ratio of the MTC nodes ρ_m, the minimum uplink transmit power P_o , and the maximum uplink transmit power P_m. Also, the model captures the impact of the system bandwidth expressed in terms of the number of resource blocks N_{RB}.

- The provided analysis reveals the significant and unexpected impact of the high density of small cells in UDNs on the maximum transmit power of the MTC nodes. This finding relaxes the requirements on the maximum transmit power which in turn allows for less complexity, brings more cost savings, and yields much longer battery life.

- This investigation provides accurate, simple, and insightful expressions. The expressions are readily readable and shows the impact of every single system parameter on the network performance allowing for guided tunability of the network.

- The results signify the asymptotic limits of the impact of all system parameters on the network performance. This allows for the efficient operation of the network by designing the system parameters which maximizes the network performance. In particular, the results show the upper bounds of the system parameters such as the density of small cells, the system bandwidth, the power truncation threshold , and the maximum transmit power where the performance saturates and no longer improves with increasing this system parameter. Accordingly, this saturation limit can be chosen as a limit for the corresponding system parameter.

6.4 System Model

In this section, we present the aspects of the considered system model.

6.4.1 Network Model

We consider the uplink transmission of measurement reports and readings of mMTC nodes in IoT applications. A UDN comprised of a surplus of small cells is assumed to collect the transmitted data from the MTC nodes. Using stochastic geometry [104], the BSs of the UDN are modeled as a Homogeneous Poisson Point Process (HPPP), Φ_s, with a density λ_s which is independent of the MTC nodes. MTC nodes are modeled as independent HPPP, Φ_m, with a density of λ_m. The characteristics of the traffic in IoT applications suggest a sporadic nature with a long duty cycle. Accordingly, only a fraction $\rho_m \in [0, 1]$ of the MTC nodes is assumed to be active and transmitting data at any given time. In general, ρ_m is a random variable and can be modeled by the Beta distribution $Beta(x, y)$ where $x = 3$ and $y = 4$ [142]. Due to the complexity constraints on the mMTC nodes, each node is equipped with a single antenna. A node is associated to the BS with the strongest average received power, i.e., the closest BS.

6.4.2 Propagation Model

The considered propagation environment consists of two components: large-scale fading component modeled by a stretched exponential path loss (SEPL) and a small-scale multi-path fading component modeled by $(\alpha - \mu)$ channel fading model [148]. In the SEPL model [2], the transmit signal power decays with the distance r as $e^{-ar^{\beta}}$. The SEPL model

accurately captures the signal propagation properties in UDN environments featuring short distances (5m − 350m) between the (serving/interfering) BSs and the associated users [149]. A recent study shows that the SEPL model fits accurately to the propagation environment in UDNs (e.g., see [2, Table I] where a comprehensive survey of several path loss models is provided). The parameters of the SEPL model, i.e., (a and β), are used to tune the model to capture different propagation scenarios. In particular, this model describes propagation environments where obstructions are the main cause of attenuation, with a being the average multiplicative attenuation, and r^{β} represents the scaling of the number of obstructions in the bath [2]. Interestingly, the special values of (a and β) given by (0.3 and 2/3) and (0.94 and 1/2) provide limiting cases of the multi-slope propagation which is a piecewise propagation model with accurate results confirmed by measurements. Accordingly, this model is adopted by the 3GPP standardization community [150].

The $\alpha-\mu$ distribution is a general fading model which includes many important fading models as special cases, namely, Gamma distribution, Nakagami-m distribution, Weibull distribution, Rayleigh distribution, and Rician distribution. The Cumulative Distribution Function (CDF) of the fading channel gain is given by:

$$F_X(x) = \frac{\gamma(\mu, \mu x^{\alpha/2})}{\Gamma(\mu)}, \tag{6.1}$$

where $\Gamma(n) = \int_0^{\infty} t^n e^{-t} \mathrm{d}t$ is the gamma function, and for integer positive n, $\Gamma(n) = (n-1)!$ and $\gamma(n, x) = \int_0^{x} t^n e^{-t} \mathrm{d}t$ is the lower incomplete gamma function. In Table 6.1 some special cases of the $\alpha - \mu$ distribution are presented.

Table 6.1: Special Cases of $\alpha - \mu$ Distribution

α	μ	distribution
α	1	Weibull
2	1	Rayleigh
2	m	Nakagami-m
2	1/2	one-sided Gaussian
2	$\frac{(K+1)^2}{2K+1}$	Rician

Denote by h_o the fading channel gain of the useful signal link between the mMTC

node and the serving BS, which is modeled using the general $\alpha - \mu$ distribution. Also, denote by h_u the fading channel gain of the interfering nodes connecting to other cells which is modeled as a Rayleigh fading channel. We assume that the channel fading gains of all interfering nodes are independent and identically distributed (i.i.d), i.e., channel gains are independent of each other and independent of the locations of the nodes.

It is worth mentioning that shadowing is not considered in this investigation where we focus on the impact of the UDN system parameters, the power control parameters, and the IoT deployment scenario on the system performance.

6.4.3 Power Control Model

Each MTC node transmits in the uplink with a maximum power P_m to satisfy the limited transmission power constraints. The nodes employ a truncated channel inversion (TCI) power control policy. In TCI power control, a node transmits with a power P where the setting of the power takes into consideration the path loss in order to invert the channel with a truncation cutoff threshold set to P_o, with $P_o > P_{sensitivity}$ being the average received power at the BS and $P_{sensitivity}$ being the minimum received power of the BS. In other words, if the transmit power required to invert the channel exceeds the maximum transmit power P_m, the MTC node is considered to be in a power control outage. Accordingly, the setting of the uplink transmit power in each MTC nodes is given by:

$$P = \begin{cases} P_o e^{ar^\beta} & \text{if } \; P_o \leq P_o e^{ar^\beta} \leq P_m, \\ 0 & \text{otherwise.} \end{cases} \tag{6.2}$$

Practically, the MTC node estimates the path loss to the serving cell e^{ar^β} through measuring the reference signals' received power and by knowing the reference signals' transmission power from the system information sent on the control channels [145]. In addition, the power control parameters P_o and P_m are known parameters where P_o is broadcasted on the control channel of the serving cell and P_m is a design parameter of the MTC nodes. Interestingly, the 3GPP LTE standard adopted another power control scheme where no truncation occurs [145]. In other words, the setting of the power $P = \min(P_o e^{ar^\beta}, P_m)$ takes place. In this investigation, we adopted the TCI power control scheme for the sake of tractability. However, we provide the power control outage for both techniques in Section 6.5.1 and show in the simulation results' section that there is

no difference between the two power control schemes in terms of the power control outage.

Due to the randomness of the locations of both the serving cells and the connected MTC devices, the link distances in both the main links and the interfering links are all random. Consequently, the transmit power P of any given MTC node can be modelled by a random variable which ranges from P_o to P_m. Section 6.5.1 is devoted to studying the statistical properties of this random quantity which plays a main role in the coverage performance of the network which is then investigated in Section 6.5.2.

6.4.4 Interference Model

We assume that each BS has N_{RB} uplink orthogonal resource blocks (RBs), each of a bandwidth B_{RB} where a node transmits its data using only one resource block at any given time. The MTC node selects an orthogonal resource randomly in a uniformly distributed manner from the N_{RB} resources with a probability of $1/N_{RB}$. Furthermore, MTC nodes transmit to the small cells using time slotted Random Access CHannel (RACH). This is more suitable to model the uplink transmission traffic, that is sporadic in nature, from a massive number of nodes [141]. Accordingly, we assume that the interference generated from mMTC nodes connecting to the same BS (i.e., intra-cell interference) is perfectly mitigated via advanced physical and access layer techniques. These techniques are tailored to the specific requirements of mMTC deployment scenarios (e.g., see the techniques discussed in [141]). In other words, only the inter-cell interference is accounted for in the analysis, and further analysis of the system considering the intra-cell interference is left for future investigation. Moreover, the inter-cell interference from each node on the tagged channel at the tagged BS is restricted to be less than P_o. This can be explained considering the assumed association criteria. Since each node is connected to the nearest BS, and the transmission power is adjusted such that the received power at the serving cell is P_o, consequently, the received interference at any BS will be upper bounded by P_o as illustrated in Fig. 6.1.

6.4.5 Communication Model

We differentiate between two categories of MTC services, namely, massive MTC and critical MTC [151]. This investigation focuses on the massive MTC. MTC nodes communicate their message to the network in three different ways: (i) direct communication

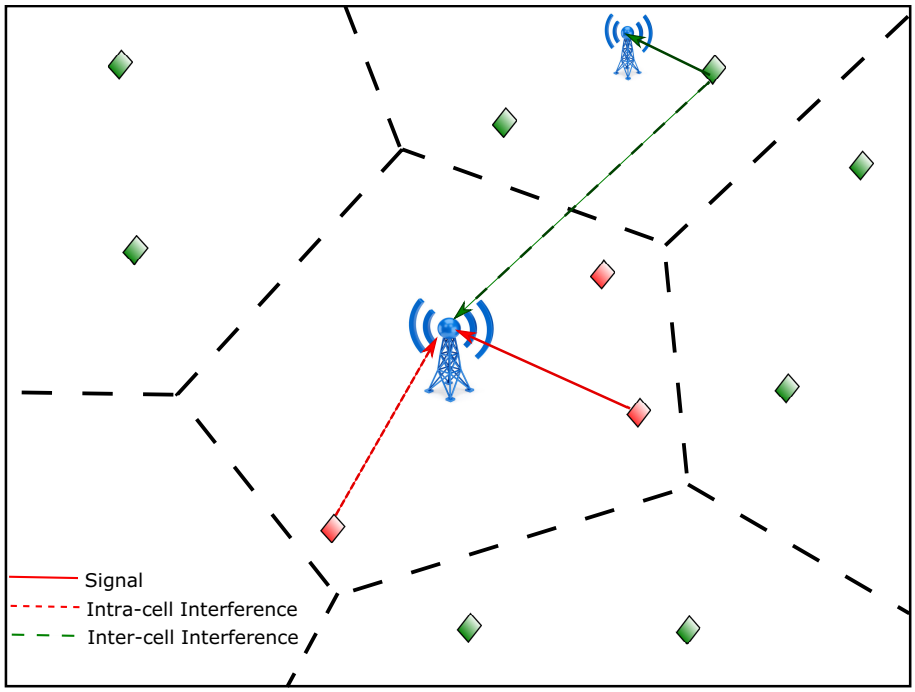

Figure 6.1: The interference from the nodes in the same cell is handled via advanced PHY layer and MAC layer techniques. Thus, we consider only the inter-cell interference which is limited to be less than P_o from each node due to the employed power control technique.

mMTC-D in which the node connects directly to the BS, (ii) aggregation mode mMTC-A where an MTC node or an HTC user aggregates the traffic and transmits to the BS, and (iii) device-to-device mode where an MTC node connects to another MTC node and transfers its message to it [139]. Particularly, in this investigation, we focus on the direct communication mode mainly because in UDNs, due to the high density of BSs, the direct communication mode is the most attractive scenario where plenty of small cells are deployed and ready to collect the traffic of the mMTC nodes [99].

6.4.6 Uplink Coverage

The harsh deployment conditions of the mMTC nodes in most applications call for coverage enhancements. Extended coverage of $15 - 20$ dB is an essential requirement of the 3GPP LTE standard Release 14 [145] and former releases. At the same time, it is desirable to minimize the transmission power of the mMTC nodes aiming at longer battery-life. These contradicting targets make the uplink coverage one of the main limiting factors to the fruition of mMTC wide deployment [139]. One can define coverage as the fraction of nodes that experience a signal with a given quality measured in terms of the signal to

interference-plus-noise ratio (SINR) or the fraction of time a given node experience the aforementioned signal quality. Supported by the above discussion, we consider the uplink coverage as the performance metric in this investigation.

The SINR of the signal received at the typical BS located at the origin from the tagged node is given by:

$$\texttt{SINR} = \frac{P_o h_o}{\sigma^2 + \mathcal{I}}, \tag{6.3}$$

where σ^2 is the noise power, and $\mathcal{I}$ is the aggregate interference on the tagged resource block in the uplink. This aggregate interference $\mathcal{I}$ is expressed as:

$$\mathcal{I} = \sum_{u \in \bar{\Phi}_m / u_o} P_u h_u e^{-a r_u^{\beta}} \mathbb{1}(P_u e^{-a r_u^{\beta}} < P_o), \tag{6.4}$$

with P_u being the transmission power from node u, h_u is the channel fading gain, and $\bar{\Phi}_m$ is the set of all interfering nodes transmitting on the tagged resource block and interfering with the transmission of the tagged MTC node u_o from outside its serving cell. Also, $\mathbb{1}(\cdot)$ is the indicator function which takes the value 1 if the argument $(\cdot)$ is true and zero otherwise. Here, the uplink coverage probability is defined as:

$$\mathcal{P}_{cov} = \mathbb{P}\left\{\texttt{SINR} > \tau\right\}, \tag{6.5}$$

with τ being the SINR threshold where it represents the SINR at which the uplink transmitted signal of an MTC device can be decoded successfully at the BS providing a predetermined level of Quality-of-Service (QoS).

6.5 Analytical Results

6.5.1 Power Control Outage

The transmission power of an active mMTC undergoes a truncated channel inversion (TCI) power control. In TCI power control, a node is declared in power outage if the required transmission power is greater than the available maximum transmission power P_m [103]. The transmission power of a node is thus adjusted such that the received power at the serving BS is P_o, i.e., the cutoff threshold. In accordance, the transmission power P of any active mMTC node is a random variable where $P \in [P_o, P_m]$. The transmission power P_o corresponds to a node which is very close to the BS, i.e., $r \sim 0$, while the transmission power P_m corresponds to the farthest node a BS can serve.

In this section, we characterize the statistical properties of the transmission power P. We provide the probability distribution function (PDF) of the transmission power and the expectation of the log-relative-power defined as $\ln\left(\frac{P}{P_o}\right)$ which appears in the expressions of the coverage probability in the next section.

A given mMTC node is declared in truncation outage if the transmission power required to reach the closest BS exceeds the available maximum transmission power P_m. Accordingly, the outage probability due to the power truncation forced by the power control mechanism can be computed as:

$$\mathcal{O}_{power} = \mathbb{P}\left\{r > r_m\right\}. \tag{6.6}$$

Since the transmission power at a given distance r is $P = P_o e^{ar^\beta}$, MTC node experience outage due to power truncation if the required power to transmit is more than the maximum available transmission power P_m or equivalently, the node is at a distance farther than r_m where $r_m = \ln^{\frac{1}{\beta}}\left(\frac{P_m}{P_o}\right)^{\frac{1}{a}}$. Since the CDF of r is $F_R(r) = 1 - e^{-\pi\lambda_s r^2}$ [58], hence, the power truncation outage probability can be expressed as:

$$\begin{aligned}\mathcal{O}_{power} &= \mathbb{P}\left\{r > r_m\right\} = 1 - \mathbb{P}\left\{r < r_m\right\} \\ &= 1 - \left(1 - e^{-\pi\lambda_s r_m^2}\right) \\ &= e^{-\pi\lambda_s r_m^2}.\end{aligned} \tag{6.7}$$

The power truncation outage $\mathcal{O}_{power}$ is a fundamental element of the coverage analysis. It represents the probability that a node is in a coverage hole due to insufficient transmission power. Obviously, this quantity is a function of the BSs density λ_s, the path loss model parameters (a and β), and the power control parameters (P_o and P_m). Considering the no-truncation power control scheme, the power control outage can be expressed as:

$$\begin{aligned}\mathcal{O}_{nt} &= \mathbb{P}\left\{h_o P_m e^{-ar^\beta} < P_o\right\} \\ &= 1 - \int_0^\infty 2\pi\lambda_s e^{-\pi\lambda_s r^2} e^{-(P_o/P_m)e^{ar^\beta}} \mathrm{d}r.\end{aligned} \tag{6.8}$$

In the next Lemma, we provide the conditional probability distribution function of the transmission power of the mMTC nodes considering the case of no power truncation outage. Remarkably, the analysis performed in this investigation considers a generic

active user which has data to transmit and do not experience outage due to insufficient transmission power.

Lemma 1. *The PDF of the uplink transmission power P of a generic active mMTC node associated to the nearest BS in a UDN environment considering a truncated channel inversion power control is expressed as:*

$$f_P(x) = \frac{2\pi\lambda_s \ln^{\frac{2}{\beta}-1}\left(\frac{x}{P_o}\right)^{\frac{1}{a}}}{a\beta x\left(1-\mathcal{O}_{power}\right)} e^{-\pi\lambda_s \ln^{\frac{2}{\beta}}\left(\frac{x}{P_o}\right)^{\frac{1}{a}}}. \tag{6.9}$$

Proof. Considering the employed power control mechanism, the transmit power $P = P_o e^{ar^\beta}$ of any active MTC device is a function of the link distance r to the serving BS where $P \in [P_o, P_m]$. Accordingly, the CDF of the transmission power P can be expressed as:

$$\begin{aligned} F_P(x) &= \mathbb{P}\left\{P \leq x\right\} = \mathbb{P}\left\{P_o e^{ar^\beta} \leq x\right\} \\ &= \mathbb{P}\left\{r \leq \ln^{1/\beta}\left(\frac{x}{P_o}\right)^{1/a}\right\} \\ &= F_R\left(\ln^{1/\beta}\left(\frac{x}{P_o}\right)^{1/a}\right). \end{aligned} \tag{6.10}$$

Considering the CDF of r, the truncated CDF of P can be written as:

$$F_P(x) = \frac{1-e^{-\pi\lambda_s \ln^{2/\beta}\left(\frac{x}{P_o}\right)^{1/a}}}{1-e^{-\pi\lambda_s \ln^{2/\beta}\left(\frac{P_m}{P_o}\right)^{1/a}}}, \tag{6.11}$$

and hence, the PDF of P can be written as:

$$\begin{aligned} f_P(x) &= \frac{dF_P(x)}{dx} \\ &= \frac{2\pi\lambda_s \ln^{\frac{2}{\beta}-1}\left(\frac{x}{P_o}\right)^{\frac{1}{a}}}{a\beta x\left(1-\mathcal{O}_{power}\right)} e^{-\pi\lambda_s \ln^{\frac{2}{\beta}}\left(\frac{x}{P_o}\right)^{\frac{1}{a}}}. \end{aligned} \tag{6.12}$$

This completes the proof. ■

Having computed the PDF of the transmission power P, we can proceed in the analysis by evaluating the moments of the log-relative-power. This result is given in the next Lemma and will be used in the coverage analysis provided in the next section.

Lemma 2. *The conditional expectation of the function* $\ln^k(P/P_o), k \in \{0, 1, 2, \cdots\}$ *is given by:*

$$\mathbb{E}_P\left[\ln^k(P/P_o)\right] = \frac{a^k \gamma\left(\frac{\beta k}{2}+1, \pi\lambda_s r_m^2\right)}{(\pi\lambda_s)^{\frac{\beta k}{2}}\left(1-\mathcal{O}_{power}\right)}. \tag{6.13}$$

Proof. The expectation of the function $\ln^k(P/P_o)$ can be expressed as:

$$\begin{aligned}
&\mathbb{E}_P\left[\ln^k(P/P_o)\right] \\
&= \int_{P_o}^{P_m} \ln^k(x/P_o) f_P(x|P_o \le P \le P_m)\mathrm{d}x && (6.14)\\
&\overset{a}{=} \frac{2\pi\lambda_s}{a\beta\left(1-\mathcal{O}_{power}\right)} \int_0^{\delta} (aw)^k w^{2/\beta-1} e^{-\pi\lambda_s w^{2/\beta}}\mathrm{d}w && (6.15)\\
&\overset{b}{=} \frac{a^k \gamma\left(\frac{\beta k}{2}+1, \pi\lambda_s r_m^2\right)}{(\pi\lambda_s)^{\frac{\beta k}{2}}\left(1-\mathcal{O}_{power}\right)}, && (6.16)
\end{aligned}$$

where step (a) is the result of the change of variables $x = P_o e^{aw}$ and $\delta = r_m^{\beta}$. Step (b) follows from simple manipulation and evaluating the integral. ■

The log-relative-power in Lemma 2 is a measure of the transmission power relative to the cutoff threshold P_o. The expected transmission power is thus scaled by the power coverage (i.e., $1 - \mathcal{O}_{power}$). Hence, a higher transmission power at the MTC nodes is required as the power truncation outage increases. At the same time, as the BSs density increases, the expected transmission power decreases. This is intuitive where a higher BSs density means a shorter distance between MTC node and its serving BS, and hence, a less power to invert the channel.

6.5.2 Uplink Coverage of Direct Communication Mode

In this section, we analyze the uplink coverage in the direct communication model. In the next theorem, we provide the general results for a generic $\alpha - \mu$ fading channel.

Theorem 1. *The uplink coverage of an active MTC node transmitting in the uplink in the direct mode communication model and considering the system model in Section 6.4 is given by:*

$$\mathcal{P}_{cov} = 1 - \mathbb{E}_{\mathcal{I}}\left[\frac{\gamma\left(\mu, \Upsilon\right)}{\Gamma(\mu)}\right], \tag{6.17}$$

and in the special case $\mu \in \mathbb{Z}^+$,

$$\mathcal{P}_{cov} = \mathbb{E}_{\mathcal{I}} \left[e^{-\Upsilon} e_{\mu-1} (\Upsilon) \right], \tag{6.18}$$

where:

$$\Upsilon = \left(\frac{\tau}{P_o} \right)^{\alpha/2} (\sigma^2 + \mathcal{I})^{\alpha/2} \mu, \tag{6.19}$$

and $e_n(x) = 1 + x + x^2/2! + \cdots + x^n/n!, n = 0, 1, 2, \cdots$, *are the partial sums of the exponential series.*

Proof. Commencing from the definition of the uplink coverage,

$$\begin{aligned} \mathcal{P}_{cov} &= \mathbb{P}\left\{ \texttt{SINR} > \tau \right\} = 1 - \mathbb{P}\left\{ \texttt{SINR} < \tau \right\} \\ &= 1 - \mathbb{P}\left\{ h_o < \frac{\tau}{P_o} (\sigma^2 + \mathcal{I}) | \mathcal{I} \right\} \\ &\overset{a}{=} 1 - \mathbb{E}_{\mathcal{I}} \left[\frac{\gamma\left(\mu, (\frac{\tau}{P_o})^{\alpha/2} (\sigma^2 + \mathcal{I})^{\alpha/2} \mu \right)}{\Gamma(\mu)} \right], \end{aligned} \tag{6.20}$$

where (a) follows from the CDF of the $\alpha - \mu$ distribution given in (6.1). Considering the identity $\gamma(n+1, x) = n! \left[1 - e^{-x} e_n(x) \right]$ for $n \in \mathbb{Z}^+$ [152, Eq. 1.2], the coverage probability in (6.18) can be obtained: ■

Evidently, the expression of the uplink coverage in Theorem 1 is intractable. Notwithstanding this tractability limitation, the above analysis provides an entry level for considering a general channel fading in the considered investigation. In quest of tractable results, we derive insightful expressions for the uplink coverage in the special case $\alpha = 2, \mu = 1$ corresponding to Rayleigh fading in the following Theorem.

Theorem 2. *The uplink coverage probability of an active mMTC node in a UDN environment satisfying the system model in Section 6.4, and considering the special case for the* $\alpha - \mu$ *distribution where* $\alpha = 2, \mu = 1$ *which corresponds to Rayleigh fading is given by:*

$$\mathcal{P}_{cov} = e^{\frac{-\tau}{\texttt{SNR}}} \mathcal{L}_I(\frac{\tau}{P_o}), \tag{6.21}$$

where

$$\mathcal{L}_I(\frac{\tau}{P_o}) = \exp\left\{ - \left(\frac{2\pi}{\beta a^{2/\beta}} \right) \left(\frac{\rho_m \lambda_m}{N_{RB}} \right) \Xi \right\}, \tag{6.22}$$

and

$$\Xi = \mathbb{E}_P \left[\int_0^{\tau} \frac{[\ln(P/P_o) + \ln(\tau/y)]^{\frac{2}{\beta}-1}}{y+1} \mathrm{d}y \right], \tag{6.23}$$

and $\mathtt{SNR} = P_o/\sigma^2$ *is the signal-to-noise ratio at the BS receiver.*

Proof. We begin by substituting the special values $\alpha = 2, \mu = 1$ in (6.18), this yields to:

$$\mathcal{P}_{cov} = \mathbb{E}_{\mathcal{I}} \left[\exp\left\{ -(\frac{\tau}{P_o})(\sigma^2 + \mathcal{I}) \right\} \right] = e^{\frac{-\tau}{\mathtt{SNR}}} \mathcal{L}_I(\frac{\tau}{P_o}) \tag{6.24}$$

The Laplace Transform (LT) of the aggregate uplink interference $\mathcal{I}$ is expressed as:

$$\begin{aligned}
&\mathcal{L}_I(s) = \mathbb{E}_{\mathcal{I}} \left[e^{-s\mathcal{I}} \right] \\
&= \mathbb{E} \left[\exp\left\{ -s \sum_{u \in \bar{\Phi}_m / u_o} P_u h_u e^{-a r_u^{\beta}} \mathbb{1}(P_u e^{-a r_u^{\beta}} < P_o) \right\} \right] \\
&\overset{a}{=} \mathbb{E}_{\bar{\Phi}_m} \left[\prod_{u \in \bar{\Phi}_m / u_o} \mathbb{E}_{P_u, h_u} \left[\exp\left\{ -s P_u h_u e^{-a r_u^{\beta}} \right\} \mathbb{1}(P_u e^{-a r_u^{\beta}} < P_o) \right] \right] \\
&\overset{b}{=} \exp\left\{ -2\pi \frac{\rho_m \lambda_m}{N_{RB}} \mathbb{E}_{P,h} \left[\int_{\ln^{\frac{1}{\beta}}(\frac{P}{P_o})^{\frac{1}{a}}}^{\infty} \left(1 - e^{-sPhe^{-ar^{\beta}}} \right) r \mathrm{d}r \right] \right\} \\
&\overset{c}{=} \exp\left\{ -2\pi \frac{\rho_m \lambda_m}{N_{RB}} \mathbb{E}_{P} \left[\int_{\ln^{\frac{1}{\beta}}(\frac{P}{P_o})^{\frac{1}{a}}}^{\infty} \left(1 - \frac{1}{1 + sPe^{-ar^{\beta}}} \right) r \mathrm{d}r \right] \right\} \\
&\overset{d}{=} \exp\left\{ \left(\frac{-2\pi \rho_m \lambda_m}{\beta a^{2/\beta} N_{RB}} \right) \mathbb{E}_P \left[\int_0^{sP_o} \frac{\left[\ln(\frac{sP}{y}) \right]^{\frac{2}{\beta}-1}}{y+1} \mathrm{d}y \right] \right\}
\end{aligned} \tag{6.25}$$

Now, we substitute for $s = \frac{\tau}{P_o}$ to obtain

$$\mathcal{L}_I(\frac{\tau}{P_o}) = \exp\left\{ -\left(\frac{2\pi}{\beta a^{2/\beta}} \right) \left(\frac{\rho_m \lambda_m}{N_{RB}} \right) \Xi \right\} \tag{6.26}$$

The set $\bar{\Phi}_m$ is a thinned version of the HPPP Φ_m with a thinning factor ρ_m / N_{RB}, where ρ_m is the fraction of MTC nodes with data to transmit and $1/N_{RB}$ is the probability of any orthogonal channel in the system to be the tagged channel. The interference power P_u received at the tagged BS serving the tagged node u_o from a given node u is restricted to be less than P_o. This is a consequence of the considered association criteria and the employed power control scheme.

We assume that the transmission power from all interfering nodes are independent. Indeed, this assumption can be justified considering the special features of UDN where the variance in the cell sizes vanishes as the density of the BSs increases. (a) follows from the independence of the transmission powers P_u, the fading channel gains h_u, and the PPP Φ_m. (b) follows from the probability generating functional (PGFL) of the PPP [105]. The integral limits in (b) consider the region where the interfering nodes reside. Since the interference power (i.e., Pe^{-ar^β}) is always less than the power truncation cutoff threshold P_o, the interfering nodes are thus located in an open disk with inner radius $r_i = \ln^{\frac{1}{\beta}}(\frac{P}{P_o})^{\frac{1}{a}}$ and outer radius at ∞. Step (c) follows from the LT of the fading gain h and finally, (d) results from the change of variables $y = sPe^{-ar^\beta}$. This completes the proof.

■

The simplified expression of the average coverage probability in (6.21) provides many insights into the network performance. Apparently, this expression is composed of two items: the exponential term $e^{\frac{-\tau}{\mathtt{SNR}}}$ which represents the noise, and the Laplace Transform (LT) term $\mathcal{L}_I(\frac{\tau}{P_o})$ representing the interference. Recall the definition of the SNR, $\mathtt{SNR} = P_o/\sigma^2$, where the power control truncation threshold P_o is the sole system parameter tuning this value. As P_o increases (i.e., a higher truncation threshold), this exponential term increases and approaches its maximum value of one asymptotically leaving the control to the LT term. One can notice that the uplink coverage performance has two regions: one region is limited by noise where the noise term dominates the coverage performance and the other is limited by interference where the interference term prevails. The border between the two regions is thus determined by the power control truncation threshold P_o. Further discussions and more deep insights regarding the uplink coverage will be discussed in the simulation results' section.

An interesting special case of the above result can be obtained by considering the special value $\beta = \frac{2}{n+1}$ with n being any non-negative integer. This special case covers a wide range of β (e.g., $\beta = 2, 1, \frac{2}{3}, \frac{1}{2}, \frac{1}{3}, \cdots$). In particular, the special values of $\beta = \frac{1}{2}$ and $\beta = \frac{2}{3}$ provide limiting cases for the multi-slope propagation model, which is recommended by the 3GPP LTE standard [147]), with an infinite number of slopes. Besides, these special values match the physical measurements of the communication links in a UDN environment, i.e., short-distance links [2]. Considering this practical special case, in the following Corollary, simpler expressions can be derived where insightful conclusions can

be obtained.

In the following Corollary, we study a special case for the path loss model parameter β. We consider the special case $\beta = \frac{2}{n+1}$ with n being any non-negative integer. This special case covers a wide range of β (e.g., $\beta = 2, 1, \frac{2}{3}, \frac{1}{2}, \frac{1}{3}, \cdots$) which resembles a multi-slope propagation model [2]. Moreover, the considered range of values in this special case matches physical measurements for the short-range communication links [2]. Given the practicality of the examined special case, simpler expressions can be derived where insightful conclusions can be obtained.

Corollary 1. *Considering the special case $\beta = \frac{2}{n+1}$ where $n \in \mathbb{Z}$ is any non-negative integer, Theorem 2 can be simplified to:*

$$\mathcal{P}_{cov} = e^{\frac{-\tau}{SNR}} \mathcal{L}_I \left(\frac{\tau}{P_o} \right), \tag{6.27}$$

$$\mathcal{L}_I \left(\frac{\tau}{P_o} \right) = \prod_{k=0}^{n} \exp \left\{ -\xi(n) \binom{n}{k} \mathbb{E}_P \left[\ln^k \left(\frac{P}{P_o} \right) \right] \mathcal{J}_{n-k}(\tau) \right\}, \tag{6.28}$$

where

$$\mathcal{J}_v(\tau) = \int_0^{\tau} \frac{\ln^v(\tau/y)}{y+1} \mathrm{d}y, \tag{6.29}$$

$$\xi(n) = \frac{(n+1)\pi \rho_m \lambda_m}{a^{n+1} N_{RB}}, \tag{6.30}$$

and $\mathbb{E}_P[\ln^k(P/P_o)]$ is given in Lemma 2.

Proof. We begin by computing the expectation in (6.26) considering the special value $\beta = \frac{2}{n+1}$,

$$\begin{aligned} &\mathbb{E}_P \left[\int_0^{\tau} \frac{[\ln(P/P_o) + \ln(\tau/y)]^n}{y+1} \mathrm{d}y \right] = \\ &\overset{a}{=} \int_0^{\tau} \frac{\sum_{k=0}^{n} \binom{n}{k} \mathbb{E}_P[\ln^k(P/P_o)] \ln^{n-k}(\tau/y)}{y+1} \mathrm{d}y \\ &\overset{b}{=} \sum_{k=0}^{n} \binom{n}{k} \mathbb{E}_P[\ln^k(P/P_o)] \int_0^{\tau} \frac{\ln^{n-k}(\tau/y)}{y+1} \mathrm{d}y, \end{aligned} \tag{6.31}$$

(a) follows from applying the binomial theorem and (b) follows by a simple arrangement of terms and change of the order of summation and integration. The proof is completed by substituting (6.31) in (6.25). ■

By carefully examining the uplink coverage expression in Corollary 1, it can be concluded that the coverage performance improves as the number of orthogonal resources N_{RB} increases. Also, the performance deteriorates as either the density of the MTC devices λ_m or the device activity ρ_m increases. Further, as the BSs density λ_s increases the coverage performance improves. Furthermore, one can expect the saturation of the performance with the increasing number of radio resources, the higher density of BSs, or the higher power control cutoff, by considering that at some point the system becomes a noise-limited system rather than an interference-limited system.

In quest of a more simplified result, a closed-form expression for the coverage probability is derived considering a special case of the SEPL parameter at $\beta = 2$, we present this result in the following Corollary.

Corollary 2. *Considering the special case $\beta = 2$, Theorem 2 can be further simplified to:*

$$\mathcal{P}_{cov} = e^{-\left(\frac{\tau}{SNR} + \xi(0)\ln(1+\tau)\right)}. \tag{6.32}$$

Proof. The expectation in (6.23) considering the special value $\beta = 2$ can be simplified to,

$$\Xi = \mathbb{E}_P\left[\int_0^{\tau} \frac{\left[\ln(P/P_o) + \ln(\tau/y)\right]^{\frac{2}{\beta}-1}}{y+1}\mathrm{d}y\right] =$$

$$= \int_0^{\tau} \frac{1}{y+1}\mathrm{d}y = \ln(1+\tau), \tag{6.33}$$

Substituting (6.33) in (6.26) and setting $\beta = 2$ the proof is completed. ■

Finally, one more simplification of the presented analysis can be done by averaging the uplink coverage probability over all values of the mMTC activity probability ρ_m. This considers the statistical properties of the activity probability and yields the average coverage performance for a general mMTC deployment without the need to estimate the individual activity probability for each case. In the following Corollary, we present this result.

Corollary 3. *The uplink coverage probability in Corollary 1 averaged over all values of ρ_m can be expressed as:*

$$\hat{\mathcal{P}}_{cov} = \frac{e^{\frac{-\tau}{SNR}}}{B(3,4)\mathcal{G}^6} \times$$

$$\left[\left(6\mathcal{G}^2 + 48\mathcal{G} + 120\right)e^{-\mathcal{G}} + \left(2\mathcal{G}^3 - 18\mathcal{G}^2 + 72\mathcal{G} - 120\right)\right] \tag{6.34}$$

where:

$$\mathcal{G} = \sum_{k=0}^{n} \binom{n}{k} \left(\frac{(n+1)\pi\lambda_m}{a^{n+1} N_{RB}} \right) \mathbb{E}_P[\ln^k(P/P_o)] \ \mathcal{J}_{n-k}(\tau) \tag{6.35}$$

and $B(x,y) = \frac{\Gamma(x)\Gamma(y)}{\Gamma(x+y)}$ *is the beta function*

Proof. Due to the sporadic nature of the traffic in mMTC, only a fraction $\rho_m \in [0,1]$ of the entire population of the mMTC nodes will be active and transmitting at any given time. Generally, ρ_m is a random variable and can be modeled by the Beta distribution $Beta(x,y)$ where $x=3$ and $y=4$ [142]. By rearranging the terms in (6.28), the average probability of coverage $\hat{\mathcal{P}}_{cov}$ can be written as

$$\begin{aligned} \hat{\mathcal{P}}_{cov} &= \mathbb{E}_{\rho_m}\{\mathcal{P}_{cov}\} = \mathbb{E}_{\rho_m}\left\{ e^{\frac{-\tau}{\text{SNR}}} e^{-\rho_m \mathcal{G}} \right\} \\ &= e^{\frac{-\tau}{\text{SNR}}} \int_0^1 e^{-x\mathcal{G}} f_{\rho_m}(x) \mathrm{d}x \\ &= e^{\frac{-\tau}{\text{SNR}}} \int_0^1 e^{-x\mathcal{G}} \frac{1}{B(3,4)} x^2 (1-x)^3 \mathrm{d}x \end{aligned} \tag{6.36}$$

By evaluating the integral in (6.36), we arrive at the result of the Corollary. This completes the proof. ■

6.6 Simulation Results

In this section, we assess the accuracy of the analytical results when compared to simulations. We present numerical results considering a wide range of the system parameters including BSs density, mMTC devices density and activity ratio, maximum available transmission power, power truncation cutoff threshold, parameters of the path loss model, and the number of orthogonal resource blocks. We realize the considered scenario by the generation of Homogeneous Poisson Point Process (HPPP) corresponding to the densities of the BSs and the mMTC devices along with the activation probability. A simulation area of 1 km^2 is considered where we generated 1000 spatial realizations of the PPP. Moreover, the channel variations are simulated by a realization of a 100 time slots drawn from an exponential random variable with a mean of one. We consider a BS density of

$\lambda_s = 1000$ cells/km^2, a coverage threshold of $\tau = 0$ dB, power truncation cutoff threshold of $P_o = -100$ dBm, a maximum transmission power $P_m = 20$ dBm, an mMTC activation probability of $\rho_m = 0.1$, and SEPL parameters of $a = 0.94, \beta = 0.5$. Furthermore, we assume that the number of available resource blocks for each BS is $N_{RB} = 100$ and each MTC device is allocated only one resource block with a bandwidth of 180 kHz, thus the noise power $\sigma^2 = -121.45$ dBm.

6.6.1 Simulation Setup

In this section, we assess the accuracy of the analytical results when compared to simulations. We present numerical results considering a wide range of the system parameters including BSs density, mMTC devices density and activity ratio, maximum available transmission power, power truncation cutoff threshold, parameters of the path loss model, and the number of orthogonal resource blocks. We realize the considered scenario by the generation of Homogeneous Poisson Point Process (HPPP) corresponding to the densities of the BSs and the mMTC devices along with the activation probability. A square simulation area of 1 km $\times$ 1 km = 1 km^2 is considered where we generated 1000 spatial realizations of the PPP. Moreover, the channel variations are simulated by a realization of a 100 time slots drawn from an exponential random variable with a mean of one. We consider a BS density of $\lambda_s = 1000$ cells/km^2, a coverage threshold of $\tau = 0$ dB, power truncation cutoff threshold of $P_o = -100$ dBm, a maximum transmission power $P_m = 20$ dBm, an mMTC activation probability of $\rho_m = 0.1$, and SEPL parameters of $a = 0.94, \beta = 0.5$. Furthermore, we assume that the number of available resource blocks for each BS is $N_{RB} = 100$ and each MTC device is allocated only one resource block with a bandwidth of 180 kHz, thus the noise power $\sigma^2 = -121.45$ dBm.

We consider the following simulation procedure to simulate the network environment modeled in this investigation.

1. A number of BSs is generated following a Poisson distribution with density λ_s BSs/km^2 and distributed uniformly in the simulation area. We consider a high density of the small cells as a feature of the dense networks.

2. A number of active MTC devices is generated in the same simulation area as well. The locations of the active MTC devices follow a Poisson distribution with den-

sity $\rho_m \lambda_m$ devices/km^2. Similarly, the devices are distributed uniformly over the simulation area.

3. Each active MTC device is associated to the nearest BS and randomly allocated an orthogonal resource block from the available resource blocks N_{RB}.

4. An MTC is considered in power control outage if the required transmission power exceeds the maximum transmit power P_m.

5. Independent channel gains are generated for the links between all active devices and their serving BSs and drawn from an exponential distribution with mean one.

6. The uplink SINR of the link between each active device and its tagged BS is computed.

7. The realization of the BSs and devices PPP is repeated N_m times and the generation of the independent fading channels is repeated for N_t time slots. In the simulations, we have considered $N_m = 1000$ and $N_t = 100$.

8. As a last step, the average coverage for the respective links between the active MTC devices and the tagged BSs is calculated as $P_{avg} = \frac{1}{N_m N_t} \sum_{m=1}^{N_m} \sum_{t=1}^{N_t} \mathbb{1}(\mathtt{SINR}_{m,t} > \tau)$.

6.6.2 Power Control Outage

Fig. 6.2 depicts the power control outage for the TCI power control scheme adopted in this investigation and the no-truncation power control scheme. Interestingly, the power control outage of both schemes is indistinguishable. The parameters controlling this quantity includes the BSs density λ_s, the path loss model parameters (a and β), and the power control parameters (P_o and P_m). Notably, this outage vanishes at low density of the BSs. Accordingly, at higher BSs density, there will be no outage due to the limited transmission power of MTC nodes. In order to show the impact of the maximum transmission power P_m on the power control outage, Fig. 6.3 depicts the outage versus the ratio P_m/P_o for different cell density λ_s. The results show that the outage decreases very fast with the ratio P_m/P_o especially for a high density of small cells. One can conclude that in the UDN environment, the maximum transmission power P_m is no longer the parameter that impacts the power control outage of the MTC node, rather it is the density of small cells.

Fig. 6.4 depicts the power control outage versus the power truncation threshold for different density of small cells and different combinations of the SEPL propagation parameters. The results show that the power control outage significantly increases with higher power truncation threshold. However, for higher cell densities ($\lambda_s > 1000$ cells / km^2), the outage is very low even at relatively high truncation threshold for the considered maximum transmission power P_m. This signifies very interesting conclusions regarding the impact of the UDN on the system performance. At high density of small cells, the outage due to the truncation threshold is almost negligible while in the same time increasing the truncation threshold means higher transmission power and as a byproduct higher SINR and higher uplink coverage performance.

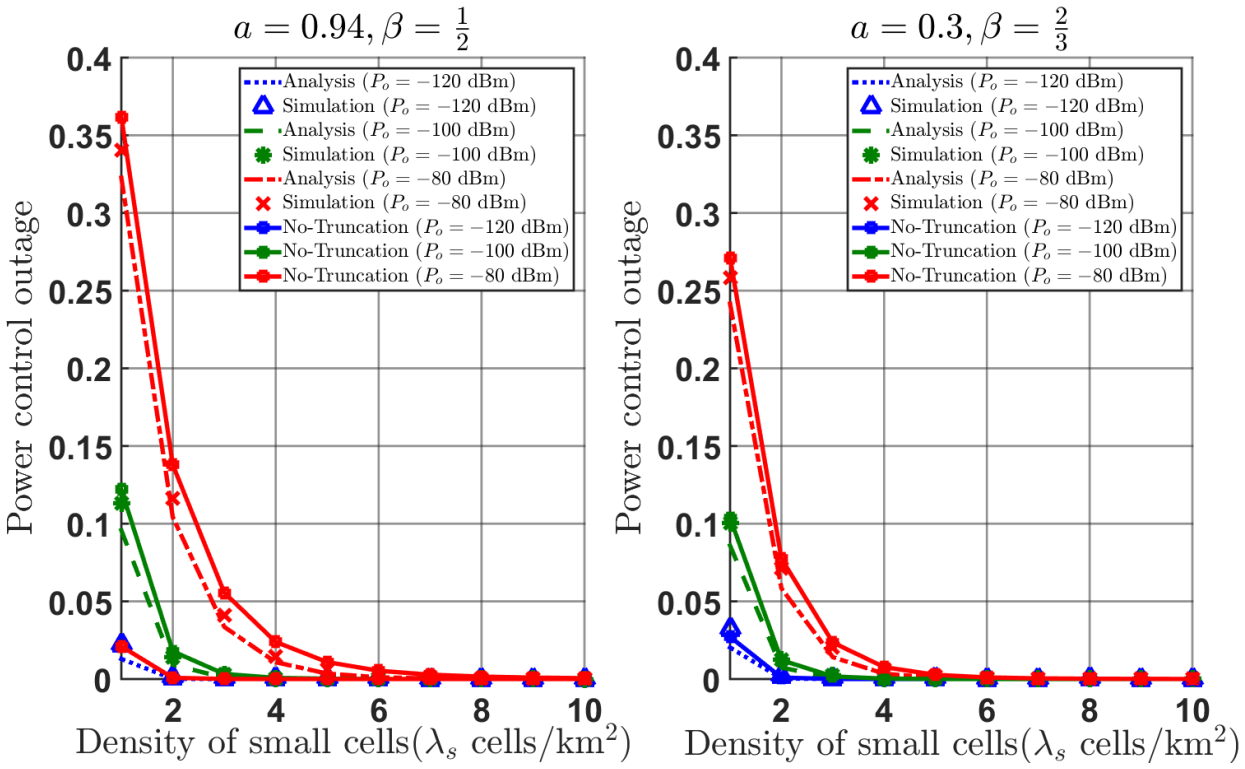

Figure 6.2: Power control outage for the truncation and no-truncation power control schemes versus the density of small cells considering different power truncation cutoff threshold P_o and different combinations of the path loss model parameters a and β, ($P_m = 20$ dBm).

6.6.3 Coverage Threshold

Fig. 6.5 depicts the uplink coverage for a typical active MTC device in a massive deployment scenario versus the coverage threshold τ. The results show the uplink coverage performance for different MTC population density in two different power truncation cutoff

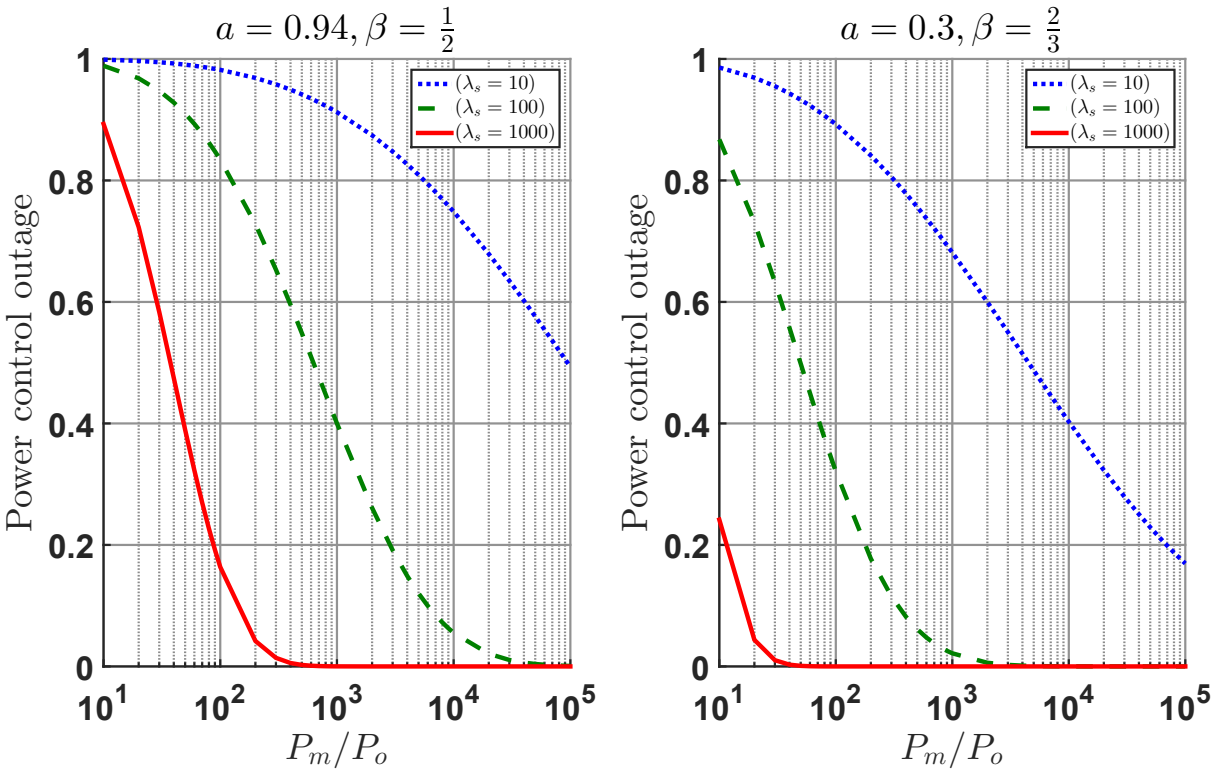

Figure 6.3: Power control outage versus the ratio P_m/P_o considering different density of small cells λ_s and different combinations of the path loss model parameters a and β, ($\lambda_m = 10^5$ nodes/km^2 and $\rho_m = 0.1$).

threshold scenarios where the small cells' density is 1000 BSs/km^2. The uplink coverage is significantly high at relatively low coverage thresholds. The results show that 80% of the time, the MTC population experiences an SINR of at most 0 dB. It is important to realize that in most of MTC applications, the nodes may experience poor received signal due to the harsh deployment conditions (e.g., basements, underground facilities, and concrete constructions). The coverage performance also shows a tendency to decline as the density of the mMTC nodes increases which can be intuitively explained by considering that the number of resource blocks in each small cell is a limited resource. In other words, as more nodes are deployed, more interference on each uplink resource is expected. On the other hand, the performance of the uplink coverage improves significantly with higher power truncation threshold even in high densities of mMTC nodes. Furthermore, the impact of the mMTC nodes density on the coverage tends to diminish as the power truncation threshold P_o gets smaller. In the limiting case, for a very small P_o, the coverage performance becomes independent of the mMTC devices density (as seen from the case of $P_o = -110$ dBm compared to $P_o = -100$ dBm). At relatively low P_o, the network becomes noise-limited rather than interference-limited. Lowering P_o

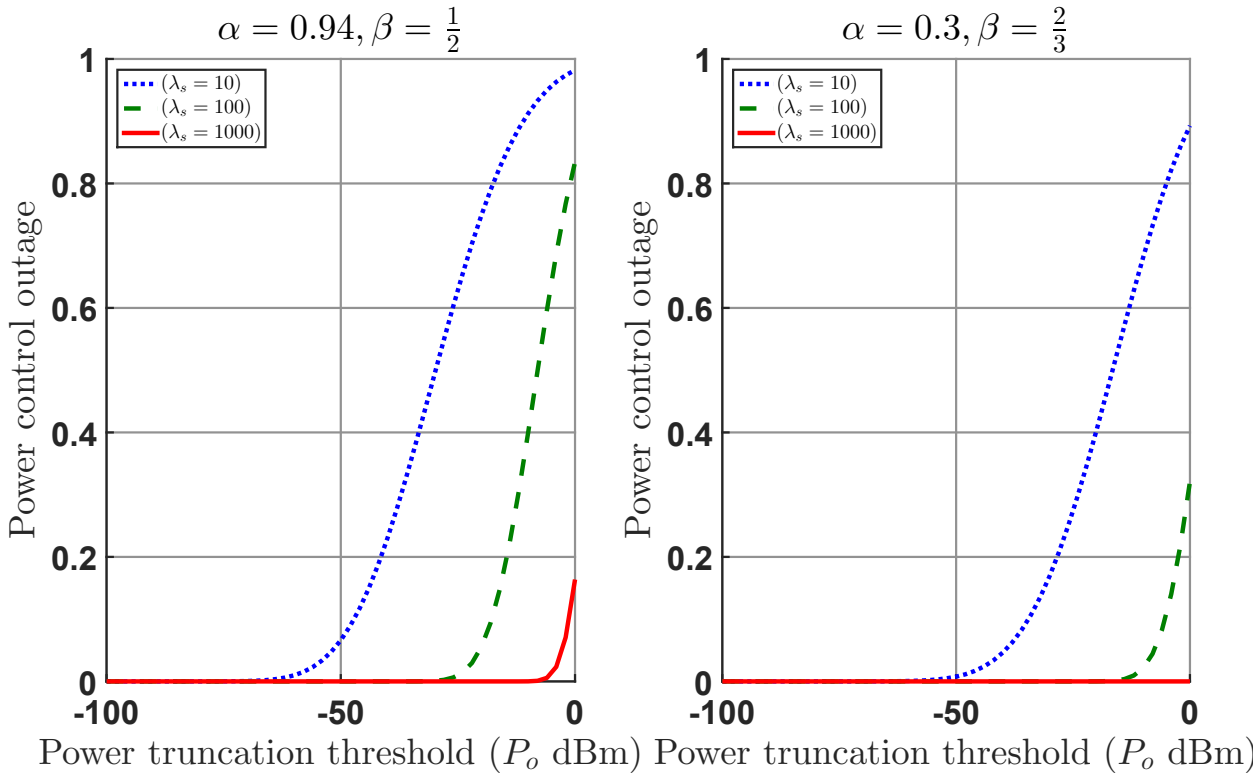

Figure 6.4: Power control ' outage versus the power truncation threshold P_o considering different density of small cells λ_s and different combinations of the path loss model parameters a and β, ($Pm = 20$ dBm, $\lambda_m = 10^5$ nodes/km^2, and $\rho_m = 0.1$).

is translated to a lower transmission power which in turn limits the interference seen in the uplink. Moreover, the noise power becomes of a comparable value to the received signal. Consequently, the impact of the increased density becomes negligible in terms of accumulated interference. On the contrary, higher P_o means higher transmission power and as a byproduct higher SINR. It is worth mentioning also that the high density of the small cells yields shorter distances to MTC devices which significantly reduces the impact of the inter-cell interference.

In Fig. 6.6, the coverage probability is plotted in two different combinations of the path loss model parameters. The coverage probability shows a slight change in both scenarios while the choice of the propagation parameters provides two realistic combinations which match the physical measurements [2].

6.6.4 Density of Small Cells

UDN is featured by the high density of small cells. In Fig. 6.7, we assess the impact of the density of the BSs on the uplink coverage performance where it is depicted versus

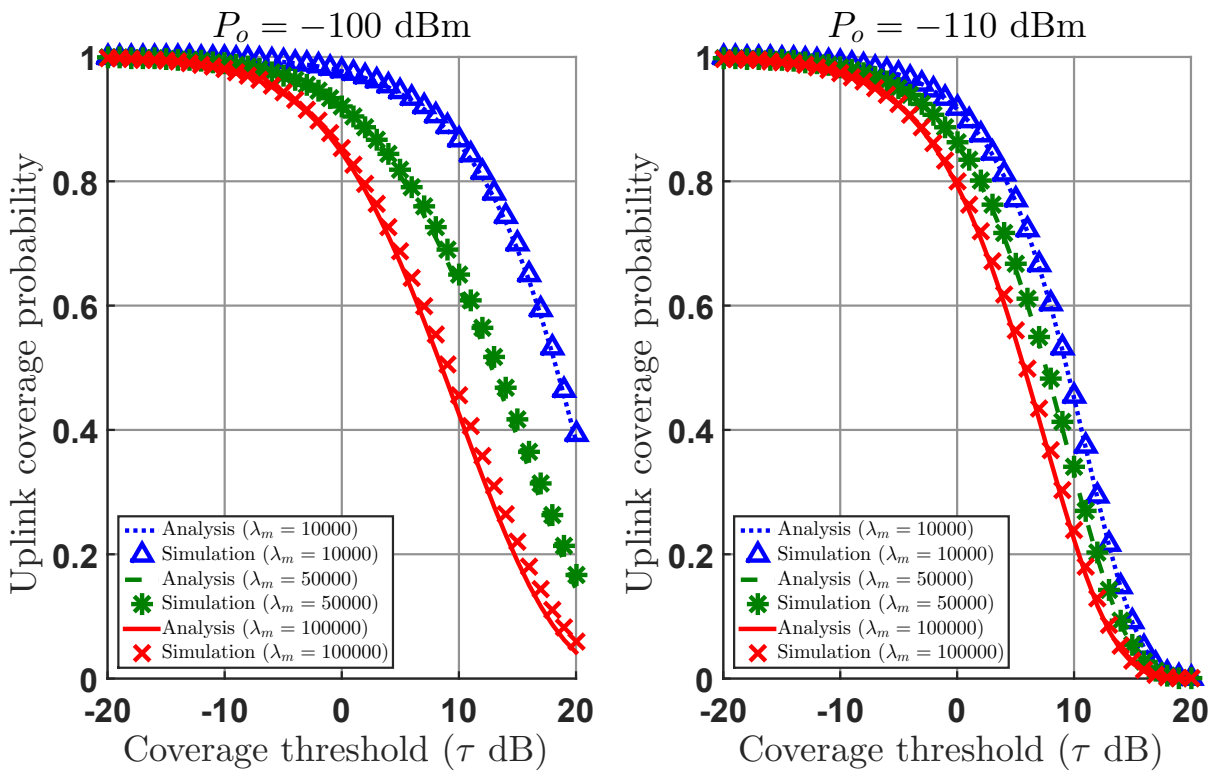

Figure 6.5: Coverage probability versus coverage threshold considering different MTC node density λ_m and different power truncation threshold P_o

the density of BSs for different densities of MTC devices. A coverage threshold of $\tau = 0$ dB and two different power control truncation thresholds $P_o = -100$ dBm and $P_o = -110$ dBm are considered. The dramatic improvement of the uplink coverage with the increasing density of BSs suggests a significant impact of the density on the network performance. However, the coverage probability saturates and reaches a maximum at a given BSs density which is distinct for different density of MTC devices and different power truncation threshold. The increasing density of small cells brings the BSs closer to the MTC devices which in turn lowers the required transmit power of these devices. Accordingly, the aggregate interference in the network diminishes leaving the devices with increasing uplink coverage probability. This coverage probability is higher for larger power control truncation threshold since this provides a higher received signal strength as compared to the aggregate interference. Since the aggregate interference gets lower with higher density of BSs, at some point the aggregate interference becomes less than the noise and the network performance switches to the noise-limited region. At this point, the density of the BSs no longer affects the network performance and the uplink coverage saturates. Consequently, network designers can decide the density of a UDN to provide

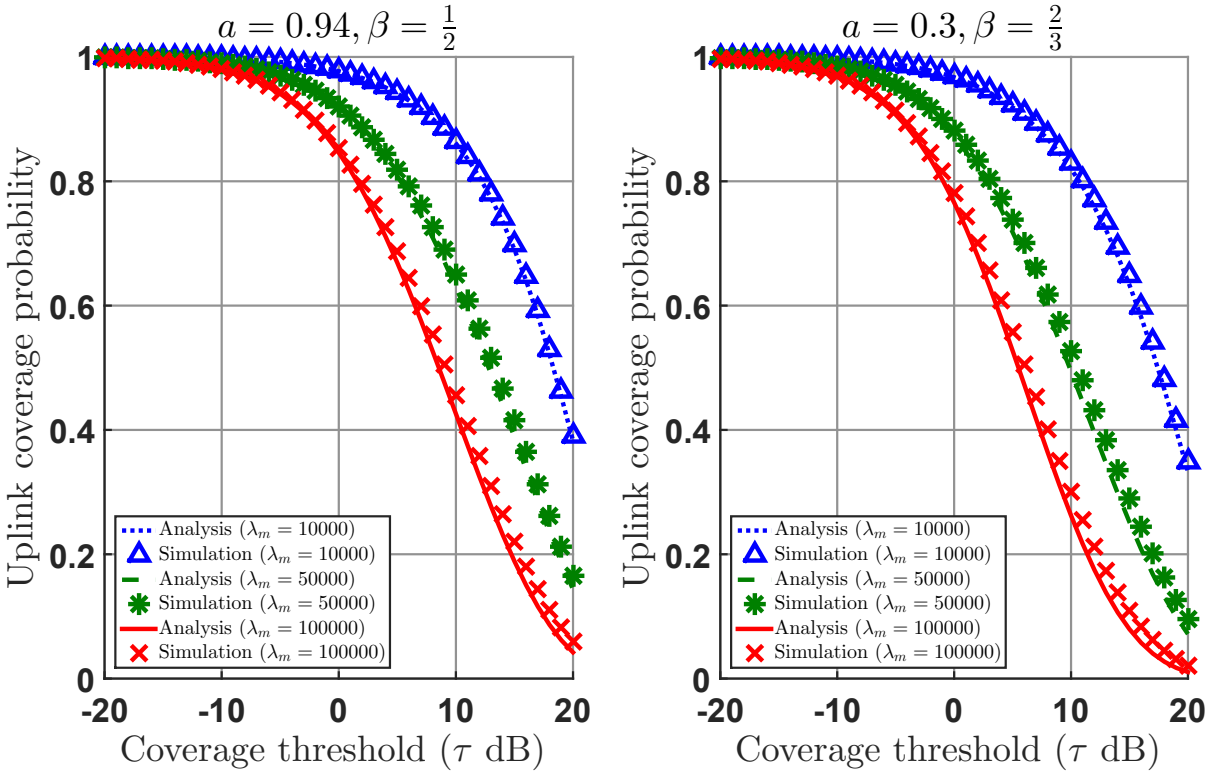

Figure 6.6: Coverage probability versus coverage threshold considering different MTC node density λ_m and different combinations of the path loss model parameters a and β

a predetermined coverage for a given density of MTC devices and a given power control truncation threshold.

In Fig. 6.8, the uplink coverage performance is depicted for two different combinations of the path loss model. In this scenario, the path loss model has a significant impact on the uplink coverage for different BSs density. Obviously, the small cells' density directly affects the link distance between the MTC node and the BS. This explains the significant impact of the path loss model parameters on the coverage probability when depicted against the BSs density.

6.6.5 Density of mMTC Devices

Considering different small cells' density and two different power truncation thresholds, Fig. 6.9 depicts the uplink coverage probability versus the mMTC devices' density at a coverage threshold of 0 dB The results show that the coverage probability significantly declines with the density of the MTC nodes in low small cells' density. This behavior is completely altered in higher BSs densities where the coverage probability decreases with the MTC devices' density in a much slower pace than in higher small cells' densities. In

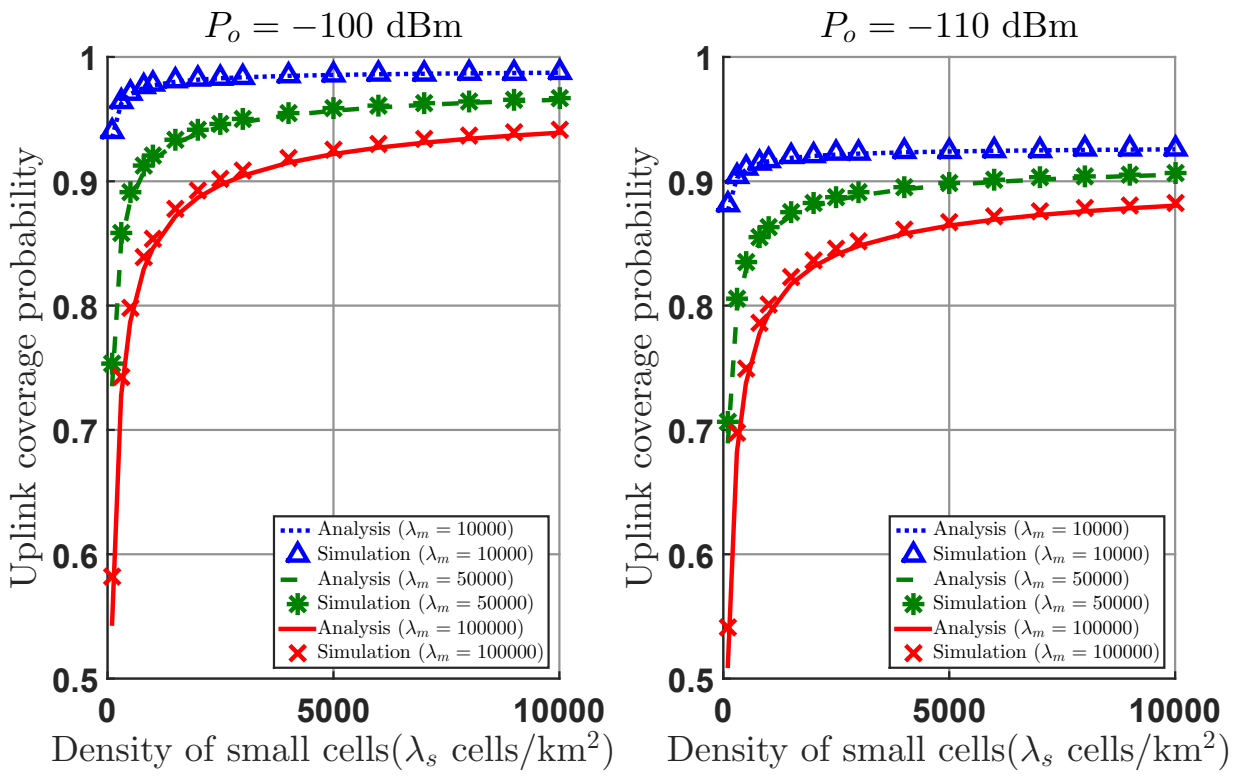

Figure 6.7: Coverage probability versus small cells' density considering different MTC node density λ_m and different power truncation threshold P_o

Fig. 6.10, the coverage performance is plotted for different combinations of the path loss parameters. In conclusion, higher MTC devices' density along with higher small cells' density translates to links with a shorter distance where the path loss parameters come to the scene to impact the uplink coverage performance.

6.6.6 Orthogonal Resource Blocks

Fig. 6.11 depicts the uplink coverage probability versus the number of orthogonal channels for different MTC devices' density at a coverage threshold of 0 dB. The results show that increasing the bandwidth significantly improves the coverage. However, this is tightly related to the density of the MTC devices. At lower MTC nodes' densities, there is a maximum number of orthogonal resources beyond which no significant improvement in the uplink coverage is achieved.

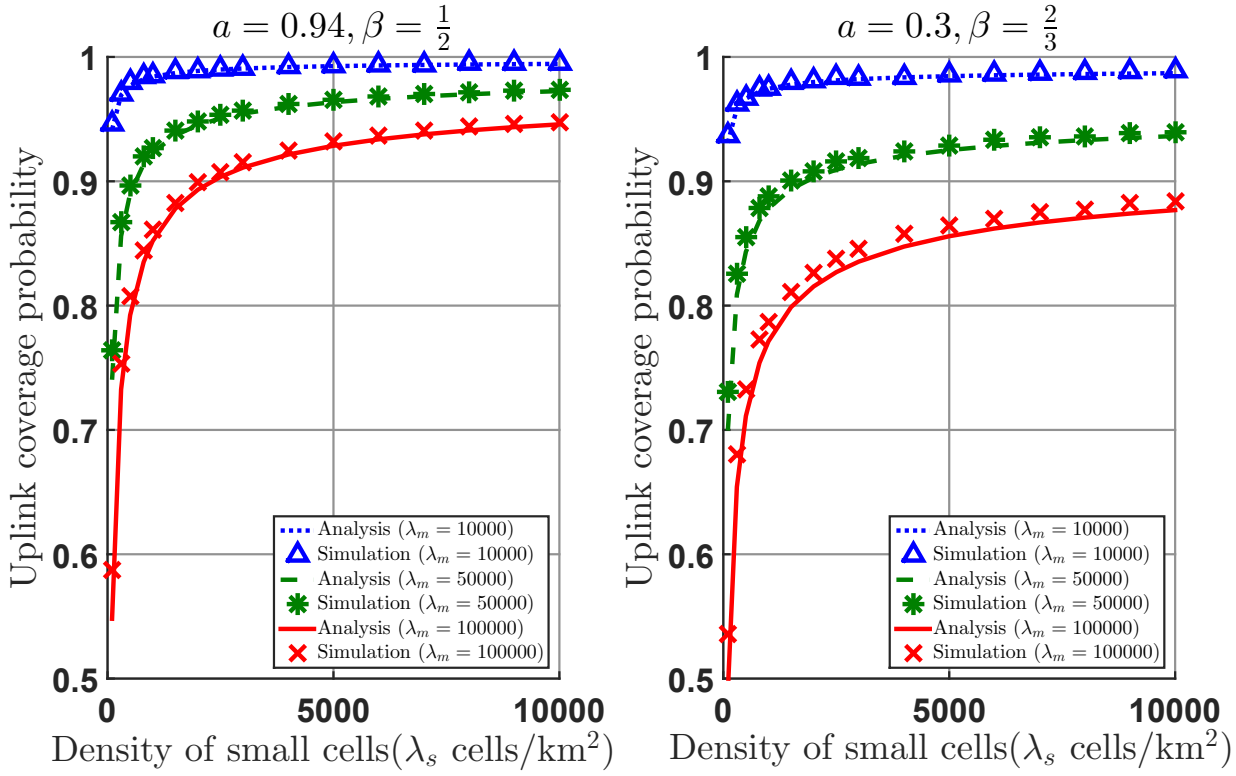

Figure 6.8: Coverage probability versus small cells' density considering different MTC node density λ_m and different combinations of the path loss model parameters a and β

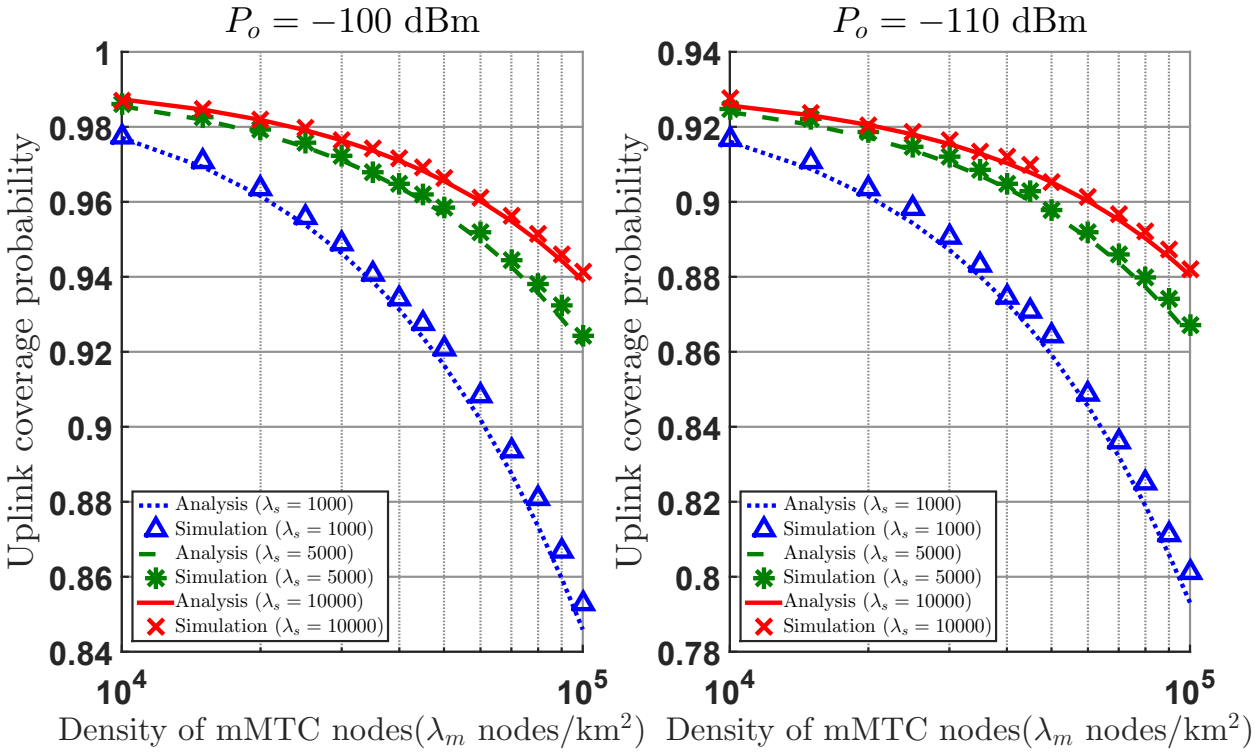

Figure 6.9: Coverage probability versus mMTC devices' density considering different small cells' density λ_s and different power truncation threshold P_o

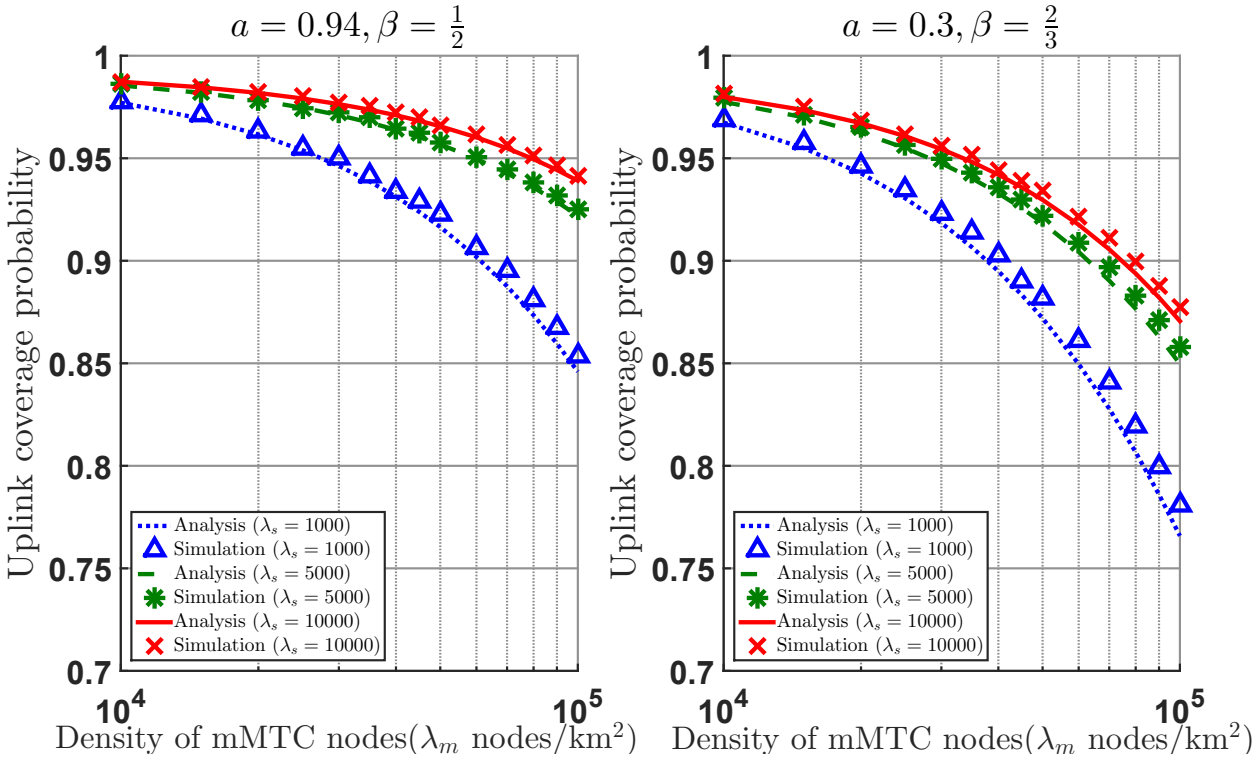

Figure 6.10: Coverage probability versus mMTC devices' density considering different small cells' density λ_s and different combinations of the path loss model parameters a and β

6.6.7 Power Truncation Cutoff Threshold

To zoom in on the impact of the power truncation threshold on the uplink coverage probability, Fig. 6.12 depicts the coverage probability versus the power truncation threshold for different MTC devices' density. We consider two different densities of small cells and the coverage probability is computed at a coverage threshold of 0 dB.

Confirming the previously discussed finding, lowering the power control cutoff threshold P_o negatively impacts the uplink coverage until it becomes indifferent to the density of MTC devices. On the other side, increasing P_o dramatically improves the uplink coverage. Even though, at some critical point, the uplink coverage performance is no longer affected by the increase of the cutoff threshold P_o where this critical saturation point is a function of both the density of the small cells and the MTC devices. This can be explained by recalling our finding that the uplink coverage performance has two regions: a noise-limited region and an interference-limited one with P_o being the system parameter that controls the boundary between them.

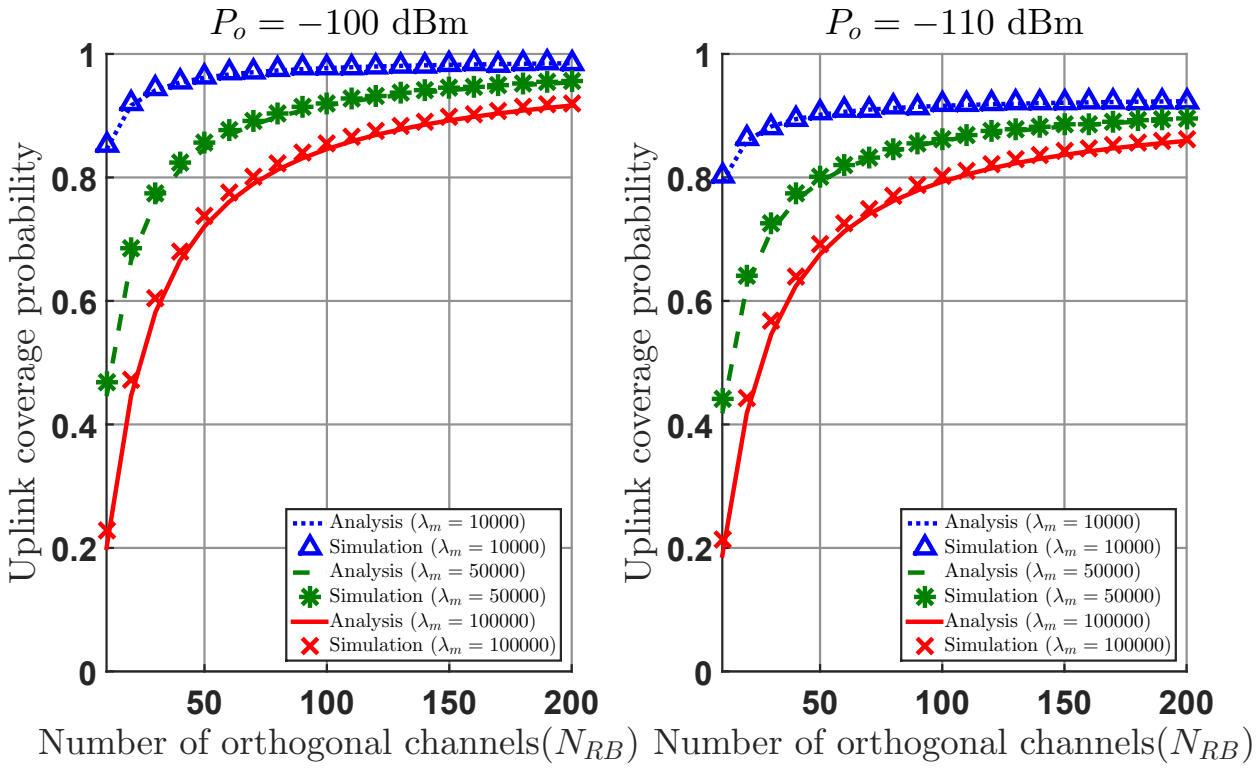

Figure 6.11: Coverage probability versus the number of orthogonal resources considering different mMTC devices' density λ_m and different power truncation threshold P_o

6.6.8 Maximum Transmission Power

Fig. 6.13 depicts the uplink coverage probability versus the maximum transmission power for different densities of MTC devices. We consider two different combinations of the SEPL model. The results show that the coverage probability does not vary with the maximum transmission power in a wide range (0 to 20 dBm). This can be justified by noting that as the density of small cells increases, the distance between the MTC nodes and its serving cells shrinks. Hence, the transmission power required to satisfy the power control cutoff threshold becomes smaller. Accordingly, a higher maximum transmission power will not affect the coverage probability as long as the transmitted signal can be received at the serving BS with the designated cutoff power.

Considering small cells in UDNs as a future possibility for serving massive MTC brings many opportunities. Firstly, the maximum transmission power can be reduced significantly from the current standard. One can suggest as low as 0-10 dBm (which corresponds to 1-10 mW)). This is due to the short link distance between the serving cell and the MTC nodes. Accordingly, this allows for more cost savings in the fabrication of the

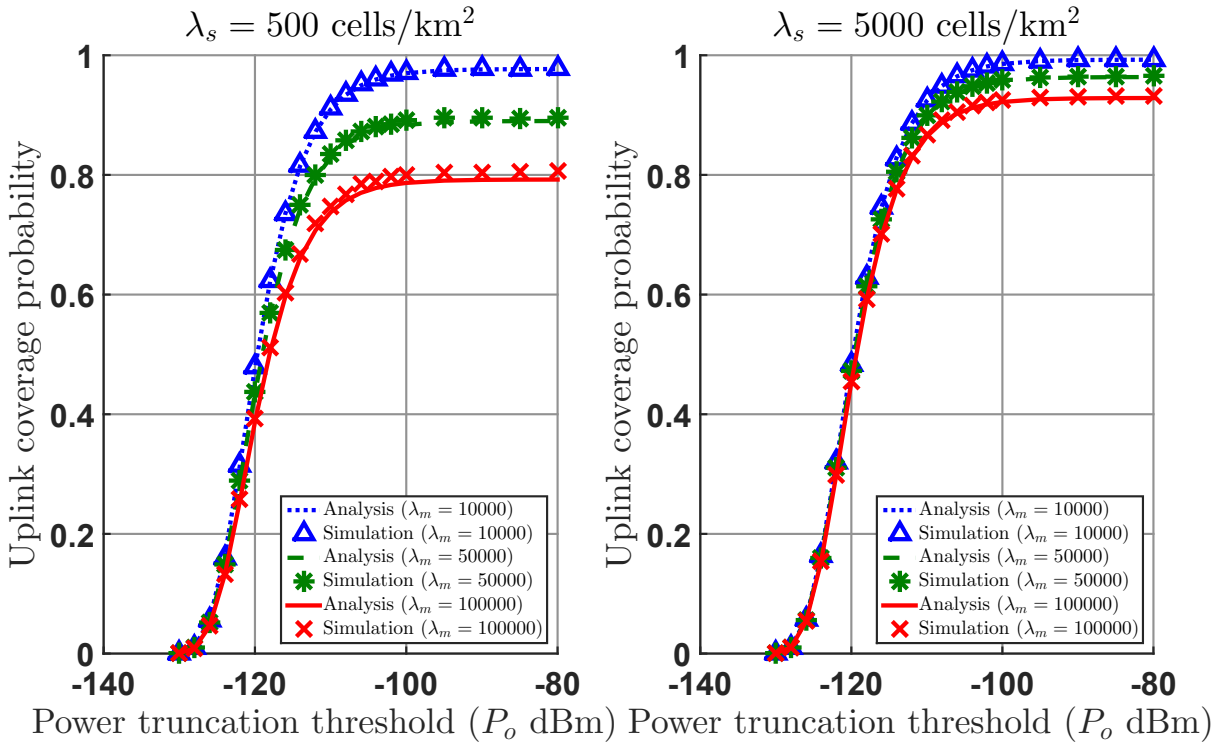

Figure 6.12: Coverage probability versus power truncation threshold considering different mMTC devices' density λ_m and different number of orthogonal resources N_{RB}

MTC nodes. Secondly, the reduction in transmit power significantly extends the battery life which can be increased to several tens of years instead of a maximum of 10 years in the current NB-IoT standard (LTE Release 13 and beyond) [145]. To summarize, aiming at a much lower transmit power from the current standard will have a double-fold gain: lower cost and longer battery life. Here, we propose that UDNs can provide this reduction of transmission power by providing short links to the massive MTC nodes, especially indoor.

6.7 Conclusion

We investigated the uplink coverage of mMTC devices deployed in massive amounts considering UDN environment. The special features of UDN is considered in the analysis. The uplink coverage is challenging in MTC applications due to the limited energy of the battery-powered MTC devices and the harsh deployment scenarios. The significant impact of the density of small cells, the available bandwidth, and the power control cutoff threshold on the uplink coverage performance is assessed by both analytical and simulation results. Remarkably, there is a critical saturation point where increasing these

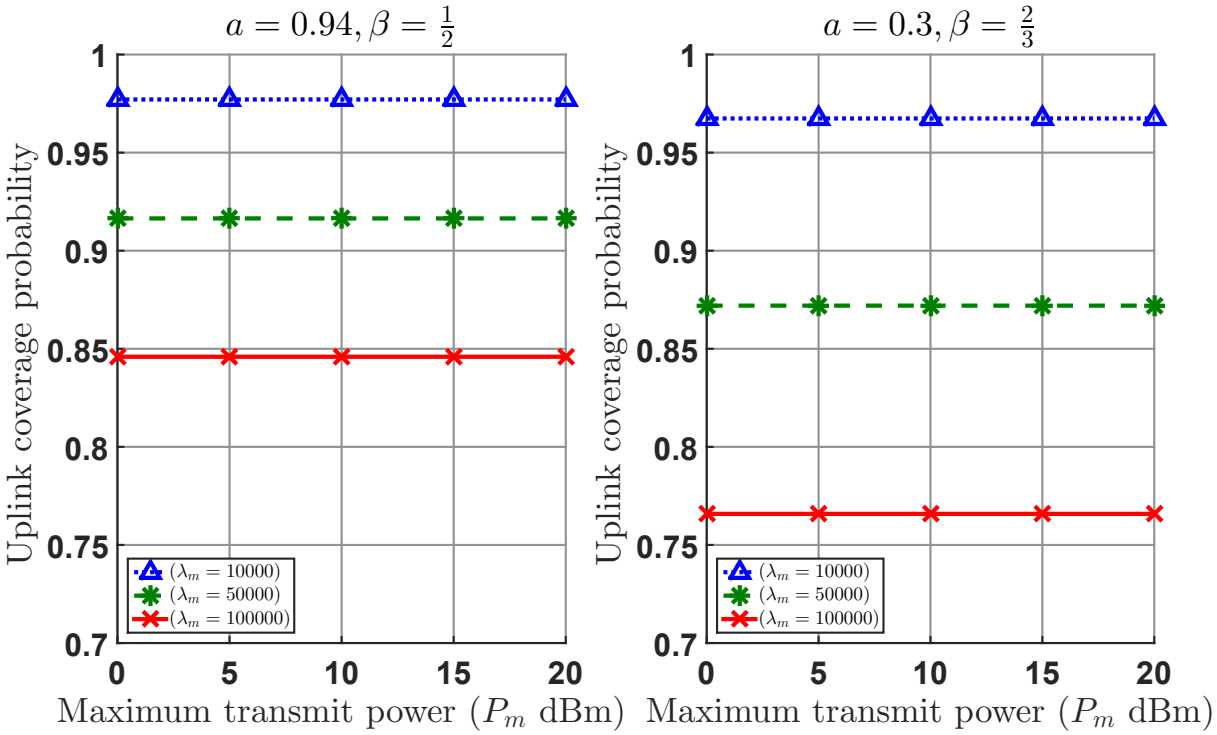

Figure 6.13: Coverage probability versus maximum transmission power considering different mMTC devices' density λ_m and different power truncation threshold P_o (Small cells' density $\lambda_s = 1000$ cells/km^2.

system parameters has no further impact on the performance. One interesting finding is that the uplink coverage performance has two distinct regions of operation, noise-limited region and interference-limited one. Another important finding is that the uplink coverage performance of a massive MTC deployment scenario in UDN environment is no longer affected by the maximum transmit power of the device, thanks to the high density of the serving small cells.

7. Coexistence of MTC and HTC in UDN

7.1 Introduction

The coexistence of Machine-Type Communication (MTC) communication and Human-Type Communication (HTC) communication is inevitable in 5G networks where Cellular Internet of Things (C-IoT) [153] emerges as a promising alternative to support IoT services [144]. Ultra-Dense Network (UDN) is widely believed to be a key enabling technology in 5G networks to support dense MTC communication as well as high traffic load HTC communication [58]. The network densification in UDNs brings the cells much closer to the users which improves their link quality. In addition, the increasing frequency reuse significantly improves the network throughput available to the end users. However, this comes with the cost of severe interference experienced by the users due to the increasing number of base stations (BSs) . The mitigation of this excessive interference is crucial to the fruition of network densification. One simple interference mitigation scheme is to turn off the inactive BSs due to lack of connected users [154], which is termed as idle mode capability.

The key requirements of Cellular Internet of Things (C-IoT) which have been addressed in LTE Release 13 are cost reduction, reduced power consumption and enhanced coverage [153]. Massive deployment of MTC devices is a main feature of the future applications of IoT. Accordingly, connectivity would be a major problem where millions of MTC devices can exist in the coverage area of one macrocell. In this scenario, UDNs will play a dominant role to provide a scalable connectivity solution. Offloading of such immense connectivity load to the dense small cell network emerges as a viable solution. The traffic of MTC communications is featuring special characteristics. In particular, MTC

traffic is mostly in the uplink with very short messages to report a reading of a sensor or a smart meter [144]. Moreover, in many scenarios, the traffic of MTC devices is sporadic with a long duty cycle. Accordingly, only a ratio of the population of MTC devices will be active and transmitting at any given time. In addition, due to the harsh deployment scenarios of some IoT applications, MTC devices may experience poor signal quality. Hence, the enhanced coverage is a basic requirement in C-IoT where $15-20$ dB improved coverage would be required when compared to regular HTC communication [153].

7.2 State-of-the-Art and Contributions

While some recent studies considered the impact of Machine-Type Communication (MTC) traffic on Human-Type Communication (HTC) users in LTE [155], traditional cellular networks [156] and fiber-wireless (FiWi) smart grid communications [157], to the best of our knowledge, we are the first to address the impact of the coexistence of MTC and HTC communications on the network performance in UDNs. In this investigation, we study the downlink network performance in terms of the coverage probability and the cell load where we proposed two association schemes for the MTC devices, namely, *Connect-to-Closest (C2C)* and *Connect-to-Active (C2A)*. The network performance is then analyzed and compared in both association schemes.

7.3 System Model

We consider a dense small cell network comprised of BSs equipped with advanced idle mode capabilities. The BSs turn off if no users are connected in order to mitigate their interference. We consider the standard tools of stochastic geometry to model the network nodes [104] where the locations of the BSs, HTC users, MTC devices are modeled as independent Homogeneous Poisson Point Process (HPPP) Φ_s, Φ_h and Φ_m with a density λ_s, λ_h and λ_m, respectively. All BSs, HTC users and MTC devices are assumed to deploy a single antenna, BSs transmit with a unit power, and all component carriers are utilized in each cell, i.e., frequency reuse factor of one. Due to the nature of the MTC traffic which is mainly sporadic with a long duty cycle for transmission [157], we assume that at any given time only ρ_m of the MTC devices are ready to transmit. Thus, only $\rho_m\lambda_m$ of the MTC devices will be active at any given time. We consider ρ_m as a constant in

this investigation for simplicity, however, the modelling of ρ_m as a random variable will be considered in future research.

We evaluate the performance with regard to a typical user at the origin which represents the average performance of all users and is allowed with the aid of Slivnyak's theorem [105]. Moreover, we consider the analysis of the performance metrics with respect to each type of users, i.e., MTC and HTC. In this case, we consider a typical HTC user and a typical MTC device each of which is located at the origin in the respective analysis to evaluate the average performance of each users' group. HTC users connect to the BS providing the maximum average received power which is the nearest BS. We consider two association schemes in case of MTC devices and we compare their performance. In the first association scheme, *connect to closest (C2C)* BS, an MTC device connects to the nearest BS and turns it on if it is in idle mode. The second association scheme, *connect to active (C2A)* BS, differs only in one aspect, the MTC device connects to the nearest active BS activated by an HTC user instead of activating the nearest BS to its location.

The propagation environment considered in this system model consists of two components; large scale fading and small scale fading. Large scale fading is modeled by Stretched Exponential Path-Loss (SEPL) model with parameters (α and β) [158]. In SEPL model, the transmit signal experiences exponential attenuation with the distance to the transmitter r, thus the received signal power from a BS transmitting with a unit power is $e^{-\alpha r^{\beta}}$. Small scale fading is modeled by independent and identically distributed (i.i.d) multipath fading channels which follows Rayleigh distribution. Without loss of generality, we assume similar fading channels for HTC users and MTC devices. Accordingly, the power fading channel gain of the serving BS, h_o, and the interfering BSs, h_b, follow exponential distribution with mean one.

In UDNs, the interference-limited scenario is a typical scenario where the aggregate interference from active cells is much greater than the noise power. Accordingly, the downlink signal to interference ratio (SIR) can be expressed as:

$$\mathtt{SIR} = \frac{\mathcal{S}}{\mathcal{I}_a} = \frac{h_o e^{-\alpha r^{\beta}}}{\sum_{b \in \Phi_a / b_o} h_b e^{-\alpha r_b^{\beta}}} \tag{7.1}$$

where $\Phi_a \subset \Phi_s$ is the interfering BSs point process which is the set of all active cells. The BS activation probability is in general location dependent, and hence, the interfering BSs

form a nonhomogeneous PPP [54]. In UDNs, considering the high density of small cells, the variance in cell sizes becomes very small and this location dependency vanishes. Based on this discussion and the approximation proposed in [54, Lemma (1)], we can model the interfering BSs as a HPPP Φ_a which represents a thinned version of the original small cells PPP Φ_s with a thinning probability p_a, and a density $p_a\lambda_s$. Remarkably, the BS activation probability can be given in terms of the relative density of the cells to the density of the users [20]:

$$p_a = 1 - \left[1 + \tfrac{1}{3.5\kappa}\right]^{-3.5} \tag{7.2}$$

where $\kappa = \frac{\lambda_s}{\lambda_u}$ is the network densification ratio and λ_u is the users' density.

Interestingly, in the considered association scenarios, the BS activation probability differs according to the association model. In *C2C* association, the density of users is the density of the merged PPP of the HTC users and MTC devices. Considering the properties of Poisson processes, the users' density in this case is the sum of the individual densities, i.e., $\lambda_u = \lambda_h + \rho_m\lambda_m$. On the other hand, in *C2A* association, we consider only the activated BSs from HTC users. Therefore, the users' density in this case is λ_h. To summarize, we consider two different activation probabilities to perform the thinning of the interferers process, $p_{cc} = 1 - [1 + 1/3.5\kappa_{cc}]^{-3.5}$ in *C2C* association scheme and $p_{ca} = 1 - [1 + 1/3.5\kappa_{ca}]^{-3.5}$ in *C2A* association scheme where $\kappa_{cc} = \lambda_s/(\lambda_h + \rho_m\lambda_m)$ and $\kappa_{ca} = \lambda_s/\lambda_h$.

To evaluate and compare the performance of the two association schemes, we consider two performance metrics. The first metric is the downlink coverage probability of HTC users and MTC devices $\mathcal{P}_h(\tau_h)$ and $\mathcal{P}_m(\tau_m)$, respectively, which can be defined as:

$$\mathcal{P}_h(\tau_h) = \mathbb{P}\left\{\mathtt{SIR}_h \geq \tau_h\right\} \tag{7.3}$$

$$\mathcal{P}_m(\tau_m) = \mathbb{P}\left\{\mathtt{SIR}_m \geq \tau_m\right\} \tag{7.4}$$

where τ_h is the coverage threshold and $\mathtt{SIR}_h$ is the SIR with respect to the HTC users. Also, τ_m is the coverage threshold and $\mathtt{SIR}_m$ is the SIR with respect to the MTC devices. Notably, we use two different coverage thresholds for the evaluation of the coverage probability of MTC and HTC users due to the difference in coverage requirements between them [153]. The second metric we consider is the average cell load of HTC users $\mathcal{L}_h$ and the average cell load of MTC devices $\mathcal{L}_m$ which can be defined as:

$$\mathcal{L}_h = \frac{N_h}{N_{s,HTC}} \quad \text{users/cell} \tag{7.5}$$

$$\mathcal{L}_m = \frac{N_m}{N_{s,MTC}} \quad \text{devices/cell} \tag{7.6}$$

where N_h, N_m, $N_{s,HTC}$ and $N_{s,MTC}$ are the average number of HTC users, MTC devices, BSs serving HTC users and BSs serving MTC devices in a given area, respectively. The average cell load provides a good measure for the loading of cells of both communication types assuming the homogenous traffic of HTC users and the homogeneous uplink traffic of MTC devices in most scenarios. In particular, the average cell load metric addresses the MTC connectivity load on the cells where the random access in initial cell association is a major bottleneck [159].

7.4 Analytical Results

7.4.1 Downlink Coverage

General Scenario

In this section, we investigate the downlink coverage probability of MTC and HTC users in UDNs. To simplify the presentation of results, we consider a general user type with density λ_u and general association scheme in the analysis of the downlink coverage probability, then we specialize the results for MTC and HTC users considering the *C2C* and *C2A* association schemes. In what follows we provide the general result and two special case simplifications.

Theorem 1. *The downlink coverage probability of a general user type in UDNs satisfying the system model presented in Section 7.3 is given by:*

$$\mathcal{P}_c(\tau) = \int_0^\infty 2\pi\lambda_s r e^{-\pi\lambda_s r^2} \mathcal{L}_{\mathcal{I}_a}(\tau e^{\alpha r^\beta}) \mathrm{d}r \tag{7.7}$$

where:

$$\mathcal{L}_{\mathcal{I}_a}(\tau e^{\alpha r^\beta}) = \exp\left\{ (-1)^{\frac{2}{\beta}} \frac{2\pi\lambda_a \tau}{\beta \alpha^{\frac{2}{\beta}}} \int_0^1 \frac{\left(\ln(x) - \alpha r^\beta\right)^{\frac{2-\beta}{\beta}}}{1+\tau x} \mathrm{d}x \right\} \tag{7.8}$$

and $\lambda_a = p_a \lambda_s$.

Proof. We follow a similar approach to the proof provided in [122] considering the SEPL model and the idle mode capabilities of the BSs. Accordingly, the interfering BSs point

process Φ_a in our system model is a thinned version of the small cells point process Φ_s with a density $p_a\lambda_s$ where p_a depends mainly on the relative density of the small cells to the users. ■

In the following corollary, we simplify the result considering the special value $\beta = \frac{2}{n+1}$ where $n \in \{0, 1, 2, 3, \cdots\}$ which corresponds to the values $\beta = 2, 1, \frac{2}{3}, \frac{1}{2}, \cdots$.

Corollary 1. *Considering the special case $\beta = \frac{2}{n+1}$ where $n \in \{0, 1, 2, 3, \cdots\}$, the downlink coverage probability stated in Theorem 1 simplifies to*

$$\mathcal{P}_c(\tau) = \int_0^\infty 2\pi\lambda_s r e^{-\pi\lambda_s r^2} \exp\left\{\sum_{k=0}^{n} \lambda_a a_k(\tau) r^{\frac{2k}{n+1}}\right\} \mathrm{d}r \tag{7.9}$$

where

$$a_k(\tau) = \frac{\pi(n+1)!}{k!\alpha^{n-k+1}} \mathrm{Li}_{(n-k+1)}(-\tau) \tag{7.10}$$

and $\mathrm{Li}_{(k)}(\cdot)$ is the k^{th} order poly-logarithmic function [134], which can be expressed as:

$$\mathrm{Li}_{(n-k+1)}(\tau) = -\frac{\tau}{\Gamma(n-k+1)} \int_0^\infty \frac{x^{n-k}}{e^x - \tau} \mathrm{d}x \tag{7.11}$$

For the special value $\beta = 2$ which corresponds to $n = 0$, the downlink coverage probability is further simplified to,

$$\mathcal{P}_c(\tau) = \exp\left\{-\frac{\pi\lambda_a}{\alpha} \ln(1+\tau)\right\}. \tag{7.12}$$

Proof. The proof follows similar steps to the proof presented in [2], however we use the expression of $\mathcal{L}_{\mathcal{I}_a}(\tau e^{\alpha r^\beta})$ presented in (7.8). ■

In the following subsections we provide the downlink coverage results of HTC users and MTC devices considering *C2C* and *C2A* association schemes. We consider the special case in (7.12), however the general result can be specialized for the considered association schemes in a similar manner. The tuning of the general result to match the association schemes mainly depends on the identification of two parameters in the general result. The first parameter is λ_s, the density of the small cells point process from which a given user selects one for association. The second parameter is λ_a, the density of interfering BSs.

C2C Association

In *C2C* association, MTC devices and HTC users are allowed to connect to the closest BS which provides the maximum average received power. Consequently, any small cell can be chosen for association by both HTC users and devices users with a density λ_s. In this case, the interfering BSs PPP is a thinned version of the small cells PPP Φ_s with a thinning probability p_{cc}, hence, the density of interfering BSs is $\lambda_a = p_{cc}\lambda_s$. Based on this, the downlink coverage probability of HTC users is given by:

$$\mathcal{P}_h^{C2C}(\tau_h) = \exp\left\{-\frac{\pi p_{cc}\lambda_s}{\alpha}\ln(1+\tau_h)\right\}. \tag{7.13}$$

Similarly, the downlink coverage probability of MTC devices is given by:

$$\mathcal{P}_m^{C2C}(\tau_m) = \exp\left\{-\frac{\pi p_{cc}\lambda_s}{\alpha}\ln(1+\tau_m)\right\}. \tag{7.14}$$

C2A Association

In *C2A* association, an HTC user connects to the closest BS if it is active or activate it if it is in idle mode, whereas MTC devices are allowed only to connect to the active BSs which are activated by the HTC users. In this scenario, HTC users can connect to any BS in the small cells PPP Φ_s with a density of λ_s. On the other hand, MTC devices are allowed only to connect to a BS in the active small cells PPP Φ_a which is a thinned version of the small cells PPP Φ_s with a thinning probability p_{ca}. Similarly, the interfering BSs PPP in this scenario is a thinned version of Φ_s with a probability p_{ca} and a density of interfering BSs $\lambda_a = p_{ca}\lambda_s$. As a result, we can express the downlink coverage probability for HTC users as:

$$\mathcal{P}_h^{C2A}(\tau_h) = \exp\left\{-\frac{\pi p_{ca}\lambda_s}{\alpha}\ln(1+\tau_h)\right\}. \tag{7.15}$$

and for MTC devices, the downlink coverage probability is given by:

$$\mathcal{P}_m^{C2A}(\tau_m) = \exp\left\{-\frac{\pi p_{ca}\lambda_s}{\alpha}\ln(1+\tau_m)\right\}. \tag{7.16}$$

7.4.2 Average Cell Load

In this section, we turn our attention to another performance metric, the average cell load measured in the number of connected users to a given cell. In the following theorem we provide the main results for the average cell load considering both users' types and the two investigated association schemes.

Theorem 2. *The average cell load of HTC users in UDNs satisfying the system model presented in Section 7.3 is given by:*

$$\mathcal{L}_h = \frac{\lambda_h}{p_a \lambda_s} \quad users/cell \tag{7.17}$$

where p_a is given in (7.2) with $\kappa = \lambda_s/\lambda_h$. Similarly, the average cell load of MTC devices can be expressed as:

$$\mathcal{L}_m = \frac{\rho_m \lambda_m}{p_a \lambda_s} \quad users/cell \tag{7.18}$$

where $p_a = p_{cc}$ in case of C2C *association and $p_a = p_{ca}$ in case of* C2A *association.*

Proof. HTC users are drawn form an HPPP Φ_h with a density λ_h, hence, the average number of active HTC users in a given area A is $\lambda_h A$. In a similar way, the average number of active MTC devices in a given area A is $\rho_m \lambda_m A$. The number of active BSs depends mainly on the considered association scheme. In *C2C* association, the average number of active BSs in a given area A is $p_{cc}\lambda_s A$, and in *C2A* association this can be given by $p_{ca}\lambda_s A$. Substituting in the average cell load as defined in (7.5) and (7.6) we obtain the expressions in (7.17) and (7.18). ■

7.5 Simulation Results

In this section, we assess the accuracy of the analytical results by simulating the system model provided in Section 7.3. The network is realized by the generation of HPPP with corresponding densities for the small cells, HTC users and MTC devices. We consider a square area with a side of $300m$ where we generated 100 spatial realizations of the PPP. The channel variation is simulated by a realization of 10 time slots drawn from an exponential random variable with a mean one. We consider a SEPL model $e^{-\alpha r^{\beta}}$ to compute the path losses for the serving BS links as well as the interference links.

7.5.1 Downlink Coverage Probability

Figure 7.1 depicts the downlink coverage probability of HTC users and MTC devices. We consider different coverage thresholds τ_h and τ_m to highlight the different coverage requirements for both types of users. The downlink coverage of HTC users improves significantly when we consider the *C2A* association scheme. A 5x enhancement is achieved

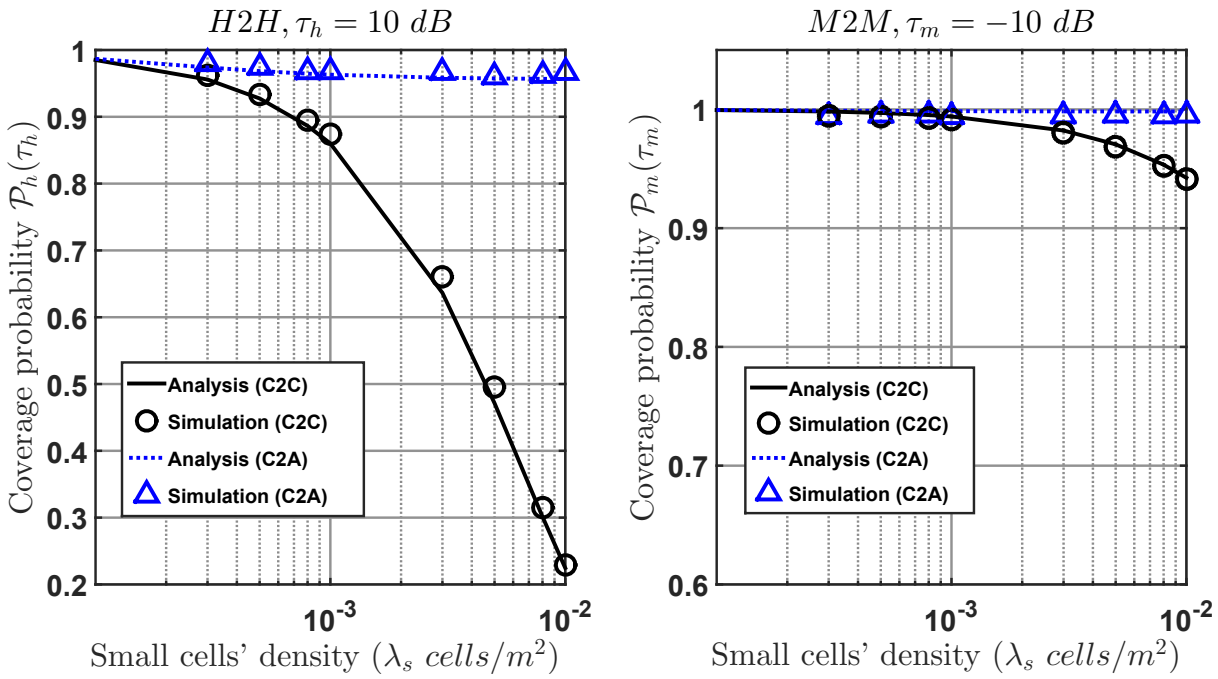

Figure 7.1: Downlink coverage probability versus the small cells' density λ_s with HTC users' density of $\lambda_h = 300\ users/km^2$, MTC devices' density of $\lambda_m = 1\ users/m^2$ and activity probability of $\rho_m = 0.1$.

in the downlink coverage at small cells density of $10,000\ cells/km^2$. On the other hand, the coverage probability in case of MTC devices improves in higher small cell densities considering the *C2A* association. The significant improvement of the coverage probability in case of HTC users is due to the mitigation of the severe interference from the large number of active cells in case of *C2C* association scheme. This interference mitigation takes place by turning off most of the BSs that would be activated to serve the MTC devices in their vicinity. Instead, those MTC devices are associated to the active BSs which are already activated by the HTC users. In Figure 7.2, the downlink coverage probability is depicted once again versus the MTC devices' density. The increasing density of MTC devices means more activated small cells in case of *C2C* association. Consequently, the *C2A* association scheme shows a similar behavior where the coverage probability improves significantly, especially, in high MTC devices' density.

7.5.2 Average Cell Load

The average cell load of HTC and MTC devices is depicted versus the small cells' density in Figure 7.3. The results show that the average cell load decreases with higher cell densities. Intuitively, more small cells translates to less load per cell. However, in *C2A*

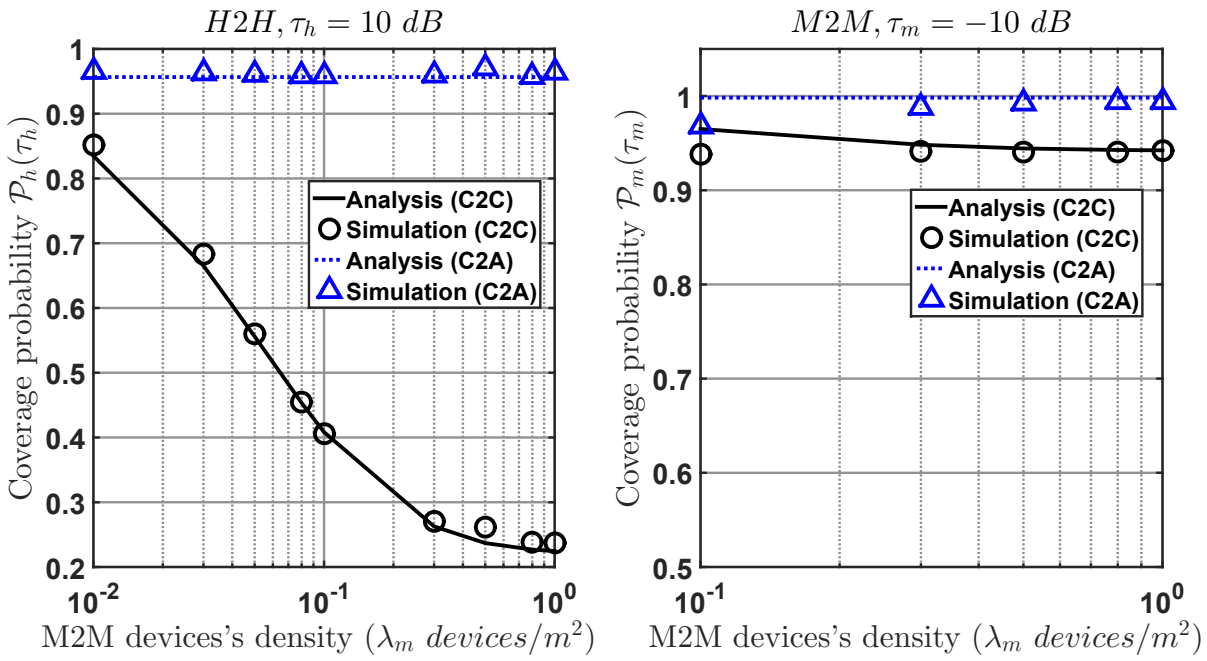

Figure 7.2: Downlink coverage probability versus the MTC devices' density λ_m with small cells' density of $\lambda_s = 0.01$ $cells/m^2$, HTC users' density of $\lambda_h = 300$ $users/km^2$ and activity probability of $\rho_m = 0.1$.

association, the average cell load of MTC devices is significantly higher than the case of *C2C* association. In *C2A* association scheme, the MTC devices are only allowed to connect to the nearest active cell which limits the number of serving cells. On the other hand, the average cell load considering HTC users is indistinguishable with respect to the two association schemes. This is intuitive since in both cases the number of HTC serving BSs depends only on the HTC users' density.

In Figure 7.4, the average cell load is depicted versus the MTC devices' density. The average cell load of MTC devices increases significantly as the MTC density increases considering the *C2A* association scheme. On the contrary, in *C2C* association scheme, the average cell load increases slightly as the density of MTC devices increases. To explain, in *C2C* association, more active MTC devices activate more cells which results in almost constant average cell load. Moreover, the average cell load of HTC users is independent of the MTC devices' density as depicted in Figure 7.4.

7.6 Conclusions

In this investigation, we studied the impact of the coexistence of MTC devices and HTC users on the performance of UDNs. We investigated two association schemes, namely,

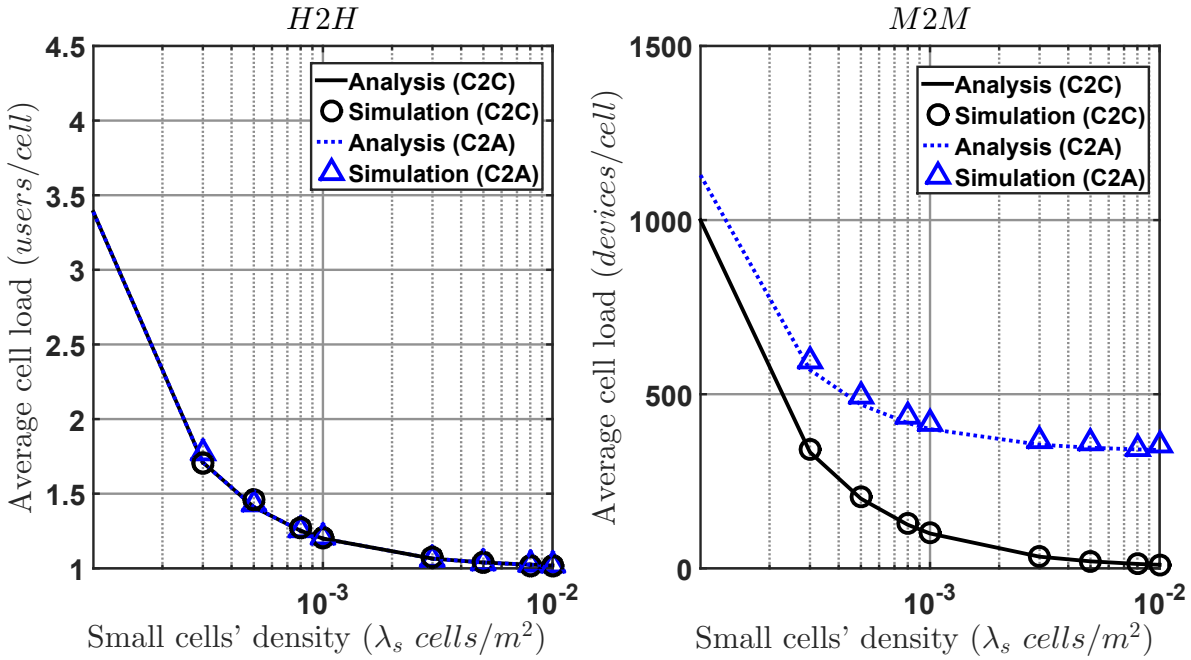

Figure 7.3: Average cell load versus the small cells' density λ_s with HTC users' density of $\lambda_h = 300$ $users/km^2$, MTC devices' density of $\lambda_m = 1$ $users/m^2$ and activity probability of $\rho_m = 0.1$.

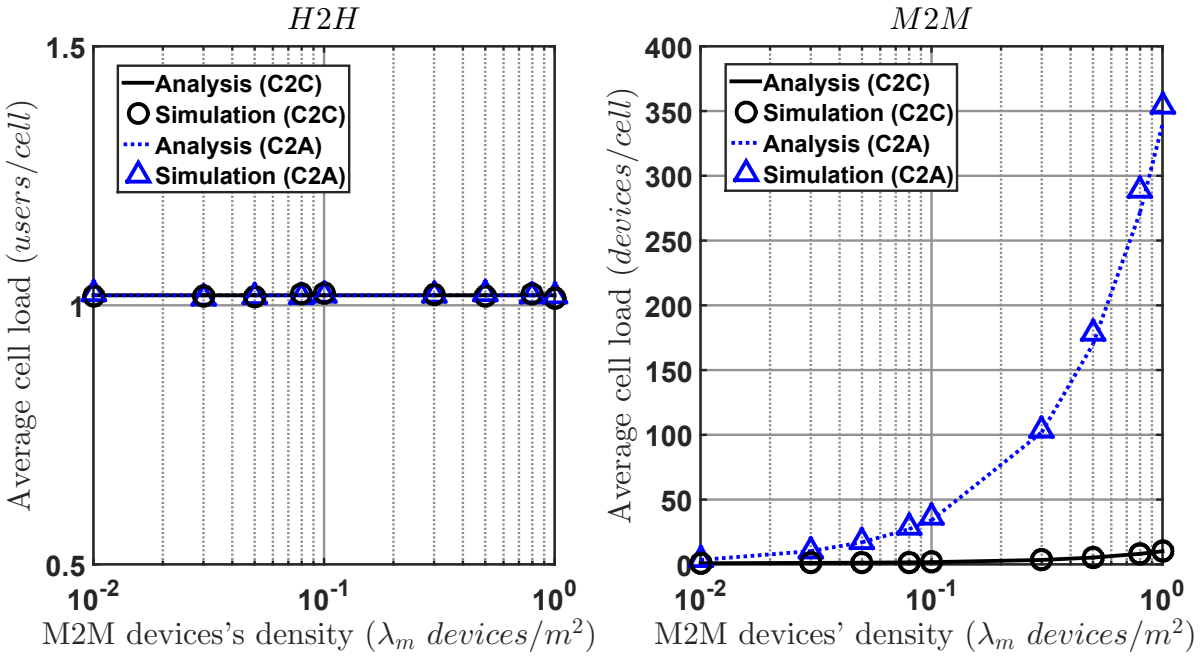

Figure 7.4: Average cell load versus the MTC devices' density λ_m with small cells' density of $\lambda_s = 0.01$ $cells/m^2$, HTC users' density of $\lambda_h = 300$ $users/km^2$ and activity probability of $\rho_m = 0.1$.

connect to closest (C2C) BS and *connect to active (C2A)* BS. The network performance in terms of downlink coverage probability and average cell load is analyzed and the analytical results are assessed through simulations. The investigation of the proposed system model shows a tradeoff between the two performance metrics with respect to the considered

association schemes. Accordingly, this suggests the design of association schemes to find a balance between them. On the positive side, the consideration of UDNs to support MTC devices traffic provides a scalable and a viable solution to the connectivity problem in future massive deployments of MTC devices.

8. Uplink Performance of Combined HTC and MTC considering NOMA in UDNs

8.1 Introduction

Network densification is a trend in mobile communication since the first generation in the 80s while considered one of the preeminent technologies to satisfy the stringent requirements in the 5G networks. Ultra-Dense Network (UDN) is then the ultimate of this trend [58]. In this way, immense number of small cells are deployed in hot-spots where enormous traffic is generated and massive number of access requests is expected. This provides full coverage, uniform capacity to HTC users, and massive connectivity to MTC devices. To this end, advanced access techniques are required to provide such massive connectivity without jeopardizing the high data rates and bandwidth efficiency, thanks to NOMA.

Fostering such massive connectivity in MTC use case scenario requires a different radio access technology (RAT). To this end, NOMA is a very promising technology where multiple users are encouraged to use a shared frequency resource simultaneously [160]. This provides many useful advantages which include: better connectivity and higher spectral efficiency when compared to Orthogonal Multiple Access (OMA). However, this comes at the cost of increased intra-cell interference. Consequently, Successive Interference Cancellation (SIC) is employed at the receivers in order to mitigate this excessive interference [161]. In NOMA, two or more users are grouped together and are allocated a single radio resource to transmit or receive data. To maximize the multiplexing gain in NOMA, the grouped users must have a relative difference in their propagation environ-

ment conditions [160]. In the special case of a 2-UE (User Equipment) pair NOMA, one of the users must have a much better propagation environment than the other to fully acquire the gain of NOMA over OMA. In fact, this is a natural scenario when an HTC user is paired with an MTC device considering the harsh deployment scenarios of MTC devices (e.g., basements, underground facilities, and concrete constructions). When SIC is applied, the signal of the stronger user (e.g., HTC user) is decoded first and then subtracted from the composite signal before the signal of the weaker user (e.g., MTC device) can be decoded.

8.2 State-of-the-Art

Considering NOMA in either UDN or MTC has recently attracted increasing attention and efforts (eg. see [162–175]). A qualitative general framework of Power-Domain NOMA (PD-NOMA) and Code-Domain NOMA (CD-NOMA) to serve massive connectivity in Heterogeneous UDN is proposed in [163]. In [164], an access framework is investigated to group BSs in a User-Centric UDN deploying NOMA. Also, a resource allocation problem of the grouped BSs is formulated and solved using tools from optimization theory. In [165], the interference management problem in UDN is addressed and discussed considering NOMA. Enabling vehicular networks is one of the main potential applications in 5G networks, however, the massive connectivity requirements would be one of the limiting factors [166]. Scheduling and resource allocation of such scenarios is thus investigated in [166]. Also, NOMA is compared to OMA considering Visible Light communication (VLC) in UDN [167]. Support of MTC in mmWaves is then investigated in [168], grant-free NOMA for massive MTC connectivity is addressed in [169, 174], and a multi-user detection grant-free NOMA considering adaptive compressed sensing is investigated in [171]. NOMA alongside TDMA are investigated in energy efficient resource allocation scenario in order to support MTC in [170], and the fundamental limits of deploying NOMA in cellular massive IoT is discussed and studied in [173].

In [172], the average success probability and the average number of served MTC devices in aggregation communication mode is investigated where tools from stochastic geometry are utilized and two resource scheduling strategies are proposed and compared, namely a random strategy, and a channel-aware strategy. However, only MTC devices

are considered in this investigation, while the coexistence of HTC users and MTC devices is inevitable in next generation networks, especially UDN. Also, the high density of BSs is not considered in this study. In [175], the downlink and uplink of NOMA-based multiple access in a dense network are investigated considering a single type of UE. A power back-off scheme is employed in the uplink to guarantee a distinctive received power at the BS form the two paired devices. Although considering a dense network, the distinguishing features of such network are not addressed by the authors in [175]. Simple power decay path-loss model is assumed and no idle mode capabilities are considered in the BSs. Moreover, the impact of serving different types of UEs (e.g., HTC and MTC) is not investigated.

8.3 Contributions

Different from previous work, in this investigation we model the uplink coverage of HTC users and MTC devices paired together in NOMA-based radio access. To this end, we employ techniques from stochastic geometry for accurate modeling of the considered scenario. The inherent randomness of the locations of HTC users, massive MTC devices and dense small cells, encourages the use of stochastic techniques to approach the investigated problem. In what follows we summarize the contributions of this study as compared to previous work in the literature:

- The distinguishing features of UDN are considered in modelling the propagation environment where a Stretched Exponential Path-Loss (SEPL) model is used to capture the short-link distances.
- The idle mode of the BSs in UDNs is considered in the analysis where most of the cells are turned off to mitigate interference.
- An efficient association scheme, namely, connect-to-active (C2A) association is proposed to address the association of the MTC devices to the active cells activated by the HTC users. Accordingly, HTC users and MTC devices can be paired in NOMA-based radio access.
- The two types of UEs, i.e., HTC and MTC are fully characterized by their densities and power control parameters.

- Closed-form and easy-computable analytical results are derived for the considered performance metrics.

8.4 System Model

In this section, we present the details of the considered system model

8.4.1 Network Model

The uplink of a UDN is considered where two types of user nodes coexist in the network, namely, HTC users and MTC devices. In this scenario, both HTC users and MTC devices represent transmitters while BSs of the UDN act as receivers. We consider a single tier of small cells where the BSs are distributed according to a Homogeneous Poisson Point Process (HPPP) Φ_s with a density λ_s. Independently from the BSs distribution, the HTC users and the MTC nodes are modeled as two other independent HPPPs Φ_h and Φ_m with densities λ_h and λ_m, respectively. Notably, we assume that $\lambda_s \gg \lambda_h$, $\lambda_m \gg \lambda_h$. With the aspects of the traffic of MTC devices in mind, we assume that only a fraction $\rho_m \in [0, 1]$ of the MTC devices are active and are having packets to transmit [142]. All BSs, HTC users, and MTC nodes are assumed to deploy a single antenna and the whole bandwidth spectrum is reused in all cells i.e., we assume a frequency reuse factor of one.

8.4.2 Propagation Model

The propagation model considers path loss and fast fading components. The path loss is modeled by a stretched exponential path-loss (SEPL) where the transmit signal power decays with the distance r as $e^{-\alpha r^{\beta}}$. This model captures the signal propagation properties in UDN environments featuring short distances between the (serving/interfering) BSs and the associated users. Here, α and β are the model parameters which are used to tune it to capture different propagation environment. SEPL model describes the propagation scenarios where the attenuation is mainly caused by obstacles adding an average multiplicative attenuation of α, with the number of obstacles in the path scaling as r. This scaling is determined by the parameter β, where $\beta = 1$ provides a linear scaling, $\beta = 2$ provides a quadratic scaling and so on [2]. The 3GPP specifications, however, recommend the adoption of the multi-slope path loss model for dense networks [147]. In

the multi-slope path loss model, different distance ranges are subject to different path loss exponents. Analytically, the SEPL model provides a better alternative that is continuous and bounded where it can be easily incorporated in stochastic geometry analysis [2]. Moreover, the SEPL model can be seen as a limiting case for the multi-slope model with an infinite number of slopes.

Each link between an HTC user and a BS is subject to fast fading and is denoted by g_{hu}. Similarly, denote by g_{mu} the fast fading channel between an MTC node and a BS. Also, denote by g_{ho} and g_{mo} the fading gain of the useful link between an HTC user and its serving BS and an MTC node and its serving BS, respectively. We assume that the channel fading gains of all interfering nodes are independent and identically distributed (i.i.d), i.e., channel gains are independent of each other and independent of the locations of the nodes. Additionally, we assume that all fading channels follow a Rayleigh fading model, hence the channel power gains follow an exponential distribution with a mean of one i.e., exp(1).

8.4.3 Cell Association Model

We assume that HTC users associate to the BS with the strongest long-term average received power i.e., the nearest BS. A BS is considered in idle mode if no HTC users are associated to it, consequently, it is turned off to save energy and to mitigate interference. Accordingly, the BSs point process Φ_s is thinned with a probability $p_a = 1 - p_o$ forming another HPPP Φ_a with a density $\lambda_a = p_a \lambda_s$, where p_o is the probability of a BS being in idle mode and it is given by [176]:

$$p_o = \left(\frac{3.5\kappa}{1 + 3.5\kappa} \right)^{3.5}, \tag{8.1}$$

where $\kappa = \frac{\lambda_s}{\lambda_h}$. On the other hand, MTC nodes are allowed only to associate to the active BSs Φ_a, we call this *Connect-to-Active (C2A) association* [177].

8.4.4 Uplink Interference Model

The bandwidth allocated to each BS is divided into N_{RB} uplink orthogonal resource blocks (RBs), each of a bandwidth B_{RB}. An HTC user associated to a given BS is allocated an equal fraction $1/N_{htc}$ of the total available uplink resource blocks, where N_{htc} is the number of HTC users associated to this BS. Thus, the allocation of uplink resources for the HTC

users is orthogonal. In addition, we assume that each HTC user always has data ready to be send in its queue, i.e., full-buffer traffic model. On the other hand, an MTC node occupies only one radio block at any given time to transmit the available data packet. This orthogonal resource block is selected randomly in a uniformly distributed manner from the N_{RB} available uplink resources with a probability of $1/N_{RB}$. It is worth mentioning that the interference seen in the tagged resource block is from a single HTC user only in each cell. This is because of the orthogonal allocation of the resources for the HTC users. Moreover, we assume that the interference generated from MTC nodes connecting to the same BS (i.e., intra-cell interference) is perfectly mitigated via advanced physical and access layer techniques. These techniques are tailored to the specific requirements of MTC deployment scenarios (e.g., see the techniques discussed in [141]). In other words, only the inter-cell interference is accounted for in the analysis for both HTC users and MTC nodes.

8.4.5 Power Control Model

Each HTC user transmits in the uplink with a maximum power P_h^{max} to satisfy the limited transmit power constraints. The users thus employ a truncated channel inversion (TCI) power control policy. In TCI power control, an HTC transmits with a power P_h such that the average received power at the BS is P_{ho}. The transmission in the uplink is truncated if the required transmit power to invert the channel is more than the maximum transmit power P_h^{max}. Accordingly, P_{ho} is the receiving power threshold at the BS where $P_{ho} > P_{sensitivity}$, with $P_{sensitivity}$ being the minimum received power of the BS. In this way, a given HTC user is in a power outage if the required transmit power is greater than P_h^{max}. Hence, the transmit power can be expressed as:

$$P_h = \begin{cases} P_{ho}e^{\alpha R_h^{\beta}} & \text{if } \; P_{ho} \leq P_{ho}e^{\alpha R_h^{\beta}} \leq P_h^{max} \\ 0 & \text{otherwise} \end{cases} \tag{8.2}$$

Similarly, the MTC nodes undergo TCI power control policy with the power given by:

$$P_m = \begin{cases} P_{mo}e^{\alpha R_m^{\beta}} & \text{if } \; P_{mo} \leq P_{mo}e^{\alpha R_m^{\beta}} \leq P_m^{max} \\ 0 & \text{otherwise} \end{cases} \tag{8.3}$$

where $P_{mo} \ll P_{ho}$ and $P_m^{max} \ll P_h^{max}$.

Practically, a UE estimates the path loss to the serving cell $e^{ar^{\beta}}$ through measuring the reference signals' received power and by knowing the reference signals' transmission power from the system information sent on the control channels [145]. In addition, the power control parameters P_{uo} and P_u^{max} are known parameters where P_{uo} is broadcasted on the control channel of the serving cell and P_u^{max} is a design parameter of this UE, with $u \in \{m, h\}$. Interestingly, the 3GPP LTE standard adopts another power control scheme where no truncation occurs [145]. In other words, the setting of the power $P_u = \min(P_{uo}e^{ar_u^{\beta}}, P_u^{max})$ takes place. In this investigation, we adopt the TCI power control scheme for the sake of tractability.

Remarkably, the transmission power of a given node P_u is a random variable due to the randomness of the link distance r_u. Evidently, this is a direct consequence of the random distribution of the small cells, the HTC users, and the MTC nodes. In Section 8.5.1, we provide a statistical characterization of the transmission power P_u which is an essential element in studying the uplink coverage of the considered scenario.

8.4.6 Uplink NOMA Model

We assume a fully-loaded system where all active cells perform a 2-UE uplink NOMA, with one user being the HTC user and the other is the MTC node. In uplink NOMA, 2 UEs are allowed to transmit on the same resource block at the same time, where the gain of NOMA maximized with a larger difference between the channel conditions and transmit powers of both users. The pairing of the two users is random pairing, where the locations of the two UEs forming the NOMA pair are selected randomly from the HTC users and MTC nodes associated to a given cell. Since an MTC node requires a single resource block to transmit its packet, a pair of an HTC user and an MTC node is associated to a tagged resource block. In other words, we assume that on each resource block there is a NOMA pair that is composed of an HTC user and an MTC node. We further assume that the HTC user has a better channel condition and transmit power than the MTC node, i.e., $g_{ho} > g_{mo}$ and $P_h > P_m$. Consequently, the received signal of the HTC user is always decoded first at the BS with the signal of the MTC device treated as noise. Using SIC, the signal of the HTC user is perfectly removed from the composite signal and then the received signal of the MTC node can be decoded.

8.4.7 Performance Metrics

The SINR of the signal received at the typical BS located at the origin from the tagged HTC user and the tagged MTC device are given by:

$$\texttt{SINR}_h = \frac{P_{ho} g_{ho}}{P_{mo} g_{mo} + \mathcal{I}_m + \mathcal{I}_h + \sigma^2} \tag{8.4}$$

$$\texttt{SINR}_m = \frac{P_{mo} g_{mo}}{\mathcal{I}_m + \mathcal{I}_h + \sigma^2} \tag{8.5}$$

where σ^2 is the noise power, $\mathcal{I}_h$ is the aggregate interference from the HTC users on the tagged resource block from outside the tagged cell in the uplink, and $\mathcal{I}_m$ is the aggregate interference from the MTC devices on the tagged resource block from outside the tagged cell in the uplink. This aggregate interference $\mathcal{I}_h$ and $\mathcal{I}_m$ can be expressed as:

$$\mathcal{I}_m = \sum_{j \in \bar{\Phi}_m / UE_o^m} P_{mj} g_{mj} e^{-\alpha R_m^\beta} \mathbb{1}\left(P_{mj} e^{-\alpha R_m^\beta} < P_{mo}\right), \tag{8.6}$$

$$\mathcal{I}_h = \sum_{j \in \bar{\Phi}_h / UE_o^h} P_{hj} g_{hj} e^{-\alpha R_h^\beta} \mathbb{1}\left(P_{hj} e^{-\alpha R_h^\beta} < P_{ho}\right), \tag{8.7}$$

where P_{mj} is the transmission power of MTC device j, g_{mj} is its channel fading gain, and $\bar{\Phi}_m$ is the set of all interfering MTC devices transmitting on the tagged resource block and interfering with the transmission of the tagged device UE_o^m from outside its serving cell. Also, P_{hj} is the transmission power of HTC user j, g_{hj} is its channel fading gain, and $\bar{\Phi}_h$ is the set of all interfering HTC users transmitting on the tagged resource block and interfering with the transmission of the tagged device UE_o^h from outside its serving cell. In addition, $\mathbb{1}(\cdot)$ is the indicator function which takes the value 1 if its argument $(\cdot)$ is true and zero otherwise.

We consider two performance metrics in this investigation, namely, the uplink coverage probability and the uplink network throughput. In what follows, we discuss the considered performance metrics.

8.4.7.1 Uplink Coverage

The uplink coverage probability for both types of devices can be defined as:

$$\mathcal{P}_h^U(\tau_h) = \mathbb{P}\left\{\texttt{SINR}_h > \tau_h\right\}, \tag{8.8}$$

$$\mathcal{P}_m^U(\tau_m, \tau_h) = \mathbb{P}\left\{\texttt{SINR}_m > \tau_m, \texttt{SINR}_h > \tau_h\right\}, \tag{8.9}$$

The uplink coverage of the MTC devices $\mathcal{P}_m^U(\tau_m, \tau_h)$ is defined in terms of both the coverage threshold of both the MTC devices τ_m and the HTC users τ_h. This is a consequence of the decoding order of the composite signal received at the BS from a pair of an HTC user and an MTC device. The received signal of the MTC device cannot be decoded successfully unless the received signal of the HTC user decoded first. Thus, an MTC device is in outage if the paired HTC user is in outage.

8.4.7.2 Network Throughput

The network throughput can be defined as [2]:

$$\mathcal{R}_h^U(\tau_h) = p_a \lambda_s \log_2(1+\tau_h)\mathcal{P}_h^U(\tau_h), \tag{8.10}$$

$$\mathcal{R}_m^U(\tau_m, \tau_h) = \rho_m \lambda_m \log_2(1+\tau_m)\mathcal{P}_m^U(\tau_m, \tau_h), \tag{8.11}$$

8.5 Analytical Results

8.5.1 Uplink Power Control Analysis in NOMA

The power control procedure of both HTC users and MTC devices has a significant impact on the network performance. Power control is a means of interference mitigation in the uplink, hence, it influences the performance. Both HTC users and MTC devices undergo a truncated channel inversion (TCI) power control. An active HTC user adjusts its transmission power such that the received power at the serving BS is P_{ho}. Accordingly, an HTC user is considered in power outage if the required transmission power P_h exceeds the available maximum power P_h^{max}. Since, the locations of all HTC users and BSs are drawn from a random process, therefore, the transmission power P_h of any active HTC user is a random variable where $P_h \in [P_{ho}, P_h^{max}]$. The transmission power P_{ho} corresponds to a user which is very close to the BS, i.e., $r \sim 0$, while the transmission power P_h^{max} corresponds to the farthest user a BS can serve. Likewise, an MTC device applies the same procedure to adjust its transmission power P_m with a cutoff threshold of P_{mo} and a maximum transmit power of P_m^{max}, i.e., $P_m \in [P_{mo}, P_m^{max}]$.

In this section, we characterize the statistical properties of the transmission power of the typical MTC device and the typical HTC user P_m and P_h, respectively. We provide the probability distribution function (PDF) of the transmission power and the expectation

of the log-relative-power defined as $\ln\left(\frac{Pm}{P_{mo}}\right)$ and $\ln\left(\frac{Ph}{P_{ho}}\right)$ which appear in the expressions of the coverage probability in the next section.

A given HTC user is in power control outage when the transmission power required to reach the closest BS exceeds the available maximum transmission power P_h^{max}. Accordingly, the outage probability due to the power truncation forced by the power control mechanism can be computed as:

$$\mathcal{O}_h = \mathbb{P}\left\{r > r_h\right\}. \tag{8.12}$$

Since the transmission power at a given distance r is $P = P_{ho}e^{ar^{\beta}}$, an HTC user experiences outage due to power truncation if the required power to transmit is more than the maximum available transmission power P_h^{max} or equivalently, the node is at a distance farther than r_h where $r_h = \ln^{\frac{1}{\beta}}\left(\frac{P_h^{max}}{P_{ho}}\right)^{\frac{1}{a}}$. Since the CDF of r is $F_R(r) = 1 - e^{-\pi\lambda_s r^2}$ [58], hence, the power control outage probability can be expressed as:

$$\begin{aligned}\mathcal{O}_h &= \mathbb{P}\left\{r > r_h\right\} = 1 - \mathbb{P}\left\{r < r_h\right\} \\ &= 1 - \left(1 - e^{-\pi\lambda_s r_h^2}\right) \\ &= e^{-\pi\lambda_s r_h^2}.\end{aligned} \tag{8.13}$$

Similarly, the power control outage of an MTC device can be defined as:

$$\mathcal{O}_m = \mathbb{P}\left\{r > r_m\right\}. \tag{8.14}$$

However, the CDF of r in the case of MTC devices is $F_R(r) = 1 - e^{-\pi p_a \lambda_s r^2}$ since the MTC devices can connect only to active small cells. Accordingly, the power control outage of MTC devices can be expressed as:

$$\mathcal{O}_m = e^{-\pi p_a \lambda_s r_m^2}. \tag{8.15}$$

where $r_m = \ln^{\frac{1}{\beta}}\left(\frac{P_m^{max}}{P_{mo}}\right)^{\frac{1}{a}}$.

In the next Lemma, we provide the conditional probability distribution function (PDF) of the transmission power of a generic active HTC user.

Lemma 1. *The PDF of the uplink transmission power P_h of a generic active HTC user associated to the nearest BS in a UDN environment considering a truncated channel inversion power control is expressed as:*

$$f_{P_h}(x) = \frac{2\pi\lambda_s \ln^{\frac{2}{\beta}-1}\left(\frac{x}{P_{ho}}\right)^{\frac{1}{\alpha}}}{a\beta x\left(1-\mathcal{O}_h\right)} e^{-\pi\lambda_s \ln^{\frac{2}{\beta}}\left(\frac{x}{P_{ho}}\right)^{\frac{1}{a}}}. \tag{8.16}$$

Proof. The transmission power of a given active HTC user is a function of the distance to its serving BS due to the employed truncation channel inversion power control. The transmission power of HTC user at a distance r from the serving BS is $P_h = P_{ho}e^{ar^\beta}$. Moreover, the transmission power is constrained by the maximum transmission power P_h^{max} and is lower bounded by the minimum received power at the BS P_{ho}. The CDF of the transmission power P_h can be expressed as:

$$\begin{aligned} F_{P_h}(x) &= \mathbb{P}\left\{P_h \leq x\right\} = \mathbb{P}\left\{P_{ho}e^{ar^\beta} \leq x\right\} = \mathbb{P}\left\{r \leq \ln^{1/\beta}\left(\frac{x}{P_{ho}}\right)^{1/a}\right\} \\ &= F_R\left(\ln^{1/\beta}\left(\frac{x}{P_{ho}}\right)^{1/a}\right). \end{aligned} \tag{8.17}$$

Considering the CDF of r, the truncated CDF of P_h can be written as:

$$F_{P_h}(x) = \frac{1 - e^{-\pi\lambda_s \ln^{2/\beta}\left(\frac{x}{P_{ho}}\right)^{1/a}}}{1 - e^{-\pi\lambda_s \ln^{2/\beta}\left(\frac{P_h^{max}}{P_{ho}}\right)^{1/a}}} \tag{8.18}$$

and hence, the PDF of P_h can be written as:

$$f_{P_h(x)} = \frac{dF_{P_h}(x)}{dx} = \frac{2\pi\lambda_s \ln^{\frac{2}{\beta}-1}\left(\frac{x}{P_{ho}}\right)^{\frac{1}{\alpha}}}{a\beta x\left(1-\mathcal{O}_h\right)} e^{-\pi\lambda_s \ln^{\frac{2}{\beta}}\left(\frac{x}{P_{ho}}\right)^{\frac{1}{a}}} \tag{8.19}$$

This completes the proof. ■

Similarly, in the next Lemma, we provide the conditional probability distribution function (PDF) of the transmission power of a generic active MTC device.

Lemma 2. *The PDF of the uplink transmission power P_m of a generic active MTC device associated to the nearest BS in a UDN environment considering a truncated channel inversion power control is expressed as:*

$$f_{P_m}(x) = \frac{2\pi p_a\lambda_s \ln^{\frac{2}{\beta}-1}\left(\frac{x}{P_{mo}}\right)^{\frac{1}{\alpha}}}{a\beta x\left(1-\mathcal{O}_m\right)} e^{-\pi p_a\lambda_s \ln^{\frac{2}{\beta}}\left(\frac{x}{P_{mo}}\right)^{\frac{1}{a}}}. \tag{8.20}$$

Proof. Similarly, the transmission power of a given active MTC device is a function of the distance to its serving BS and is given by $P_m = P_{mo}e^{ar^\beta}$. Moreover, $P_m \in [P_{mo}, P_m^{max}]$, therefore, the CDF of the transmission power P_m can be expressed as:

$$F_{P_m}(x) = \mathbb{P}\left\{P_m \leq x\right\} = \mathbb{P}\left\{P_{mo}e^{ar^\beta} \leq x\right\} = \mathbb{P}\left\{r \leq \ln^{1/\beta}\left(\frac{x}{P_{mo}}\right)^{1/a}\right\}$$
$$= F_R\left(\ln^{1/\beta}\left(\frac{x}{P_{mo}}\right)^{1/a}\right). \tag{8.21}$$

Considering the association scheme of the MTC devices, the CDF of r is $F_R(r) = 1 - e^{-\pi p_a \lambda_s r^2}$ since the MTC devices can connect only to active small cells. Hence, the truncated CDF of P_m can be written as:

$$F_{P_m}(x) = \frac{1 - e^{-\pi p_a \lambda_s \ln^{2/\beta}\left(\frac{x}{P_{mo}}\right)^{1/a}}}{1 - e^{-\pi p_a \lambda_s \ln^{2/\beta}\left(\frac{P_m^{max}}{P_{mo}}\right)^{1/a}}} \tag{8.22}$$

and hence, the PDF of P_m can be written as:

$$f_{P_m(x)} = \frac{dF_{P_m}(x)}{dx} = \frac{2\pi p_a \lambda_s \ln^{\frac{2}{\beta}-1}\left(\frac{x}{P_{mo}}\right)^{\frac{1}{\alpha}}}{a\beta x\left(1 - \mathcal{O}_m\right)} e^{-\pi p_a \lambda_s \ln^{\frac{2}{\beta}}\left(\frac{x}{P_{mo}}\right)^{\frac{1}{a}}} \tag{8.23}$$

This completes the proof.

■

In the next two Lemmas, we use the PDF of the transmission power P_h and P_m computed for both the HTC users and the MTC device, respectively, to proceed in the analysis. To this end, we evaluate the moments of the log-relative-power $\ln^k(P_h/P_{ho})$ and $\ln^k(P_m/P_{mo})$ of the HTC users and the MTC devices, respectively. These will be used in the uplink coverage and network throughput analysis provided in the next section.

Lemma 3. *The conditional expectation of the function* $\ln^k(P_h/P_{ho}), k \in \{0, 1, 2, \cdots\}$ *is given by:*

$$\mathbb{E}_{P_h}\left[\ln^k(P_h/P_{ho})\right] = \frac{a^k \gamma\left(\frac{\beta k}{2} + 1, \pi\lambda_s r_h^2\right)}{\left(\pi\lambda_s\right)^{\frac{\beta k}{2}}\left(1 - \mathcal{O}_h\right)}. \tag{8.24}$$

Proof. The expectation of the function $\ln^k(P_h/P_{ho})$ can be expressed as:

$$\begin{aligned}
&\mathbb{E}_{P_h}\left[\ln^k(P_h/P_{ho})\right] \\
&= \int_{P_{ho}}^{P_m^{max}} \ln^k(x/P_{ho}) f_{P_h}(x)\mathrm{d}x && (8.25)\\
&\overset{a}{=} \frac{2\pi\lambda_s}{a\beta\left(1-\mathcal{O}_h\right)} \int_0^{\delta} (aw)^k w^{2/\beta-1} e^{-\pi\lambda_s w^{2/\beta}}\mathrm{d}w && (8.26)\\
&\overset{b}{=} \frac{a^k\gamma\left(\frac{\beta k}{2}+1, \pi\lambda_s r_h^2\right)}{(\pi\lambda_s)^{\frac{\beta k}{2}}\left(1-\mathcal{O}_h\right)}, && (8.27)
\end{aligned}$$

where step (a) is the result of the change of variables $x = P_{ho}e^{aw}$ and $\delta = r_h^{\beta}$. Step (b) follows from simple manipulation and evaluating the integral. ■

Likewise, we evaluate the moments of the log-relative-power of the transmission power of an active MTC device P_m.

Lemma 4. *The conditional expectation of the function* $\ln^k(P_m/P_{mo}), k \in \{0, 1, 2, \cdots\}$ *is given by:*

$$\mathbb{E}_{P_m}\left[\ln^k(P_m/P_{mo})\right] = \frac{a^k\gamma\left(\frac{\beta k}{2}+1, \pi p_a\lambda_s r_m^2\right)}{(\pi p_a\lambda_s)^{\frac{\beta k}{2}}\left(1-\mathcal{O}_m\right)}. \tag{8.28}$$

Proof. Following similar steps as in the proof of Lemma 3, we arrive at the result given in this Lemma. ■

The log-relative-power in Lemma 3 and 4 is a measure of the transmission power P_h and P_m relative to the cutoff threshold P_{ho} and P_{mo}, respectively. The expected transmission power is thus scaled by the power control coverage (i.e., $1-\mathcal{O}_h$ and $1-\mathcal{O}_m$, respectively). Hence, a higher transmission power at the HTC users and the MTC devices is required as the power control outage increases. At the same time, as the BSs density increases, the expected transmission power decreases. This is intuitive where a higher BSs density means a shorter distance between either HTC users or MTC devices and its serving BS, and hence, a less power to invert the channel.

8.5.2 Uplink NOMA Coverage and Throughput Analysis

In this section, a comprehensive analysis is provided for the performance metrics discussed in the system model.

8.5.2.1 Uplink NOMA Coverage Analysis

We start off by analyzing the uplink NOMA coverage in the considered scenario where we employ random pairing of an HTC user and an MTC device to form a 2-U group. From now on, we assume that the HTC users enjoy a much favorable propagation environment than the one corresponding to the paired MTC device. Since, in a typical UDN, the density of the small cells exceeds the density of the active HTC users, therefore, HTC users will always be at a close proximity to the serving cell probably with a Line-of-Sight (LOS) connection. Nevertheless, the MTC devices are usually deployed in harsh deployment scenarios leaving them with terrible propagation conditions. Focusing on the aspects of the NOMA-based coexistence of HTC users and MTC devices, we consider Rayleigh fading for the sake of tractable and insightful results. In the following theorem, we calculate the average uplink coverage probability for the typical HTC user.

Theorem 1. *The uplink coverage probability of the tagged HTC which is paired in a 2-UE group with a randomly chosen MTC device on the tagged resource block considering the system model in Section 8.4 is given by:*

$$\mathcal{P}_h^U(\tau_h) = \begin{cases} \mu e^{-\frac{2\delta_h}{\mathit{SNR}_h}} \mathcal{L}_{I_h}\left(\frac{2\delta_h}{P_{ho}}\right) \mathcal{L}_{I_m}\left(\frac{2\delta_h}{P_{ho}}\right) + \nu e^{-\frac{\tau_h}{\mathit{SNR}_h}} \mathcal{L}_{I_h}\left(\frac{\tau_h}{P_{ho}}\right) \mathcal{L}_{I_m}\left(\frac{\tau_h}{P_{ho}}\right), & \text{if } \tau_h \frac{P_{mo}}{P_{ho}} < 1 \\ \nu e^{-\frac{\tau_h}{\mathit{SNR}_h}} \mathcal{L}_{I_h}\left(\frac{\tau_h}{P_{ho}}\right) \mathcal{L}_{I_m}\left(\frac{\tau_h}{P_{ho}}\right), & \text{if } \tau_h \frac{P_{mo}}{P_{ho}} \geq 1 \end{cases} \tag{8.29}$$

where $\delta_h = \frac{\tau_h}{1-\tau_h \frac{P_{mo}}{P_{ho}}}$, $\mathit{SNR}_h = \frac{P_{ho}}{\sigma^2}$, $\mu = \frac{\tau_h \frac{P_{mo}}{P_{ho}} - 1}{\tau_h \frac{P_{mo}}{P_{ho}} + 1}$, $\nu = \frac{2}{\tau_h \frac{P_{mo}}{P_{ho}} + 1}$ *and*

$$\mathcal{L}_{I_h}(s) = \exp\left\{ -\left(\frac{2\pi}{\beta \alpha^{2/\beta}}\right) (p_a \lambda_s) \, \mathbb{E}_{P_h} \left[\int_0^{sP_{ho}} \frac{\left[\ln\left(\frac{sP_h}{y}\right)\right]^{\frac{2}{\beta}-1}}{y+1} \mathrm{d}y \right] \right\} \tag{8.30}$$

$$\mathcal{L}_{I_m}(s) = \exp\left\{ -\left(\frac{2\pi}{\beta \alpha^{2/\beta}}\right) \left(\frac{\rho_m \lambda_m}{N_{RB}}\right) \mathbb{E}_{P_m} \left[\int_0^{sP_{mo}} \frac{\left[\ln\left(\frac{sP_m}{y}\right)\right]^{\frac{2}{\beta}-1}}{y+1} \mathrm{d}y \right] \right\} \tag{8.31}$$

Proof. Since $g_h > g_m$, the uplink coverage probability of the typical HTC user paired with a random MTC device can be computed as follows:

$$\begin{aligned} \mathcal{P}_h^U(\tau_h) &= \mathbb{P}\left\{ \mathtt{SINR}_h > \tau_h, g_h > g_m \right\} \\ &= \mathbb{P}\left\{ g_h > g_m, g_h > \tau_h \frac{P_{mo}}{P_{ho}} g_m + \frac{\tau_h}{P_{ho}} \left(\mathcal{I}_h + \mathcal{I}_m + \sigma^2 \right) \right\} \end{aligned} \tag{8.32}$$

Firstly, if $\tau_h \frac{P_{mo}}{P_{ho}} \geq 1$, then $A_h = \frac{\tau_h}{P_{ho}} \left(P_{mo} g_m + \mathcal{I}_h + \mathcal{I}_m + \sigma^2\right) > g_m$, and hence:

$$\mathcal{P}_h^U(\tau_h) = \mathbb{P}\left\{g_h > A_h\right\} \tag{8.33}$$

Since g_h and g_m both follow exponential distribution with mean one, therefore the order statistics of g_h and g_m is given by $f_{g_h g_m}(g_h, g_m) = 2 f_{g_h} f_{g_m} = 2e^{-g_h - g_m}$ [178]. Accordingly, the uplink coverage probability can be expressed as:

$$\begin{aligned}
\mathcal{P}_h^U(\tau_h) &= \mathbb{E}\left[\int_{g_m=0}^{\infty} \int_{g_h=A_h}^{\infty} f_{g_h g_m}(g_h, g_m) \mathrm{d}g_h \mathrm{d}g_m\right] \\
&= 2 \int_{g_m=0}^{\infty} e^{-(1+\tau_h \frac{P_{mo}}{P_{ho}}) g_m} \mathrm{d}g_m \mathbb{E}\left[exp\left\{-\frac{\tau_h}{P_{h_o}}\left(\mathcal{I}_h + \mathcal{I}_m + \sigma^2\right)\right\}\right] \\
&= \frac{2}{\tau_h \frac{P_{mo}}{P_{ho}} + 1} e^{-\frac{\tau_h}{\mathtt{SNR}_h}} \mathcal{L}_{I_h}\left(\frac{\tau_h}{P_{ho}}\right) \mathcal{L}_{I_m}\left(\frac{\tau_h}{P_{ho}}\right),
\end{aligned} \tag{8.34}$$

Secondly, in case of $\tau_h \frac{P_{mo}}{P_{ho}} < 1$,

$$\begin{aligned}
&\mathcal{P}_h^U(\tau_h) = \mathbb{P}\left\{g_h > g_m, g_m > A_h\right\} + \mathbb{P}\left\{g_h > A_h, g_m < A_h\right\} \\
&= \mathbb{E}\left[\int_{g_m=\frac{\frac{\tau_h}{P_{ho}}(\mathcal{I}_h + \mathcal{I}_m + \sigma^2)}{1-\tau_h \frac{P_{mo}}{P_{ho}}}}^{\infty} \int_{g_h=g_m}^{\infty} f_{g_h g_m}(g_h, g_m) \mathrm{d}g_h \mathrm{d}g_m \right. \\
&\left. + \int_{g_m=0}^{\frac{\frac{\tau_h}{P_{ho}}\left(\mathcal{I}_h + \mathcal{I}_m + \sigma^2\right)}{1-\tau_h \frac{P_{mo}}{P_{ho}}}} \int_{g_h=A_h}^{\infty} f_{g_h g_m}(g_h, g_m) \mathrm{d}g_h \mathrm{d}g_m\right] \\
&= e^{-\frac{2\delta_h}{\mathtt{SNR}_h}} \mathcal{L}_{I_h}\left(\frac{2\delta_h}{P_{ho}}\right) \mathcal{L}_{I_m}\left(\frac{2\delta_h}{P_{ho}}\right) - \frac{2}{\tau_h \frac{P_{mo}}{P_{ho}} + 1} e^{-\frac{2\delta_h}{\mathtt{SNR}_h}} \mathcal{L}_{I_h}\left(\frac{2\delta_h}{P_{ho}}\right) \mathcal{L}_{I_m}\left(\frac{2\delta_h}{P_{ho}}\right) \\
&+ \frac{2}{\tau_h \frac{P_{mo}}{P_{ho}} + 1} e^{-\frac{\tau_h}{\mathtt{SNR}_h}} \mathcal{L}_{I_h}\left(\frac{\tau_h}{P_{ho}}\right) \mathcal{L}_{I_m}\left(\frac{\tau_h}{P_{ho}}\right) \\
&= \frac{\tau_h \frac{P_{mo}}{P_{ho}} - 1}{\tau_h \frac{P_{mo}}{P_{ho}} + 1} e^{-\frac{2\delta_h}{\mathtt{SNR}_h}} \mathcal{L}_{I_h}\left(\frac{2\delta_h}{P_{ho}}\right) \mathcal{L}_{I_m}\left(\frac{2\delta_h}{P_{ho}}\right) + \frac{2}{\tau_h \frac{P_{mo}}{P_{ho}} + 1} e^{-\frac{\tau_h}{\mathtt{SNR}_h}} \mathcal{L}_{I_h}\left(\frac{\tau_h}{P_{ho}}\right) \mathcal{L}_{I_m}\left(\frac{\tau_h}{P_{ho}}\right)
\end{aligned} \tag{8.35}$$

Now, we move attention to the Laplace Transform (LT) of the PDF of the aggregate

uplink interference $\mathcal{I}_h$ which is expressed as:

$$\begin{aligned}
&\mathcal{L}_{\mathcal{I}_h}(s) = \mathbb{E}_{\mathcal{I}_h}\left[e^{-s\mathcal{I}_h}\right] \\
&= \mathbb{E}\left[\exp\left\{-s\sum_{j\in\bar{\Phi}_h/UE_o^h} P_{hj}g_{hj}e^{-\alpha r^\beta}\mathbb{1}\left(P_{hj}e^{-\alpha r^\beta}\right)\right\}\right] \\
&\overset{a}{=} \mathbb{E}_{\bar{\Phi}_h}\left[\prod_{j\in\bar{\Phi}_h/UE_o^h}\mathbb{E}_{P_h,g_h}\left[\exp\left\{-sP_{hj}g_{hj}e^{-ar^\beta}\right\}\mathbb{1}(P_{hj}e^{-ar^\beta} < P_o)\right]\right] \\
&\overset{b}{=} \exp\left\{-2\pi p_a\lambda_s\mathbb{E}_{P_h,g_h}\left[\int_{\ln^{\frac{1}{\beta}}(\frac{P_h}{P_{ho}})^{\frac{1}{\alpha}}}^{\infty}\left(1-e^{-sP_hg_he^{-ar^\beta}}\right)r\mathrm{d}r\right]\right\} \\
&\overset{c}{=} \exp\left\{-2\pi p_a\lambda_s\mathbb{E}_{P_h}\left[\int_{\ln^{\frac{1}{\beta}}(\frac{P_h}{P_{ho}})^{\frac{1}{\alpha}}}^{\infty}\left(1-\frac{1}{1+sP_he^{-ar^\beta}}\right)r\mathrm{d}r\right]\right\} \\
&\overset{d}{=} \exp\left\{\left(\frac{-2\pi p_a\lambda_s}{\beta a^{2/\beta}}\right)\mathbb{E}_{P_h}\left[\int_0^{sP_{ho}}\frac{\left[\ln(\frac{sP_h}{y})\right]^{\frac{2}{\beta}-1}}{y+1}\mathrm{d}y\right]\right\}
\end{aligned} \tag{8.36}$$

Since the HTC users are allocated orthogonal resources in each BS, only one HTC user is considered in the uplink aggregate interference. Accordingly, the set of interfering users in the uplink on the tagged resource block $\bar{\Phi}_h$ is a thinned version of the HPPP Φ_h with a thinning factor $p_a\lambda_s$, where p_a is the probability of active BSs. We assume that the transmission power from all interfering users are independent. Indeed, this assumption can be justified considering the special features of UDN where the variance in the cell sizes vanishes as the density of the BSs increases. (a) follows from the independence of the transmission powers P_{hj}, the fading channel gains g_{hj}, and the PPP Φ_h. (b) follows from the probability generating functional (PGFL) of the PPP [105]. The integral limits in (b) consider the region where the interfering nodes reside. Since the interference power (i.e., $P_he^{-ar^\beta}$) is always less than the power truncation cutoff threshold P_{ho}, the interfering HTC users are thus located in an open disk with inner radius $r = \ln^{\frac{1}{\beta}}(\frac{P_h}{P_{ho}})^{\frac{1}{\alpha}}$ and outer radius at ∞. Step (c) follows from the LT of the fading gain g_h and finally, (d) results from the change of variables $y = sP_he^{-ar^\beta}$. This completes the proof.

Similarly, we can derive the Laplace Transform (LT) of the PDF of the aggregate

uplink interference $\mathcal{I}_m$ which is expressed as:

$$\mathcal{L}_{\mathcal{I}_m}(s) = \mathbb{E}_{\mathcal{I}_m}\left[e^{-s\mathcal{I}_m}\right] = \exp\left\{\left(\frac{-2\pi\rho_m\lambda_m}{\beta a^{2/\beta}N_{RB}}\right)\mathbb{E}_{P_m}\left[\int_0^{sP_{mo}}\frac{\left[\ln\left(\frac{sP_m}{y}\right)\right]^{\frac{2}{\beta}-1}}{y+1}\mathrm{d}y\right]\right\} \tag{8.37}$$

By combining the results in (8.34), (8.35), (8.36), and (8.37) the proof is complete.

■

Theorem 1 presents an interesting result where the uplink coverage of the HTC users has two distinct regions of operation with regard to the coverage threshold τ_h with the boundary set as $\tau_h = \frac{P_{ho}}{P_{mo}}$. Interestingly, this boundary is a function of the ratio of the power control cutoff threshold of the HTC users and the MTC devices which highlights the significant impact of the power control procedure on the network performance. Moreover, the uplink coverage consists of three components representing the effect of the noise, the uplink interference of the HTC users, and the uplink interference of the MTC devices. While the exponential noise term is a function of two system parameters, namely, the coverage threshold and the HTC power control cutoff threshold, further, the HTC interference term $\mathcal{L}_h$ shows the impact of the SEPL model (α and β), the BSs activity probability p_a, and the density of the small cells λ_s. Note that $\lim_{\lambda_s\to\infty} p_a\lambda_s = \lambda_h$ which also establishes the connection between the uplink coverage performance and the density of the active HTC users. On the other hand, the MTC interference term $\mathcal{L}_m$ represents the impact of the density of the active MTC devices $\rho_m\lambda_m$ and the available bandwidth N_{RB}. For the sake of more simplification, in the following corollaries, we consider some special cases of the SEPL model parameter β where these special cases provide a tractable alternative for the multi-slope path loss model recommended by the 3GPP. [2, 147].

Corollary 1. *In the special case $\beta = \frac{2}{n+1}$, where $n \in \mathbb{Z}$ is any non-negative integer, the uplink coverage given in Theorem 1 can be simplified to:*

$$\mathcal{P}_h^U(\tau_h) = \begin{cases} \mu e^{-\frac{2\delta_h}{SNR_h}}\mathcal{L}_{I_h}\left(\frac{2\delta_h}{P_{ho}}\right)\mathcal{L}_{I_m}\left(\frac{2\delta_h}{P_{ho}}\right) + \nu e^{-\frac{\tau_h}{SNR_h}}\mathcal{L}_{I_h}\left(\frac{\tau_h}{P_{ho}}\right)\mathcal{L}_{I_m}\left(\frac{\tau_h}{P_{ho}}\right), & \text{if } \tau_h\frac{P_{mo}}{P_{ho}} < 1 \\ \nu e^{-\frac{\tau_h}{SNR_h}}\mathcal{L}_{I_h}\left(\frac{\tau_h}{P_{ho}}\right)\mathcal{L}_{I_m}\left(\frac{\tau_h}{P_{ho}}\right), & \text{if } \tau_h\frac{P_{mo}}{P_{ho}} \geq 1 \end{cases} \tag{8.38}$$

where

$$\mathcal{L}_{I_h}(s) = \exp\left\{-\Upsilon(n)\binom{n}{k}\mathbb{E}_{P_h}\left[\ln^k\left(\frac{P_h}{P_{ho}}\right)\right]\ \mathcal{J}_{n-k}(sP_{ho})\right\} \tag{8.39}$$

$$\mathcal{L}_{I_m}(s) = \exp\left\{-\xi(n)\binom{n}{k}\mathbb{E}_{P_m}\left[\ln^k\left(\frac{P_m}{P_{mo}}\right)\right]\ \mathcal{J}_{n-k}(sP_{mo})\right\} \tag{8.40}$$

and

$$\mathcal{J}_v(x) = \int_0^x \frac{\ln^v(x/y)}{y+1}\mathrm{d}y, \tag{8.41}$$

$$\Upsilon(n) = \frac{(n+1)\pi p_a \lambda_s}{a^{n+1}}, \tag{8.42}$$

$$\xi(n) = \frac{(n+1)\pi \rho_m \lambda_m}{a^{n+1} N_{RB}}, \tag{8.43}$$

$\mathbb{E}_{P_h}[\ln^k(P_h/P_{ho})]$ *and* $\mathbb{E}_{P_m}[\ln^k(P_m/P_{mo})]$ *are given in Lemma 3 and Lemma 4, respectively*

.

Proof. By substituting the value of $\beta = \frac{2}{n+1}$ in (8.30) and (8.31), respectively, we get:

$$\mathcal{L}_{I_h}(s) = \exp\left\{-\left(\frac{(n+1)\pi p_a \lambda_s}{a^{n+1}}\right)\mathbb{E}_{P_h}\left[\int_0^{sP_{ho}} \frac{\left(\ln(\frac{P_h}{P_{ho}}) + \ln(\frac{sP_{ho}}{y})\right)^n}{y+1}\mathrm{d}y\right]\right\} \tag{8.44}$$

$$\mathcal{L}_{I_m}(s) = \exp\left\{-\left(\frac{(n+1)\pi \rho_m \lambda_m}{a^{n+1} N_{RB}}\right)\mathbb{E}_{P_m}\left[\int_0^{sP_{mo}} \frac{\left(\ln(\frac{P_m}{P_{mo}}) + \ln(\frac{sP_{mo}}{y})\right)^n}{y+1}\mathrm{d}y\right]\right\} \tag{8.45}$$

Using the binomial expansion and by simple mathematical manipulation, we arrive at the result in the Corollary. This completes the proof. ■

A closed-form version of the results presented in Theorem 1 can be further derived by considering the special case $\beta = 2$. In the following corollary we lay out this result.

Corollary 2. *In the special case $\beta = 2$, the uplink coverage given in Theorem 1 can be simplified to:*

$$\mathcal{P}_h^U(\tau_h) =$$

$$\begin{cases} \mu \exp\left\{-\left(\frac{2\delta_h}{SNR_h} + \frac{\pi p_a \lambda_s}{\alpha}\ln(1+2\delta_h) + \frac{\pi \rho_m \lambda_m}{\alpha N_{RB}}\ln\left(1+2\delta_h\frac{P_{mo}}{P_{ho}}\right)\right)\right\} + \\ \nu \exp\left\{-\left(\frac{\tau_h}{SNR_h} + \frac{\pi p_a \lambda_s}{\alpha}\ln(1+\tau_h) + \frac{\pi \rho_m \lambda_m}{\alpha N_{RB}}\ln\left(1+\tau_h\frac{P_{mo}}{P_{ho}}\right)\right)\right\}, & \text{if } \tau_h\frac{P_{mo}}{P_{ho}} < 1 \\ \nu \exp\left\{-\left(\frac{\tau_h}{SNR_h} + \frac{\pi p_a \lambda_s}{\alpha}\ln(1+\tau_h) + \frac{\pi \rho_m \lambda_m}{\alpha N_{RB}}\ln\left(1+\tau_h\frac{P_{mo}}{P_{ho}}\right)\right)\right\}, & \text{if } \tau_h\frac{P_{mo}}{P_{ho}} \geq 1 \end{cases}$$

Proof. By substituting the value of $\beta = 2$ in (8.30) and (8.31), respectively, and by evaluating the resulting integral we arrive at the results in the Corollary. This completes the proof. ■

To complement our analysis, in the following theorem we compute the average uplink coverage of the typical MTC device which is paired with the typical HTC user in the same uplink NOMA-group. In uplink NOMA, the signal of the user with stronger channel conditions, here it is the HTC user, has to be decoded successfully first before decoding the signal of the weaker user, i.e., the MTC device. Accordingly, the uplink coverage of the MTC device is a function of the coverage threshold of the HTC user. To clarify this, in a given NOMA-pair, if the decoding of the HTC user signal failed, so is the decoding of the MTC device's signal. Therefore, the coverage requirements of the HTC user has to be satisfied firstly, and then the decoding of the MTC device signal can be achieved successfully. Theorem 2 presents this result.

Theorem 2. *The uplink coverage probability of the tagged MTC device which is paired in a 2-UE group with a randomly chosen HTC user with a coverage threshold τ_h on the tagged resource block considering the system model in Section 8.4 is given by:*

$$\mathcal{P}_m^U(\tau_m, \tau_h) =$$

$$\begin{cases} \nu e^{-\frac{\Psi}{\mathit{SNR}_h}} \mathcal{L}_{I_m}\left(\frac{\Psi}{P_{ho}}\right) \mathcal{L}_{I_h}\left(\frac{\Psi}{P_{ho}}\right), & \text{if } \tau_h \frac{P_{mo}}{P_{ho}} \geq 1 \\ \mu e^{-\frac{2\delta_h}{\mathit{SNR}_h}} \mathcal{L}_{I_m}\left(\frac{2\delta_h}{P_{ho}}\right) \mathcal{L}_{I_h}\left(\frac{2\delta_h}{P_{ho}}\right) + \nu e^{-\frac{\Psi}{\mathit{SNR}_h}} \mathcal{L}_{I_m}\left(\frac{\Psi}{P_{ho}}\right) \mathcal{L}_{I_h}\left(\frac{\Psi}{P_{ho}}\right), & \text{if } \tau_h \frac{P_{mo}}{P_{ho}} < 1, \frac{\delta_h}{P_{ho}} \geq \frac{\tau_m}{P_{mo}} \\ e^{-2\frac{\tau_m}{\mathit{SNR}_m}} \mathcal{L}_{I_m}\left(\frac{2\tau_m}{P_{mo}}\right) \mathcal{L}_{I_h}\left(\frac{2\tau_m}{P_{mo}}\right), & \text{if } \tau_h \frac{P_{mo}}{P_{ho}} < 1, \frac{\delta_h}{P_{ho}} < \frac{\tau_m}{P_{mo}} \end{cases}$$

where $\mathit{SNR}_m = \frac{P_{mo}}{\sigma^2}$, *and* $\Psi = \tau_h + \tau_m \frac{P_{ho}}{P_{mo}} + \tau_m \tau_h$

$$\mathcal{L}_{I_h}(s) = \exp\left\{ -\left(\frac{2\pi}{\beta \alpha^{2/\beta}}\right) (p_a \lambda_s) \, \mathbb{E}_{P_h} \left[\int_0^{sP_{ho}} \frac{\left[\ln\left(\frac{sP_h}{y}\right)\right]^{\frac{2}{\beta}-1}}{y+1} \mathrm{d}y \right] \right\} \tag{8.46}$$

$$\mathcal{L}_{I_m}(s) = \exp\left\{ -\left(\frac{2\pi}{\beta \alpha^{2/\beta}}\right) \left(\frac{\rho_m \lambda_m}{N_{RB}}\right) \mathbb{E}_{P_m} \left[\int_0^{sP_{mo}} \frac{\left[\ln\left(\frac{sP_m}{y}\right)\right]^{\frac{2}{\beta}-1}}{y+1} \mathrm{d}y \right] \right\} \tag{8.47}$$

Proof. Since an HTC user and an MTC device are paired together on a given resource block, the successful decoding of the HTC packet must happen first before the decoding of the MTC packet. Consequently, The uplink coverage probability of the typical MTC

device who is paired with a random HTC user is a function of the coverage threshold of both devices, thus, it is expressed as:

$$\begin{aligned}\mathcal{P}_m^U(\tau_m,\tau_h) &= \mathbb{P}\left\{\mathtt{SINR}_m > \tau_m, \mathtt{SINR}_h > \tau_h, g_h > g_m\right\}\\ &= \mathbb{P}\left\{g_h > g_m, g_h > \tau_h\tfrac{P_{mo}}{P_{ho}}g_m + \tfrac{\tau_h}{P_{ho}}\left(\mathcal{I}_h+\mathcal{I}_m+\sigma^2\right), g_m > \frac{\tau_m}{P_{mo}}\left(\mathcal{I}_h+\mathcal{I}_m+\sigma^2\right)\right\}\end{aligned}$$

There are many cases to consider in the computation of this probability. When $\tau_h\frac{P_{mo}}{P_{ho}} > 1$,

$$\begin{aligned}\mathcal{P}_m^U(\tau_m,\tau_h) &= \mathbb{P}\left\{g_h > \tfrac{\tau_h}{P_{ho}}\left(P_{mo}g_m+\mathcal{I}_h+\mathcal{I}_m+\sigma^2\right), g_m > \frac{\tau_m}{P_{mo}}\left(\mathcal{I}_h+\mathcal{I}_m+\sigma^2\right)\right\}\\ &= \mathbb{E}\left[\int_{g_m=\frac{\tau_m}{P_{mo}}(\mathcal{I}_h+\mathcal{I}_m+\sigma^2)}^{\infty}\int_{g_h=\frac{\tau_h}{P_{ho}}(P_{mo}g_m+\mathcal{I}_h+\mathcal{I}_m+\sigma^2)}^{\infty} f_{g_hg_m}(g_h,g_m)\mathrm{d}g_h\mathrm{d}g_m\right]\\ &= \frac{2}{\tau_h\frac{P_{mo}}{P_{ho}}+1}\mathbb{E}\left[\exp\left\{-\frac{\tau_h}{P_{ho}}\left(\mathcal{I}_h+\mathcal{I}_m+\sigma^2\right)\right\}\exp\left\{-\frac{\tau_m}{P_{mo}}\left(\tau_h\frac{P_{mo}}{P_{ho}}+1\right)\left(\mathcal{I}_h+\mathcal{I}_m+\sigma^2\right)\right\}\right]\\ &= \frac{2}{\tau_h\frac{P_{mo}}{P_{ho}}+1}e^{-\frac{\Psi}{\mathtt{SNR}_h}}\mathcal{L}_{I_m}\left(\frac{\Psi}{P_{ho}}\right)\mathcal{L}_{I_h}\left(\frac{\Psi}{P_{ho}}\right)\end{aligned} \tag{8.48}$$

where $\Psi = \tau_h + \tau_m\frac{P_{ho}}{P_{mo}} + \tau_m\tau_h$. When $\tau_h\frac{P_{mo}}{P_{ho}} \le 1$, there are two cases, firstly, $\frac{\delta_h}{P_{ho}} > \frac{\tau_m}{P_{mo}}$:

$$\begin{aligned}\mathcal{P}_m^U(\tau_m,\tau_h) &= \mathbb{P}\left\{g_h > g_m, g_m > \frac{\delta_h}{P_{ho}}\left(\mathcal{I}_h+\mathcal{I}_m+\sigma^2\right)\right\}\\ &+ \mathbb{P}\left\{g_h > \tfrac{\tau_h}{P_{ho}}\left(P_{mo}g_m+\mathcal{I}_h+\mathcal{I}_m+\sigma^2\right), \frac{\tau_m}{P_{mo}}\left(\mathcal{I}_h+\mathcal{I}_m+\sigma^2\right) < g_m < \frac{\delta_h}{P_{ho}}\left(\mathcal{I}_h+\mathcal{I}_m+\sigma^2\right)\right\}\\ &= \mathbb{E}\left[\int_{g_m=\frac{\delta_h}{P_{ho}}(\mathcal{I}_h+\mathcal{I}_m+\sigma^2)}^{\infty}\int_{g_h=g_m}^{\infty} f_{g_hg_m}(g_h,g_m)\mathrm{d}g_h\mathrm{d}g_m\right]\\ &+ \mathbb{E}\left[\int_{g_m=\frac{\tau_m}{P_{mo}}(\mathcal{I}_h+\mathcal{I}_m+\sigma^2)}^{\frac{\delta_h}{P_{ho}}\left(\mathcal{I}_h+\mathcal{I}_m+\sigma^2\right)}\int_{g_h=\frac{\tau_h}{P_{ho}}(P_{mo}g_m+\mathcal{I}_h+\mathcal{I}_m+\sigma^2)}^{\infty} f_{g_hg_m}(g_h,g_m)\mathrm{d}g_h\mathrm{d}g_m\right]\\ &= \frac{\tau_h\frac{P_{mo}}{P_{ho}}-1}{\tau_h\frac{P_{mo}}{P_{ho}}+1}e^{-\frac{2\delta_h}{\mathtt{SNR}_h}}\mathcal{L}_{I_m}\left(\frac{2\delta_h}{P_{ho}}\right)\mathcal{L}_{I_h}\left(\frac{2\delta_h}{P_{ho}}\right) + \frac{2}{\tau_h\frac{P_{mo}}{P_{ho}}+1}e^{-\frac{\Psi}{\mathtt{SNR}_h}}\mathcal{L}_{I_m}\left(\frac{\Psi}{P_{ho}}\right)\mathcal{L}_{I_h}\left(\frac{\Psi}{P_{ho}}\right)\end{aligned} \tag{8.49}$$

Secondly, $\frac{\delta_h}{P_{ho}} \le \frac{\tau_m}{P_{mo}}$:

$$\begin{aligned}\mathcal{P}_m^U(\tau_m,\tau_h) &= \mathbb{P}\left\{g_h > g_m, g_m > \frac{\tau_m}{P_{mo}}\left(\mathcal{I}_h+\mathcal{I}_m+\sigma^2\right)\right\}\\ &= \mathbb{E}\left[\int_{g_m=\frac{\tau_m}{P_{mo}}(\mathcal{I}_h+\mathcal{I}_m+\sigma^2)}^{\infty}\int_{g_h=g_m}^{\infty} f_{g_hg_m}(g_h,g_m)\mathrm{d}g_h\mathrm{d}g_m\right]\\ &= e^{-\frac{2\tau_m}{\mathtt{SNR}_m}}\mathcal{L}_{I_m}\left(\frac{2\tau_m}{P_{mo}}\right)\mathcal{L}_{I_h}\left(\frac{2\tau_m}{P_{mo}}\right)\end{aligned} \tag{8.50}$$

By combining the results in (8.48), (8.49), and (8.50), we get the result in Theorem 2. This completes the proof. ■

Different from the uplink coverage of the HTC users, the uplink coverage of the MTC devices has three regions of operation. Notably, the boundaries of these regions are all controlled by the ratio of the power truncation cutoff threshold $\frac{P_{ho}}{P_{mo}}$. More tractable results are then presented in the following corollaries considering the special cases $\beta\frac{2}{n+1}$ and $\beta = 2$.

Corollary 3. *In the special case $\beta = \frac{2}{n+1}$, where $n \in \mathbb{Z}$ is any non-negative integer, the uplink coverage given in Theorem 2 can be simplified to:*

$$\mathcal{P}_m^U(\tau_m, \tau_h) =$$

$$\begin{cases} \nu e^{-\frac{\Psi}{SNR_h}} \mathcal{L}_{I_m}\left(\frac{\Psi}{P_{ho}}\right) \mathcal{L}_{I_h}\left(\frac{\Psi}{P_{ho}}\right), & \text{if } \tau_h \frac{P_{mo}}{P_{ho}} \geq 1 \\ \mu e^{-\frac{2\delta_h}{SNR_h}} \mathcal{L}_{I_m}\left(\frac{2\delta_h}{P_{ho}}\right) \mathcal{L}_{I_h}\left(\frac{2\delta_h}{P_{ho}}\right) + \nu e^{-\frac{\Psi}{SNR_h}} \mathcal{L}_{I_m}\left(\frac{\Psi}{P_{ho}}\right) \mathcal{L}_{I_h}\left(\frac{\Psi}{P_{ho}}\right), & \text{if } \tau_h \frac{P_{mo}}{P_{ho}} < 1, \frac{\delta_h}{Pho} \geq \frac{\tau_m}{P_{mo}} \\ e^{-2\frac{\tau_m}{SNR_m}} \mathcal{L}_{I_m}\left(\frac{2\tau_m}{P_{mo}}\right) \mathcal{L}_{I_h}\left(\frac{2\tau_m}{P_{mo}}\right), & \text{if } \tau_h \frac{P_{mo}}{P_{ho}} < 1, \frac{\delta_h}{Pho} < \frac{\tau_m}{P_{mo}} \end{cases}$$

where

$$\mathcal{L}_{I_h}(s) = \exp\left\{-\Upsilon(n)\binom{n}{k}\mathbb{E}_{P_h}\left[\ln^k\left(\frac{P_h}{P_{ho}}\right)\right] \mathcal{J}_{n-k}(sP_{ho})\right\} \tag{8.51}$$

$$\mathcal{L}_{I_m}(s) = \exp\left\{-\xi(n)\binom{n}{k}\mathbb{E}_{P_m}\left[\ln^k\left(\frac{P_m}{P_{mo}}\right)\right] \mathcal{J}_{n-k}(sP_{mo})\right\} \tag{8.52}$$

and

$$\mathcal{J}_v(x) = \int_0^x \frac{\ln^v(x/y)}{y+1}\mathrm{d}y, \tag{8.53}$$

$$\xi(n) = \frac{(n+1)\pi\rho_m\lambda_m}{a^{n+1}N_{RB}}, \tag{8.54}$$

$$\Upsilon(n) = \frac{(n+1)\pi p_a\lambda_s}{a^{n+1}}, \tag{8.55}$$

$\mathbb{E}_{P_h}[\ln^k(P_h/P_{ho})]$ *and* $\mathbb{E}_{P_m}[\ln^k(P_m/P_{mo})]$ *are given in Lemma 3 and Lemma 4, respectively*

.

Proof. Follow similar approach to the proof of Corollary 1. ■

Corollary 4. *In the special case $\beta = 2$, the uplink coverage given in Theorem 2 can be*

simplified to:

$$\mathcal{P}_m^U(\tau_m,\tau_h) =$$

$$\begin{cases} \nu \exp\left\{-\left(\frac{\Psi}{\mathit{SNR}_h}+\frac{\pi p_a\lambda_s}{\alpha}\ln\left(1+\Psi\right)+\frac{\pi\rho_m\lambda_m}{\alpha N_{RB}}\ln\left(1+\Psi\frac{P_{mo}}{P_{ho}}\right)\right)\right\}, & \textit{if}\ \ \tau_h\frac{P_{mo}}{P_{ho}}\geq 1 \\ \mu \exp\left\{-\left(\frac{2\delta_h}{\mathit{SNR}_h}+\frac{\pi p_a\lambda_s}{\alpha}\ln\left(1+2\delta_h\right)+\frac{\pi\rho_m\lambda_m}{\alpha N_{RB}}\ln\left(1+2\delta_h\frac{P_{mo}}{P_{ho}}\right)\right)\right\}+ & \\ \nu \exp\left\{-\left(\frac{\Psi}{\mathit{SNR}_h}+\frac{\pi p_a\lambda_s}{\alpha}\ln\left(1+\Psi\right)+\frac{\pi\rho_m\lambda_m}{\alpha N_{RB}}\ln\left(1+\Psi\frac{P_{mo}}{P_{ho}}\right)\right)\right\}, & \textit{if}\ \ \tau_h\frac{P_{mo}}{P_{ho}}<1, \\ & \frac{\delta_h}{P_{ho}}\geq\frac{\tau_m}{P_{mo}} \\ \exp\left\{-\left(\frac{2\tau_m}{\mathit{SNR}_h}+\frac{\pi p_a\lambda_s}{\alpha}\ln\left(1+2\tau_m\frac{P_{ho}}{P_{mo}}\right)+\frac{\pi\rho_m\lambda_m}{\alpha N_{RB}}\ln\left(1+2\tau_m\right)\right)\right\}, & \textit{if}\ \ \tau_h\frac{P_{mo}}{P_{ho}}<1, \\ & \frac{\delta_h}{P_{ho}}\leq\frac{\tau_m}{P_{mo}} \end{cases}$$

Proof. Follow similar approach to the proof of Corollary 2. ■

8.5.2.2 Uplink NOMA Network Throughput Analysis

Considering the definition of the network throughput given in Section 8.4, it is given by:

$$\mathcal{R}_h^U(\tau_h) = p_a\lambda_s\log_2(1+\tau_h)\mathcal{P}_h^U(\tau_h), \tag{8.56}$$

$$\mathcal{R}_m^U(\tau_m,\tau_h) = \rho_m\lambda_m\log_2(1+\tau_m)\mathcal{P}_m^U(\tau_m,\tau_h), \tag{8.57}$$

By plugging the expressions of the uplink coverage probability given in Theorem 1 , 2 and Corollaries 1 - 4, we obtain the general form expressions of the network throughput for HTC and MTC as well as the special cases.

8.6 Simulation Results

To assess the accuracy of the analytical results, system-level Monte Carlo simulations are performed. The presented numerical results in this section are chosen to show the impact of all system parameters on the network performance. The system parameters considered include: the densities of BSs, HTC users, and MTC devices, the activity ratio of the MTC devices, the power control parameters of HTC users and MTC devices, the system bandwidth, and the parameters of the path loss model. The network is modeled by generating Homogeneous Poisson Point Process (HPPP) to abstract the locations of the BSs, HTC users, and MTC devices. We assume a simulation area of 1 km^2 where 1000 spatial realizations are generated. In addition, a 100 channel gain realizations drawn

from an exponential random variable with a mean of one are generated to simulate the channel variations. We consider a BS density of $\lambda_s = 1000$ cells/km^2, HTC users' density of a $\lambda_h = 500$ users/km^2, MTC devices' density of a $\lambda_m = 2 \times 10^5$ users/km^2 with activity ratio 0.1, a coverage thresholds of $\tau_h = 0$ dB, $\tau_M = -20$ dB, power control parameters for the HTC users $P_{ho} = -90$ dBm and $P_h^{max} = 20$ dBm, power control parameters for the MTC devices $P_{mo} = -110$ dBm and $P_m^{max} = 2$ dBm , and SEPL parameters of $a = 0.94, \beta = 0.5$. Furthermore, we assume that the number of available resource blocks for each BS is $N_{RB} = 100$ and each MTC device is allocated only one resource block with a bandwidth of 180 kHz, thus the noise power $\sigma^2 = -121.45$ dBm. On the other hand, the HTC users are allocated all the available resource blocks.

8.6.1 Simulation Setup

We consider the following simulation procedure to simulate the network environment modeled in this investigation.

1. A number of BSs is generated following a Poisson distribution with density λ_s BSs/km^2 and distributed uniformly in the simulation area. We consider a high density of the small cells as a feature of the dense networks.

2. A number of HTC users with density λ_h users/km^2 and MTC devices with density λ_m devices/km^2 are generated in the same simulation area as well. The locations of HTC users and MTC devices follow a Poisson distribution . Similarly, the users/devices are distributed uniformly over the simulation area.

3. Each HTC user is associated to the nearest BS and allocated N_{RB}/K of the resource blocks where K is the number of the HTC users associated to this BS. Also, each MTC device is associated to the nearest active BS and randomly paired with an HTC user and allocated an orthogonal resource block from the available resource blocks N_{RB}.

4. An HTC user or MTC device is considered active if the required transmission power is not greater than P_h^{max} or P_m^{max}, respectively.

5. Independent channel gains are generated for the links between all active HTC uses and MTC devices and their serving BSs and drawn from an exponential distribution

with mean one.

6. The uplink SINR of the link between each active HTC user/ MTC device and its tagged BS is computed. The SINR of an active MTC is only considered in the computation of the average uplink coverage if the SINR of the paired HTC user exceeds its uplink coverage QoS target.

7. Also, the uplink network throughput R of each HTC user and MTC device is computed.

8. The realization of the BSs and devices PPP is repeated N_m times and the generation of the independent fading channels is repeated for N_t time slots. In the simulations, we have considered $N_m = 1000$ and $N_t = 100$.

9. The average uplink coverage for the respective links between the active HTC users and MTC devices and the tagged BSs is calculated as $P_{avg} = \frac{1}{N_m N_t} \sum_{m=1}^{N_m} \sum_{t=1}^{N_t} \mathbb{1}(\mathtt{SINR}_{m,t} > \tau)$.

10. Finally, the average uplink network throughput of the HTC users and MTC devices is computed as $R_{avg} = \frac{1}{N_m N_t} \sum_{m=1}^{N_m} \sum_{t=1}^{N_t} R_{m,t}$.

8.6.2 Coverage Threshold

Fig. 8.1 shows the uplink coverage of a typical pair of HTC user and MTC device versus the coverage threshold τ_h and τ_m, respectively, in a NOMA-based deployment scenario. For the typical MTC device, the performance threshold of the paired HTC user is set to $\tau_h = 0$ dB. . Thus, the coverage performance of the typical MTC devices is capped by the coverage of the paired HTC user where the signal of the MTC device cannot be detected if the signal of the user is not recoverable at this threshold. The uplink coverage is depicted for three different densities of the small cells, namely, 10^3, 5×10^3, and 10^4 cells/km^2 where the performance improves as the density of the small cells gets higher. However, this improvement shows a tendency to saturate at higher densities. This behaviour is similar for both MTC devices and HTC users. Remarkably, the uplink coverage of the HTC users exceeds 85% at a coverage threshold of $\tau_h = 0$ dB. This shows that the NOMA based multiple access is not negatively impacting the HTC performance while it provides a good performance for the paired MTC devices.

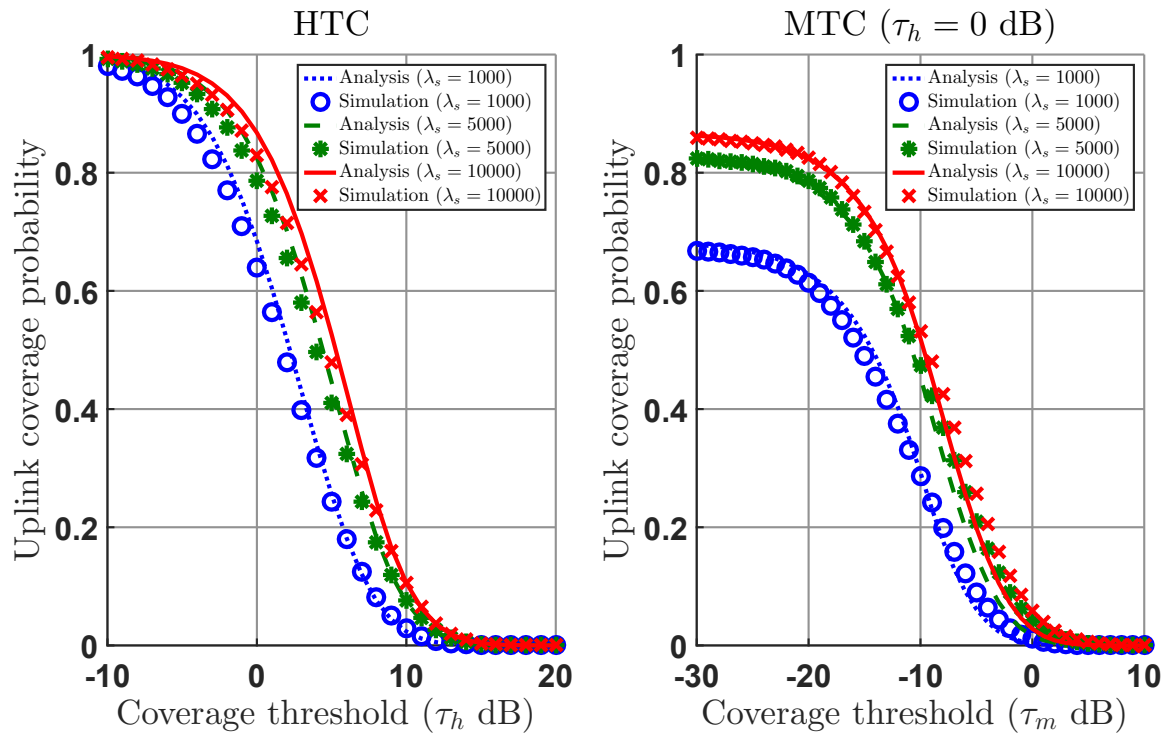

Figure 8.1: Uplink coverage probability versus coverage threshold considering different density of BSs λ_s (Density of MTCDs $\lambda_m = 0.2$ devices/m^2 and $\rho_m = 0.1$).

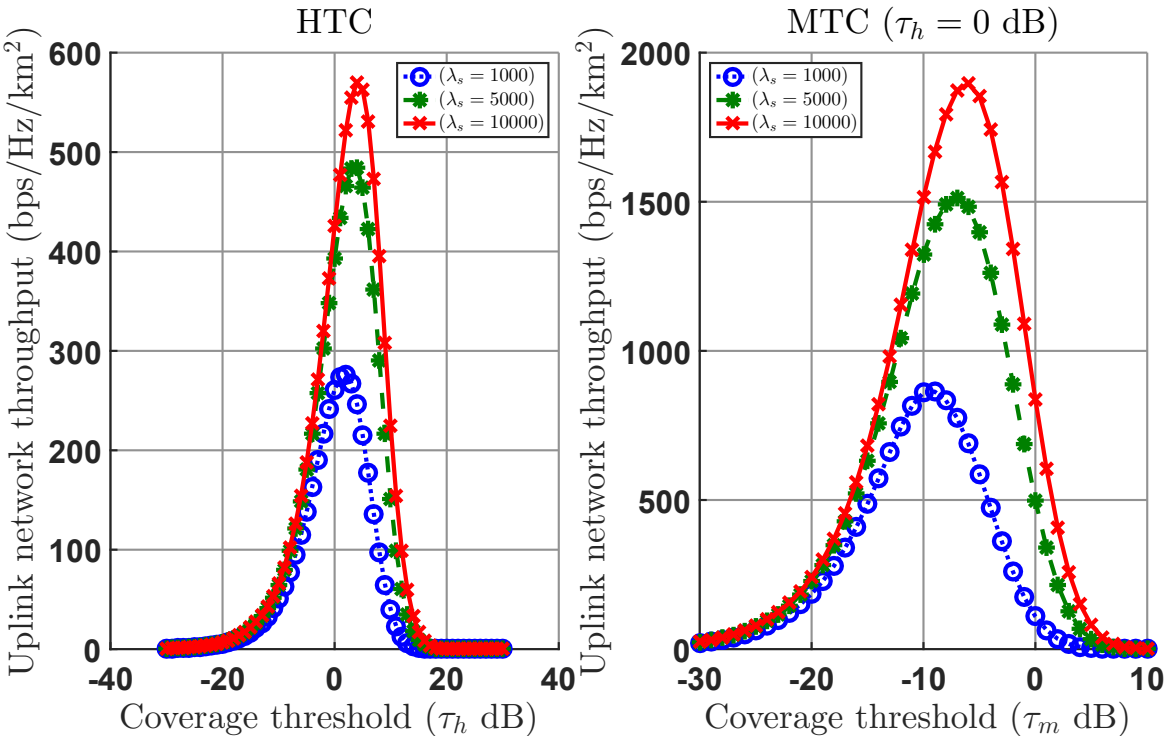

Figure 8.2: Uplink network throughput versus coverage threshold considering different density of BSs λ_s (Density of MTCDs $\lambda_m = 0.2$ devices/m^2 and $\rho_m = 0.1$).

To further evaluate the network performance, the network throughput is plotted against the coverage threshold in Fig. 8.2 for different densities of small cells. As depicted in the figure, the network throughput starts off at zero for very small coverage thresholds, increases until reaching a maximum value, and then falling down back to zero at relatively high coverage thresholds. This behaviour can be explained by recalling the definition of the network throughput where it consists of two components: $\log_2(1+\tau)$ which is increasing with the coverage threshold taking values from zero to infinity, and the coverage probability $\mathcal{P}(\tau)$ which is, in the contrary, decreasing from one to zero. The maximum value of the network throughput and the coverage threshold at which this maximum value is achieved are however different for HTC users from MTC devices, and different for different densities of small cells. Further examination of the results conveys more interesting outcomes where the network throughput is slightly improving with the density of small cells while it is significantly improving at the corresponding maximum point of each density. More on this in the next section.

8.6.3 Density of Small Cells

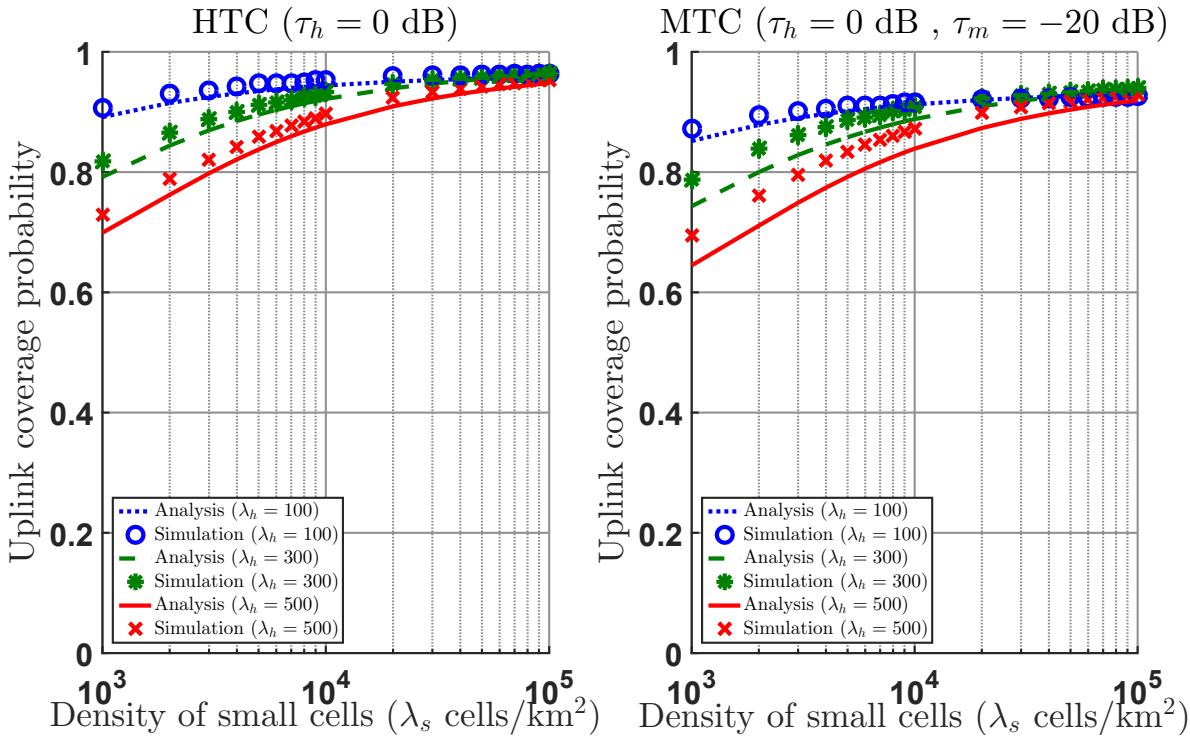

Figure 8.3: Uplink coverage probability versus density of small cells considering different density of HTC users λ_h (Density of MTCDs $\lambda_m = 0.2$ devices/m^2 and $\rho_m = 0.1$).

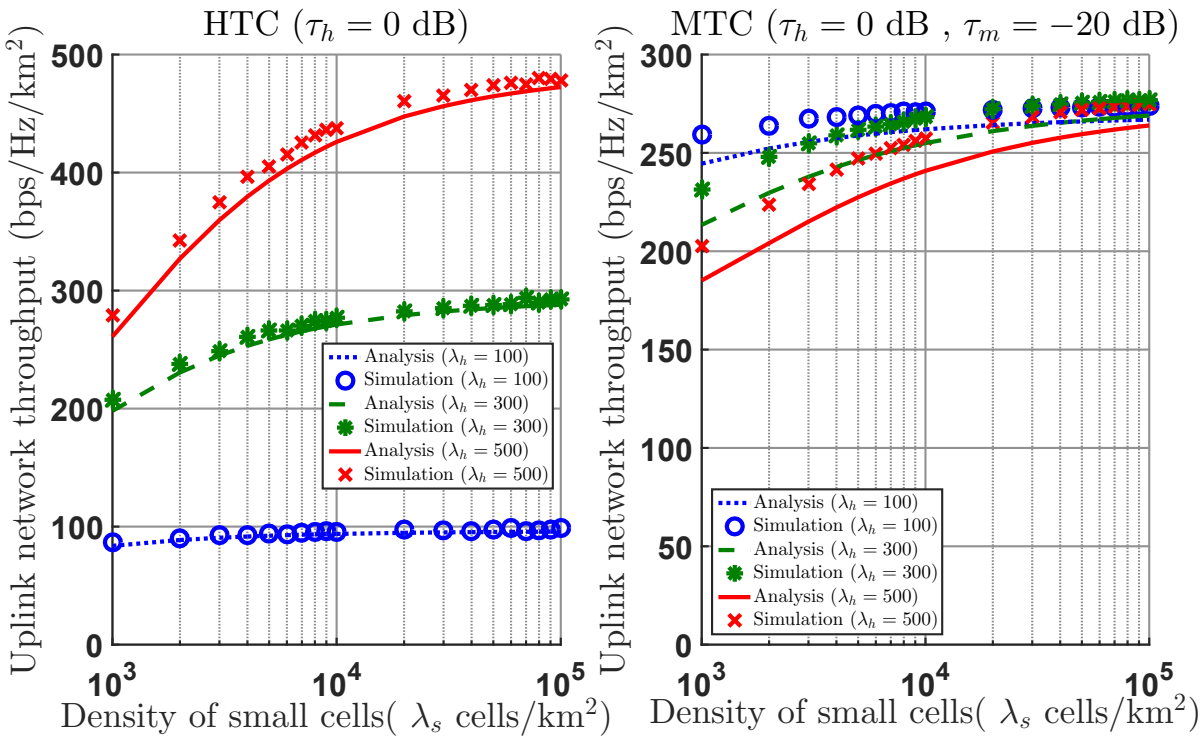

Figure 8.4: Uplink network throughput versus density of small cells considering different density of HTC users λ_h (Density of MTCDs $\lambda_m = 0.2$ devices/m^2 and $\rho_m = 0.1$).

Fig. 8.3 further confirms the increase of the uplink coverage of both HTC users and MTC devices with higher density of small cells. However, this increase comes to and end saturating at very high BSs' densities. The higher the density of the cells, the shorter the distance from both HTC users and MTC devices to the serving BS, and consequently, the better the uplink coverage performance. In the contrary, the uplink coverage probability declines with higher density of HTC users at smaller density of cell. However, the pace of the coverage performance decay with the density of HTC users declines with higher densities of small cells. More HTC users activates more cells, and since we only consider the inter-cell interference, increasing the number of HTC users per unit area increases the uplink interference, and in turn negatively impacts the uplink coverage performance. On the other hand, at very high densities of small cells, the distance between either the HTC users or the MTC devices and the serving BS becomes very short giving more advantage to the increasing signal power over the increasing interference power, until the coverage becomes indistinguishable for distinct densities of HTC users.

The same performance, in terms of the uplink network throughput, holds for the MTC devices as depicted Fig. 8.4. Conversely, the network throughput performance is reversed

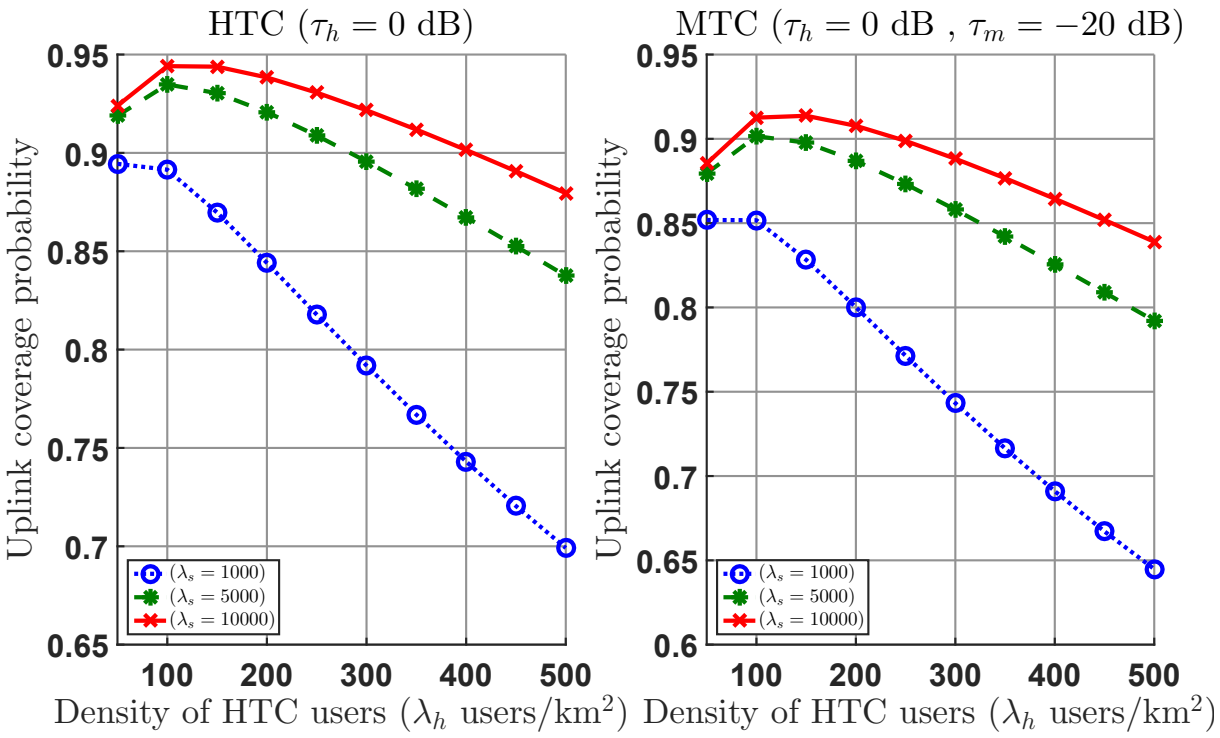

Figure 8.5: Uplink coverage probability versus density of HTC users considering different density of small cells λ_s (Density of MTCDs $\lambda_m = 0.2$ devices/m^2 and $\rho_m = 0.1$).

when switching focus to the HTC users. In particular, the uplink network throughput of MTC devices increases with the density of small cells and decreasing with the density of HTC users. For the HTC users, the uplink network throughput is still increases with the density of small cells, but in a much slower rate for smaller densities of HTC users. One can explain this behaviour by recalling the definition of the uplink network throughput of the HTC users where it linearly increases with the density of active cells. Remember also that the number of active cells increases with either increasing of the number of cells or the number of HTC users per unit area. However, for smaller densities of HTC users, the number of active cells saturates faster with higher density of BSs reaching a maximum which is the density of the HTC users itself. This takes place when each user exactly activates a single cell. Differently, the uplink throughput performance shows a dramatic increase with the density of the HTC users. For the same reasons mentioned above, a higher number of HTC users per unit area is translated to a larger number of activated cells, and hence, a much higher uplink network throughput.

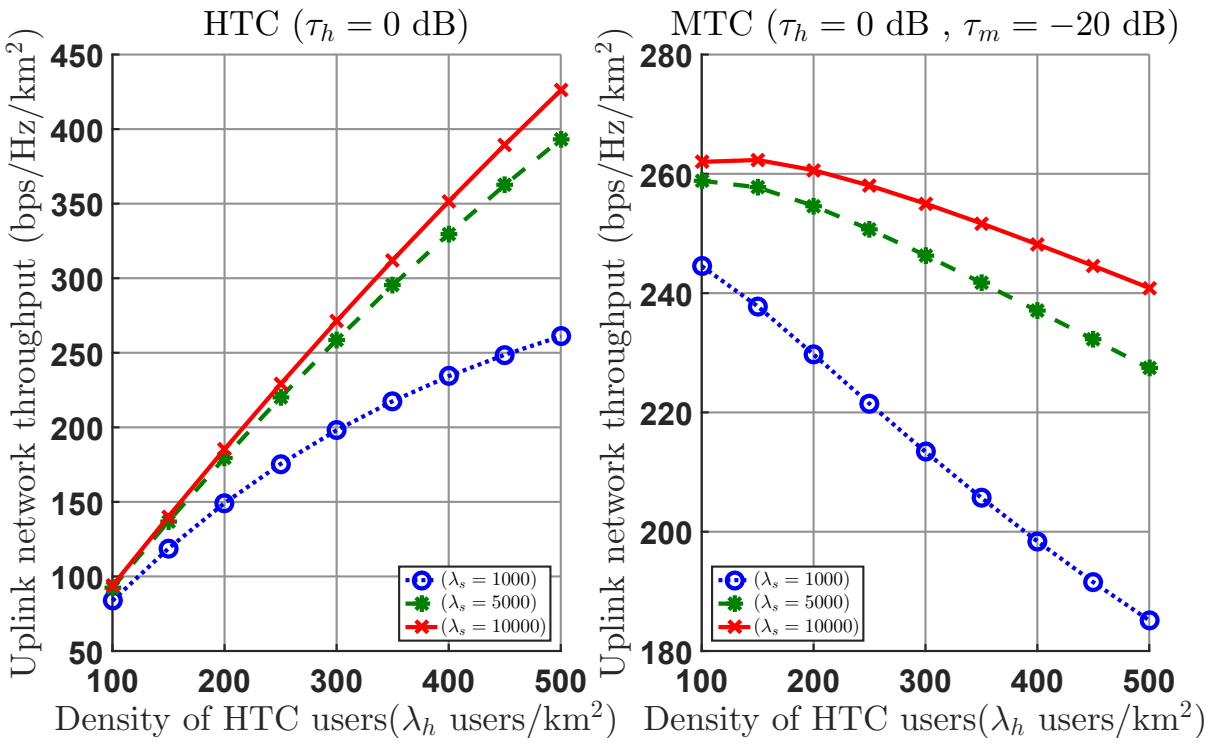

Figure 8.6: Uplink network throughput versus density of HTC users considering different density of small cells λ_s (Density of MTCDs $\lambda_m = 0.2$ devices/m^2 and $\rho_m = 0.1$).

8.6.4 Density of HTC Users

Focusing on the impact of the HTC density on the uplink network performance, the uplink coverage probability and the uplink network throughput are depicted in Figures 8.5 and 8.6. The results confirm the previously discussed conclusions. Remarkably, for larger densities of small cells ($\gg 1000$ BSs/km^2), the uplink coverage probability of HTC users and the uplink coverage probability of MTC devices get improved with the density of HTC users approaching a maximum at a certain density of HTC users, then declines at a faster rate afterwards.

8.6.5 Density of MTC Devices

Fig. 8.7 depicts the uplink coverage probability against the density of MTC devices considering different densities of small cells. The coverage performance deteriorates with the increasing number of MTC nodes per unit area since this reflects more interfering nodes on the tagged resource block. This impact is similar for the HTC users and the MTC devices. At the same time, increasing the density of small cells significantly improves

the uplink coverage where more cells means more reuse of the resources, and hence, more room for the interference generated from the increasing number of MTC nodes for a given resource block.

While the uplink network throughput of the HTC users depicted in Fig. 8.8 shows a similar tendency to decrease with the increasing density of MTC devices, instead, the uplink network throughput of the MTC devices dramatically increases with the increasing density of the MTC devices. Back to the expression of the uplink throughput of the MTC devices, it has a linear relation with the density of the MTC devices, which explains the previously mentioned behaviour.

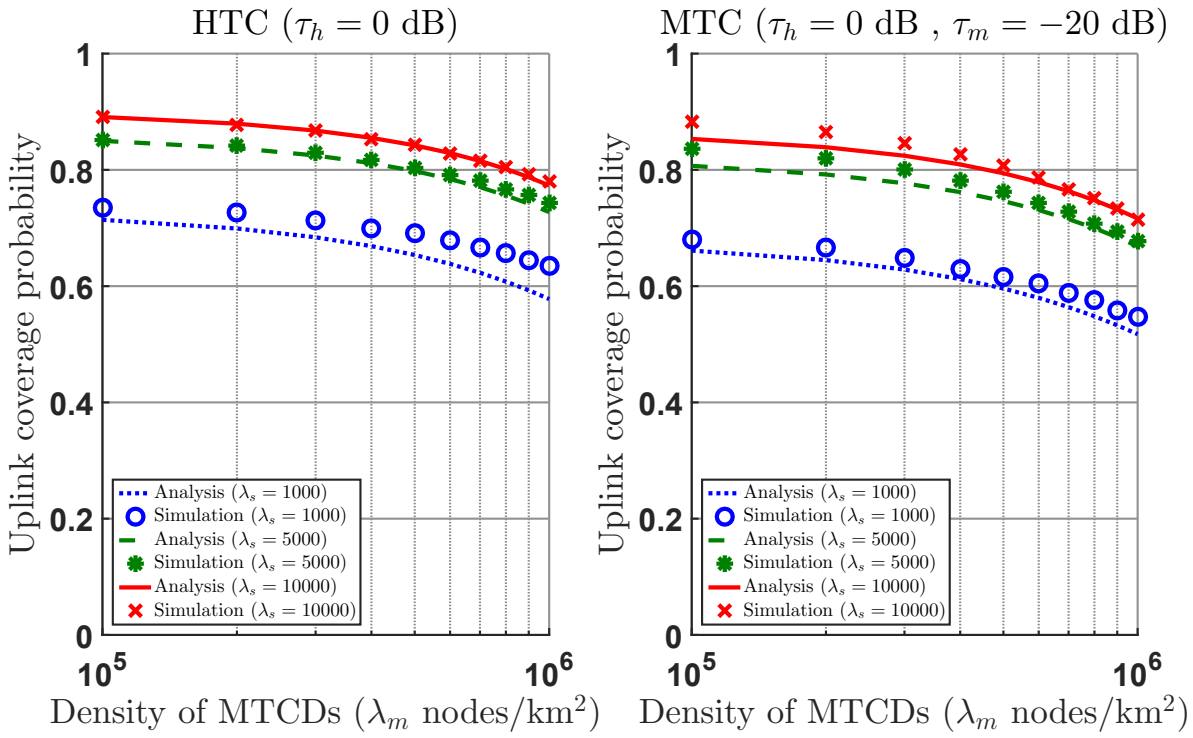

Figure 8.7: Uplink coverage probability versus density of MTC devices considering different density of small cells λ_s ($\rho_m = 0.1$).

8.6.6 Power Truncation Cutoff Threshold

Turning our focus to the power control parameters, in Figures 8.9 and 8.10, we depict the uplink coverage probability and the uplink network throughput against the ratio between the power control truncation cutoff threshold of the HTC users and that of the MTC devices. The results show no difference in the performance of the coverage when compared to the throughput. Since the uplink network throughput of both HTC users and

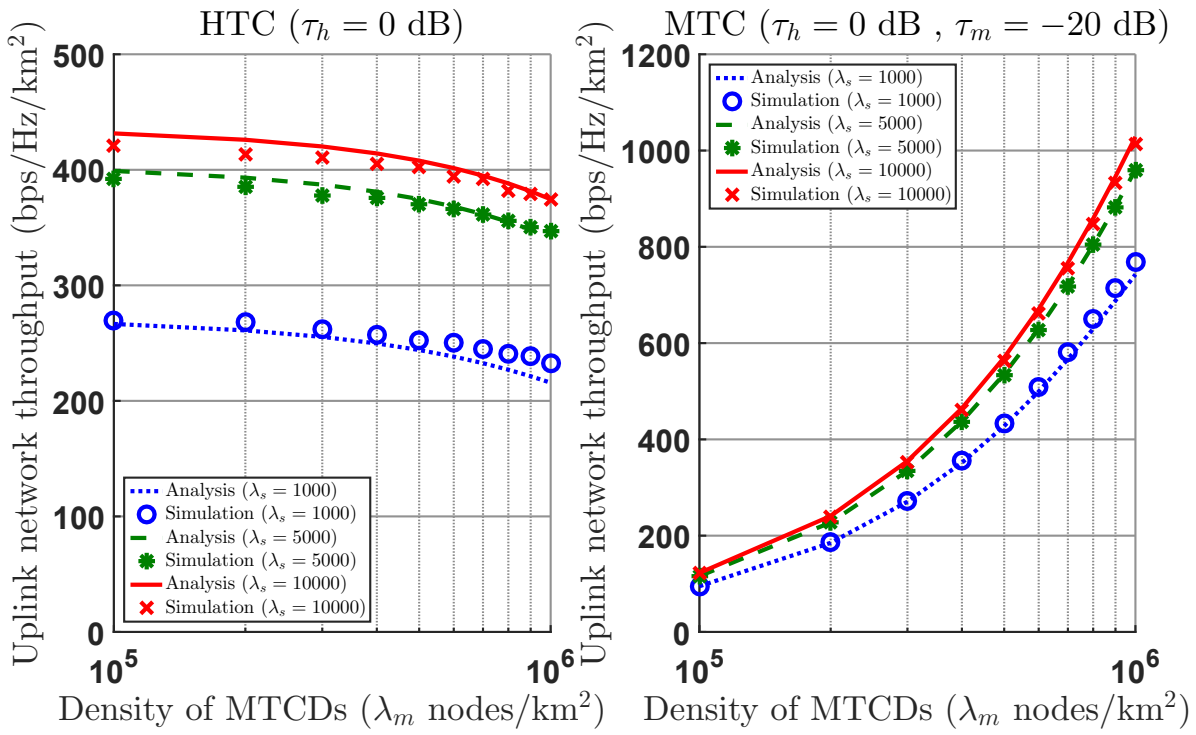

Figure 8.8: Uplink network throughput versus density of MTC devices considering different density of small cells λ_s ($\rho_m = 0.1$).

MTC devices is only a function of the power control parameters in terms of the coverage term, the uplink network throughput becomes a scaled version of the uplink coverage probability of the HTC users and MTC devices with the scale being the density of active cells or the density of active MTC nodes, respectively.

Either the coverage or the network throughput of the HTC users monotonically increases with the power cutoff ratio reaching a saturation value at a certain ratio. On the other side, the performance with respect to the MTC devices is entirely different. The uplink coverage probability and network throughput both increases significantly improves with increasing the power cutoff ratio until reaching a maximum, then the performance turns upside down afterwards. Increasing the power control cutoff threshold of the HTC users, with respect to that of the MTC devices, increases the received signal power of the HTC users at the serving cell, which in turn improves the uplink coverage and the uplink network throughput. Besides, deploying more small cells brings the BSs closer to the HTC users, and hence, reducing their transmit power which significantly decreases the uplink interference enhancing the coverage and the throughput performance even more. Moreover, by closely examining this performance, one can notice that the maximum point is the same for distinct densities of small cells.

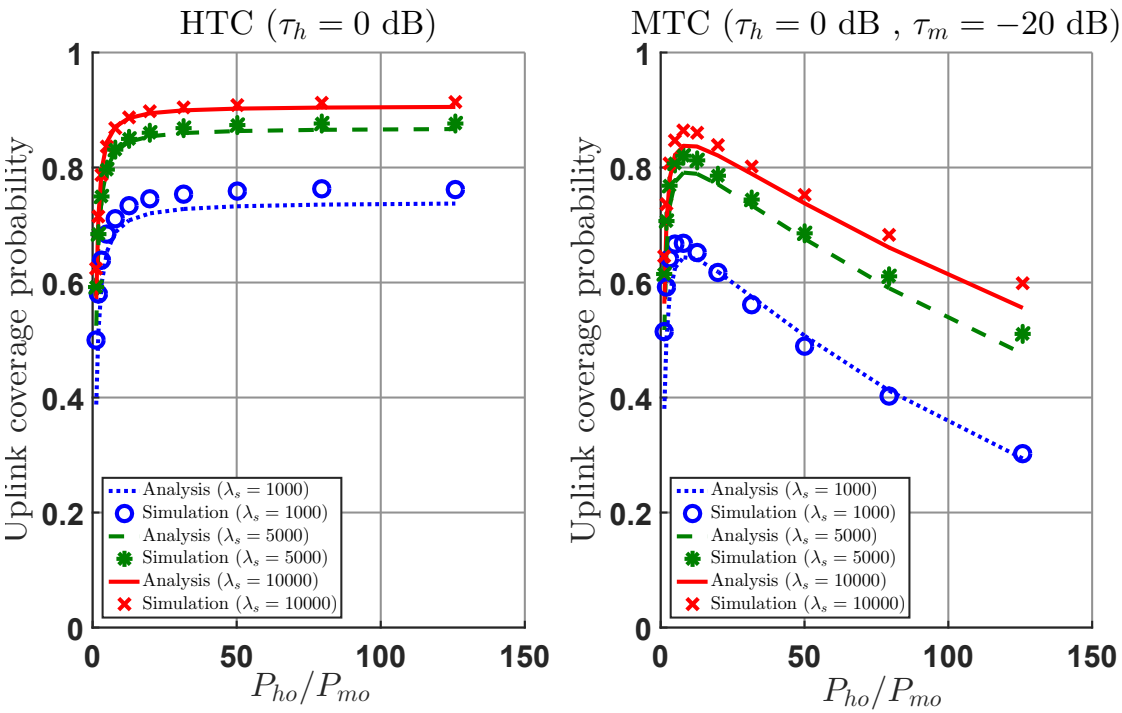

Figure 8.9: Uplink coverage probability versus the ratio of the power control cutoff threshold of HTC users and MTC devices considering different density of small cells λ_s (Density of MTCDs $\lambda_m = 0.2$ devices/m^2 and $\rho_m = 0.1$).

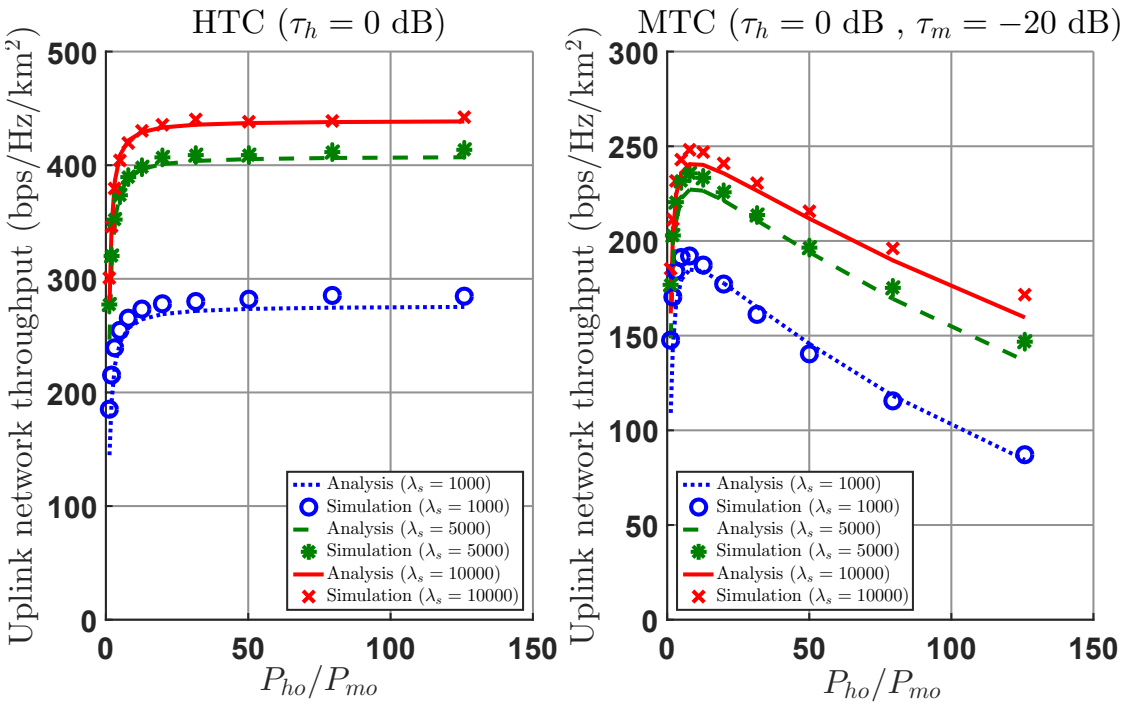

Figure 8.10: Uplink network throughput versus the ratio of the power control cutoff threshold of HTC users and MTC devices considering different density of small cells λ_s (Density of MTCDs $\lambda_m = 0.2$ devices/m^2 and $\rho_m = 0.1$).

8.6.7 Number of Resource Blocks

Fig. 8.11 depicts the uplink coverage against the number of resource blocks considering three distinct densities of MTC devices, namely, 10^5 , 5×10^5, and 10^6 nodes/km^2. The uplink coverage probability improves with larger number of resource blocks due to decreasing the number of active MTC devices transmitting on a given resource block. At some point, more resource block no longer improves the coverage performance since the aggregate interference from the MTC devices becomes very small as compared to that of the HTC users. Moreover, the coverage performance deteriorates with increasing the density of MTC devices where more interferes contribute to the uplink aggregate interference.

In Fig. 8.12, the uplink network throughput is depicted versus the number of resource blocks. Similarly, the network throughput of the HTC users and MTC devices improves with increasing the number of resource blocks approaching a saturation at the same point where the coverage saturates. Moreover, the uplink network throughput of the HTC users decreases with higher density of MTC devices. Nevertheless, the uplink network throughput significantly improves with the increasing number of MTC devices per unit area. Recall that the uplink throughput of the MTC devices linearly increases with the density of active MTC devices, which in turn is a linear function of the density of MTC devices.

8.7 Conclusions

Inevitable coexistence of HTC users and massive MTC devices is a feature of the next generation of cellular network. Satisfying the requirements of both deployment scenarios is challenging. While the HTC users demand an extremely high data rate with relatively small number of active user, the MTC devices require a massive number of connections each of which is injecting small packets in a sporadic nature. In this work, we investigate a NOMA-based radio access where a pair of an HTC user and an MTC device is encouraged to use the same resource block in the uplink simultaneously. This allows to host the diverse requirements of both types of users while operating the network at its optimal point. The results confirm this claim where both types of users, i.e., HTC and MTC, enjoy a high uplink coverage and an enormous uplink network throughput. The analytical results which

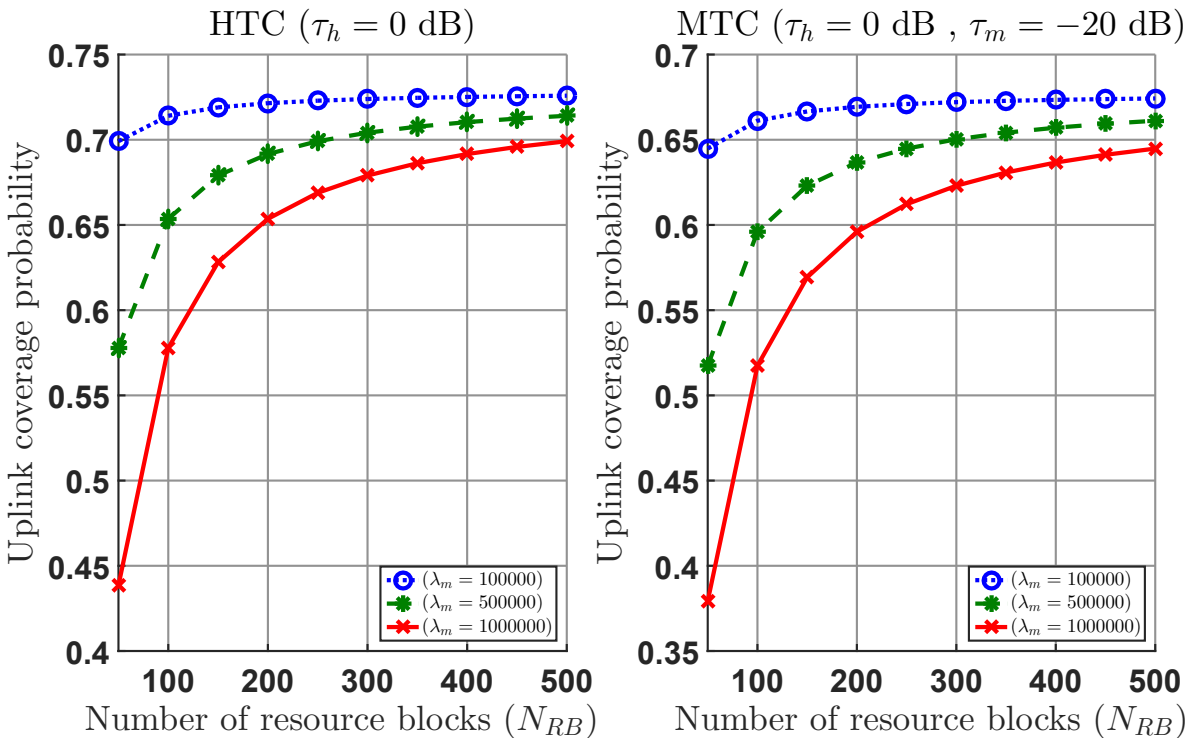

Figure 8.11: Uplink coverage probability versus the number of resource blocks considering different density of MTC devices λ_m ($\rho_m = 0.1$).

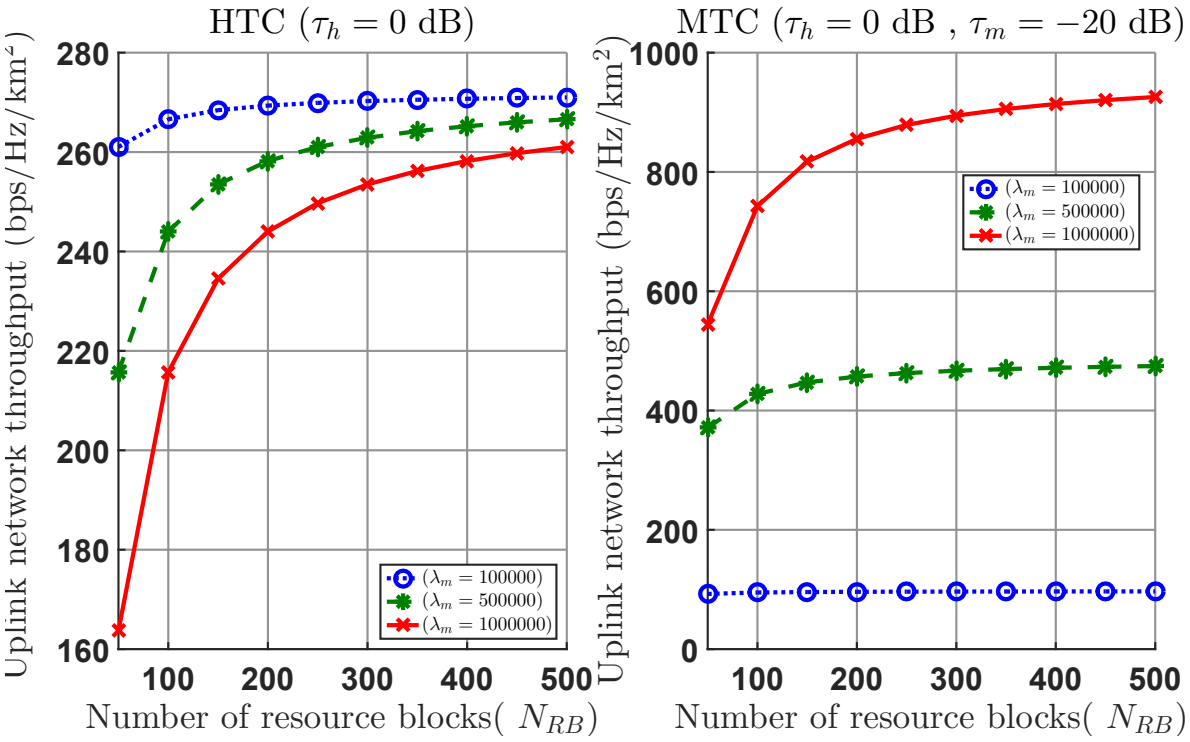

Figure 8.12: Uplink network throughput versus the number of resource blocks considering different density of MTC devices λ_m ($\rho_m = 0.1$).

are validated by extensive Monte Carlo simulations provide a mathematical framework to assess the performance of such scenario and to tune the system parameters to operate the network at an optimal and efficient point. Increasing the density of small cells and the available bandwidth significantly improves the network performance. On the other side, the power control parameters has to be tuned carefully to approach the optimal performance of both the uplink coverage and the uplink network throughput.

9. Conclusions, Limitations, and Future Work

9.1 Conclusions

Ultra-dense networks (UDNs) are fundamentally different from traditional mobile networks and even Heterogeneous Networks (HetNets). Accordingly, this suggests a distinct treatment when it comes to the performance evaluation of such networks, i.e., UDNs. These differences include: close proximity of many cells to a given user, potential inactivity of most BSs due to lack of users, drastic inter-cell interference in hot-spots, limitation of the capacity by virtue of the backhaul bottleneck, and fundamentally different propagation environment. In this thesis, we identified the distinguishing traits of UDNs and the challenges of addressing them in accurate modelling and rigorous performance analysis. Tackling these challenges has been the main goal of this thesis which leads to a better understanding of network densification and its potential applications in Internet-of-Things (IoT) and Physical Layer Security (PLS). Significant contributions have been made in this thesis, which is evident from the track record of publications that resulted from this research work. We briefly summarize these achievements:

1. We developed a mathematical framework for the computation of the average downlink rate of the connections from the typical user to many BSs in its neighborhood. The framework provides a high degree of accuracy as confirmed by our extensive simulations for the considered system model. The performance of the multiple association sheds light on the gains and losses of such association scheme. Although the average rate decreases when connecting to farther cells, this is compensated by expanding beyond the bottleneck of the limited backhaul capacity. The aggregate downlink rate of the connections to many cells exceeds the limits imposed by the

backhaul capacity of the individual cells. Moreover, considering general channel fading distributions in both the signal and the interference links provides a way to handle different propagation environment in dense networks.

2. We investigated the downlink performance of UDNs where inactive BSs are turned off to mitigate their interference. We employ Stretched Exponential Path-Loss (SEPL) model to capture the propagation environment in UDN where the serving and interfering BSs are within short distances from the user. The idle mode capability imposes an upper-bound on the system interference where at very high small cells' densities the number of active BSs converges to the number of the active users, e.g., each user activates the closest BS to its location. The impact of bounding the interference on the network performance influences the coverage as well as the capacity of the network. To summarize, under the utilized assumptions, the coverage probability as well as the capacity are invariant with the small cells' density at high densities. However, it is strongly tied to the user's density. Moreover, the coverage probability and the network throughput never drop to zero at very high BSs density due to the interference upper-bound set by the density of the active users.

3. We studied the secrecy capacity of UDNs where our findings clearly show the high secrecy capacity of such networks which is an inherent feature by virtue of the high density of the small cells. Users in dense networks connect via strong connections to very close cells. The close proximity of the small cells to the users induces a secure environment where the cells can whisper encoded messages to the legitimate users confusing the Eves and providing the users with high average secrecy rate. The average secrecy rate in UDNs is an increasing function in the small cells density even with the consideration of LOS transmission in the leakage link. On the contrary, the average secrecy rate decreases in environments with high users density where the activation of more BSs results in increasing the interference in the main link which in turn negatively impacts the average secrecy rate.

4. We investigated the uplink coverage of mMTC devices deployed in massive amounts considering UDN environment. The special features of UDN is considered in the analysis. The uplink coverage is challenging in MTC applications due to the limited energy of the battery-powered MTC devices and the harsh deployment scenarios.

The significant impact of the density of small cells, the available bandwidth, and the power control cutoff threshold on the uplink coverage performance is assessed by both analytical and simulation results. Remarkably, there is a critical saturation point where increasing these system parameters has no further impact on the performance. One interesting finding is that the uplink coverage performance has two distinct regions of operation, noise-limited region and interference-limited one. Another important finding is that the uplink coverage performance of a massive MTC deployment scenario in UDN environment is no longer affected by the maximum transmit power of the device, thanks to the high density of the serving small cells. This finding relaxes the requirements on the maximum transmit power of the MTC devices which in turn allows for less complexity, brings more cost savings, and yields much longer battery life.

5. We studied the impact of the coexistence of MTC devices and HTC users on the downlink performance of UDNs. We investigated two association schemes, namely, *connect to closest (C2C)* BS and *connect to active (C2A)* BS. The network performance in terms of downlink coverage probability and average cell load is analyzed and the analytical results are assessed through simulations. The investigation of the proposed system model shows a tradeoff between the two performance metrics with respect to the considered association schemes. Accordingly, this suggests the design of association schemes to find a balance between them. On the positive side, the consideration of UDNs to support MTC devices traffic provides a scalable and a viable solution to the connectivity problem in future massive deployments of MTC devices.

6. We investigated the impact of employing advanced radio access techniques on the uplink performance of UDNs considering the coexistence of HTC users and MTC devices. To this end, a NOMA-based radio access is studied where a pair of an HTC user and an MTC device is encouraged to use the same resource block in the uplink simultaneously. This allows to host the diverse requirements of both types of users while operating the network at its optimal point. The results confirm this claim where both types of users, i.e., HTC and MTC, enjoy a high uplink coverage and an enormous uplink network throughput. The analytical results which are validated by extensive Monte Carlo simulations provide a mathematical framework to assess the

performance of such scenario and to tune the system parameters to operate the network at an optimal and efficient point. Increasing the density of small cells and the available bandwidth significantly improves the network performance. On the other side, the power control parameters has to be tuned carefully to approach the optimal performance of both the uplink coverage and the uplink network throughput.

9.2 Limitations

The close evaluation of the performance of UDNs reveals how network densification would be a candidate technology to satisfy the various diverse requirements of the next generation of mobile communications, namely 5G. The high density of the small cells results in high spectrum reuse, close proximity of the BSs to the users, and smooth uniform coverage. Consequently, UDNs provide a huge data rate per unit area to satisfy the enhanced Mobile Broadband (eMBB) use case and a massive connectivity to satisfy the massive Machine-Type Communications (mMTC) use case. Moreover, further evaluation of the performance of dense networks would reveal their suitability to satisfy the Ultra-Reliable Low-Latency Communications (URLLC) use case.

However, the main limitation of UDNs is the restricted mobility where the small cells in a dense network fail to serve high speed users. The small coverage area of the individual small cells results in frequent handovers in the case of fast-moving users, which introduces intolerable signaling overhead in the radio access network. Accordingly, UDN would not be an option to serve autonomous vehicles, unless they are in parking lots or in a congested downtown. Notwithstanding, clustering of many small cells provides a solution to the frequent handovers problem where a cluster of small cells cooperates to serve a user or a set of users. In this scenario, the handover procedure will simply reduces to adding or removing cells to a given cluster. Even in this case, only users with slow or moderate speeds can be accommodated in a dense network.

9.3 Future Work

Further in-depth investigations are required to layout a concrete understanding of the control parameters to optimize the operation of a dense network. The tradeoffs between different performance metrics such as the area spectral efficiency, the energy efficiency, the

coverage/outage probability, and the network throughput require the understanding of the individual effect of the controlling parameters specifically the density of BSs, the number of antennae per BS, the transmission power, and the idle mode capabilities. Another challenge in the accurate modelling of UDNs is the consideration of vertical densification where the small cell BSs are densified in the elevation plane. In this context, the 3D modelling of the dense cellular network is crucial to the performance evaluation of such densification alternative. In this section, we layout some interesting directions of research to further extend the results contributed in this thesis:

- **User Association** The user association has been studied extensively in traditional networks and HetNets. However, in the scenario of dense networks, there are unique challenges that need to be considered and accurately investigated. This is even more involving when considering the co-existence of both HTC users and MTC devices. The drastic interference amongst the nearby cells due to the LOS transmission requires proposing innovative association rules to exploit the idle mode capabilities of the small cell BSs. The backhauling is another limiting factor that must be considered while associating an HTC user or an MTC node to a cell. Another challenge to the association of users to cells in a dense network is the mobility management, where fast users would generate many handover events if they are associated to cells with small coverage area. Effective collaborative-based solutions are required to account for these unique challenges where dual connectivity provides a practical alternative.

  Another important open problem is the applicability of range expansion in dense scenarios where the interference would be a limiting factor. The common understanding is that 5G networks would be a mix of many radio access technologies (RATs) such as cellular networks, WiFi, and mmWaves networks. This introduces another research venue which is the multiple association of a user to many cells in different RATs. To explain, a user might connect to a macrocell and many small cells in a cellular network, to a WiFi access point, and to a mmWaves cell simultaneously. Moreover, the study of backhaul-aware association in UDN is still an open problem. Moreover, the consideration of Quality-of-Service (QoS), Quality-of-Experience (QoE), and Quality-of-Physical Experience (QoPE) [179] in dense networks is missing in the current published work, although it is very relevant to

the admission of a user to a given cell.

- **Backhauling** The backhauling is identified as the bottleneck for the wide deployment of dense networks. The provisioning of ideal backhaul to all small cells in a dense network is challenging. Accordingly, the wireless backhauling emerges as a viable alternative. There are many wireless backhauling techniques including mmWaves links, relays links, and massive-MIMO backhaul links. Certainly, one of the open problems is the study of the effect of the wireless backhauling on the user experience in a dense network environment. Another open problem is the consideration of realistic traffic distributions and user distributions to evaluate the performance of wireless backhauling networks in UDN.

- **Interference Management** Interference management is of a predominant influence on the operation of a dense network. Imagine a wireless network with immense number of cells that operate in co-channel scenario. Undoubtedly, the interference could be the limiting factor on the fruition of such dense network dispelling the densification gains. The coordinated interference management is challenging with such a large number of neighboring cells. The curse of dimensionality arose uniquely in dense networks while considering collaborative interference management. The consideration of idle mode capabilities in modelling interference problems in UDN would be another interesting problem. The performance evaluation of proactive turning off of lightly-loaded dominant interferers could yield interesting results. The reduced distance between the cells in the vicinity of the same user makes the interferes as strong as the servers due to the LOS components, and this uniquely challenges the interference management in dense networks. A multi-domain interference management is another interesting problem, where the interference management is performed in frequency, time, space domains simultaneously. Also, the consideration of realistic user and traffic distributions although beneficial, but still an open problem to consider in dense networks.

- **Energy Efficiency** The power consumption plays a main role in specifying the OPEX of a dense network. In spite of the small footprint of a small cell, the aggregate consumed power of a large number of such cells is immense. Energy efficiency refers to the number of transmitted bits per unit energy. Thus, increasing the en-

ergy efficiency conflicts with the link quality, and hence the QoS. The maximization of energy efficiency considering the user experience is an interesting model to be investigated in UDN. Another setting which has a great impact on the successful deployment of dense networks is the energy efficient wireless backhauling. Thus considering a joint backhaul-aware energy efficient association of users to cells in a dense network would yield interesting results.

- **Small Cell Discovery** The detection of cells in close proximity of a given user in a cellular network is crucial to the optimal operation of the network. However, this becomes more important and much harder in a densified network. Many small cells are in the vicinity of a user and the efficient detection of them is not an easy task. The main challenge in this context is how to manage the reuse of synchronization signals in neighboring small cells, which are in the interference range of each other, in order to ease the cell discovery task. Optimization of cell discovery in terms of time and energy-efficiency is an open problem in UDN scenarios. Moreover, the exploitation of location data and fingerprints in optimizing small cell discovery [82] is an interesting direction to investigate.

- **Propagation Modelling** Another open research direction in the study of dense networks is the consideration of 3D channel modelling. Also, the consideration of multi-slope path loss models requires further investigation in different densification contexts. The modelling of channel fading to account for the propagation characteristics in UDN suggests the use of Rician fading model which requires further rigorous investigation.

References

[1] M. D. Renzo, A. Guidotti, and G. E. Corazza, "Average rate of downlink heterogeneous cellular networks over generalized fading channels: A stochastic geometry approach," *IEEE Trans. Commun.*, vol. 61, no. 7, pp. 3050–3071, July 2013.

[2] A. AlAmmouri, J. G. Andrews, and F. Baccelli, "SINR and throughput of dense cellular networks with stretched exponential path loss," *IEEE Trans. Wireless Commun.*, vol. 17, no. 2, pp. 1147–1160, Feb. 2018.

[3] K. David and H. Berndt, "6G vision and requirements: Is there any need for beyond 5G?" *IEEE Veh. Technol. Mag.*, vol. 13, no. 3, pp. 72–80, Sep. 2018.

[4] M. Chen, K. Gaither, N. W. John, and B. Mccann, "An information-theoretic approach to the cost-benefit analysis of visualization in virtual environments," *IEEE Transactions on Visualization and Computer Graphics*, vol. 25, no. 1, pp. 32–42, Jan. 2019.

[5] T. Wright, S. de Ribaupierre, and R. Eagleson, "Leap motion performance in an augmented reality workspace: Integrating devices with an interactive platform," *IEEE Consumer Electronics Magazine*, vol. 8, no. 1, pp. 36–41, Jan 2019.

[6] A. Al-Fuqaha, M. Guizani, M. Mohammadi, M. Aledhari, and M. Ayyash, "Internet of Things: A survey on enabling technologies, protocols, and applications," *IEEE Commun. Surveys Tuts.*, vol. 17, no. 4, pp. 2347–2376, Fourth quarter 2015.

[7] D. López-Pérez and M. Ding, "A brief history on the theoretical analysis of dense small cell wireless networks," *CoRR*, vol. abs/1812.02269, 2018. [Online]. Available: http://arxiv.org/abs/1812.02269

[8] C. Martin. (2017) North american consumers to have 13 connected devices. [Online]. Available: https://www.mediapost.com/publications/article/302663/north-american-consumers-to-have-13-connected-devi.html

[9] Cisco, "Cisco visual network index: Global mobile traffic forecast update 2014-2019," White Paper, May 2015.

[10] D. Porcino and W. Hirt, "Ultra-wideband radio technology: Potential and challenges ahead," *IEEE Commun. Mag.*, vol. 41, no. 7, pp. 66–74, July 2003.

[11] L. Atzori, A. Iera, and G. Morabito, "The Internet of Things: A survey," *Computer networks*, vol. 54, no. 15, pp. 2787–2805, 2010.

[12] S. Severi, F. Sottile, G. Abreu, C. Pastrone, M. Spirito, and F. Berens, "M2M technologies: Enablers for a pervasive Internet of Things," in *Proc. European Conf. on Networks and Communications (EuCNC), 2014*, Bologna, Italy, June 2014, pp. 1–5.

[13] R. R. Tyagi, K.-D. Lee, F. Aurzada, S. Kim, and M. Reisslein, "Efficient delivery of frequent small data for U-healthcare applications over LTE-Advanced networks," in *Proc. of the 2nd ACM international workshop on Pervasive Wireless Healthcare*, Hilton Head, SC, June 2012, pp. 27–32.

[14] K. M., S. M., and R. M. Banakar, "Evolution of IoT in smart vehicles: An overview," in *Proc. IEEE Int. Conf. on Green Computing and Internet of Things (ICGCIoT), 2015*, Noida, India, Oct. 2015, pp. 804–809.

[15] R. Khan, S. U. Khan, R. Zaheer, and S. Khan, "Future Internet: The Internet of Things architecture, possible applications and key challenges," in *Proc. IEEE 10th Int. Conf. on Frontiers of Information Technology (FIT), 2012*, Islamabad, Pakistan, Dec. 2012, pp. 257–260.

[16] N. Bhushan, J. Li, D. Malladi, R. Gilmore, D. Brenner, A. Damnjanovic, R. Sukhavasi, C. Patel, and S. Geirhofer, "Network densification: The dominant theme for wireless evolution into 5G," *IEEE Commun. Mag.*, vol. 52, no. 2, pp. 82–89, Feb. 2014.

[17] P. Pirinen, "A brief overview of 5G research activities," in *Proc. 1st Int. Conf. on 5G for Ubiquitous Connectivity (5GU), 2014*, Akaslompolo, Finland, Nov. 2014, pp. 17–22.

[18] I. Hwang, B. Song, and S. Soliman, "A holistic view on hyper-dense heterogeneous and small cell networks," *IEEE Commun. Mag.*, vol. 51, no. 6, pp. 20–27, June 2013.

[19] J. Zander and P. Mähönen, "Riding the data tsunami in the cloud: Myths and challenges in future wireless access," *IEEE Commun. Mag.*, vol. 51, no. 3, pp. 145–151, Mar. 2013.

[20] S. M. Yu and S.-L. Kim, "Downlink capacity and base station density in cellular networks," in *Proc. 11th Int. Symp. Modeling Optimization in Mobile, Ad Hoc Wireless Networks (WiOpt), 2013*, Tsukuba, Japan, May 2013, pp. 119–124.

[21] D. David López-Pérez, M. Ding, H. Claussen, and A. Jafari, "Towards 1 Gbps/UE in cellular systems: Understanding ultra-dense small cell deployments," *IEEE Commun. Surveys Tuts.*, vol. 17, no. 4, pp. 2078 – 2101, Fourth quarter 2015.

[22] S. Stefanatos and A. Alexiou, "Access point density and bandwidth partitioning in ultra dense wireless networks," *IEEE Trans. Commun.*, vol. 62, no. 9, pp. 3376–3384, Sept. 2014.

[23] S. Lee and K. Huang, "Coverage and economy of cellular networks with many base stations," *IEEE Commun. Lett.*, vol. 16, no. 7, pp. 1038–1040, July 2012.

[24] J. Park, S.-L. Kim, and J. Zander, "Asymptotic behavior of ultra-dense cellular networks and its economic impact," in *Proc. IEEE Global Communications Conf. (GLOBECOM), 2014*, Austin, TX, Dec. 2014, pp. 4941–4946.

[25] M. Ding, D. Lopez-Perez, G. Mao, P. Wang, and Z. Lin, "Will the area spectral efficiency monotonically grow as small cells go dense?" in *Proc. IEEE Global Communications Conf. (GLOBECOM), 2015*, San Diego, CA, Dec. 2015, pp. 1–7.

[26] J. Deissner and G. Fettweis, "A study on hierarchical cellular structures with inter-layer reuse in an enhanced GSM radio network," in *Proc. IEEE Int. Workshop on Mobile Multimedia Communications (MoMuC '99) , 1999*, San Diego, CA, Nov. 1999, pp. 243–251.

[27] J. Boccuzzi and M. Ruggiero, *Femtocells: design and applications.* McGraw-Hill, 2011.

[28] J. Andrews, H. Claussen, M. Dohler, S. Rangan, and M. Reed, "Femtocells: Past, present, and future," *IEEE J. Sel. Areas Commun.*, vol. 30, no. 3, pp. 497–508, Apr. 2012.

[29] A. Damnjanovic, J. Montojo, Y. Wei, T. Ji, T. Luo, M. Vajapeyam, T. Yoo, O. Song, and D. Malladi, "A survey on 3GPP heterogeneous networks," *IEEE Wireless Commun.*, vol. 18, no. 3, pp. 10–21, June 2011.

[30] D. David López-Pérez, I. Guvenc, G. de la Roche, M. Kountouris, T. Quek, and J. Zhang, "Enhanced intercell interference coordination challenges in heterogeneous networks," *IEEE Wireless Commun.*, vol. 18, no. 3, pp. 22–30, June 2011.

[31] M. Peng, Y. Li, Z. Zhao, and C. Wang, "System architecture and key technologies for 5G heterogeneous cloud radio access networks," *IEEE Network*, vol. 29, no. 2, pp. 6–14, Mar. 2015.

[32] J. Andrews, "Seven ways that HetNets are a cellular paradigm shift," *IEEE Commun. Mag.*, vol. 51, no. 3, pp. 136–144, Mar. 2013.

[33] H. Claussen, I. Ashraf, and L. T. Ho, "Dynamic idle mode procedures for femtocells," *Bell Labs Technical Journal*, vol. 15, no. 2, pp. 95–116, 2010.

[34] C. Li, J. Zhang, and K. Letaief, "User-centric intercell interference coordination in small cell networks," in *Proc. IEEE Int. Conf. Communications (ICC), 2014*, Sydney, NSW, June 2014, pp. 5747–5752.

[35] C. Li, J. Zhang, M. Haenggi, and K. Letaief, "User-centric intercell interference nulling for downlink small cell networks," *IEEE Trans. Commun.*, vol. 63, no. 4, pp. 1419–1431, Apr. 2015.

[36] M. Polignano, P. Mogensen, P. Fotiadis, L. Chavarria, I. Viering, and P. Zanier, "The inter-cell interference dilemma in dense outdoor small cell deployment," in *Proc. IEEE 79th Vehicular Technology Conf. (VTC Spring), 2014*, Seoul, Korea(South), May 2014, pp. 1–5.

[37] B. Soret, K. Pedersen, N. Jørgensen, and V. Fernández-López, "Interference coordination for dense wireless networks," *IEEE Commun. Mag.*, vol. 53, no. 1, pp. 102–109, Jan. 2015.

[38] X. Wang, E. Visotsky, and A. Ghosh, "Dynamic cell muting for ultra dense indoor small cell deployment scenario," in *Proc. ICC Workshops*, London, UK, June 2015, pp. 148–153.

[39] D. Chen, T. Quek, and M. Kountouris, "Backhauling in heterogeneous cellular networks: Modeling and tradeoffs," *IEEE Trans. Wireless Commun.*, vol. 14, no. 6, pp. 3194–3206, June 2015.

[40] Y.-N. R. Li, H. Xiao, J. Li, and H. Wu, "Wireless backhaul of dense small cell networks with high dimension MIMO," in *IEEE Globecom Workshops (GC Wkshps), 2014*, Austin, TX, Dec. 2014, pp. 1254–1259.

[41] B. Li, D. Zhu, and P. Liang, "Small cell in-band wireless backhaul in massive MIMO systems: A cooperation of next-generation techniques," *IEEE Trans. Wireless Commun.*, vol. 14, no. 12, pp. 7057–7069, Dec. 2015.

[42] X. Ge, H. Cheng, M. Guizani, and T. Han, "5G wireless backhaul networks: challenges and research advances," *IEEE Network*, vol. 28, no. 6, pp. 6–11, Nov. 2014.

[43] P. Amin, N. Kibret, E. Mutafungwa, B. Haile, J. Hamalainen, and J. Nurminen, "Performance study for off-grid self-backhauled small cells in dense informal settlements," in *Proc. IEEE 25th Annu. Symp. Personal, Indoor, and Mobile Radio Communication (PIMRC), 2014*, Washington DC, Sept. 2014, pp. 1652–1657.

[44] A. Gupta, X. Zhang, and J. Andrews, "SINR and throughput scaling in ultradense urban cellular networks," *IEEE Wireless Commun. Lett.*, vol. 4, no. 6, pp. 605–608, Dec. 2015.

[45] C. Galiotto, N. K. Pratas, L. Doyle, and N. Marchetti, "Effect of LOS/NLOS propagation on ultra-dense networks," *CoRR*, vol. abs/1507.01757, 2015. [Online]. Available: http://arxiv.org/abs/1507.01757

[46] J. Carle, J.-F. Myoupo, and D. Seme, "A basis for 3D cellular networks," in *Proc. 15th Int. Conf. Information Networking, 2001.*, Beppu City, Oita, Jan. 2001, pp. 631–636.

[47] C. Decayeux and D. Seme, "A new model for 3D cellular mobile networks," in *Proc. 3rd Int. Workshop on Parallel and Distributed Computing*, July 2004, pp. 22–28.

[48] Z. Pan and Q. Zhu, "Modeling and analysis of coverage in 3D cellular networks," *IEEE Commun. Lett.*, vol. 19, no. 5, pp. 831–834, May 2015.

[49] K. Zheng, L. Zhao, J. Mei, B. Shao, W. Xiang, and L. Hanzo, "Survey of large-scale MIMO systems," *IEEE Commun. Surveys Tuts.*, vol. 17, no. 3, pp. 1738–1760, Third quarter 2015.

[50] J. Zhang, C. Pan, F. Pei, G. Liu, and X. Cheng, "Three-dimensional fading channel models: A survey of elevation angle research," *IEEE Commun. Mag.*, vol. 52, no. 6, pp. 218–226, June 2014.

[51] S. Akoum and J. Acharya, "Full-dimensional MIMO for future cellular networks," in *Proc. IEEE Radio and Wireless Symp. (RWS), 2014*, Newport Beach, CA, Jan. 2014, pp. 1–3.

[52] R. Heath, S. Peters, Y. Wang, and J. Zhang, "A current perspective on distributed antenna systems for the downlink of cellular systems," *IEEE Commun. Mag.*, vol. 51, no. 4, pp. 161–167, Apr. 2013.

[53] J. Wu, Z. Zhang, Y. Hong, and Y. Wen, "Cloud radio access network (C-RAN): a primer," *IEEE Network*, vol. 29, no. 1, pp. 35–41, Jan. 2015.

[54] J. Park, S. L. Kim, and J. Zander, "Tractable resource management with uplink decoupled millimeter-wave overlay in ultra-dense cellular networks," *IEEE Trans. Wireless Commun.*, vol. 15, no. 6, pp. 4362–4379, June 2016.

[55] L. Su, C. Yang, and C. L. I, "Energy and spectral efficient frequency reuse of ultra dense networks," *IEEE Trans. Wireless Commun.*, vol. 15, no. 8, pp. 5384–5398, Aug 2016.

[56] N. Yang, L. Wang, G. Geraci, M. Elkashlan, J. Yuan, and M. D. Renzo, "Safeguarding 5G wireless communication networks using physical layer security," *IEEE Commun. Mag.*, vol. 53, no. 4, pp. 20–27, Apr. 2015.

[57] M. Ding, P. Wang, D. López-Pérez, G. Mao, and Z. Lin, "Performance impact of LoS and NLoS transmissions in dense cellular networks," *IEEE Trans. Wireless Commun.*, vol. 15, no. 3, pp. 2365–2380, Mar. 2016.

[58] M. Kamel, W. Hamouda, and A. Youssef, "Ultra-dense networks: A survey," *IEEE Commun. Surveys Tuts.*, vol. 18, no. 4, pp. 2522–2545, Fourth quarter 2016.

[59] Qualcomm, "1000x: More small cells hyper-dense small cell deployments," White Paper, June 2014.

[60] Nokia, "Ultra dense network (UDN)," White Paper, 2016.

[61] C. Coletti, L. Hu, N. Huan, I. Z. Kovács, B. Vejlgaard, R. Irmer, and N. Scully, "Heterogeneous deployment to meet traffic demand in a realistic LTE urban scenario," in *Proc. IEEE Vehicular Technology Conference (VTC Fall) 2012*, Quebec City, QC, Sept. 2012, pp. 1–5.

[62] D. Liu, L. Wang, Y. Chen, M. Elkashlan, K. K. Wong, R. Schober, and L. Hanzo, "User association in 5G networks: A survey and an outlook," *IEEE Commun. Surveys Tuts.*, vol. PP, no. 99, pp. 1–1, 2016.

[63] C.-H. Liu and L.-C. Wang, "Random cell association and void probability in poisson-distributed cellular networks," in *Proc. IEEE Int. Conf. Communications (ICC), 2015*, London, UK, June 2015, pp. 2816–2821.

[64] F. Tavares, G. Berardinelli, N. Mahmood, T. Sorensen, and P. Mogensen, "Inter-cell interference management using maximum rank planning in 5G small cell networks," in *Proc. 11th Int. Symp. Wireless Communications Systems (ISWCS), 2014*, Barcelona, Spain, Aug. 2014, pp. 628–632.

[65] A. Y. Al-Zahrani, F. R. Yu, and M. Huang, "A joint cross-layer and colayer interference management scheme in hyperdense heterogeneous networks using mean-field game theory," *IEEE Trans. Veh. Technol.*, vol. 65, no. 3, pp. 1522–1535, Mar. 2016.

[66] O. Guéant, J.-M. Lasry, and P.-L. Lions, "Mean field games and applications," in *Paris-Princeton lectures on mathematical finance 2010*. Springer, 2011, pp. 205–266.

[67] L. Liu, V. Garcia, L. Tian, Z. Pan, and J. Shi, "Joint clustering and inter-cell resource allocation for CoMP in ultra dense cellular networks," in *Proc. IEEE Int. Conf. Communications (ICC), 2015*, London, UK, June 2015, pp. 2560–2564.

[68] G. Yuehong, C. Lei, Z. Xin, Z. Yajun, and Z. Yunfei, "Enhanced power allocation scheme in ultra-dense small cell network," *China Communications*, vol. 13, no. 2, pp. 21–29, Feb. 2016.

[69] Y. Sun, Y. Chang, M. Hu, and B. Wang, "A cluster-based hybrid access strategy using non-cooperative game theory for ultra-dense HetNet," in *Proc. IEEE High Performance Computing and Communications (HPCC), 2015*, New York, USA, Aug. 2015, pp. 14–19.

[70] M.-J. Cho, T.-W. Ban, B. C. Jung, and H. J. Yang, "A distributed scheduling with interference-aware power control for ultra-dense networks," in *Proc. IEEE Int. Conf. Communications (ICC), 2015*, London, UK, June 2015, pp. 1661–1666.

[71] N. Wang, E. Hossain, and V. Bhargava, "Backhauling 5G small cells: A radio resource management perspective," *IEEE Wireless Commun.*, vol. 22, no. 5, pp. 41–49, Oct. 2015.

[72] E. Björnson, L. Sanguinetti, and M. Kountouris, "Energy-efficient future wireless networks: A marriage between massive MIMO and small cells," in *Proc. IEEE 16th Int. Workshop on Signal Processing Advances in Wireless Communications (SPAWC), 2015*, Stockholm, Sweden, June 2015, pp. 211–215.

[73] E. Björnson, L. Sanguinetti, and M. Kountouris, "Deploying dense networks for maximal energy efficiency: Small cells meet massive MIMO," *IEEE J. Sel. Areas Commun.*, vol. 34, no. 4, pp. 832–847, Apr. 2016.

[74] C. Li, J. Zhang, and K. Letaief, "Throughput and energy efficiency analysis of small cell networks with multi-antenna base stations," *IEEE Trans. Wireless Commun.*, vol. 13, no. 5, pp. 2505–2517, May 2014.

[75] S. Yunas, M. Valkama, and J. Niemelä, "Spectral and energy efficiency of ultra-dense networks under different deployment strategies," *IEEE Commun. Mag.*, vol. 53, no. 1, pp. 90–100, Jan. 2015.

[76] Q. Ren, J. Fan, X. Luo, Z. Xu, and Y. Chen, "Analysis of spectral and energy efficiency in ultra-dense network," in *Proc. IEEE Int. Conf. Communication Workshop (ICCW), 2015*, London, UK, June 2015, pp. 2812–2817.

[77] S. Samarakoon, M. Bennis, W. Saad, M. Debbah, and M. Latva-aho, "Energy-efficient resource management in ultra dense small cell networks: A mean-field approach," in *Proc. IEEE Global Communications Conf. (GLOBECOM), 2015*, San Diego, CA, Dec. 2015, pp. 1–6.

[78] S. Samarakoon, M. Bennis, W. Saad, M. Debbah, and M. Latva-aho, "Ultra dense small cell networks: Turning density into energy efficiency," *IEEE J. Sel. Areas Commun.*, vol. PP, no. 99, pp. 1–1, Mar. 2016.

[79] C. Yang, "A unified design of spectrum, energy, and cost efficient ultra-dense small cell networks," in *Proc. Int. Conf. on Wireless Communications Signal Processing (WCSP), 2015*, Nanjing, China, Oct. 2015, pp. 1–4.

[80] Q. Li, R. Hu, Y. Qian, and G. Wu, "Cooperative communications for wireless networks: techniques and applications in LTE-advanced systems," *IEEE Wireless Commun.*, vol. 19, no. 2, Apr. 2012.

[81] S. Singh, "Load balancing in heterogeneous cellular networks," Ph.D. dissertation, The University of Texas at Austin, 2014.

[82] A. Prasad, O. Tirkkonen, P. Lunden, O. Yilmaz, L. Dalsgaard, and C. Wijting, "Energy-efficient inter-frequency small cell discovery techniques for LTE-advanced heterogeneous network deployments," *IEEE Commun. Mag.*, vol. 51, no. 5, pp. 72–81, May 2013.

[83] P. Shuai, T. En, J. Huilin, P. Zhiwen, L. Nan, and Y. Xiaohu, "An improved graph coloring based small cell discovery scheme in LTE hyper-dense networks," in *Proc. IEEE Wireless Communications and Networking Conf. Workshops (WCNCW), 2015*, New Orleans, LA, Mar. 2015, pp. 17–22.

[84] I. F. Akyildiz, W.-Y. Lee, M. C. Vuran, and S. Mohanty, "Next generation/dynamic spectrum access/cognitive radio wireless networks: a survey," *Computer Networks*, vol. 50, no. 13, pp. 2127–2159, 2006.

[85] E. Obregon, K. W. Sung, and J. Zander, "On the sharing opportunities for ultra-dense networks in the radar bands," in *Proc. IEEE Int. Symp. on Dynamic Spectrum Access Networks (DYSPAN), 2014*, McLean, VA, Apr. 2014, pp. 215–223.

[86] Y. Teng, Y. Wang, and K. Horneman, "Co-primary spectrum sharing for denser networks in local area," in *Proc. 9th Int. Conf. on Cognitive Radio Oriented Wireless Networks and Communications (CROWNCOM), 2014*, Oulu, Finland, June 2014, pp. 120–124.

[87] A. H. Jafari, D. Lopez-Perez, M. Ding, and J. Zhang, "Study on scheduling techniques for ultra dense small cell networks," in *Proc. IEEE 82nd Vehicular Technology Conf. (VTC Fall), 2015*, Boston, MA, Sept. 2015, pp. 1–6.

[88] J. Chen, Z. Gao, and Q. Zhao, "Load-aware dynamic spectrum access in ultra-dense small cell networks," in *Proc. Int. Conf. on Wireless Communications Signal Processing (WCSP), 2015*, Nanjing, China, Oct. 2015, pp. 1–5.

[89] H. D. Nguyen and S. Sun, "Closed-form performance bounds for stochastic geometry-based cellular networks," *IEEE Trans. Wireless Commun.*, vol. 16, no. 2, pp. 683–693, Feb. 2017.

[90] M. D. Renzo, "Stochastic geometry modeling and analysis of multi-tier millimeter wave cellular networks," *IEEE Trans. Wireless Commun.*, vol. 14, no. 9, pp. 5038–5057, Sept. 2015.

[91] P. Herath, W. A. Krzymień, and C. Tellambura, "Coverage and rate analysis for limited information cell association in stochastic-layout cellular networks," *IEEE Trans. Veh. Technol.*, vol. 65, no. 9, pp. 6962–6971, Sept. 2016.

[92] X. Zhang and J. G. Andrews, "Downlink cellular network analysis with multi-slope path loss models," *IEEE Trans. Commun.*, vol. 63, no. 5, pp. 1881–1894, May 2015.

[93] C. Rosa, K. Pedersen, H. Wang, P. H. Michaelsen, S. Barbera, E. Malkamaki, T. Henttonen, and B. Sebire, "Dual connectivity for lte small cell evolution: functionality and performance aspects," *IEEE Commun. Mag.*, vol. 54, no. 6, pp. 137–143, June 2016.

[94] M. I. Kamel, W. Hamouda, and A. M. Youssef, "Multiple association in ultra-dense networks," in *Proc. IEEE Inter. Conf. on Commun. (ICC) 2016*, Kuala Lumpur, Malaysia, May 2016, pp. 1–6.

[95] H. M. Wang, T. X. Zheng, J. Yuan, D. Towsley, and M. H. Lee, "Physical layer security in heterogeneous cellular networks," *IEEE Trans. Commun.*, vol. 64, no. 3, pp. 1204–1219, Mar. 2016.

[96] H. Wu, X. Tao, N. Li, and J. Xu, "Secrecy outage probability in multi-RAT heterogeneous networks," *IEEE Communications Letters*, vol. 20, no. 1, pp. 53–56, Jan. 2016.

[97] Y. J. Tolossa, S. Vuppala, and G. Abreu, "Secrecy rate analysis in multi-tier heterogeneous networks over generalized fading model," *IEEE Internet Things J.*, vol. 4, no. 1, pp. 101–110, Feb. 2017.

[98] J. Wang, J. Lee, and T. Q. S. Quek, "Optimal cooperative range of distributed transmitters for communications secrecy," in *Proc IEEE 17th International Workshop on Signal Processing Advances in Wireless Communications (SPAWC)*, July 2016, pp. 1–5.

[99] T. Kwon and J. M. Cioffi, "Random deployment of data collectors for serving randomly-located sensors," *IEEE Trans. Wireless Commun.*, vol. 12, no. 6, pp. 2556–2565, June 2013.

[100] D. Malak, H. S. Dhillon, and J. G. Andrews, "Optimizing data aggregation for uplink machine-to-machine communication networks," *IEEE Trans. Commun.*, vol. 64, no. 3, pp. 1274–1290, Mar. 2016.

[101] S. N. Swain, R. Thakur, and S. R. M. Chebiyyam, "Coverage and rate analysis for facilitating machine-to-machine communication in LTE-A networks using device-to-device communication," *IEEE Trans. Mobile Comput.*, vol. 16, no. 11, pp. 3014–3027, Nov. 2017.

[102] M. Shehab, H. Alves, and M. Latva-aho, "Effective capacity and power allocation for machine-type communication," *IEEE Trans. Veh. Commun.*, pp. 1–1, 2019.

[103] H. ElSawy and E. Hossain, "On stochastic geometry modeling of cellular uplink transmission with truncated channel inversion power control," *IEEE Trans. Wireless Commun.*, vol. 13, no. 8, pp. 4454–4469, Aug. 2014.

[104] H. ElSawy, A. Sultan-Salem, M. S. Alouini, and M. Z. Win, "Modeling and analysis of cellular networks using stochastic geometry: A tutorial," *IEEE Commun. Surveys Tuts.*, vol. 19, no. 1, pp. 167–203, First quarter 2017.

[105] M. Haenggi, *Stochastic Geometry for Wireless Networks.* Cambridge Univ. Press, 2012.

[106] D. Stoyan, W. Kendall, and J. Mecke, *Stochastic Geometry and its Applications.* John Wiley and Sons, 1995.

[107] H. Dhillon, R. Ganti, F. Baccelli, and J. Andrews, "Modeling and analysis of K-tier downlink heterogeneous cellular networks," *IEEE J. Sel. Areas Commun.*, vol. 30, no. 3, pp. 550–560, Apr. 2012.

[108] S. Singh, F. Baccelli, and J. Andrews, "On association cells in random heterogeneous networks," *IEEE Wireless Commun. Lett.*, vol. 3, no. 1, pp. 70–73, Feb. 2014.

[109] S. Singh, H. Dhillon, and J. Andrews, "Offloading in heterogeneous networks: Modeling, analysis, and design insights," *IEEE Trans. Wireless Commun.*, vol. 12, no. 5, pp. 2484–2497, May 2013.

[110] J. Andrews, S. Buzzi, W. Choi, S. Hanly, A. Lozano, A. Soong, and J. Zhang, "What will 5G be?" *IEEE J. Sel. Areas Commun.*, vol. 32, no. 6, pp. 1065–1082, June 2014.

[111] L. Zhang, H.-C. Yang, and M. Hasna, "Generalized area spectral efficiency: An effective performance metric for green wireless communications," *IEEE Trans. Commun.*, vol. 62, no. 2, pp. 747–757, Feb. 2014.

[112] R. Jain, D.-M. Chiu, and W. R. Hawe, *A quantitative measure of fairness and discrimination for resource allocation in shared computer system.* Eastern Research Laboratory, Digital Equipment Corporation Hudson, MA, 1984, vol. 38.

[113] N. Bhushan, J. Li, D. Malladi, R. Gilmore, D. Brenner, A. Damnjanovic, R. T. Sukhavasi, C. Patel, and S. Geirhofer, "Network densification: The dominant theme for wireless evolution into 5G," *IEEE Commun. Mag.*, vol. 52, no. 2, pp. 82–89, Feb. 2014.

[114] U. Siddique, H. Tabassum, E. Hossain, and D. I. Kim, "Wireless backhauling of 5g small cells: challenges and solution approaches," *IEEE Wireless Commun.*, vol. 22, no. 5, pp. 22–31, Oct. 2015.

[115] G. Piro, C. Ceglie, D. Striccoli, and P. Camarda, "3D video transmissions over LTE: A performance evaluation," in *Proc. IEEE EUROCON, 2013*, July 2013, pp. 177–185.

[116] Qualcomm, "Neighborhood small cells for hyper-dense deployments: Taking hetnets to the next level," White Paper, Feb. 2013.

[117] J. Zhu and P. R. Kinget, "Frequency-translational quadrature-hybrid receivers for very-low-noise, frequency-agile, scalable inter-band carrier aggregation," *IEEE J. Solid-State Circuits*, vol. PP, no. 99, pp. 1–15, 2016.

[118] G. Yuan, X. Zhang, W. Wang, and Y. Yang, "Carrier aggregation for LTE-advanced mobile communication systems," *IEEE Commun. Mag.*, vol. 48, no. 2, pp. 88–93, Feb. 2010.

[119] J. Liu and W. Xiao, "Advanced carrier aggregation techniques for multi-carrier ultra-dense networks," *IEEE Commun. Mag.*, vol. 54, no. 7, pp. 61–67, July 2016.

[120] J. F. Monserrat, I. Alepuz, J. Cabrejas, V. Osa, J. López, R. García, M. J. Domenech, and V. Soler, "Towards user-centric operation in 5G networks," *EURASIP Journal on Wireless Communications and Networking*, vol. 2016, no. 1, p. 1, 2016.

[121] S. Ahmad and D. Datla, "Distributed power allocations in heterogeneous networks with dual connectivity using backhaul state information," *IEEE Trans. Wireless Commun.*, vol. 14, no. 8, pp. 4574–4581, Aug 2015.

[122] J. Andrews, F. Baccelli, and R. Ganti, "A tractable approach to coverage and rate in cellular networks," *IEEE Trans. Commun.*, vol. 59, no. 11, pp. 3122–3134, Nov. 2011.

[123] J. Venkataraman, M. Haenggi, and O. Collins, "Shot noise models for outage and throughput analyses in wireless ad hoc networks," in *Proc. IEEE Military Commun. Conf. (MILCOM2006)*, Washington, DC, Oct. 2006, pp. 1–7.

[124] K. A. Hamdi, "A useful lemma for capacity analysis of fading interference channels," *IEEE Trans. Commun.*, vol. 58, no. 2, pp. 411–416, Feb. 2010.

[125] M. Haenggi, J. G. Andrews, F. Baccelli, O. Dousse, and M. Franceschetti, "Stochastic geometry and random graphs for the analysis and design of wireless networks," *IEEE J. Sel. Areas Commun.*, vol. 27, no. 7, pp. 1029–1046, Sept. 2009.

[126] H. P. Keeler, "Notes on the Poisson point process," Technical Reports, Weierstrass Institute, Tech. Rep., 2016.

[127] H. Thompson, "Distribution of distance to nth neighbour in a population of randomly distributed individuals," *Ecology*, vol. 37, no. 2, pp. 391–394, 1956.

[128] M. K. Simon and M.-S. Alouini, *Digital communication over fading channels*. John Wiley & Sons, 2005, vol. 95.

[129] M. Abramowitz and I. A. Stegun, *Handbook of mathematical functions: with formulas, graphs, and mathematical tables*. Courier Corporation, 1964, vol. 55.

[130] A. Goldsmith, *Wireless Communications*. Cambridge University Press, 2005.

[131] ArrayComm, http://www.arraycomm.com/technology/coopers-law/.

[132] J. G. Andrews, X. Zhang, G. D. Durgin, and A. K. Gupta, "Are we approaching the fundamental limits of wireless network densification?" *IEEE Commun. Mag.*, vol. 54, no. 10, pp. 184–190, Oct. 2016.

[133] I. Ashraf, F. Boccardi, and L. Ho, "Sleep mode techniques for small cell deployments," *IEEE Commun. Mag.*, vol. 49, no. 8, pp. 72–79, Aug. 2011.

[134] E. W. Weisstein, "Polylogarithm. From MathWorld–A Wolfram Web Resource,," http://mathworld.wolfram.com/Polylogarithm.html.

[135] A. Mukherjee, S. A. A. Fakoorian, J. Huang, and A. L. Swindlehurst, "Principles of physical layer security in multiuser wireless networks: A survey," *IEEE Commun. Surveys Tuts.*, vol. 16, no. 3, pp. 1550–1573, Third quarter 2014.

[136] J. Barros and M. R. D. Rodrigues, "Secrecy capacity of wireless channels," in *Proc. IEEE Int. Symp. on Inf. Theory*, July 2006, pp. 356–360.

[137] L. Wang, "Physical layer security in wireless networks: Design and enhancement." Ph.D. dissertation, Queen Mary University of London, 2015.

[138] Z. Dawy, W. Saad, A. Ghosh, J. G. Andrews, and E. Yaacoub, "Toward massive machine type cellular communications," *IEEE Wireless Communications*, vol. 24, no. 1, pp. 120–128, Feb. 2017.

[139] A. Osseiran, J. F. Monserrat, and P. Marsch, *5G mobile and wireless communications technology.* Cambridge University Press, 2016.

[140] M. Elsaadany, A. Ali, and W. Hamouda, "Cellular LTE-A technologies for the future Internet-of-Things: Physical layer features and challenges," *IEEE Commun. Surveys Tuts.*, vol. 19, no. 4, pp. 2544–2572, Fourthquarter 2017.

[141] C. Bockelmann, N. Pratas, H. Nikopour, K. Au, T. Svensson, C. Stefanovic, P. Popovski, and A. Dekorsy, "Massive machine-type communications in 5G: physical and MAC-layer solutions," *IEEE Communications Magazine*, vol. 54, no. 9, pp. 59–65, Sept. 2016.

[142] E. Soltanmohammadi, K. Ghavami, and M. Naraghi-Pour, "A survey of traffic issues in machine-to-machine communications over LTE," *IEEE Internet Things J.*, vol. 3, no. 6, pp. 865–884, Dec. 2016.

[143] G. Naddafzadeh-Shirazi, L. Lampe, G. Vos, and S. Bennett, "Coverage enhancement techniques for machine-to-machine communications over LTE," *IEEE Commun. Mag.*, vol. 53, no. 7, pp. 192–200, July 2015.

[144] S. Chen, R. Ma, H. H. Chen, H. Zhang, W. Meng, and J. Liu, "Machine-to-machine communications in ultra-dense networks: A survey," *IEEE Commun. Surveys Tuts.*, vol. 19, no. 3, pp. 1478–1503, Thirdquarter 2017.

[145] 3GPP TS 36.213, v14.5.0, "LTE; evolved universal terrestrial radio access (E-UTRA); physical layer procedures," 3GPP, Tech. Rep., Jan. 2018.

[146] M. Kamel, W. Hamouda, and A. Youssef, "Uplink coverage of machine-type communications in ultra-dense networks," in *IEEE Global Communications Conference (GLOBECOM2018)*, Abu Dhabi, UAE, Dec. 2018, pp. 1–6.

[147] 3GPP TR 36.814, v9.0.0, "Further advancements for e-utra physical layer aspects," 3GPP, Tech. Rep., Mar. 2010.

[148] M. D. Yacoub, "The $\alpha - \mu$ distribution: A physical fading model for the stacy distribution," *IEEE Trans. Veh. Technol.*, vol. 56, no. 1, pp. 27–34, Jan. 2007.

[149] M. Kamel, W. Hamouda, and A. M. Youssef, "Coverage and capacity analysis with stretched exponential path loss in ultra-dense networks," in *IEEE Global Communications Conference (GLOBECOM 2017)*, Dec. 2017, pp. 1–6.

[150] M. Ding, D. López-Pérez, G. Mao, and Z. Lin, "Performance impact of idle mode capability on dense small cell networks," *IEEE Trans. Veh. Technol.*, vol. 66, no. 11, pp. 10 446–10 460, Nov 2017.

[151] Ericsson, "Cellular networks for massive IoT: Enabling low power wide area applications," White Paper, Jan. 2016.

[152] W. Gautschi, "The incomplete gamma functions since Tricomi," in *In Tricomi's Ideas and Contemporary Applied Mathematics, Atti dei Convegni Lincei, n. 147, Accademia Nazionale dei Lincei*. Citeseer, 1998.

[153] A. Rico-Alvarino, M. Vajapeyam, H. Xu, X. Wang, Y. Blankenship, J. Bergman, T. Tirronen, and E. Yavuz, "An overview of 3GPP enhancements on machine to machine communications," *IEEE Commun. Mag.*, vol. 54, no. 6, pp. 14–21, June 2016.

[154] C. Hoymann, D. Larsson, H. Koorapaty, and J. F. Cheng, "A lean carrier for LTE," *IEEE Commun. Mag.*, vol. 51, no. 2, pp. 74–80, Feb. 2013.

[155] T. P. C. de Andrade, C. A. Astudillo, and N. L. S. da Fonseca, "Impact of M2M traffic on human-type communication users on the LTE uplink channel," in *Proc. IEEE Latin-American Conference on Communications 2015 (LATINCOM)*, Arequipa, Peru, Nov. 2015, pp. 1–6.

[156] M. Centenaro and L. Vangelista, "A study on M2M traffic and its impact on cellular networks," in *Proc. IEEE 2nd World Forum on Internet of Things 2015 (WF-IoT)*, Milan, Italy, Dec. 2015, pp. 154–159.

[157] M. Lévesque, F. Aurzada, M. Maier, and G. Joós, "Coexistence analysis of H2H and M2M traffic in FiWi smart grid communications infrastructures based on multi-tier business models," *IEEE Trans. Commun.*, vol. 62, no. 11, pp. 3931–3942, Nov. 2014.

[158] M. Franceschetti, J. Bruck, and L. J. Schulman, "A random walk model of wave propagation," *IEEE Trans. Antennas Propag.*, vol. 52, no. 5, pp. 1304–1317, May 2004.

[159] A. Laya, C. Kalalas, F. Vazquez-Gallego, L. Alonso, and J. Alonso-Zarate, "Goodbye, ALOHA!" *IEEE Access*, vol. 4, pp. 2029–2044, Apr. 2016.

[160] H. Tabassum, M. S. Ali, E. Hossain, M. J. Hossain, and D. I. Kim, "Uplink vs. downlink noma in cellular networks: Challenges and research directions," in *2017 IEEE 85th Vehicular Technology Conference (VTC Spring)*, June 2017, pp. 1–7.

[161] X. Zhang and M. Zhang, "Successive interference cancellation in downlink heterogeneous cellular networks," in *IEEE Globecom Workshops 2013 (GC Wkshps)*, Dec. 2013, pp. 730–735.

[162] S. K. Sharma and X. Wang, "Towards massive machine type communications in ultra-dense cellular iot networks: Current issues and machine learning-assisted solutions," *arXiv preprint arXiv:1808.02924*, 2018.

[163] Z. Qin, X. Yue, Y. Liu, Z. Ding, and A. Nallanathan, "User association and resource allocation in unified noma enabled heterogeneous ultra dense networks," *IEEE Commun. Mag.*, vol. 56, no. 6, pp. 86–92, June 2018.

[164] Y. Liu, X. Li, F. R. Yu, H. Ji, H. Zhang, and V. C. M. Leung, "Grouping and cooperating among access points in user-centric ultra-dense networks with non-orthogonal multiple access," *IEEE J. Sel. Areas Commun.*, vol. 35, no. 10, pp. 2295–2311, Oct. 2017.

[165] J. Liu, M. Sheng, L. Liu, and J. Li, "Interference management in ultra-dense networks: Challenges and approaches," *IEEE Netw.*, vol. 31, no. 6, pp. 70–77, Nov. 2017.

[166] B. Di, L. Song, Y. Li, and Z. Han, "V2X meets noma: Non-orthogonal multiple access for 5G-enabled vehicular networks," *IEEE Wireless Commun.*, vol. 24, no. 6, pp. 14–21, Dec. 2017.

[167] S. Feng, R. Zhang, W. Xu, and L. Hanzo, "Multiple access design for ultra-dense vlc networks: Orthogonal vs non-orthogonal," *IEEE Transactions on Communications*, vol. 67, no. 3, pp. 2218–2232, Mar. 2019.

[168] T. Lv, Y. Ma, J. Zeng, and P. T. Mathiopoulos, "Millimeter-wave noma transmission in cellular m2m communications for internet of things," *IEEE Internet Things J.*, vol. 5, no. 3, pp. 1989–2000, June 2018.

[169] Y. Du, C. Cheng, B. Dong, Z. Chen, X. Wang, J. Fang, and S. Li, "Block-sparsity-based multiuser detection for uplink grant-free noma," *IEEE Trans. Wireless Commun.*, vol. 17, no. 12, pp. 7894–7909, Dec. 2018.

[170] Z. Yang, W. Xu, Y. Pan, C. Pan, and M. Chen, "Energy efficient resource allocation in machine-to-machine communications with multiple access and energy harvesting for iot," *IEEE Internet Things J.*, vol. 5, no. 1, pp. 229–245, Feb. 2018.

[171] Y. Du, B. Dong, Z. Chen, X. Wang, Z. Liu, P. Gao, and S. Li, "Efficient multi-user detection for uplink grant-free noma: Prior-information aided adaptive compressive sensing perspective," *IEEE J. Sel. Areas Commun.*, vol. 35, no. 12, pp. 2812–2828, Dec. 2017.

[172] O. L. Alcaraz López, H. Alves, P. H. Juliano Nardelli, and M. Latva-aho, "Aggregation and resource scheduling in machine-type communication networks: A stochastic geometry approach," *IEEE Trans. Wireless Commun.*, vol. 17, no. 7, pp. 4750–4765, July 2018.

[173] M. Shirvanimoghaddam, M. Condoluci, M. Dohler, and S. J. Johnson, "On the fundamental limits of random non-orthogonal multiple access in cellular massive iot," *IEEE J. Sel. Areas Commun.*, vol. 35, no. 10, pp. 2238–2252, Oct. 2017.

[174] R. Abbas, M. Shirvanimoghaddam, Y. Li, and B. Vucetic, "A novel analytical framework for massive grant-free noma," *IEEE Trans. Commun.*, vol. 67, no. 3, pp. 2436–2449, Mar. 2019.

[175] Z. Zhang, H. Sun, and R. Q. Hu, "Downlink and uplink non-orthogonal multiple access in a dense wireless network," *IEEE J. Sel. Areas Commun.*, vol. 35, no. 12, pp. 2771–2784, Dec. 2017.

[176] M. Kamel, W. Hamouda, and A. Youssef, "Performance analysis of multiple association in ultra-dense networks," *IEEE Trans. Commun.*, vol. 65, no. 9, pp. 3818–3831, Sept. 2017.

[177] M. Kamel, W. Hamouda, and A. Youssef, "Downlink coverage and average cell load of M2M and H2H in ultra-dense networks," in *Proc. IEEE Personal, Indoor and Mobile Radio Communications (PIMRC), 2017*, Montreal, QC, Oct. 2017.

[178] H. A. David and H. N. Nagaraja, "Order statistics," *Encyclopedia of Statistical Sciences*, vol. 9, 2004.

[179] W. Saad, M. Bennis, and M. Chen, "A vision of 6G wireless systems: Applications, trends, technologies, and open research problems," *arXiv preprint arXiv:1902.10265*, 2019.

Appendix:
List of Publications

Journal Articles

1. **M. Kamel**, W. Hamouda, and A. Youssef, "Performance analysis of multiple association in ultra-dense networks," *IEEE Trans. Commun.*, vol. 65, no. 9, pp. 3818-3831, Sept. 2017.

2. **M. Kamel**, W. Hamouda, and A. Youssef, "Physical layer security in ultra-dense networks," *IEEE Wireless Commun. Lett.*, vol. 6, no. 5, pp. 690-693, Oct. 2017.

3. **M. Kamel**, W. Hamouda, and A. Youssef, "Ultra-dense networks: A survey," *IEEE Commun. Surveys Tuts.*, vol. 18, no. 4, pp. 2522–2545, Fourth quarter 2016.

Conference Proceedings

1. M. Elbayoumi, **M. Kamel**, W. Hamouda and A. Youssef, "Capacity Analysis of Downlink NOMA-Based Coexistent HTC/MTC in UDN" *Proc. IEEE International Conference on Communications, Signal Processing, and their Applications (ICCSPA), 2019*, Sharjah, UAE, Mar. 2109

2. **M. Kamel**, W. Hamouda and A. Youssef, "Uplink coverage of machine-type communications in ultra-dense networks," *Proc. IEEE Global Communications Conf. (GLOBECOM), 2018*, pp. 1-6, Abu Dhabi, United Arab Emirates, Dec. 2018.

3. **M. Kamel**, W. Hamouda, and A. M. Youssef, "Downlink coverage and average cell load of M2M and H2H in ultra-dense networks," in *Proc. IEEE Personal, Indoor and Mobile Radio Communications (PIMRC), 2017*, Montreal, Oct. 2017.

4. **M. Kamel**, W. Hamouda, and A. M. Youssef, "Coverage and capacity analysis with stretched exponential path loss in ultra-dense networks," in *Proc. IEEE Global Communications Conf. (GLOBECOM), 2017*, Singapore, Dec. 2017.

5. **M. Kamel**, W. Hamouda, and A. M. Youssef, "Average downlink rate in ultra-dense networks," in *Proc. IEEE Inter. Conf. on Commun. (ICC) 2017*, pp. 1–6, Paris, France, May 2017.

6. **M. Kamel**, W. Hamouda, and A. M. Youssef, "Multiple association in ultra-dense networks," in *Proc. IEEE Inter. Conf. on Commun. (ICC) 2016*, pp. 1–6, Kuala Lumpur, Malaysia, May 2016.